

The Effect of Mean Stresses on
Short Fatigue Crack
Growth Behaviour

By

Chun Hui Wang

Thesis submitted to the University of Sheffield for the Degree of Doctor
of Philosophy in the Faculty of Engineering

University of Sheffield

Department of Mechanical and Process Engineering

June 1990

Summary

The Effects of Mean Stresses on Short Fatigue Crack Growth Behaviour

This thesis investigates the effects of mean stresses on the fatigue behaviour of short cracks and related mechanisms. An experimental programme was carried out to investigate the effect of mean stresses on short fatigue crack growth behaviour and fatigue life in air. The material used was a 1.99% NiCrMo steel. Specimens with a shallow hour-glass profile were tested under torsional and uniaxial loading with various alternating and mean stress levels. Crack propagation was monitored by means of a surface replication technique applied periodically during the tests. Several results have been obtained:

1.) A plasticity localization period is found under stress-controlled conditions, in which no crack initiation occurred. Under tensile mean stress loading, the number of cycles spent in this phase is given by

$$N_0 = 2.97 \times 10^{66} e^{-\sigma_m/51.5} \sigma_a^{-23} \quad (1)$$

For mean stress torsional loading, dominant cracks tend to initiate from inclusions with no plasticity localization period.

2.) Mean shear stress is found to increase microstructurally short crack (MSC) growth rate under torsional loading (hence stage I, mode II cracks) and this effect is independent of the polarity of the mean shear stress. MSC growth rate under mean shear stress torsional loading can be expressed as,

$$\frac{d a}{d N} = 3.68 \times 10^{-52} e^{\tau_m/62.6} \tau_a^{19.07} (d_1 - a) \quad (\mu m/cycle) \quad (2)$$

where $d_1 = 167 \mu m$ and is independent of the mean shear stress level. Here τ_m and τ_a are the mean and alternating shear stress, respectively.

3.) Physically short cracks (PSCs) growing under mixed mode (I and II) are also strongly influenced by mean shear stress. Mean shear stress may affect crack growth path but with no effect of polarity on the fatigue lifetime of isotropic materials. The PSC growth rate under torsional mean shear stress is,

$$\frac{d a}{d N} = 1.09 \times 10^{-34} e^{\tau_m/66.5} \tau_a^{11.715} a - D \quad (\mu m/cycle) \quad (3)$$

where $D = 5.1 \times 10^{-4} \mu/cycle$.

4.) While mean tensile stress significantly enhances the short crack growth rate and reduces fatigue lifetime, mean compressive stress does not show any beneficial or harmful effect for the present material. The MSC growth phase for mean tensile stress uniaxial loading is given as an upper bound by

$$\frac{d a_s}{d N} = 3.894 \times 10^{-78} e^{\sigma_m/43.1} \sigma_a^{27.2} (d_2 - a_s) \quad (\mu m/cycle) \quad (4)$$

where d_2 equals $50 \mu m$. For compressive mean stress loading, the MSC growth rate is identical to that under zero mean stress loading.

5.) The physically short crack (PSC) growth rate under tensile mean stress loading is given by

$$\frac{d a_s}{d N} = 2.346 \times 10^{-58} e^{\sigma_m/56.1} \sigma_a^{19.33} a_s^{1.405} - D \quad (\mu m/cycle) \quad (5)$$

where $D = 2.76 \times 10^{-34} e^{\sigma_m/137} \sigma_a^{11.1} (\mu m/cycle)$. But low compressive mean stress ($-200 \text{ MPa} \leq \sigma_m \leq 0 \text{ MPa}$) does not alter the PSC growth rate, i.e the PSC growth rate is identical to that under zero mean stress loading.

6.) A new model is proposed, in which three stress parameters (macro shear stress amplitude, macro mean shear stress and macro maximum normal stress) are incorporated to unify the effects of the mean stresses. This model states that the MSC growth rate is controlled by as 'effective shear stress amplitude', i.e.

$$\tau_a^* = \tau_a e^{|\tau_m|/1194} + 0.218 \times \sigma_{n,max} \quad (6)$$

Here τ_a , τ_m and $\sigma_{n,max}$ are the mean shear stress, alternating shear stress and maximum normal stress on the MSC plane.

Satisfactory predictions of the MSC growth rate and high cycle fatigue lifetime data from the following four types of tests have been achieved on the basis of this model: (a) fully reversed torsion tests ($R = -1$); (b) mean torsional shear stress tests; (c) fully reversed uniaxial loading ($R = -1$); (d) mean stress uniaxial tests (tensile or compressive mean stress loading).

Preface

This dissertation is based on the findings of research carried out in the Department of Mechanical and Process Engineering at the University of Sheffield.

The content of this dissertation is original except where specific references are made to other work. No part of this thesis has been submitted to any other university for any degree or qualification.

Chun Hui Wang

Sheffield, June 1990.

Acknowledgements

I wish to thank the head of the Department of Mechanical and Process Engineering for the use of the laboratory facilities. I am especially grateful to my supervisor, Professor K. J. Miller, for his guidance, generous help and encouragement. Helpful discussions with Dr. M. W. Brown, Dr. E. R. de los Rios, Dr. J. Yates and Dr. R. Akid are also gratefully acknowledged.

I am indebted to the British Council and the Chinese Government for the award of a scholarship. I should also like to thank the generous assistance of GEC Turbine Generators Ltd for providing specimens and information about the material. Helpful discussion with Dr. R. Suhr, the Head of the Fatigue Testing Group of GEC's Turbine Generators Ltd is also gratefully acknowledged.

The high cycle uniaxial fatigue tests were carried out at the Health and Safety Executive, Sheffield: I am especially grateful to Mr. Peter Bann for his help in the use of the Instron machine.

Finally I would like to thank my wife for her support and understanding.

C. H. Wang

Contents

Summary	I
Preface	III
Acknowledgments	IV
Contents	V
Nomenclature	VIII
1 Introduction and Theoretical Considerations	1
1.1 Historical Background	1
1.2 Effects of Mean Stress on the Fatigue Limit	2
1.2.1 Effect of Mean Axial Stress	2
1.2.2 Effect of Mean Shear Stress	5
1.3 Crack Initiation and Propagation	6
1.4 Multi-Axial Fatigue	7
1.5 Linear Fracture Mechanics	10
1.6 Non-linear Fracture Mechanics	15
1.7 Short Crack Growth	19
1.7.1 A General Review	19
1.7.2 Microstructurally Short Crack (MSC) Growth	20
1.7.3 Physically Short Crack (PSC) Growth	22
1.8 Comments	23
References	25
Figures and Tables	29
2 Experimental Work	35
2.1 Material	35
2.2 Test Facilities and Design of Grips	36
2.3 Specimen Design and Preparation	37

2.4	Experimental Techniques	38
2.4.1	Torsion Tests	38
2.4.2	Tensile Tests	40 ^{4/}
2.4.3	Crack Detection	42
2.5	Test Programmes	44
	References	47
	Figures and Tables	48
3	Torsion Tests: Results and Analyses	56
3.1	Effect of Mean Shear Stress on Cyclic Shear Plastic Deformation	56
3.2	Tests Results	58
3.3	Stage I Crack Growth	59
3.4	Effects of Inclusions	61
3.5	Transient and Stage II Crack Propagation	62
3.5.1	Transient Behaviour	62
3.5.2	Stage II Growth and Theoretical Modelling	64
3.6	Polarity of Mean Shear Stress	66
3.7	Discussion and Conclusions	68
	References	70
	Figures and Tables	71
4	Uniaxial Tests: Results and Analyses	87
4.1	The Stress-Strain Relationship	87
4.2	Fully Reversed Uniaxial Fatigue Tests	89
4.2.1	Conventional Fatigue Results	89
4.2.2	Crack Growth Data	90
4.3	High-Cycle Uniaxial Asymmetrical Fatigue Tests	93
4.3.1	Conventional Fatigue Tests; Results and Analyses	93
4.3.2	Fractographic Studies	98
4.3.3	Crack Growth Results	100

References	102
Figures and Tables	103
5 Stress Ratio Effects: A Literature Survey	124
5.1 Introduction	124
5.2 Stress Ratio Effects on Long Crack Growth	125
5.3 Closure of Long Cracks	126
5.4 Effects of Stress Ratio on Threshold	130
5.5 Effects of Mean Stress on Short Crack Growth	132
5.6 Comments	134
References	135
Figures and Tables	138
6 Analyses of Crack Growth Results	140
6.1 The Limits of LEFM	140
6.2 Generation of Crack Growth Data	142
6.3 Microstructurally Short Crack Growth in Torsion	143
6.3.1 Introduction	143
6.3.2 MSC Growth under Various Mean Stress Torsional Loading ..	144
6.4 Analysis of Physically Short Crack Growth in Torsion	147
6.4.1 Derivation of the Crack Growth Equation	147
6.4.2 Effect of Mean Shear stress on PSC Growth and Its Modelling	151
6.5 Torsional Fatigue Life Prediction	153
6.6 MSC Growth under Uniaxial Loading	154
6.6.1 Fully Reversed Loading	154
6.6.2 Effect of Mean Axial Stress	155
6.7 PSC Growth under Uniaxial Loading	158
6.7.1 Fully Reversed Loading	158
6.7.2 Uniaxial Loading under Mean Stress	160
6.8 Uniaxial Fatigue Lifetime Prediction	161
6.9 Summary	161

References	164
Figures and Tables	165
7 Discussion and Future Work	202
7.1 Torsional Mean Stress and Cyclic Plastic Strain	202
7.2 Plasticity Localization	203
7.2.1 Role of Stress Level and Microstructure	203
7.2.2 Effect of Mean Stresses	204
7.3 Microstructurally Short Crack Growth	206
7.3.1 Effect of Torsional Mean Shear Stress	206
7.3.2 Mean Uniaxial Stress	207
7.4 A Model for the Effects of Mean Stress	207
7.4.1 Introduction	208
7.4.2 The Modified Model	209
7.4.3 Application of the Model to Experimental Results	211
7.4.4 Comments	212
7.5 Physically Short Crack Growth	214
7.5.1 Torsional Loading	214
7.5.2 Uniaxial Loading	215
7.6 Effect of Mean Stress and Closure of Short Cracks	217
7.7 Fatigue Life Prediction	219
7.8 Future Work	220
References	222
Figures and Tables	224
8 Conclusions	231
Appendices	237
Appendix A: Torsion Tests Data	237
Appendix B: Uniaxial Tests Data	243

Nomenclature

The symbols most frequently used in the text are listed below. Those which are rarely used are defined in their context.

a	crack length
a_f	Crack length at failure
a_s	Surface crack length
a_{th}	Crack length at threshold
$CTOD$	Crack tip opening displacement
d	Predominant microstructural dimension
E	Young's modulus
G	Modulus of rigidity
K	Stress intensity factor
K_t	Stress concentration factor
K_f	Notch fatigue factor
K_{th}	Threshold stress intensity factor
n	Strain hardening exponent
n'	Cyclic hardening exponent
N	Cycles
N_f	Cycles to failure
r_0	Minimum radius of specimen cross-section
r_p	Plastic zone size
$r_{p,rev}$	Cyclic (reversed) plastic zone size
$r_{p,mon}$	Monotonic plastic zone size
S	Stress
R	Stress ratio (S_1/S_2)
T	Torque
X	Distance from crack tip
Y	Geometry factor

Θ	Angle of twist
θ	Angle of twist per unit length
ϵ	Normal strain
σ	Normal stress
γ	Engineering shear strain
ν	Poisson's ratio
τ	Shear stress
τ_u	Ultimate torsional strength
σ_u	Ultimate tensile strength
λ	Biaxial stress ratio (σ_2/σ_1)
Δ	Range

Subscripts:

a	amplitude
cl	closure
e	elastic
fl	fatigue limit
m	mean value
max	maximum value
min	minimum value
op	opening
p	plastic
t	total

Chapter 1

Introduction and Theoretical Considerations

1.1 Historical Background

FATIGUE has long been recognized as the worst culprit which gives rise to unexpected failures. During the years 1852 – 1870, Wohler carried out the first systematic experiments on fatigue and Wohler type curves or S–N curves are still regarded as representative of basic fatigue characteristics [1]. Although great progress has been made in the study of fatigue ever since these pioneering days, fatigue failures are still the major causes for disastrous failures. Examples are the failure of Comet aircraft in the 1950's, a DC-10 airliner in 1979.

Fatigue occurs over a certain period of time, through cyclic loading frequently at stresses below that which would cause immediate failure. The cyclic stress can be at a zero mean stress but at an amplitude (S_a) as shown in Fig.1.1a, or there can be a superimposed mean stress (S_m) as in Fig.1.1b. In practice, many components and structures are subjected to unsymmetrical loading. Common examples are due to steady end loads, residual stresses, shrink fits, unsymmetrical twisting of shafts, and so on. A large number of failures are closely associated with high mean stress [2].

1.2 Effects of Mean Stress

The mean stress can have a substantial influence on fatigue behaviour as is shown in Fig.1.2, where S_a is plotted against the number of cycles to failure N_f for a given mean stress.

Conventional test programmes generally involve establishing S-N curves for a series of values of mean stresses for different materials. In order to avoid the necessity of carrying out such comprehensive tests, attempts have been made to construct maps and relationships to enable the prediction of the fatigue limit under different mean stresses.

1.2.1 Effects of Mean Axial Stress

Numerous investigations of the influence of tensile mean stress on long-life fatigue strength has been made. A number of empirical relationships has been proposed to account for the effect of mean tensile stress [3]. However, the study of compressive mean stress is relatively rare, partly because compressive mean stress is difficult to superimpose and partly because many data showed compressive mean stress was not harmful. In general, tensile mean stress is detrimental while compressive mean stress may be regarded as beneficial.

The fatigue strength of a material under unsymmetrical loading can be represented on a diagram in which the fluctuating stress S_a is plotted against the mean stress S_m as shown in Fig.1.3, which is commonly referred to as a $R - M$ diagram, where R is the stress range, equal to twice the amplitude of fluctuating stress. Points S_0 and S_u are the alternating fatigue stress for a given endurance and static tensile strength, respectively. The curve joining the two points represents the contour of a given endurance for various combinations of static and fluctuating stresses. This is the classical approach to predicting the fatigue life of a component.

To compare the behaviour of different metals, a dimensionless approach is com-

monly adopted, in which the ratio of fluctuating stress to the alternating fatigue strength is plotted against the ratio of mean stress to tensile strength as shown in Fig.1.4.

Among those empirical relationships proposed (e.g. [3] [4]), the most frequently used are listed below,

$$\text{Modified Goodman Law, } \frac{S_a}{S_0} + \frac{S_m}{S_u} = 1 \quad (1.1)$$

$$\text{Gerber's Law, } \frac{S_a}{S_0} + \left(\frac{S_m}{S_u}\right)^2 = 1 \quad (1.2)$$

$$\text{Soderberg's Law, } \frac{S_a}{S_0} + \frac{S_m}{S_y} = 1 \quad (1.3)$$

$$\text{Morrow's law, } \frac{S_a}{S_0} + \frac{S_m}{\sigma_t} = 1 \quad (1.4)$$

$$\text{Heywood's Law, } \frac{\sigma}{\sigma_u} = \left(1 - \frac{\sigma_m}{\sigma_u}\right) \left\{ \frac{\sigma_0}{\sigma_u} + \gamma \left(1 - \frac{\sigma_0}{\sigma_u}\right) \right\} \quad (1.5)$$

where

$$\gamma = \left(\frac{\sigma_m}{3\sigma_u}\right) \left(2 + \frac{\sigma_m}{\sigma_u}\right) \quad \text{for steels} \quad (1.6)$$

$$\gamma = \left(\frac{\sigma_m}{\sigma_u}\right) \left\{1 + \left(\frac{n\sigma_u}{2200}\right)^4\right\}^{-1} \quad \text{for aluminium alloys} \quad (1.7)$$

Here σ_t is the true fracture stress of specimen. The term n is the logarithm of the life at which the fatigue strength is estimated. Heywood's expression degenerates to the modified Goodman relationship when $\gamma = 0$.

A survey of the literature showed that 90 percent of the data lay above the Goodman line, and fall mainly between the modified Goodman curve and Gerber's parabola [3] [5]. However, some of the low- and medium-strength aluminium alloys exhibit marked mean stress effect, with values lying below the Goodman line. Such alloys have a high ratio of zero mean stress fatigue limit to tensile strength. The Soderberg criterion is on the conservative side, as shown in Fig.1.4. It was also

reported that a more accurate prediction of the effect of mean stress can be obtained by using the true fracture stress of the material rather than the ultimate tensile strength [3].

Some of the very early experimental results implied that mean compressive stress would also reduce the fatigue limit. Gerber may have proposed his parabolic relationship in order to allow for the reduction. However, subsequent data shows that fatigue limit does not decrease below the zero mean stress fatigue limit, provided the specimen does not yield or buckle under the maximum compressive stress, as reported in reference [3]. For some materials fatigue limit increases with the increasing mean compressive stress.

Also shown in Fig.1.3 are two lines and drawn at 45° from yield stress and the ultimate tensile stress, respectively. Along the first line, the sum of mean stress and fluctuating stress equals the yield stress, while along the second line, the sum equals the ultimate tensile stress. Clearly, all components are required to operate below the second line to avoid immediate failure while some are required to operate below the first line to avoid gross yielding, especially for high strength materials.

All these approaches have to be modified for notches, size, surface finish, and environmental effects when their application is made to the design of components. For example, stress concentrations are frequently encountered in engineering applications. However, due to the lack of the understanding of the basic mechanisms of fatigue with mean stress, different authors treat these effects in different ways. One criterion based on the work of Snow and Langer quoted in [6] is reviewed here.

The simple Goodman criterion is used. For small external mean stress, the local mean stress is increased by K_t (or if known by K_f). The original Goodman line is modified accordingly. As the external mean stress is increased, a point will be reached when the material at the stress concentration yields and beyond this point it is suggested that any further increase of mean stress has no effect. The modified design criterion is shown in Fig.1.5.

Such a criterion is strictly based on the assumption and some experimental data

that the maximum stress at stress concentration should not exceed the yield stress, which may not be true under some circumstances e.g. cyclic hardening of some materials can produce a cyclic yield stress level above the static yield stress.

1.2.2 Effect of Mean Shear Stress

In contrast to the study of axial mean stress, very little work has been done on the influence of mean shear stress on the torsional fatigue limit. A review of the then available literature on steels, aluminium alloys, and copper alloys by Smith in 1942 [7] concluded that mean shear stress had little effect on the torsional fatigue limit, especially when maximum shear stress is below the monotonic shear yield stress of the material. The results are quoted here in Fig.1.6a, which cites many technical papers in reference [3] and [4]. This conclusion has subsequently been supported by more recent work [8] [9] and is widely accepted.

The results reported by Gough [10] also confirmed the above conclusion. He stated that the effect of mean shear stress is to increase the maximum shear stress for a given stress range hereby influencing the crystallographic structure of materials. This was supported by X-ray diffraction studies that indicated a breakdown of the original grains sub-grains or crystallites [3].

The data reported by Smith are replotted in Fig.1.6b assuming that torsional fatigue limits of materials are two thirds of their yield strengths. One interesting observation is that the data and diagram presented by Smith (Fig.1.6a) seems to suggest that the direction of the mean shear has a marked effects on fatigue endurance (the diagram does not exhibit a symmetry about the $\tau_m = 0$ axis). Contrary to the study on mean uniaxial stresses (which can be divided into mean tensile stress and mean compressive stress), no discussion can be located in the literature with regard to this respect. More discussion on this issue will be presented in Section 3.6 in relation to the experiments conducted in the present research.

1.3 Crack Initiation and Propagation

To understand and quantify the effect of mean stress it is obvious that the mechanisms involved in the fatigue process need to be studied. It follows therefore that the birth and growth of cracks needs to be reviewed.

Extensive studies have shown that cyclic plastic deformation is essential for fatigue damage. For instance, the plastic strain amplitude at the fatigue limit of smooth specimens is of the order of 10^{-5} for all materials [1]. It is now clear that elastic deformation is fully reversible and cannot cause any damage. It is the plastic deformation which causes irreversible changes in the material structure, which is the most basic aspect of fatigue.

Fatigue processes can be considered under three consecutive and partly overlapping stages, (1) Cyclic hardening /or softening; (2) Crack initiation and (3) Crack propagation. For a polycrystalline ductile metal, the above three stages are generally related to free surface events. Surface grains can deform plastically and fracture more easily at a surface because they are not only in intimate contact with the environment which always assists fatigue damage, but also, they are the only ones not wholly supported by neighbouring grains.

Other factors are also responsible for crack initiation at a surface, such as existing macroscopic stress concentration around notches, or where there is a change in shape, and additionally microscopic stress concentrations due to the surface irregularity (a surface is never ideally smooth). Three types of fatigue crack nucleation site have been observed [1] with either light or electron microscopy. Local plastic-strain concentration at or near to the surface is common for all three types. These give rise to active slip planes which form within surface grains having favourably orientated slip systems. It is here that fatigue cracks are initiated and propagate [11] [12]. Under uniaxial loading conditions, extrusions and intrusions are invariably formed and cracks start from these microscopic notches.

As there is no clear cut demarcation between initiation and crack growth, the

areas which they are referred to in the literature vary widely. It is more plausible to divide fatigue lifetime into the following four phases [11] [13], (1) nucleation of fatigue crack (defined as initiation); (2) Stage I crack growth; (3) Stage II crack propagation; (4) final rupture. Stage I cracks lie along the active slip planes, which generally coincide with the maximum shear plane [14]. In uniaxial loading the maximum shear stress lies in planes oriented at 45° to the loading direction. After penetrating the body of the material to a depth of two or three grains, cracks may become Stage II cracks, and propagate in a direction perpendicular to the maximum tensile stress. This transition from Stage I to Stage II depends on the microstructure of materials, stress levels, stress states, and so on. The mechanism for Stage II crack growth is double de-cohesion along the two maximum shear planes radiating from the crack tip.

The crack growth rate, which is one of the most important measures of the development of damage, is dominated by the shear mode during Stage I whilst the normal stress acting on the crack plane modifies the growth rate [15]. A more detailed discussion is presented in the following section.

1.4 Multi-Axial Fatigue

The multi-axial fatigue behaviour of metals has been studied since the beginning of twentieth century. A wealth of experimental data and a number of criteria are therefore available, both for high cycle fatigue and low cycle fatigue. For high cycle fatigue, due to the fact that bulk stresses are nominally elastic, most of the classical criteria are based on the onset of plasticity. The Tresca and von Mises criteria are popular for ductile materials whilst the Rankine principal stress criterion is often used for brittle materials. Gough and Sines [10] also proposed an ellipse arc criterion to correlate fatigue limit data under different combinations of stress states, but without any physical interpretation. The disadvantage of these criteria is that crack growth direction and crack plane orientation (which are very important for fatigue failure analysis and which are nearly always related to a free surface, as discussed in Section 1.3) are not taken into account especially in respect to the effect of free surface. For

low cycle fatigue, these simple criteria are unable to correlate the available results. This has led to many criteria being proposed especially when correlating low-cycle experimental data. Most of the criteria are empirical relationships and hence do not allow generalization.

The theory proposed by Brown and Miller [15] advanced the understanding of fatigue mechanisms under multi-axial stress states, and various experimental results can be correlated by this theory. The detail of the theory and relevant developments are now discussed.

The theory is proposed for fully reversed cycling loading. The stress ratios (R) of the three principal stresses are all -1 . Due to the fact that cracks are initiated from the free surface, one of the three principal stresses is zero (which can be σ_2 or σ_3). If the other two principal stresses are denoted as ξ_1 and ξ_2 ($\xi_1 \geq \xi_2$) then the biaxial ratio is $\lambda = \xi_2/\xi_1$. Positive λ and negative λ will give rise to two modes of crack growth, case A ($\lambda \leq 0$) and case B ($\lambda \geq 0$). For case A, a crack grows along the surface and therefore is less dangerous in comparison to that of case B, in which the crack propagates inwards and away from the surface.

The theory states that a plot of the maximum shear strain amplitude against the tensile strain amplitude normal to the crack plane will reveal the controlling process in fatigue crack growth for each multiaxial stress state. The two strains are represented on Mohr's circles of strain by the co-ordinates of the highest point of the largest Mohr's circle. Because the fully reversed condition is considered, the Mohr's circles represent both the maximum and minimum stress states, but with different signs.

$$\frac{\gamma}{2} = \frac{1}{2} \times \text{maximum engineering shear strain} = \frac{\epsilon_1 - \epsilon_3}{2} \quad (1.8)$$

$$\epsilon_n = \text{tensile strain on the maximum shear plane} = \frac{\epsilon_1 + \epsilon_3}{2} \quad (1.9)$$

Hence constant fatigue life contours can be represented on a Γ plane by the curve of maximum shear strain $\gamma/2$ against the tensile strain ϵ_n normal to maximum shear

plane for a given fatigue life, ie.

$$\frac{\epsilon_1 - \epsilon_3}{2} = f\left[\frac{\epsilon_1 + \epsilon_3}{2}\right] \quad (1.10)$$

where $\epsilon_1 \geq \epsilon_2 \geq \epsilon_3$.

The above theory is important in that the physics of crack growth processes is considered. The conclusion that multi-axial fatigue failures have two basic crack types indicates that conventional failure criteria are not appropriate. For low strain fatigue, similar relationships have been proposed in terms of stress, one example is the criterion by Findley [16] who concluded that the normal stress upon the maximum shear stress modifies the fatigue life, ie.

$$\tau_n = \text{constant} - f(\sigma_n) \quad (1.11)$$

In another paper [17] Kandil, Brown, and Miller attempted to quantify the function f , they suggested an equivalent strain range for case A type cracks of the form $\Delta\gamma_n + S\Delta\epsilon_n$, where S has a value of 1.0. Then the constant fatigue life contours can be expressed as

$$\Delta\gamma_n + \Delta\epsilon_n = \text{constant} \quad (1.12)$$

For low-cycle fatigue, when plastic strain amplitudes are comparable to elastic strain amplitudes, Brown and Miller theory can also be presented in terms of plastic shear strain and plastic normal strain amplitudes.

Socie *et al* [18] studied the effects of mean stress on the biaxial fatigue of Inconel 718. They suggested a modification to the above relationship to account for the effects of tensile mean stress. Constant fatigue life contours are expressed in the form,

$$\frac{1}{2}\Delta\gamma_p + \frac{1}{2}\Delta\epsilon_{np} + \sigma_n/E = \text{constant} \quad (1.13)$$

Instead of using the maximum shear strain γ_{max} , Lohr and Ellison [19] proposed a similar parameter γ^* , the shear strain driving the crack through the thickness. They

proposed the following empirical relation to correlate all multiaxial data using a single curve, ie for case B type cracks only,

$$\gamma^* + k \epsilon_n^* = \text{constant} \quad (1.14)$$

The above discussion was actually mainly concerned with Stage I crack growth. After cracks have penetrated the body of a material to a depth of the order of two or three grains, they may turn 45 degrees to a plane perpendicular to the maximum tensile strain. Cracks then grow by a double de-cohesion mechanism, in which multi-slip systems will dominate [13] [20]. Whether the above reviewed criteria are still valid in quantifying crack growth for Stage II is not yet clear.

In the above discussion, it is clear that macro-plasticity is responsible for crack growth. However, in many other cases, cracks can propagate at nominally low elastic cyclic stress levels which are only a small proportion of the yield stress. Obviously the mechanisms are modified, and crack propagation, therefore, cannot be characterised by a single law. Hence it is necessary to distinguish between these two kinds of growth. In the last two decades, much work has been done to understand these differences. Initially the first or high strain crack growth types of cracks were called “short” cracks, the later being called “long” cracks which may be characterized by LEFM.

1.5 Linear Fracture Mechanics

Many engineering components and structures contain cracklike defects, and discontinuities, etc. They can be introduced prior-to service, such as weld imperfections and geometrical discontinuities. From the point of view of continuum mechanics, a crack or a notch represents a very effective stress raiser.

It becomes very important to quantify the behaviour of a crack precisely, since even very small cracks measuring only a few tenths of a micron in length can have a substantial effect on the lifetime and safe working stress levels of a component or a

structure.

Consider a homogeneous and isotropic elastic body containing a sharp crack (crack tip radius is zero). The body is loaded by arbitrary external forces. There are three isolated modes of relative displacement of the crack surfaces which can occur as shown in Fig.1.7. Mode I is called the opening mode in which crack faces move directly apart, Mode II and Mode III are called the shear mode and the tear mode, respectively. The stress field at the crack tip can be described with the aid of the elastic parameter called the stress intensity factor K_m , in which $m = I, II$ and III . Symbols I, II, III denote the three different loading modes.

The stress distribution at the vicinity of the crack tip under plane strain condition is as follows,

$$\text{Pure Mode I} \quad K_I = Y_I \sigma \sqrt{\pi a} \quad (1.15)$$

$$\sigma_\theta = \frac{K_I}{\sqrt{2\pi r}} \left(\frac{3}{4} \cos \frac{\theta}{2} + \frac{1}{4} \cos \frac{3\theta}{2} \right) \quad (1.16)$$

$$\sigma_r = \frac{K_I}{\sqrt{2\pi r}} \left(\frac{5}{4} \cos \frac{\theta}{2} - \frac{1}{4} \cos \frac{3\theta}{2} \right) \quad (1.17)$$

$$\sigma_z = \nu(\sigma_\theta + \sigma_r) \quad (1.18)$$

$$\tau_{r\theta} = \frac{K_I}{\sqrt{2\pi r}} \left(\frac{1}{4} \sin \frac{\theta}{2} + \frac{1}{4} \sin \frac{3\theta}{2} \right) \quad (1.19)$$

where a is the crack length, Y is a geometry factor and r and θ are polar co-ordinates with the origin at the crack tip.

When the external stress level is low, elasticity conditions in the crack tip zone dominate. In other words the plastic zone does not greatly perturb the crack tip elastic stress field.

In many other cases, the external stress level is relatively high and, as a result, the plastic zone greatly changes the elastic stress-strain distribution at the crack tip. However, there is no analytical elastic-plastic solution of generally validity and completeness; hence some acceptable approximations are required.

One good approximation to reality is offered by the model that takes into account strain hardening of the material in the plastic zone, commonly known as HRR [21] [22] solution. For a material whose stress-strain relationship is linear for $\sigma < \sigma_y$ and of a power-law type for $\sigma > \sigma_y$, i.e.

$$\sigma = E\epsilon \quad \text{for } \sigma < \sigma_y$$

and

$$\sigma = \sigma_y \left(\frac{\epsilon}{\epsilon_y} \right)^n \quad \text{for } \sigma > \sigma_y \quad (1.20)$$

the stress and strain components within the plastic zone can be expressed in the form

$$\sigma_{ij} = \Phi(K_I, \sigma_y, n) \cdot \frac{g_{ij}(\theta, n)}{r^{n/(1+n)}}, \quad (1.21)$$

$$\epsilon_{ij} = \Psi(K_I, \sigma_y, n) \cdot \frac{h_{ij}(\theta, n)}{r^{1/(1+n)}} \quad (1.22)$$

where Φ and Ψ represent the intensity of the stress and strain fields, which are given by the elastic stress intensity factor and material constants σ_y and n . For the case of perfect plasticity, the stress distribution can be obtained by equating n to zero.

It should be pointed out that the HRR solution is only valid for monotonically increasing stress, no unloading is considered.

Due to the plasticity at the crack tip, cyclic loading causes redistribution of stress and strain. For simplicity, consider the ideally elastic-plastic approach to the cyclic stress case. The stress cyclically varies within limits σ and $\sigma - \Delta\sigma$ where the stress range $\Delta\sigma = 2\sigma_a$. When the stress increases from zero to σ , a plastic zone of the size given by Eq.1.23 is formed. If we reduce the stress from σ to $\sigma - \Delta\sigma$ (i.e., K_I to $K_I - \Delta K_I$), since the range of stress before reversed yielding occurs is $2\sigma_y$, the superposition of $-\Delta\sigma$ will induce a plastic zone of the size given by the following equation provided that the crack is always open,

$$r_{p,mon} = \frac{1}{2\pi} \left(\frac{K_{max}}{\sigma_y} \right)^2 \quad r_{p,rev} = \frac{1}{2\pi} \left(\frac{\Delta K}{2\sigma_y} \right)^2 \quad (1.23)$$

However, there is ample experimental evidence that fatigue cracks close at a stress equal or higher than zero [23]. Unfortunately such effect is frequently ignored in the

discussion of the reversed plastic zone size and the above equation is generally used, e.g. in reference [24].

A very important conclusion can be drawn here namely that the stress strain fields within the plastic zone (for both the elastic case or the small-scale yielding case) can be characterized by the elastic stress-intensity factor. Having established that it is the local plastic deformation which controls the crack initiation and propagation, it is the stress intensity factor alone which becomes the basis for describing the crack growth rate, the conditions of non-propagation, and so on.

Paris and Erdogan [25] first critically scrutinized crack growth under fatigue loading using LEFM and an empirical relation was proposed to correlate fatigue crack growth data, which is now known as the Paris-Erdogan Law in the literature.

$$\frac{da}{dN} = A (\Delta K)^m \quad (1.24)$$

where $\Delta K = K_{max} - K_{min}$, and A and m are material, temperature, microstructure, and stress ratio dependent. Values of m that have been reported lie typically in the range of values $2 \leq m \leq 5$.

This empirical relation is widely used, since it exposes the most important fact of the self-similarity of the fatigue crack growth process. However, it is only valid within a so-called intermediate, medium-amplitude part of the fatigue kinetic diagram.

A threshold effect is observed, as indicated in Fig.1.8, which occurs when the crack growth rate equals a value of approximately the order of an atomic distance per cycle. Hence the plot is generally split into three regions. Region B is the linear part of the growth curve and crack growth can be adequately described by the Paris-Erdogan Law.

When the maximum stress intensity factor becomes higher crack growth curve deviates from linearity. Approaching the critical stress intensity value (fracture toughness K_{Ic}), crack instability and rapid acceleration can occur and region C terminates with failure.

In region A, the applied stress intensity factor range is invariably low, and crack

growth rate is also very low. Extensive experimental data have shown that the crack growth in this region is greatly affected by microstructure, environment and stress ratio, etc.

Equation 1.24, especially in its integrated form, is widely used to evaluate the lifetime of cracked structures from a knowledge of the likely stress spectrum, initiation values of K ie K_{th} , K_{Ic} , and constants A and m .

The basis of the description of fatigue crack propagation by the stress intensity factor range ΔK are (i) crack extension is governed by a elastic stress field at the crack tip, which determines various parameters, such as plastic-zone size. For small-scale yielding, the plastic-zone size is generally taken to be less than one fiftieth of the crack length. This leads to the condition that the limiting stress amplitude is less than one third of the yield stress. More generally, for self-similitude to hold, low applied stress levels and correspondingly small local plastic zones are required. (ii) The continuum conditions of LEFM to hold. In other words, the use of LEFM may break down when the plastic-zone size at the crack tip is either less than the microstructural dimension or greater than say one fifth of the crack length.

LEFM analyses of crack growth however permit a direct and advantageous comparison between small laboratory specimens and large structures when the stress intensity factor terms (which incorporating the geometry factor and the loading factor) are identical in both cases. However, the limitations of LEFM analyses must be noted albeit its great potential and wide applicability. Recent experimental evidence has shown that for many engineering materials, LEFM can give a very non-conservative prediction of the crack growth rate and also the conditions for non-propagation under high cyclic stress levels, which is directly associated with the damage-tolerance methodologies. A more detailed discussions is presented in the next two sections.

1.6 Non-linear Fracture Mechanics

Elasto-Plastic Fracture Mechanics (EPFM) was developed to study the fracture process for high strength, high ductility materials for which crack-tip plasticity is not negligible and dominates the cracking process. Therefore the extent of plastic deformation in the crack tip region is the most important parameter, whereas in LEFM, it is the elastic stress field that characterized the cracking process through uniquely characterizing the local plastic deformation

Various approaches have been put forward to estimate the plastic deformation and associated phenomena. Among them, three are usually used, (a) Crack Tip Opening Displacement (*CTOD*); (b) Path-independent contour integrals e.g. *J* integral; (c) Fracture process zone. Since *CTOD* can provide a very plausible, albeit qualitative explanation of fatigue growth under high strain conditions, attention will now be focused on its development.

Dugdale [27] and Barenblatt [28] first proposed a strip yielding model, which allows the crack tip to blunt. The model was later developed by Burdekin and Stone [29]. This model envisages a central crack of length $2a$ lying normal to an applied stress σ as shown in Fig.1.9. Yielding occurs over a length r_p ahead of each crack tip in the form of a narrow strip zone. By removing the stress singularity (implying that the stress concentration due to the crack is relaxed), the plastic-zone size is given by,

$$r_p = c - a = a \left[\sec \left(\frac{\pi \sigma}{2 \sigma_y} \right) - 1 \right] \quad (1.25)$$

where σ_y is the yield stress, which sometimes is replaced by the ultimate tensile strength of the material σ_u . It follows that the corresponding zone is actually an unstable zone in which the maximum stress level reaches the U.T.S. The crack tip opening displacement can be obtained by using the same model,

$$CTOD = \frac{8\sigma_y}{E\pi} a \ln \left\{ \sec \left(\frac{\pi \sigma}{2 \sigma_y} \right) \right\} = \frac{8\sigma_y}{E\pi} a \ln \left\{ 1 + \frac{r_p}{a} \right\} \quad (1.26)$$

Bilby, Cottrell and Swinden [30] used a dislocation type of model, in which both the crack and plastic zone are treated as dislocation pile-ups. The theory of continuous

distributions of dislocations was applied to obtain the spread of the plastic zone. The same technique as used by Dugdale and Barenblatt was also adopted, that is the stress singularity in the solution of the equilibrium equation is also removed. The case for a mode III crack was solved analytically and similar equations are derived, ie

$$\frac{a}{c} = \cos \left(\frac{2 \tau}{\pi \tau_y} \right) \quad (1.27)$$

and the crack tip sliding displacement

$$CTSD = \frac{8\tau_y}{\pi G} a \ln \left\{ \sec \left(\frac{\pi \tau}{2 \tau_y} \right) \right\} = \frac{8\tau_y}{\pi G} a \ln \left\{ 1 + \frac{r_p}{a} \right\} \quad (1.28)$$

where G is the shear modulus.

For a mode I crack under remote tensile stress a similar solution to Dugdale and Barenblatt model was also obtained by the same authors through representing the plastic zone at crack tip by two shear bands radiating from crack tip at 45° as shown in Fig.1.9(b).

It should be pointed out that the above discussion is only valid for plane stress. Difficulties are encountered for the plane strain condition due to the presence of high triaxial stresses. Larsson and Carlsson [31] pointed out that a single parameter, such as $CTOD$, cannot characterise the crack tip field, because the stress acting parallel to the crack plane affects the spread of plasticity.

For the cyclic stress case, if no crack closure is considered, the monotonic plastic zone (sometimes called the 'forward plastic-zone') size can be obtained by replacing the stress σ with σ_{max} ; the reversed plastic-zone size and the range of crack tip opening displacement can be obtained by replacing σ with σ_a .

Similar to the applications of LEFM to fatigue crack growth, two major types of criteria have been put forward to correlate fatigue crack growth rate. Firstly, the reversed plastic-zone size, or 'severe deformation zone size' for the case when macroplasticity occurs, has received wide attention. For example, Brown and Miller [26] have shown a better correlation between cyclic plastic-zone size and fatigue crack growth rate for biaxial stress states. Previously Brown *et al* [32] had successfully related

crack growth rate to the extent of the ‘severe deformation zone’ embedded in the plastic zone at the crack tip.

Secondly, crack advance is often related to the geometry changes at the crack tip caused by the crack opening deformation. Essentially one tries to identify the irreversible new crack surface caused by sliding off. However the results of crack growth tests on a wide range of materials do not support a simple quantification of crack growth rate with $\frac{1}{2}(CTOD)$ and so crack growth is assumed to be a fraction of the crack tip opening displacement [33] [34]; ie.

$$\frac{da}{dN} = f \cdot CTOD \quad (1.29)$$

where f which varies with stress is able to correlate crack growth rate [35].

Experimental results showed that crack growth rate indicates a higher order relation to the stress level in low cycle fatigue, hence several empirical relationships have been reported in the literature, For example, Solomon [36] and Wareing [37] proposed that crack growth is strongly dependent on the cyclic plastic strain,

$$\frac{da}{dN} = YA(\Delta\epsilon_p)^\alpha \cdot a \quad (1.30)$$

where Y is a geometry factor, for example Y equals 1 for a straight crack front, and 0.25 and 0.5 for semicircular surface crack and semi-elliptical surface crack respectively. The exponent α is in the range 1 to 2. For a material obeying a cyclic stress–strain relationship,

$$\Delta\sigma = k(\Delta\epsilon_p)^{n'} \quad (1.31)$$

the growth law, expressed in terms of stress, is,

$$\frac{da}{dN} = YA(\Delta\sigma)^m \cdot a \quad (1.32)$$

where $m = \alpha/n'$. For most steels, m is the order of 10.

Tomkins and other workers [20] [38] have proposed two very plausible models for low cycle fatigue crack growth. In the first model, crack growth per cycle is considered equal to the de-cohesion caused by plastic straining,

$$\frac{da}{dN} = \delta = r_{p,rev} \cdot \epsilon_p \quad \text{for ductile steels} \quad (1.33)$$

$$\frac{da}{dN} = \delta = \int_0^{\epsilon_p} r_{p,rev} d\epsilon_p \quad \text{for high strength steels} \quad (1.34)$$

Another model [39] relates the crack growth to the plastic portion of the crack tip opening displacement δ_p , which is obtained by modifying the BCS model to account for the plastic deformation (since the BCS solution of the equilibrium equation is only a lower bound). This is done by replacing the Elastic Youngs' Modulus, E by the Secant Modulus, $\sigma / (\epsilon_e + \epsilon_p)$. Hence *CTOD* (or δ) is given by,

$$CTOD = \frac{Aa}{\beta E} \ln \sec(\beta\sigma_a) + Aa\Delta\epsilon_p \left[\frac{\beta\sigma_a}{(1+n')} + \dots \right] \quad (1.35)$$

where $A \approx 2$ for crack tip relaxation along two $\pm 45^\circ$ slip lines, and $\beta = \pi/2\sigma_u$.

While for $(\sigma_a/\sigma_u) < 0.5$,

$$\delta \simeq \frac{\pi\sigma_a^2 a}{2\sigma_u E} + \frac{\pi\sigma_a \Delta\epsilon_p a}{\sigma_u(1+n')} = \delta_e + \delta_p \quad (1.36)$$

The disadvantage of these two models is that they can only apply to cases in which cyclic plastic strain is present and it is inappropriate to extend their applications to high cycle fatigue.

The following conclusion can be drawn from the above discussion. In high strain fatigue, the Paris-Erdogan Law and the ΔK approach are not applicable, because the high order Paris Law predicts a crack growth rate in the following form which has been found not to be true.

$$\frac{da}{dN} = A(\Delta\sigma)^m \cdot a^{\frac{m}{2}} \quad (1.37)$$

The phenomenon of high stress induced crack growth has received great attention over the last two decades, and has been entitled 'short crack' growth. It is generally realised that a new approach is required and recent publications are now reviewed in the following section.

1.7 Short Crack Growth

1.7.1 A General Review

Although it has been well-established that EPFM instead of LEFM must be used for cases where small-scale yielding (SSY) is violated, LEFM sometimes is still used for studying the crack growth behaviour under high cyclic stress levels, because extensive data have been produced with the conventionally ΔK -based methodology. A typical example is the use of the stress intensity factor threshold for predicting the fatigue limit, where sometimes an imaginary ‘intrinsic crack’ length is added to the real crack length.

The application of EPFM, however, is not straight forward, because cyclic softening and hardening behaviour is invariably associated with high cyclic stress. In addition continuum mechanics may not be applicable, or at least it has to be modified when cracks are very small, ie of the order of the microstructural features (grain size, average distance between different phases, etc.) These problems lead to the investigation of “short fatigue cracks” which, in general, can be defined as cracks whose behaviour cannot be quantified by LEFM. Moreover, the application of LEFM to the characterization of sub-critical flaw growth can result in overestimates in the lifetime of defect-tolerant structures. There have been reports in the literature that failures in components with small defects occurred at shorter lives than those predicted from long crack data [40].

Generally, there are three prevailing definitions to describe a “mechanically short” crack: (i) Cracks which are of the length comparable to the scale of the microstructure (invalidation of continuum mechanics); (ii) Cracks which are of a length comparable to the scale of the local plastic zone (invalidation of the SSY condition); (iii) Cracks which are simply physically small less than 0.5 to 1.0 mm (invalidation of similitude). A crack may also be termed as “chemically short” if a corrosive environment is present. In terms of Linear Elastic Fracture Mechanics (LEFM), a more precise definition can be expressed as that a crack is considered as short crack when LEFM

cannot quantify its growth rate.

Hence short cracks can be divided into three main categories [41],

1. Microstructurally short cracks (MSC); $a < d$.
2. Physically short cracks (PSC); $d < a < \ell$.
3. Highly stressed cracks with $a > \ell$ and $\sigma_a > \frac{1}{3}\sigma_{cy}$.

where d is the dominant microstructural barrier, ℓ is the minimum crack length for which LEFM is valid.

An example can be found at a notch root, where after the initiation, crack growth actually covers all the above listed three regimes but may eventually become a LEFM type of growth in its behaviour.

The investigations to date are reviewed in detail in references [42] [43] [44]. There is now a large body of evidence showing that the growth of short cracks are faster than those predicted by LEFM. Several possible reasons have been proposed to explain the faster growth rate of short cracks under the same nominal driving force ΔK , such as high plastic zone size to crack length ratio, low crack closure level, different growth mechanisms, differences in the crack tip environments, microstructural effects, and so on. All these indicate significant differences between short cracks and long cracks.

1.7.2 Microstructurally Short Crack (MSC) Growth

In this regime, crack growth is affected by the microstructure, such as grain boundaries, orientation of grains, inclusions, etc. because the crack length is of the same order of magnitude as metallurgical features. It is therefore not appropriate to use isotropic material assumptions and the local stress-strain field is different from the remote applied stress-strain field [45]. However from an engineering viewpoint, it is the applied stress or strain that is of most concern, hence studies are usually confined to the application of applied load to quantify crack growth behaviour.

Due to the fact that a MSC is not only very small, but also may grow at a high speed, precise measurement of the crack length becomes very difficult. It follows that there are only a few experimental data available in literature on the MSC growth rate. Hobson *et al* [45] examined a medium carbon steel under push-pull tests and derived an equation for MSC growth,

$$\frac{da_s}{dN} = 1.64 \times 10^{-34} (\Delta\sigma)^{11.14} (d - a_s) \quad (1.38)$$

where a_s is the surface crack length measured from replicas, $d = 107 \mu m$. This equation actually gave the upper bound of MSC growth rate for the material.

Based on the concept that cyclic shear plastic strain controls the Stage I crack growth, Miller *et al* [46] showed that cyclic shear plastic strain $\Delta\gamma_p$ should be used for the correlation of crack growth rate of a medium carbon steel, ie

$$\frac{da_s}{dN} = 6(\Delta\gamma_p)^{2.24} (d - a_s) \quad (1.39)$$

where $d = 330 \mu m$ for torsion tests.

Other kinds of equations have also been put forward and most of them are in the general form as below,

$$\frac{da}{dN} = A(\Delta\gamma)^\alpha (d - a)^\nu a^{1-\nu} \quad (1.40)$$

here $\Delta\gamma$ is the shear strain range, and A , α and ν ($0 \leq \nu \leq 1$) are material constants. The term d is the dominant microstructural barrier which may depend on stress level and stress states [44].

All these equations exhibit a decreasing crack growth rate (except when $\nu = 0$ in the above equation) as the crack length increases in the range $0 < a < d$ for a constant stress or strain range. Such a pattern agrees with the form of MSC growth observed in experiments where the deceleration or arrest of small fatigue cracks often occurs when crack tip hit the crystallographic barriers, as found in steels, Ti alloys and Aluminium alloys [42]. Several models have been proposed for microstructural barrier blocking mechanisms [42] [47] [48]. These models almost follow the same approach, viz, the microstructural barrier blocks the spread of the plastic zone, which

is the ligament between the crack tip and the next barrier. Such a blocking effect eventually diminishes as the crack becomes longer and longer with a corresponding increase in plastic zone size.

However, the exact extent of the influence of microstructure on MSC growth is not definitive. Some workers consider that this period is the growth of a crack in the very first grain where the crack is initiated. Once the crack has overcome the barrier to Stage II, crack growth will not be affected by microstructure. This simplification can lead to a simple modeling of the Stage II crack growth. However, when the change in the crack growth path and real metallurgical features are considered, MSC growth is most likely affected by several different microstructural barriers. Besides, material anisotropy and texture may also influence MSC growth behaviour as suggested by some workers.

1.7.3 Physically Short Crack (PSC) Growth

Since microstructural effects are nearly non-existent in this regime, EPFM can be directly applied to describe this crack growth phase. One empirical relationship is,

$$\frac{da}{dN} = B \cdot (\Delta\epsilon)^\beta \cdot a \quad (1.41)$$

as proposed by Tomkins [38] from high strain push-pull fatigue tests. Equations in terms of stress are also reported, e.g. in [49],

$$\frac{da}{dN} = B \cdot (\Delta\sigma)^m \cdot a \quad (1.42)$$

where $m = 7$.

The experimentally observed threshold effect has also been taken into account by some workers [45] [46]. For instance, the fatigue limit is the boundary between non-propagation and propagation and a more general crack growth law for the PSC growth regime is of the following form,

$$\frac{da}{dN} = B \cdot (\Delta\epsilon)^\beta \cdot a - C \quad (1.43)$$

The J-integral has also been used by some workers to correlate PSC growth, although the applicability of the J-integral is questionable in these cases. Nevertheless it offers an interesting approach to unify long crack growth and short crack growth. The following results are presented by Dowling [50],

$$\frac{da}{dN} = A \cdot (\Delta J)^{m'} \quad (1.44)$$

where

$$\Delta J \simeq 3.2\Delta W_e \cdot a + 5.0\Delta W_p \cdot a \quad (1.45)$$

and

$$\Delta W_e = \frac{\Delta\sigma^2}{2E} \quad (1.46)$$

$$\Delta W_p = \frac{\Delta\sigma\Delta\epsilon_p}{1+n'} \quad (1.47)$$

here 3.2 and 5.0 are the scaling constants, which incorporate correction factors for specimen geometry and flaw shape and are derived from equivalent linear elastic solutions.

1.8 Comments

It is clear that mean stress can dramatically reduce the fatigue limit, which is one of the most important measures of the resistance of a material to fatigue loading. The effect of mean stress is of great importance to engineers, since in many applications, a high static mean load and a very low fluctuating load are operational and even inevitable. Classic design criteria are either based on the conventional S-N curves for different mean stress levels, or on empirical relationships, such as the Goodman relation or the Gerber relation, etc. The conventional approaches have some serious problems however. For instance, there is no physical understanding behind these phenomena and different workers may deal with the problem in different ways. Although many design codes have addressed mean stress effects, their application is confined to

a rather narrow region and broader generalization is not allowed due to their empirical nature. Furthermore in service loading may be more complicated due to loading changes of various amplitude, effects of defects, and so on.

LEFM, since its birth, has become an important tool for assessing structural integrity. Vast amounts of data have been accumulated, including mean stress effects (this will be reviewed in Chapter 5). Damage-Tolerance Methodologies, which are constructed on the basis of LEFM, have made it possible to evaluate the safe stress level and the lifetime of cracked components. However, due to the limits of the applicability of LEFM, these recently developed approaches cannot be applied for high stress levels. The limits of LEFM approach for asymmetrical loading will be discussed in Section 6.1 in relation the present experimental results. In particular, the Goodman or Gerber type of curves cannot be obtained from LEFM results.

The various models reviewed in this chapter have significantly advanced our understanding of the mechanisms responsible for crack growth, especially those models proposed on the basis of EPFM enabled the quantification of short crack growth under high strain. However, none of these models can predict the effect of mean stresses on short crack growth, actually this problem has not been addressed in terms of crack growth rate and no publications can be found regarding the effects of mean stress on short crack growth. The lack of published data in this area of fatigue research also strongly advocates the necessity for the present work.

Economic pressures to use materials more efficiently have made designers to make use the strength of materials more effectively and therefore more components are working at stress levels close to the yield stress. Therefore, a new approach has to be established not only to provide a better understanding of the effects of mean stress, but also to offer improved design codes for engineers.

References

1. Klesnil, M and Lukas, P. (1980) *Fatigue of Metallic Materials*, Elsevier Scientific Publishing Company.
2. Suhr, R. (1987) The Factors Affecting the High Cycle Fatigue Strength of Pressure Turbine and Generator Rotors, *GEC REVIEW*, Vol.3, No.3, pp. 171–179.
3. Frost, N. E., Marsh, K. J. and Pook, L. P. (1974) *Metal Fatigue*, Clarendon Press, Oxford.
4. Forrest, K. (1962) *Fatigue of Metals*, Pergamon Press.
5. Dolan, T. J. (1953) *Metals Engineering Design*, ASME Handbook, McGraw-Hill, New York. pp. 82.
6. Cook, N. H. (1987) *Mechanics and Materials For Design*, McGraw-Hill International Editions (McGraw-Hill Book Company).
7. Smith, J.O. (1942) Effect of Range of Stress on Fatigue Strength, *University of Illinois Engineering Department Station Bulletin 334*.
8. Findley, W. N., Mergan, F. C. and Rosenberg, A. H. (1953) *Proceedings of American Society for Testing and Materials*, 53, pp.768.
9. Chodorowski, W. T. (1956) *International Conference on Fatigue*, Institution of Mechanical Engineers, pp.122.
10. Gough, H. J. (1949) Engineering Steels Under Combined Cyclic and Static Stress, *Proceedings of Institution of Mechanical Engineers*, Vol.160, pp.472.
11. Forsyth, P. J. E. (1961) A Two Stage Process of Fatigue crack Growth, *Proceedings of Crack Propagation Symposium*, Cranfield, pp.76–94.
12. Ewing, J. A. and Humfrey, J. C. W. (1903) The Fracture of Metals under Repeated Alternations of Stress, *Philosophy Transactions of Royal Society*, 200, pp.241-250.
13. Brown, M. W. and Miller, K. J. (1979) Initiation and Growth of Cracks in Biaxial Fatigue, *Fatigue of Engineering Materials and Structures*, Vol.1, pp.231–246, 1979.
14. Fuchs, H. O. (1985) On the Definition of Planes of maximum shear strains, *Multiaxial Fatigue*, ASTM STP 853, K. J. Miller and M. W. Brown, Eds., American Society for Testing and Materials, Philadelphia, pp.5-8.

15. Brown, M. W. and Miller, K. J. (1973) A Theory for Fatigue Failure under Multiaxial Stress–Strain Conditions, *Proceedings of the Institution of Mechanical Engineers*, Vol.187 65/73, pp.745-755.
16. Findley, W. N. (1957) *Transactions, American Society of Mechanical Engineers*, Vol.79, pp.1337.
17. Kandil, F. A., Brown, M. W. and Miller, K. J. (1982) Biaxial Low-cycle Fatigue Fracture of 316 Stainless Steel at Elevated Temperatures, *Book 280*, The Metals Society, London, pp.203-210.
18. Socie, D. F., Waill, L. A. and Dittmer, D. F. (1985) Biaxial Fatigue of Inconel 718 Including Mean Stress Effects, *Multiaxial Fatigue, ASTM STP 853*, K. J. Miller and M. W. Brown, Eds., American Society for Testing and Materials, Philadelphia, pp.463-481.
19. Lohr, R. D. and Ellison, E. G. (1980) A Simple Theory for Low Cycle Multiaxial Fatigue, *Fatigue of Engineering Materials and Structures*, Vol. 3, pp.1-17.
20. Tomkins, B. (1968) Fatigue Crack Propagation—An Analysis, *Philosophical Magazine*, Vol.18, pp.1041.
21. Rice, J. R. and Rosengren, G. F. (1968) Plane Strain Deformation Near a Crack Tip in a Power–Law Hardening Material, *Journal of Mechanics and Physics of Solids*, Vol.16, pp.1-12.
22. Hutchinson, J. W. (1968) *Journal of Mechanics and Physics of Solids*, Vol.16, pp.13.
23. Elber, W. (1971) The Significance of Crack Closure, *ASTM STP 486*, pp.230.
24. Lal, K. M. and May, I. Le. (1980) An Assessment of Crack Closure in Fatigue Using the Westergaard Stress Function, *Fatigue of Engineering Materials and Structures*, Vol.3, pp.99-111.
25. Paris, P. and Erdogan, F. (1963) A Critical Analysis of Crack Propagation Laws, *Transactions ASME, Journal of Basic Engineering*, D85, pp.528-534.
26. Brown, M. W. and Miller, K. J. (1985) Mode I Fatigue Crack Growth Under Biaxial Stress at Room and Elevated Temperature, *Multiaxial Fatigue, ASTM STP 853*, K. J. Miller and M. W. Brown, Eds., American Society For Testing and Materials, Philadelphia, pp.135-152.
27. Dugdale, D. S. (1960) Yielding of Steel Sheets Containing Slits, *Journal of Mechanics and Physics of Solids*, 8, pp.100-104.
28. Barenblatt, G. I. (1962) Mathematical Theory of Equilibrium Cracks, *Advances in Applied Mechanics*, Vol.7, pp.55–129.

29. Burdekin, F. M. and Stone, O. E. M. (1966) The Crack Opening Displacement Approach to Fracture Mechanics in Yielding Materials, *Journal of Strain Analysis*, 1, pp.145-163.
30. Bilby, B.A., Cottrell, A.H. and Swinden, K.H. (1963) The Spread of Plasticity from a Notch, *Proceedings of the Royal Society of London*, A 272, pp.272-304.
31. Larsson, S. G. and Carlsson, A. J. (1973) Influence of Non-Singular Stress Terms on Small Scale Yielding at Crack Tips in Elastic-Plastic Materials, *Journal of Mechanics and Physics of Solids*, 21, pp.263-277.
32. Brown, M. W., Liu, H. W., Kfoury, A. P. and Miller, K. J. (1980) An Analysis of Fatigue Crack Growth under Yielding Conditions, *Proceedings of the Conference of the Fifth International Conference on Fracture, Cannes, France*, pp.891-899.
33. Lardner, R. W. (1968) A Dislocation Model for Fatigue Crack Growth in Metals, *Philosophical Magazine*, Vol. 17, pp.71-82.
34. Schwalbe, K. H. (1973) Approximate Calculation of Fatigue Crack Growth, *Engineering Fracture Mechanics*, Vol. 9, pp.381-396.
35. Barenblatt, G. I. (1962) *Advances in Applied Mechanics*, 7, pp.55.
36. Solomon, H. D. (1972) Low Cycle Fatigue Crack Propagation in 1018 Steel, *Journal of Materials, JMLSA*, Vol. 7, No. 3, pp.299-306.
37. Wareing, J. (1983) Mechanisms of High Temperature Fatigue and Creep—Fatigue in Engineering Materials, *Fatigue at High Temperature*, edited by R. P. Skelton, Applied Science Publishers, pp.135-185.
38. Tomkins, B. (1971) Fatigue Failure in High Strength Metals, *Philosophical Magazine*, 1971, pp.687-703.
39. Tomkins, B. (1984) High Strain Fatigue, *Subcritical Crack Growth Due to Fatigue, Stress Corrosion and Creep*, edited by L. H. Larsson, Elsevier Applied Science Publishers, pp.239-266.
40. Hicks, M. A., Howland, C. and Brown, C. W. (1983) *The Metallurgy of Light Alloys*, The Chamelon Press, London.
41. Miller, K. J. (1987) The Behaviour of Short Fatigue Cracks and Their Initiation Part I—A Review of Two Recent Books, *Fatigue AND Fracture of Engineering Materials and Structures*. Vol.10, No.1, pp.75-91.
42. Tanaka, K. (1987) Mechanisms and Mechanics of Short Fatigue Crack Propagation, *JSME International Journal, Review*, Vol.30, No.259, pp.1-13.
43. Suresh, S. and Ritchie, R. O. (1984) Propagation of Short Cracks, *International Metals Reviews*, Vol. 29, No. 6, pp.445-476.

44. Miller, K. J. (1987) The Behaviour of Short Fatigue Cracks and Their Initiation Part II—A General Summary, *Fatigue and Fracture of Engineering Materials and Structures*. Vol.10, No.2, pp.93-113.
45. Hobson, P. D., Brown, M. W. and de los Rios E. R. (1986) Two Phases of Short Crack Growth in a Medium Carbon Steel, *The Behaviour of Short Fatigue Cracks*. EGF Publication 1 (Edited by K. J. Miller and E. R. de los Rios.), pp.441-459.
46. Miller, K. J., Mohamed, H. J. and de los Rios E. R. (1986) Fatigue Damage Accumulation Above and Below the Fatigue Limit, *The Behaviour of Short Fatigue Cracks*. EGF Publication 1 (Edited by K. J. Miller and E. R. de los Rios.), pp.491-511.
47. Navarro, A. and de los Rios, E. R. (1988) Short and Long Crack Growth: A Unified Model, *Philosophical Magazine*, Vol.57, No.1, pp.15–36.
48. Navarro, A. and de Los Rios, E. R. (1988) An Alternative Model of the Blocking of Dislocations at Grain Boundaries, *Philosophical Magazine*, Vol.57, No.1 pp.37–42.
49. Scott, P. M., Tomkins. B. and Forman, A. J. E. (1982) Development of Engineering Codes of Practice for Corrosion Fatigue, *ASME Pressure Vessel and Piping Conference*, Orlando, 1982.
50. Dowling, N. E. (1977) *Cyclic Stress-Strain and Plastic Deformation aspects of Fatigue Crack Growth*, *ASTM STP 637*,, pp.97.

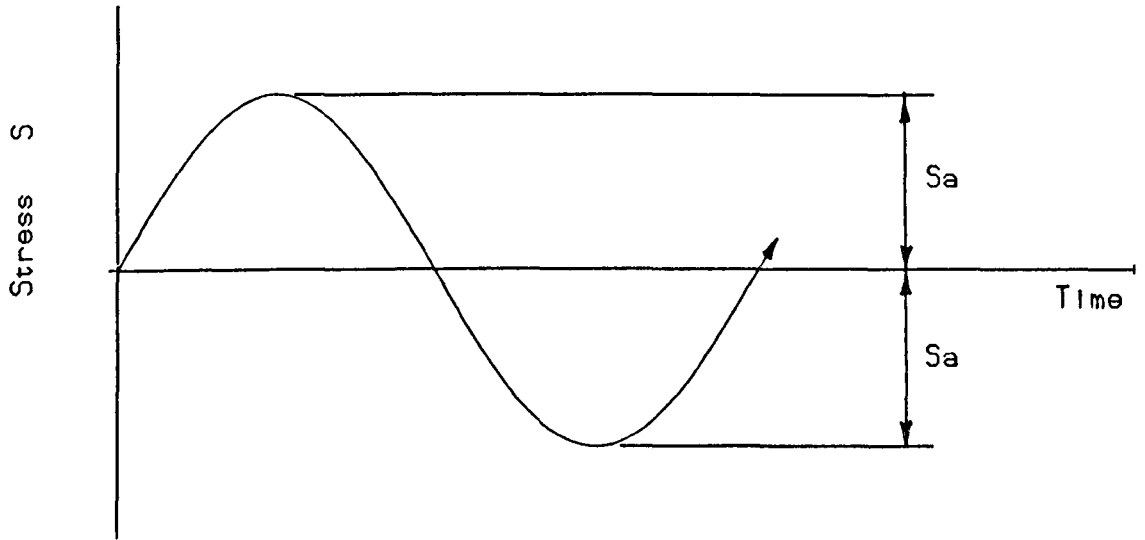


Figure 1.1a Fatigue Loading, without mean stress

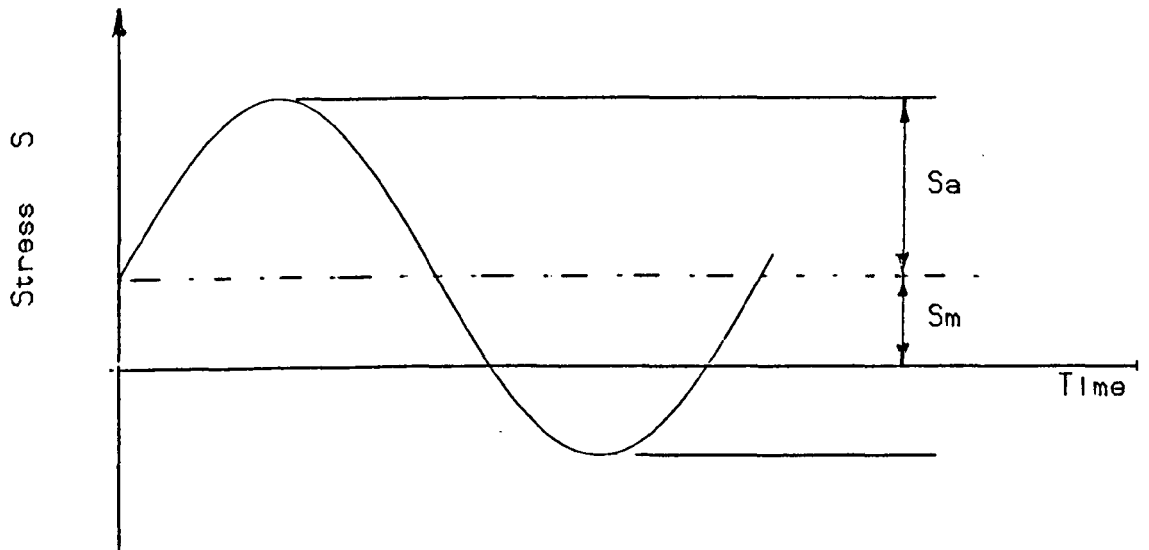


Figure 1.1b Fatigue Loading, with mean stress

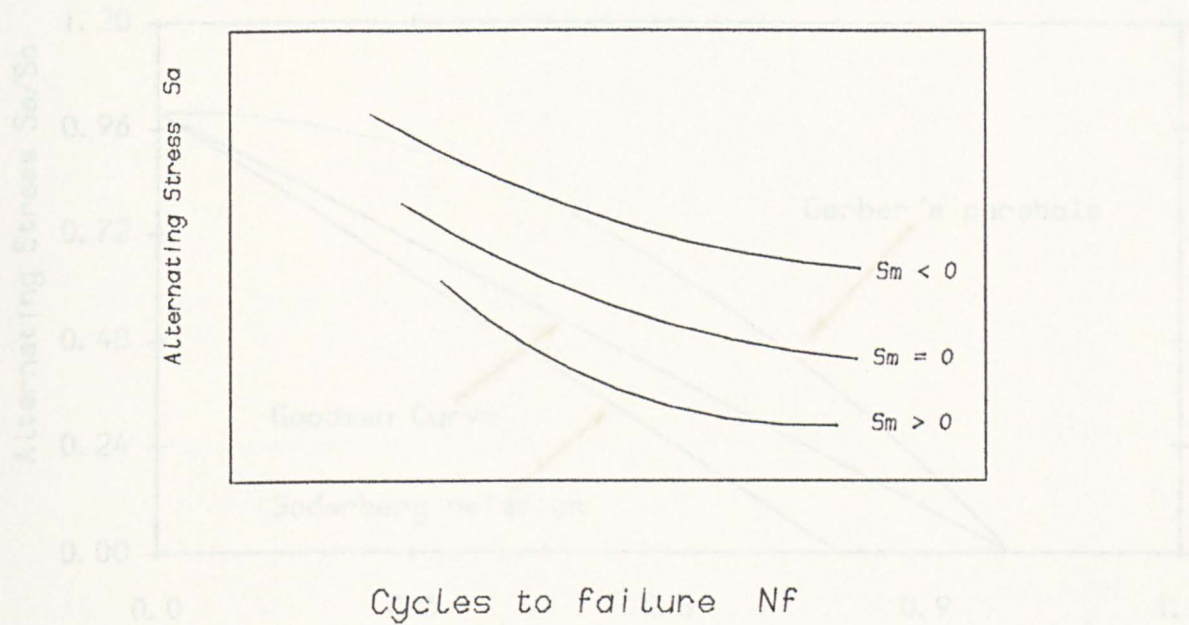


Fig.1.2 Schematic Drawing of the Effect of Mean Stress on Fatigue Life

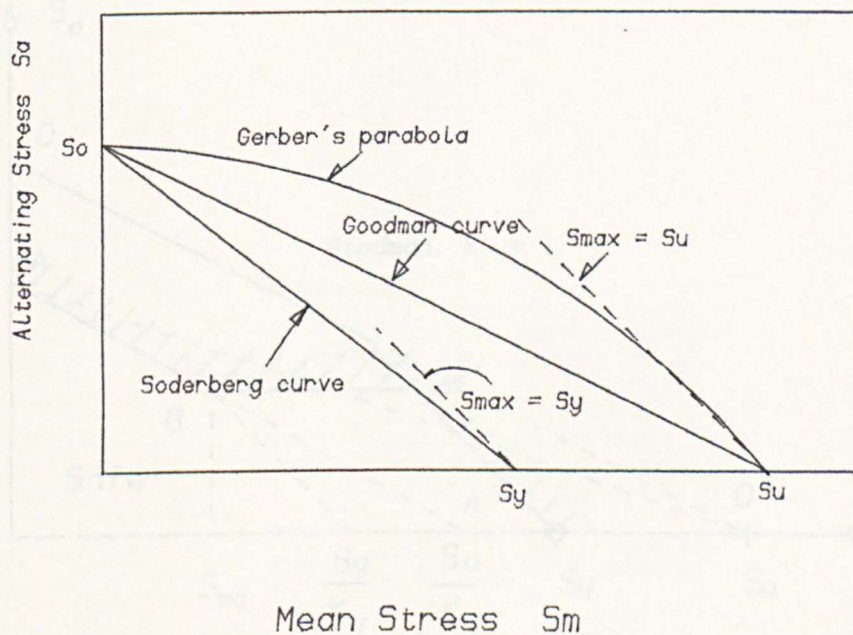


Fig.1.3 Fatigue Strength versus Static Strength (R--M diagram)

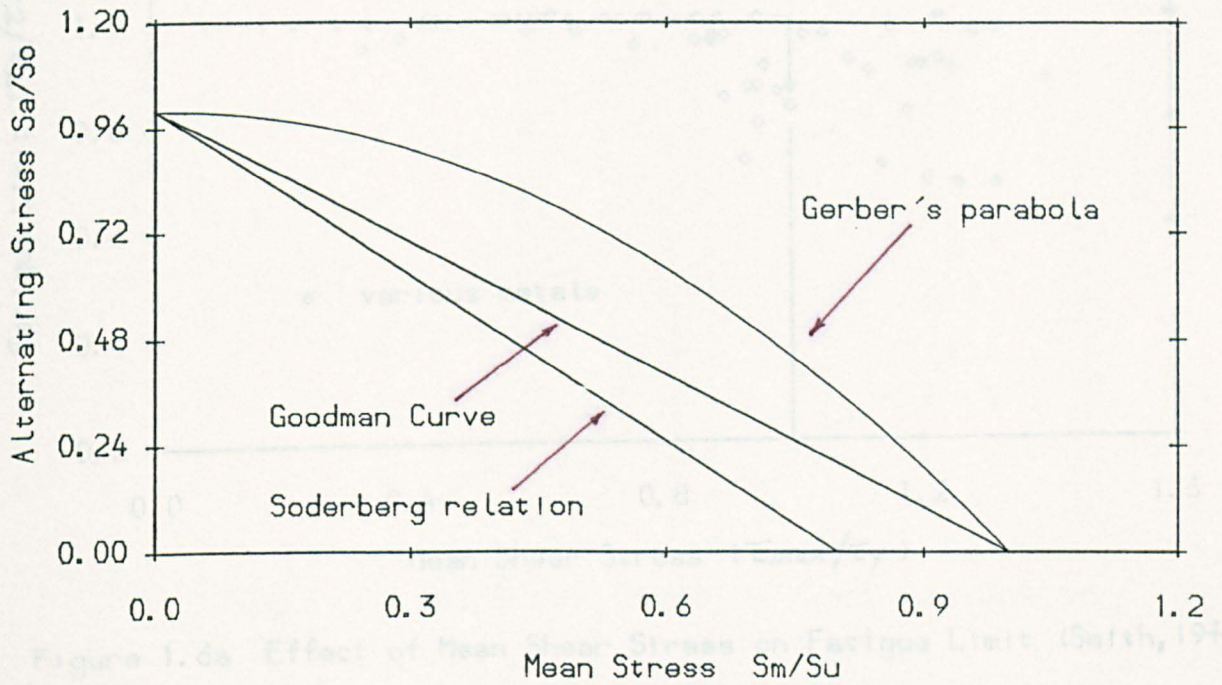


Figure 1.4 Dimensionless R--M Diagram

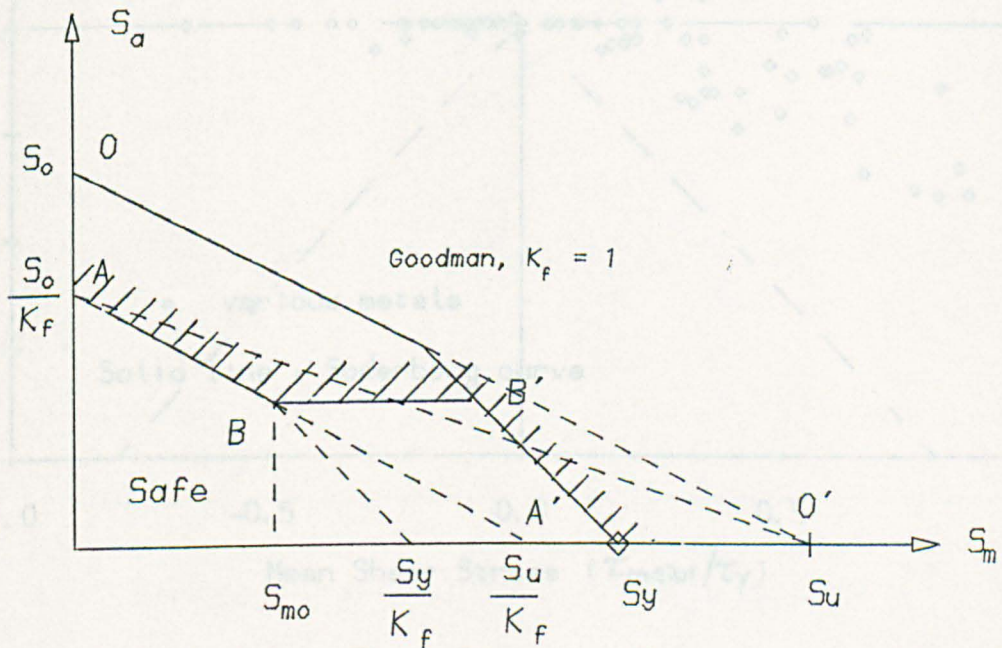


Fig.1.5 The effect of stress concentration on the Goodman diagram

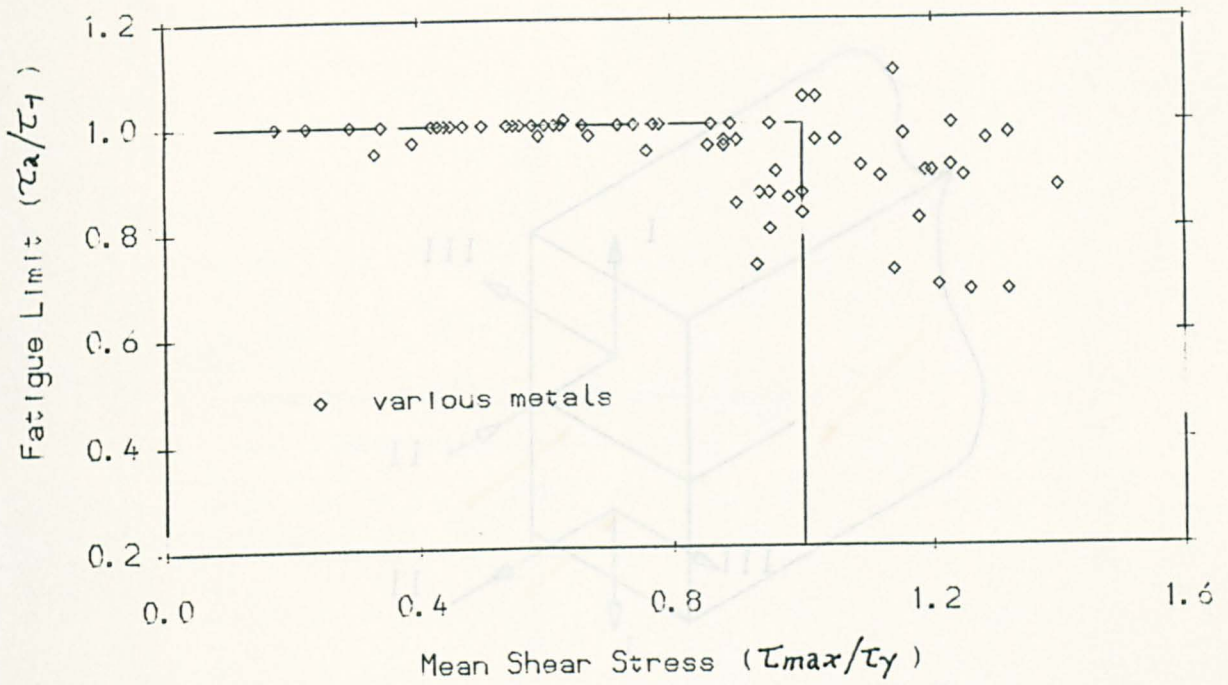


Figure 1.6a Effect of Mean Shear Stress on Fatigue Limit (Smith, 1942)

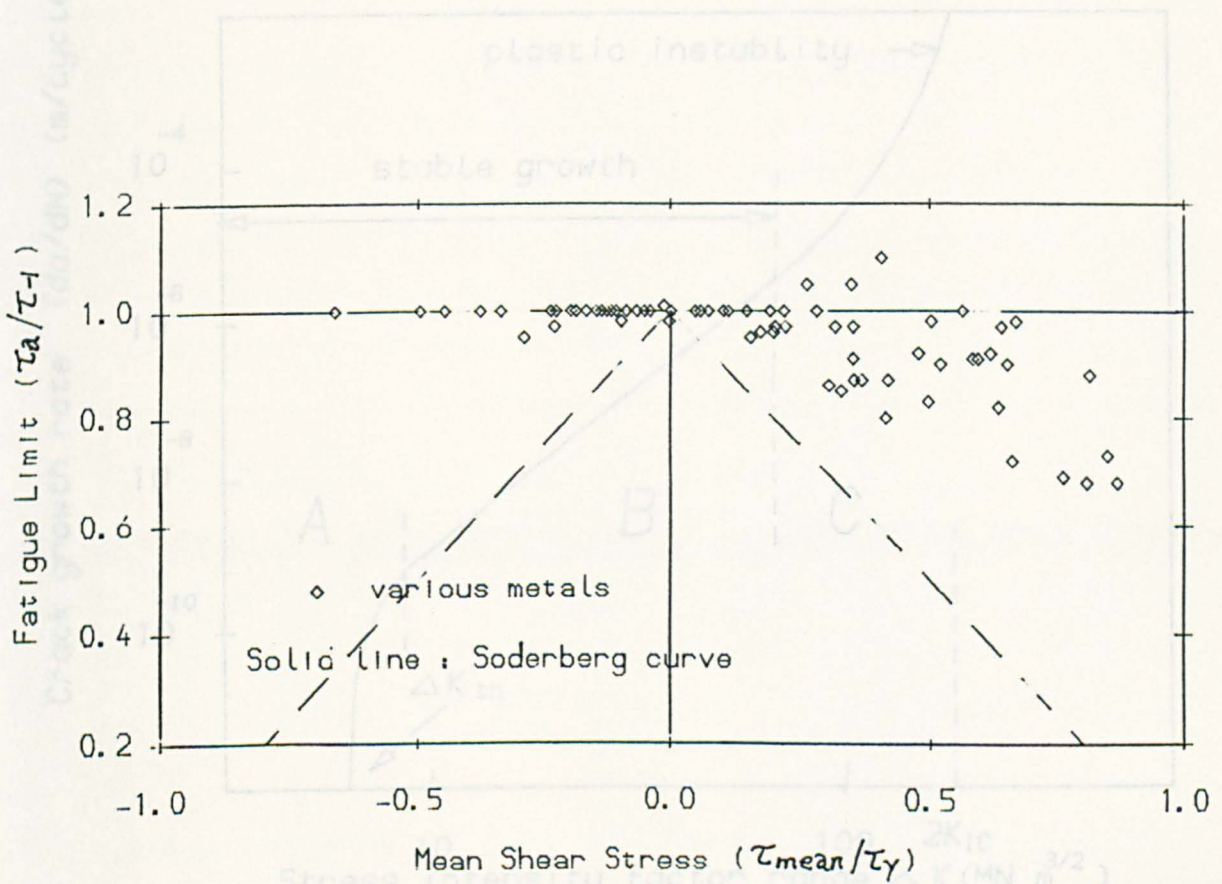


Figure 1.6b Effect of Mean Shear Stress on Fatigue Limit (dimensionless)

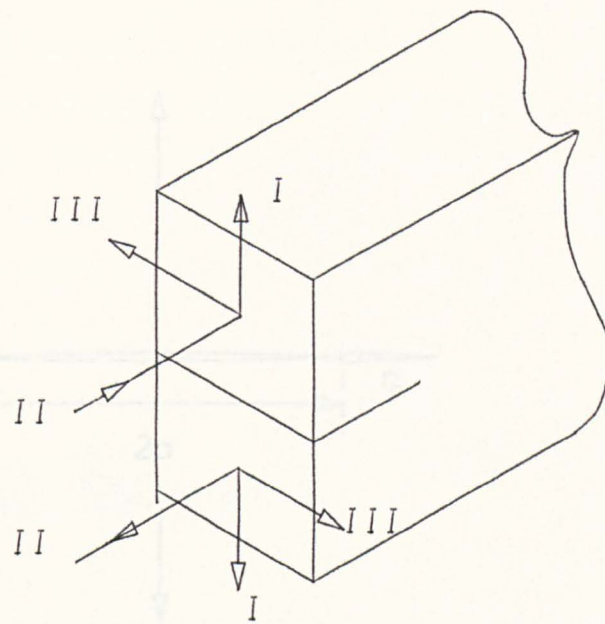


Fig.1.7 The Three Modes of Crack Extension

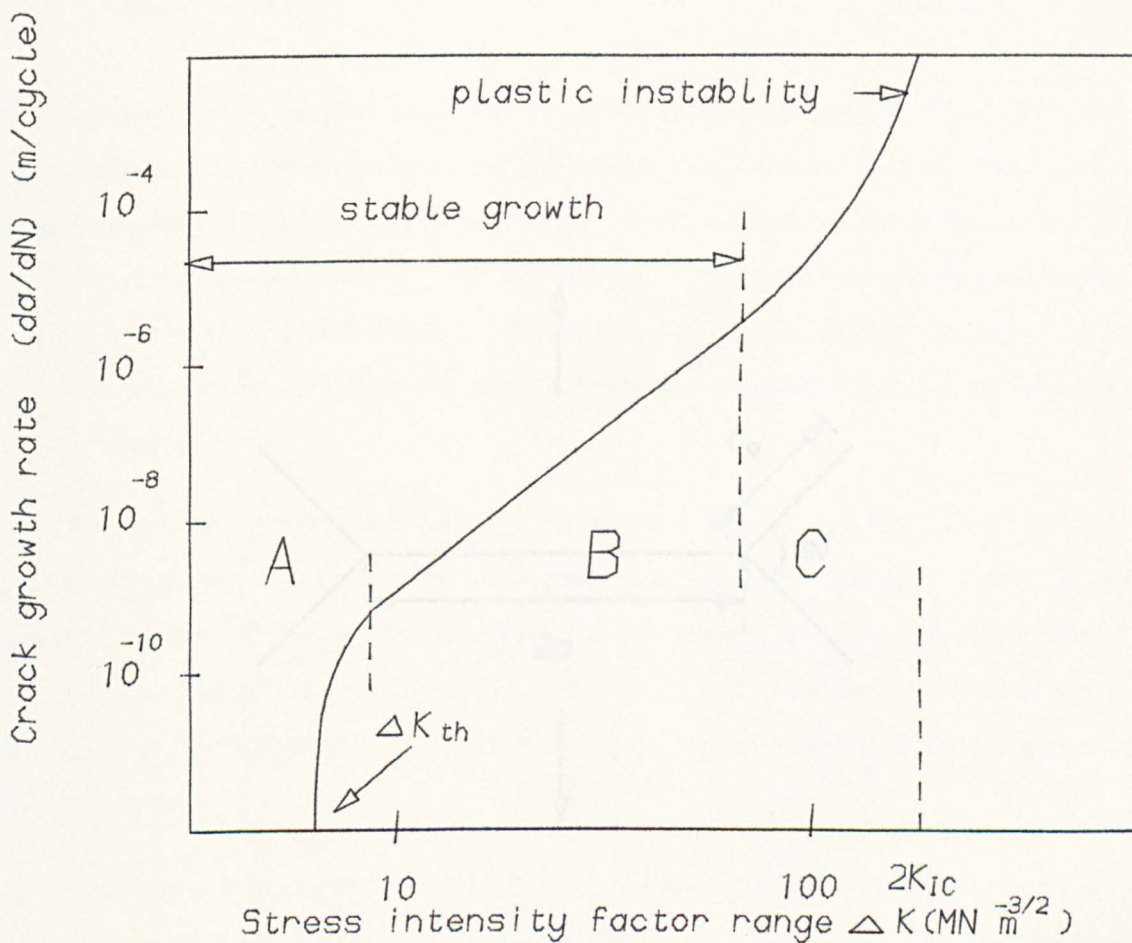
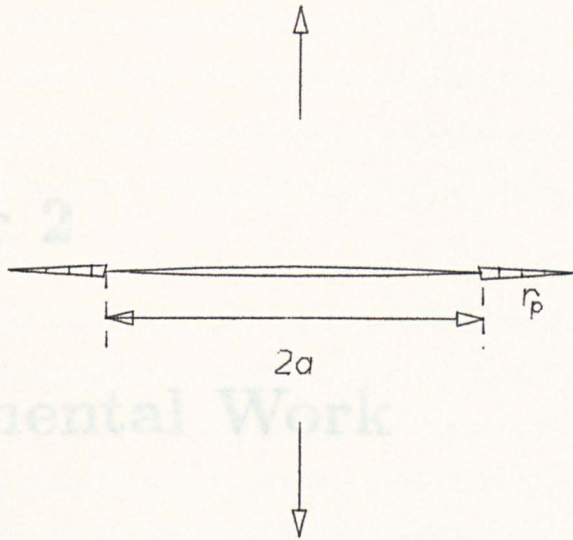


Fig.1.8 A Crack Growth Dynamics Diagram

Chapter 2

Experimental Work



(b) Dugdale-Barenblatt model

2.1 Material

A 1.29% NiCrMo rotor steel was used for all the tests in this study. The full chemical composition of the steel is shown in Table 2.1. The material is made from vacuum degassed steel, which is cast and forged, then heat treated by steam quenching from 650°C and tempered at 550°C . This procedure produces a steel with typical mechanical properties shown in Table 2.2. The material is widely used in making generator rotors and low-pressure turbine rotors. Specimens were taken from the axial direction from a forging.

The microstructure of the material, as shown in Fig. 2.2, is a tempered bainite structure. The prior austenite grain is divided into bundles, which are composed of packets which are the smallest units surrounded by high angle boundaries [1]. The average size of the prior austenite grains is $50\ \mu\text{m}$, bundles have an average size of $10\ \mu\text{m}$ and the mean value of packet size is $3\ \mu\text{m}$. The material was etched in 2% Nital solution.

Specimens were manufactured by GPC Rotors Ltd and were then given a further heat treatment of 520°C tempering for four hours to remove residual machining

(a) BCS model

Fig.1.9 Representations of a Crack with Shear Bands

Chapter 2

Experimental Work

2.1 Material

A 1.99% NiCrMo rotor steel was used for all the tests in this study. The full chemical composition of the steel is shown in Table 2.1. The material is made from vacuum degassed steel, which is cast and forged, then heat treated by steam quenching from 850°C and tempered at 590°C. This procedure produces a steel with typical mechanical properties shown in Table 2.2. The material is widely used in making generator rotors and low-pressure turbine rotors. Specimens were taken from the axial direction from a forging.

The microstructure of the material, as shown in Fig.2.1 and Fig.2.2, is a tempered bainite structure. The prior-austenite grain is divided into bundles, which are composed of packets which are the smallest units surrounded by high angle boundaries [1]. The average size of the prior-austenite grains is 50 μm , bundles have an average size of 10 μm and the mean value of packet size is 3 μm . The material was etched in 2% Nital solution.

Specimens were manufactured by GEC Rotors Ltd and were then given a further heat treatment of 590°C tempering for four hours to remove residual machining

stresses from the surface. It has been shown [Ref.2 in Chapter1] that such heat treatment does not affect the mechanical properties and microstructure. To avoid oxidation, specimens were coated with "Berkatekt" prior to the heat treatment. Some oxidization was observed and the oxidized surface layer was later removed by further polishing. Although vacuum environment is certainly preferred, it was not used due to economic reasons.

A cooling rate of less than 0.5°C per minute (furnace cooling) was used for the first eleven specimens, which are denoted by the number of the specimen being preceded by an A. Then a faster cooling rate at 10°C per minute was used for another nineteen specimens, since it was thought this would not affect the fatigue behaviour. The numbers of these nineteen specimens are preceded with B. The tempering procedures are shown in Fig.2.3. The experimental results showed that lower fatigue limit of 380 MPa was observed for the specimens which experienced a high cooling rate, in comparison to 440 MPa for the specimens cooled in the furnace (see Ref.2 in Chapter2). This reduction is possibly due to the fast cooling process producing a tensile residual stress in the specimen surface. Since the outer surface of the specimen cooled more quickly than the interior, at the time when the center of specimen was cool down, the shrinking the core would probably produce a tensile mean stress on the surface. More work is required to clarify this point. The other thirty specimens (the numbers are preceded by A) were stress relieved at lower cooling rate (less than 0.5°C). In this thesis discussions are only concerned with the material which received a furnace cooling heat treatment unless otherwise specified.

2.2 Test Facilities and Design of Grips

Three machines of different controlling systems were used for the torsion tests, the low cycle push-pull tests and the high cycle tests conducted under various mean stresses and alternating stresses.

A detailed description of the torsion machine can be found in reference [2]. This

machine monitors the maximum and minimum torques which are directly controlled by manipulating maximum and minimum deflections. The mechanical controlling system generates a sinusoidal waveform at frequencies between 0.4 and 10 Hz.

The machine used to determine the cyclic stress–strain relationship together with the low cycle fatigue tests is an electro–hydraulic servo–controlled Mayes machine with a static load capacity of ± 250 KN. Low cycle fatigue tests were conducted under load controlled mode. The gripping and extensometer arrangements are described in [3]. In this thesis the plastic strain is defined as the offset plastic strain, namely the young's modulus is taken to be the monotonic one.

An Instron Model 1603 Electro Magnetic Resonance (EMR) machine was used for high cycle fatigue at different stress ratios. The machine has a dynamic load capacity of ± 100 KN and a mean load capacity of ± 100 KN with a frequency between 100 and 300 Hz depending upon the specimen stiffness. The machine has a good accuracy in load measurement ($\pm 0.5\%$) and load control ($\pm 1\%$). A set of grips were designed, as shown in Fig.2.4, to match the Instron EMR machine and to avoid backlash under a negative stress ratio.

2.3 Specimen Design and Preparation

An hour–glass shaped specimen was chosen for the test programme. This design satisfies the requirement that the area of crack growth is limited to the central region of the specimen, thus restricting the area needed to be replicated. Moreover, the mild hour glass profile allows a superposition of compressive mean stress without causing buckling.

Specimens (A type, furnace cooled), as shown in Fig.2.5(a), were successfully used in torsion tests. However, three specimens (type B, cooled at a higher cooling rate) failed at the heads under push-pull loading condition. Subsequent examination of the failure surfaces, as shown in Fig.2.6, showed that cracks were initiated from the shoulder and propagated across the specimen causing the failure. Clearly the stress

concentration at the root of the shoulder is too high and the high yield strength of material does not allow this stress concentration to be relaxed as what would occur for a low yield stress carbon steel [3]. Hence the specimen was modified by increasing the root radius from 1 mm to 3 mm, and reducing the minimum radius of the specimen cross-section from 8 mm to 7.3 mm, as shown in Fig.2.5(b). The specimens used to determine the cyclic deformation response, as shown in Fig.2.5(c), were obtained as a result of modification of the original specimen. The strain ranges are thus limited by the shape of the specimen to avoid buckling. High strain amplitude tests were carried out on hour glass-shaped specimens.

After the heat treatment, the specimens were polished using a mechanical polishing method which involved using progressively finer grid paper and diamond polishing liquid alternatively in longitudinal and circumferential directions. In this way it is possible to remove the scratches from the previous stage. Finally, the specimens were polished until the surface roughness was $0.5\mu\text{m}$. A 2% Nital solution was used for etching for half minute at the ambient temperature to reveal the microstructure. Etching made it easier to locate cracks on replicas and to examine the effect of microstructure on short crack growth.

2.4 Experimental Techniques

2.4.1 Torsion tests

The details of the torsion testing rig have been described by Zachariah and Miller [2]. Two basic recordings were made, torque and relative twist. The first was provided through a load cell previously calibrated statically with deadweight loads on a lever arm. The second recording was made via transducers (LVTDs) and cams fixed to the specimen over a gauge length of 20mm. The two LVTD–cam combinations were calibrated by using a rig which could be fitted to the machine which provided a small definite angle.

A data logging device was used to display and record the maximum, minimum, and mean values of torque and twist angle. In the tests, the maximum and minimum torque values displayed by the data logging device were used to adjust the combination of maximum and minimum deflections while the test was running to maintain the stress-controlled condition (see next paragraph). The torque–twist curves were also recorded by an $X - Y$ plotter and from these graphs the stresses and strains were calculated.

It is difficult to achieve a stress controlled condition under torsional loading, as there is no practical method to monitor the surface stresses under unsymmetrical cyclic loading without any contact with the specimen surface such as by the use of strain gauges. Therefore a simplified method was developed in the present work, in which the modified Nadai's theory due to Brown and Carbonell [5] was taken as a starting point.

The maximum shear stress on the outer surface of the specimen can be obtained by Nadai's theory [4]. This theory has been modified to give the cyclic stress and strain distribution of an hour-glass shaped specimen under fully reversed loading [5]. For a torque-controlled test (A5) whose torque-twist curve is shown in Fig.2.7, the maximum stress and minimum stress at the outer surface can be obtained from the modified Nadai's theory as follows,

$$\tau_{max}^{(1)} = \frac{3 + n_1}{2\pi r_0^3} T_{max} \quad (2.1)$$

$$\tau_{min}^{(2)} = \tau_{max}^{(1)} - \frac{3 + n_2}{2\pi r_0^3} \Delta T = \frac{3 + n_1}{2\pi r_0^3} T_{max} - \frac{3 + n_2}{2\pi r_0^3} \Delta T \quad (2.2)$$

$$\tau_{max}^{(3)} = \tau_{min}^{(2)} + \frac{3 + n_3}{2\pi r_0^3} \Delta T = \tau_{max}^{(1)} - \frac{3 + n_2}{2\pi r_0^3} \Delta T + \frac{3 + n_3}{2\pi r_0^3} \Delta T \quad (2.3)$$

where n_1, n_2, n_3 are the slopes of the $\log T$.vs. $\log \theta$ at points 1, 2, and 3, T is the torque, and r_0 is the minimum radius of the specimen cross-section.

If the maximum and minimum torques are kept constant through the test, the change of the maximum shear stress from second cycle to k cycle is $\tau_{max}^{(2k-1)} - \tau_{max}^{(3)}$

which equals

$$\begin{aligned}
\delta\tau_{max} &= \tau_{max}^{(2k-1)} - \tau_{max}^{(3)} \\
&= \sum_{i=2}^{k-1} \frac{n_{2i+1} - n_{2i}}{2\pi r_0^3} \Delta T \\
&= -\sum_{i=3}^{k-1} \frac{n_{2i} - n_{2i-1}}{2\pi r_0^3} \Delta T + \frac{n_{2k-1} - n_4}{2\pi r_0^3} \Delta T \\
&\approx -\delta\tau_{max} + \frac{n_{2k-1} - n_4}{2\pi r_0^3} \Delta T
\end{aligned} \tag{2.4}$$

therefore

$$\delta\tau_{max} = \frac{1}{2} \frac{n_{2k-1} - n_4}{2\pi r_0^3} \Delta T \tag{2.5}$$

where $n_1, n_2, \dots, n_{2k-1}$ are the slope of the $\log T$.vs. $\log \theta$ at the points $1, 2, \dots, 2k-1$ ($n_1 < n_2 < \dots < n_{2k-1}$).

From the recorded data, it can be seen that the $T - \theta$ curves are stabilized (the shape) after only a few cycles. The difference between n_4 and n_{2k-1} is negligible when compared with $3 + n_1$. Therefore the change of the maximum shear stress during a torque- controlled test can be neglected, and so can the change of the minimum shear stress. Therefore the maximum and minimum shear stress are given by Eq.2.3 and Eq.2.2.

Cyclic creep strain per cycle depends on the stress range and the mean stress [6] [7]. Since the stress range was constant during the tests, the constancy of the measured creep strain per cycle ($\gamma_{p,1}^{cc}, \gamma_{p,2}^{cc}, \gamma_{p,3}^{cc}$ and $\gamma_{p,4}^{cc}$ as shown in the following equation are roughly equal to each other) indicated that the mean stress was not relaxed, which is in agreement with the above calculation. The characteristic values obtained for each of the eleven tests are presented in Table 2.3, in which γ_p^{cc} was taken as the average of four values calculated from the recorded torque–twist curves, i.e.

$$\begin{aligned}
\gamma_p^{cc} &= \frac{1}{4}(\gamma_{p,1}^{cc} + \gamma_{p,2}^{cc} + \gamma_{p,3}^{cc} + \gamma_{p,4}^{cc}) \\
&= \frac{1}{4} \left\{ \frac{(\Theta_2 - \Theta_1)L}{(N_2 - N_1)r_0} + \frac{(\Theta_3 - \Theta_2)L}{(N_3 - N_2)r_0} + \frac{(\Theta_4 - \Theta_3)L}{(N_4 - N_3)r_0} + \frac{(\Theta_5 - \Theta_4)L}{(N_5 - N_4)r_0} \right\} \tag{2.6}
\end{aligned}$$

where for simplicity, the specimen is approximately considered as a cylindrical bar. Terms $\Theta_1, \Theta_2, \Theta_3, \Theta_4,$ and Θ_5 are the maximum twist angle for $N_1, N_2, N_3, N_4,$ and N_5 and L is the gauge length.

2.4.2 Tensile tests

All low cycle and high cycle tests were carried out under load-controlled conditions to enable comparison and correlation on the basis of stress. For unsymmetrical loading, tests should be conducted under stress-controlled conditions in order to avoid possible relaxation of mean stress. However, it is known that dynamic creep or ratcheting can occur in the case of load-controlled unsymmetrical loading. One example is shown in Fig.2.8. The mean stress as well as the stress amplitude are constant. Under these conditions both the strain amplitude (ϵ_a) and the mean strain (ϵ_m) change constantly. Whether ratcheting ceases after a number of loading cycles or continues to the final failure depends on the material, stress amplitude, mean stress and temperature. Two kinds of failures can occur depending on the degree of ratcheting, they are dynamic creep failure and fatigue failure.

A substantial part of the dynamic creep can be approximated by the relation [8],

$$\epsilon_N = \epsilon_0 + C_1(N - 1) \quad (2.7)$$

where ϵ_0 is the deformation in the first half cycle, $C_1 = \left[\frac{d\epsilon_N}{dN} / f \right]$ which is a function of stress amplitude and mean stress level, $\frac{d\epsilon_N}{dN}$ is the dynamic creep rate, and f is frequency of the cycling. Thus if the total strain due to dynamic creep is lower than $(\epsilon_{pn})_{cyc}$ (it is suggested that $(\epsilon_{pn})_{cyc} = \epsilon_{pn}$ where ϵ_{pn} is the plastic instability strain, see reference [9]) then the prevailing mechanism is one of fatigue. Otherwise ratcheting dominates the failure process.

Therefore, ratcheting must be avoided in order to permit a study on the effects of mean stress on fatigue crack growth and fatigue tests should be within the high cycle fatigue regime. Moreover, for high mean stress levels, for example when σ_{max} approaches σ_u , special care needs to be taken to prevent high ϵ_N value. From Eq.2.7, it can be seen that ϵ_0 plays a significant role at low stress amplitude (C_1 decreases with the reduction of stress amplitude and increases with the increase of mean stress). There are two loading paths to reach σ_{max} . First, the maximum stress level is applied in the first half cycle. Secondly, the maximum stress level is increased from a low level to the required level within some cycles. Fig.2.9 shows these two

different loading paths. As cracks are initiated after many cycles, e.g. for all the fatigue tests with lives of more than one hundred thousand cycles, no cracks were detected after five thousands cycles. This means that the effect of early loading history can be neglected. One test (No.A39) showed a ratcheting failure when cycled at $\sigma_a = 280$ MPa, $\sigma_m = 504$ MPa following a loading path very close to case one (the mean stress was preset at 504 MPa on the EMR Instron machine, and the amplitude was increased rapidly from zero to the required level 280 MPa within about 80 cycles). Therefore other high mean stress tests were conducted following the second path (e.g. No.A57 and No.A58 which were cycled at the same stress range and mean stress level failed at $N_f = 9.23 \times 10^5$ and $N_f = 3.73 \times 10^5$).

The change in diameter of these specimens was measured later, the reduction was less than 0.25 %, which shows that the upper limit of the axial dynamic creep strain ϵ_p^{dc} ,

$$\epsilon_p^{dc} \leq \frac{-0.25}{-\mu} = 0.8 \quad \text{in percentage terms} \quad (2.8)$$

The cyclic creep strain per cycle (see Section 2.4.1) can also be calculated,

$$\epsilon_p^{cc} \leq \frac{0.8 \times 10^{-2}}{N_f} = 9.3 \times 10^{-9} \quad (2.9)$$

Therefore the effects of creep straining on crack growth can be neglected.

2.4.3 Crack detection

A replica technique was used to monitor crack growth behaviour. In spite of the associated disadvantages such as rest periods being introduced, the crack depth cannot be measured and automation is very difficult, the method has been widely used in short crack growth studies, for example see references [3] [10]. This is due to the fact that commonly used techniques, e.g. potential drop (D.C. or A.C. currents), ultrasonics and direct microscopical observations, are not suitable for the measurement of very short cracks.

Various types of replicating materials with suitable solvents are available. For the plain specimen case, acetate sheet with acetone solvent has proved to be the most

successful type due to its high resolution capability. In the present study, a thin sheet of replicating material with a thickness of 0.1 *mm* was used. This was found to give the most faithful reproduction of the specimen surface. Also, the thin material, after being attached to a microscope slide, allowed a shallow focus depth and a high magnification mode of observation in a microscope.

A sheet of replicating material was cut into small pieces of about 12 *mm* in width and 20 *mm* in length. Acetone was sprayed onto the specimen surface and also onto one side of the replica. The strip was then quickly held against the specimen and surface tension drew the replica onto the surface. After a couple of minutes the replica became dry and was removed with the aid of a small piece of cello tape and a pair of tweezers. Finally the replica was attached to a microscope slide by adhesive tape. Replicas were later examined under an optical microscope with image processing facilities to measure crack length.

Since more than one crack were initiated and propagated in a specimen, replicas were taken for at least twelve stages of the lifetime. Some cracks were initiated at a very late stage. Replications were made at regular evenly spaced intervals through the lifetime in order to monitor the crack growth rates.

To help with the relocation of replicas and cracks, six etch marks were placed on the specimen surface equi-distributed along two circumferences some 6 *mm* away from the minimum section of the specimen. These marks were produced by etching the specimen more deeply at those particular points. Being reproduced on the replicas, these marks greatly helped in finding a particular crack over a range of replicas. For cracks at their very early stages of development, extreme difficulties were encountered in locating them on replicas due primarily to their extreme shortness. A local coordinate was established with reference to a certain etch mark which made it easier to locate such cracks. As these marks were not made at the minimum section, cracks did not often grow from these marks. In effect, only one out of a total of three hundred cracks initiated from an etch mark.

Another technique used to help the location of cracks on replicas was that replicas

taken during the last stages of a test were examined first. Cracks were long in these stages and easy to find. Then observations and measurements were made on replicas at these precise positions at the immediately previous stage.

Attempts were made to take replicas while the test was running. Because the surface deformation was small, replicas could be made. However, cracks and their immediate proximity were found smeared when being observed under a microscope. It is postulated that this effect was due to the relative closing and opening of cracks during cycling. The closing of cracks could drive out the acetone from a crack and opening could suck the acetone back into the crack. Such movements would result in local damage to the replicas.

Fatigue tests, therefore, were stopped to take replicas. In the present study, replicas were taken at different tensile and compressive load levels. It was found that an extra tensile load was not necessary to open the crack during replication. Cracks could be observed at any load level, hence most of the replications were carried out at the mean load level although cracks would be more clearly reproduced on replicas if a tensile load was used to further open the crack.

The observation of replicas obtained with various stress levels in one cycle showed that cracks did close and open during a loading cycle (on replicas cracks showed a different contrast to the surrounding material). However, due to the limit on the accuracy of the reproduction of specimen surface and that replicas can only record the crack profile along the surface, quantitative measurements of the crack tip opening displacement and a precise determination of the opening stress level were not possible.

Most specimens were slightly etched using 2% Nital solution to facilitate the location of cracks and to determine the effects of microstructure on crack growth behaviour. Tests on unetched specimens were also carried out to study the effect of etching. The results showed that etching had no effect on the fatigue limit and crack growth, probably due the fact that etching only produced a surface roughness of 2 μm . Experimental results indicated that the major barrier to short crack growth is packet bundle boundaries and prior austenite grain boundaries. This will be discussed

later.

2.5 Test Programme

The test programme consisted of the following three series for studying the effects of mean shear stress and normal mean stress on short crack growth:

Series 1: Mean Stress Effects in Torsion Tests

Eleven specimens (A type) were tested in torsion under various mean and alternating shear stress levels under load control to study the effects of mean shear stress on the fatigue strength of the material and stages I and II crack growth.

The effect of mean shear stress is important primarily because the early fatigue life, including the crack initiation event, is dominated by shear strains developed in material slip systems and can produce a Stage I crack. At the fatigue limit stress level which separates propagating cracks from non-propagating cracks, the fatigue lifetime of a material can be determined by the behaviour of a short Stage I crack and whether it can change to a stage II crack. Apparently mean stress could affect the transition and also the short crack growth rate.

The fatigue lives ranged from ten thousand (10^4) cycles to over a million (10^6) cycles. Tests were conducted at different stress ratios ($R = -1, -0.867, -0.697, -0.555, -0.514, -0.418$) with a sinusoidal loading waveform of frequencies between 1 Hz and 3 Hz. For each test the load (torque) was monitored by means of a data-logger and this reading was then used to control the deflections in order to maintain the loads. Hysteresis loops (torque-twist curves) were also recorded at frequent intervals during the tests by an $X - Y$ plotter.

Tests were either stopped when surface cracks were longer than three millimetres (so as to protect the fracture surfaces), or continued until total fracture.

Series 2: Fully Reversed Uniaxial Tests

One load-controlled test and two strain-controlled tests were conducted on cylindrical bar specimens to obtain the cyclic stress-strain relationship.

Seven fully reversed low and high cycle uniaxial fatigue tests were carried out under load control at low frequency to obtain fatigue crack growth and fatigue lifetime data. The fatigue life ranged from a few thousands (10^3) cycles to over a million (10^6) cycles. Testing frequencies for low cycle fatigue were from 0.5 Hz–0.3Hz and the frequencies for high cycle tests were from 3 Hz to 150 Hz. High testing frequency was used to reduce testing time and, in addition, the frequency of the resonant machine cannot be adjusted.

Tests were interrupted periodically to enable plastic replication of the specimen surface. At least two tests with one stress state were carried out to enable a number of cracks to be studied for each state.

Series 3: Variable Mean and Alternating Stress Uniaxial Tests

Twenty one type A and thirteen type B specimens were tested under different combinations of stress range and mean stress level (at high frequency). Fatigue lives were all over 10^5 cycles. Stress ratio R was from -1.8 to 0.25 . Most tests were conducted on the Instron machine at a constant frequency of about 150 Hz.

To investigate the effects of testing frequencies on short crack growth behaviour, two fully reversed high cycle fatigue tests were carried out on a Mayes machine at a frequency of 2 Hz and four tests were conducted on the Instron machine at a frequency of 150 Hz. Very little effect was found, $N_f = 1.3 \times 10^5$, 1.45×10^5 cycles at $f = 2$ Hz and $N_f = 2.35 \times 10^5$, 2.20×10^5 , 2.02×10^5 and 3.0×10^5 cycles at $f = 150$ Hz. Such effects are possibly due to cracks being open for a longer time at low frequencies compared to high frequencies. As a result, cracks showed a higher growth rate under low testing frequency [11].

Results of the test programme and analyses are presented in Chapter 3 and Chapter 4.

References

1. Kotilainen, H. (1982) On the Cleavage Fracture Strength of Bainite Microstructure, *Fracture and the Role of Microstructure, Vol.1* , Proceedings of the 4th European Conference on Fracture held in Leoben, Austria.
2. Zachariah, K. P. and Miller, K. J. (1974) Fatigue Testing Rig, *Engineering* 214, pp.563–565.
3. Hobson, P. D. (1985) Short Crack Growth in Carbon Steel, *Ph.D Thesis*. University of Sheffield.
4. Nadai, A. (1956) *Theory of Flow and Fracture of Solids, Vol. 1, Ch. 21*, 2nd edition (McGraw-Hill Book Co.,New York).
5. Carbonell, E. P. and Brown, M. W. (1986) A Study of Short Crack Growth in Torsional Low Cycle Fatigue for a Medium Carbon Steel, *Fatigue & Fracture of Engineering Materials and Structures, Vol.9, No.1*, pp. 15–33.
6. Oldroyd, P. W. and Radon, J. C. (1979) Reversal of Cyclic Creep in Mild Steel and Copper, *Fatigue of Engineering Materials and Structures, Vol.1*, pp. 297–306.
7. Pilo, D., Reik, W., Mayr, P. and Machrauch, E. (1979) Cyclic Induced Creep of a Plain Carbon Steel at Room Temperature, *Fatigue of Engineering Materials and Structures, Vol. 1*, pp. 287–295.
8. Klesnil, M. and Lukas, P. (1980) *Fatigue of Metallic Materials*, Elsevier Scientific Publishing Company.
9. Feltner, C. E. (1963) *Acta Metallurgica, Vol.11*, pp.803.
10. Lankford, J. and Barbee, J. G. (1974) SEM Characterization of Fatigue Crack Tip Deformation in Stainless Steel Using a Positive Replica Technique, *Journal of Material Science, Vol.9*, pp.1096–1908.
11. Miller, K. J. (1970) *Ph.D thesis*, London University.

Table 2.1: Chemical Composition (% Wt) (Reminder Ferrite)

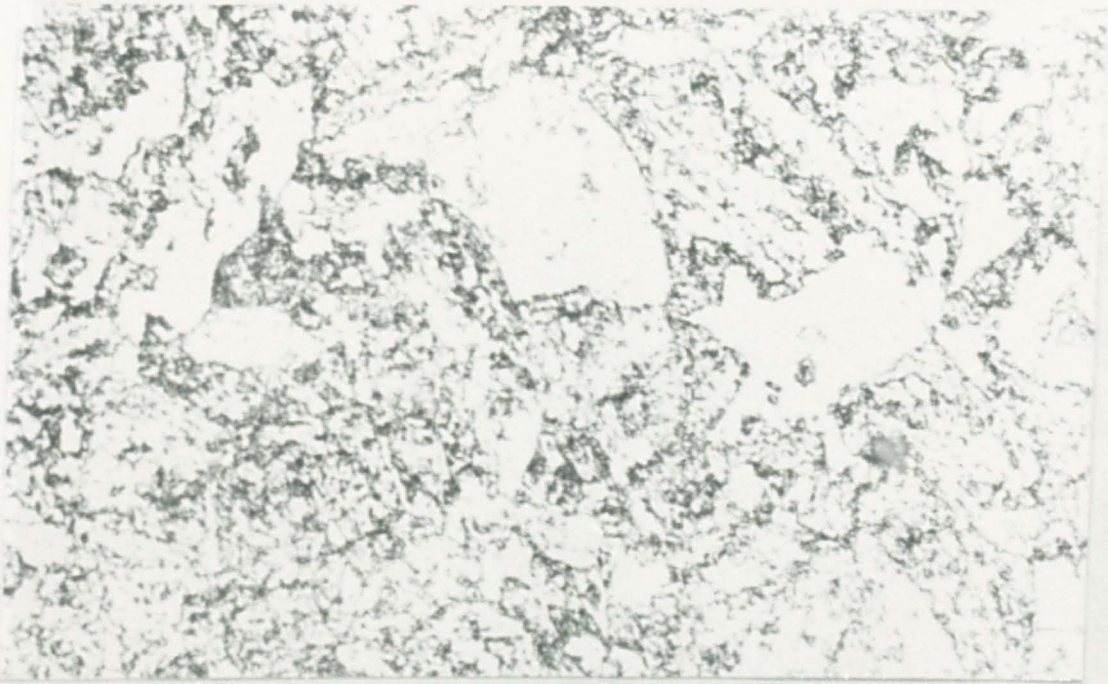
C	Si	Mn	S	P	Ni	Cr	Mo	V
0.29	0.21	0.55	0.01	0.005	1.99	1.3	0.57	0.09

Table 2.2: Mechanical Properties

Yield Strength (0.2 proof stress) (MPa)	Ultimate Tensile Strength (MPa)	Hardness	Elongation ϵ_f	Reduction in Area (%)
710	840	280 HV	18.3	63

Table 2.3: Torsion Test Results

Test No.	Minimum radius (mm)	ΔT (N·m)	$\Delta \tau$ (MPa)	τ_m (MPa)	$\Delta \gamma_t$ (%)	$\Delta \gamma_p$ (%)	γ_p^{cc}	N_f cycles
A1	3.96	56.7	576	-79	0.728	0.020	1.70×10^{-8}	196500
A2	3.96	65.2	586	+118	0.774	0.053	3.03×10^{-7}	43787
A3	3.97	55.3	560	+52	0.704	0.015	1.52×10^{-9}	530000
A4	3.95	54.7	556	+84	0.704	0.020	4.30×10^{-9}	255150
A5	3.94	55.1	574	+90	0.732	0.026	2.06×10^{-8}	171902
A6	3.95	54.7	560	-112	0.721	0.033	1.40×10^{-7}	126792
A7	3.95	55.1	568	+116	0.732	0.034	3.52×10^{-7}	134600
A8	3.95	54.7	560	0.0	0.696	0.006	0	1200000
A9	3.94	54.7	560	+20	0.709	0.008	1.21×10^{-10}	900000
A10	3.94	54.9	563	0.0	0.700	0.008	0	1080000
A11	3.96	67.7	660	0.0	0.827	0.060	0	84529



—
10 μm

Fig.2.1 Microstructure in Axial Direction



—
10 μm

Fig:2.2 Microstructure in Radial Direction

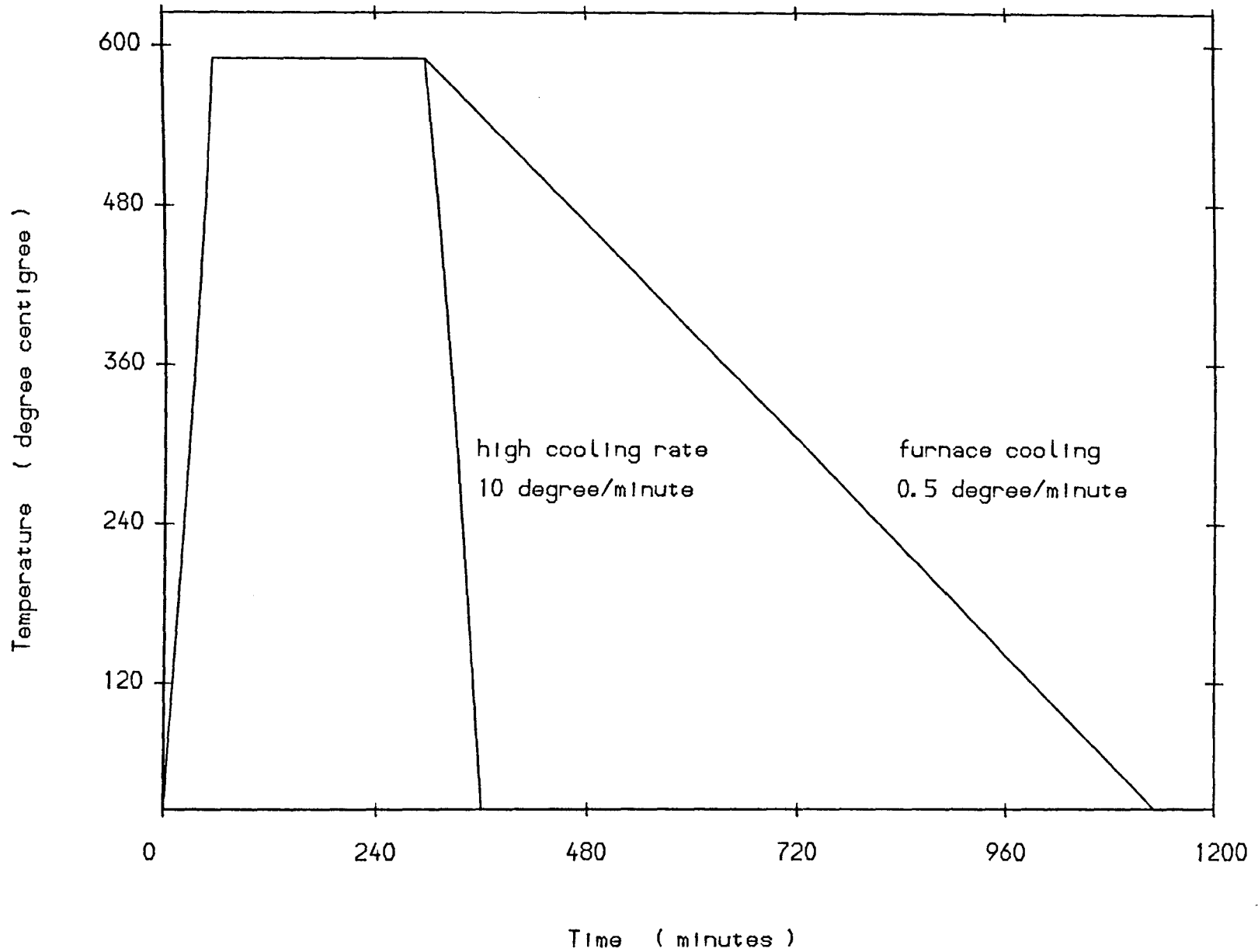
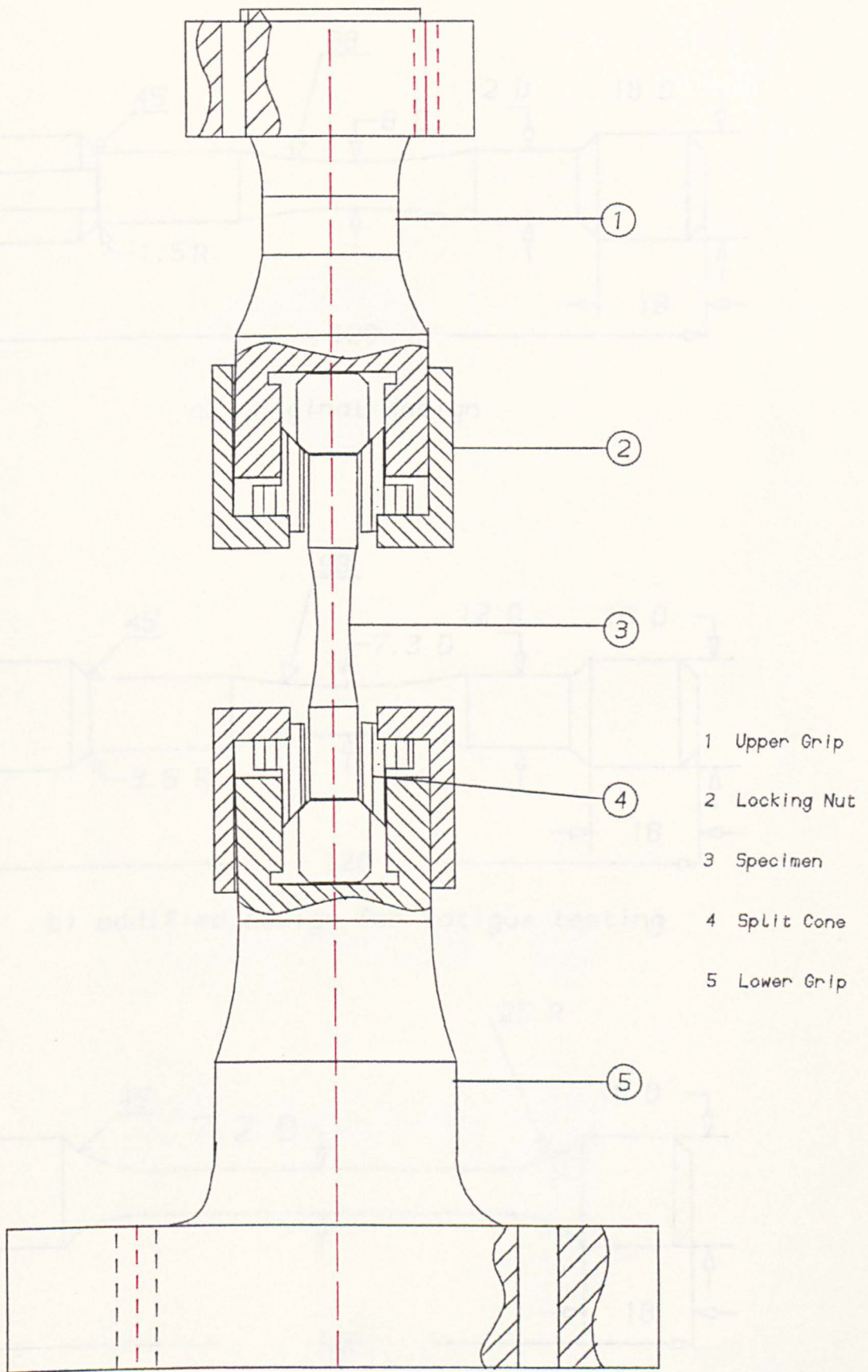
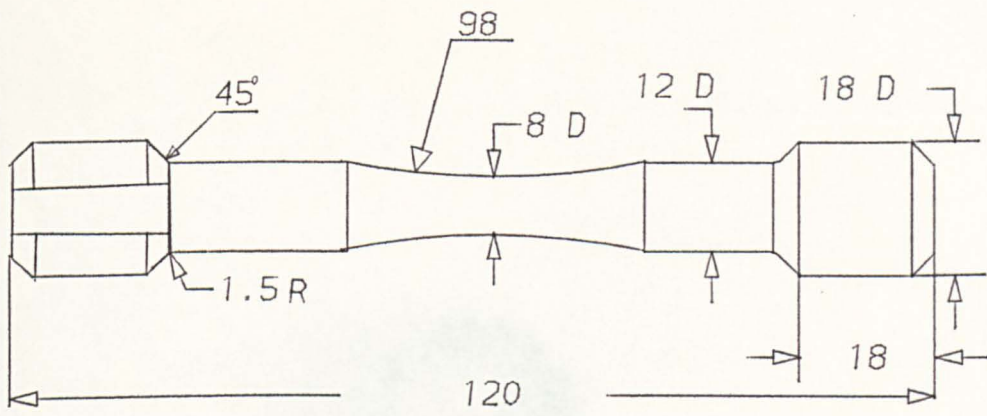


Fig. 2.3 Tempering Heat Treatment Procedure

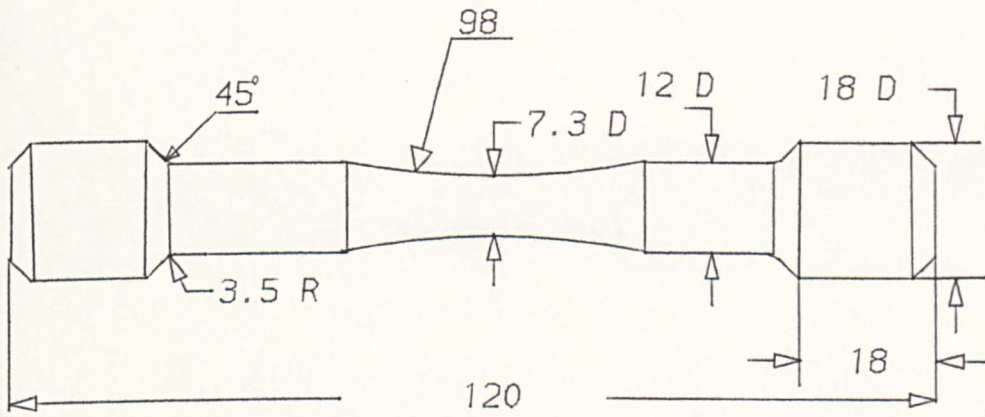


Scale 1:1.5

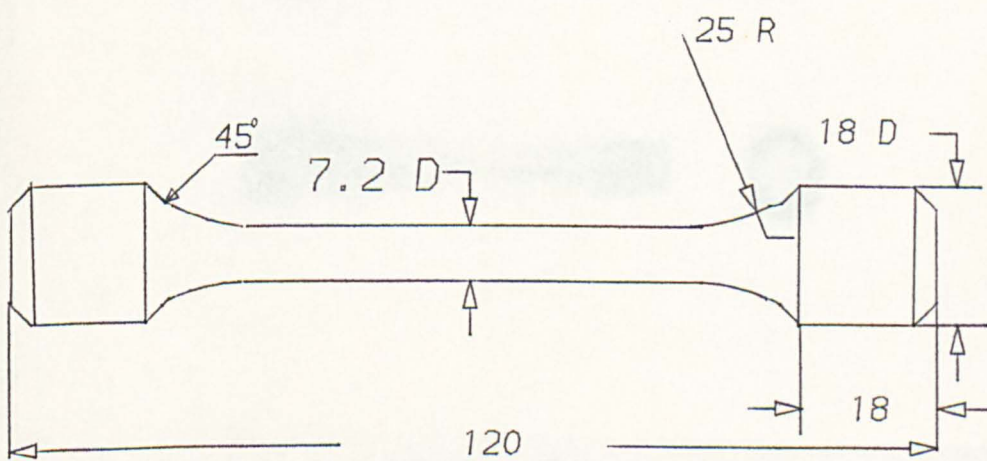
Fig.2.4 Design of Grips (for Instron machine)



a) original design



b) modified design for fatigue testing



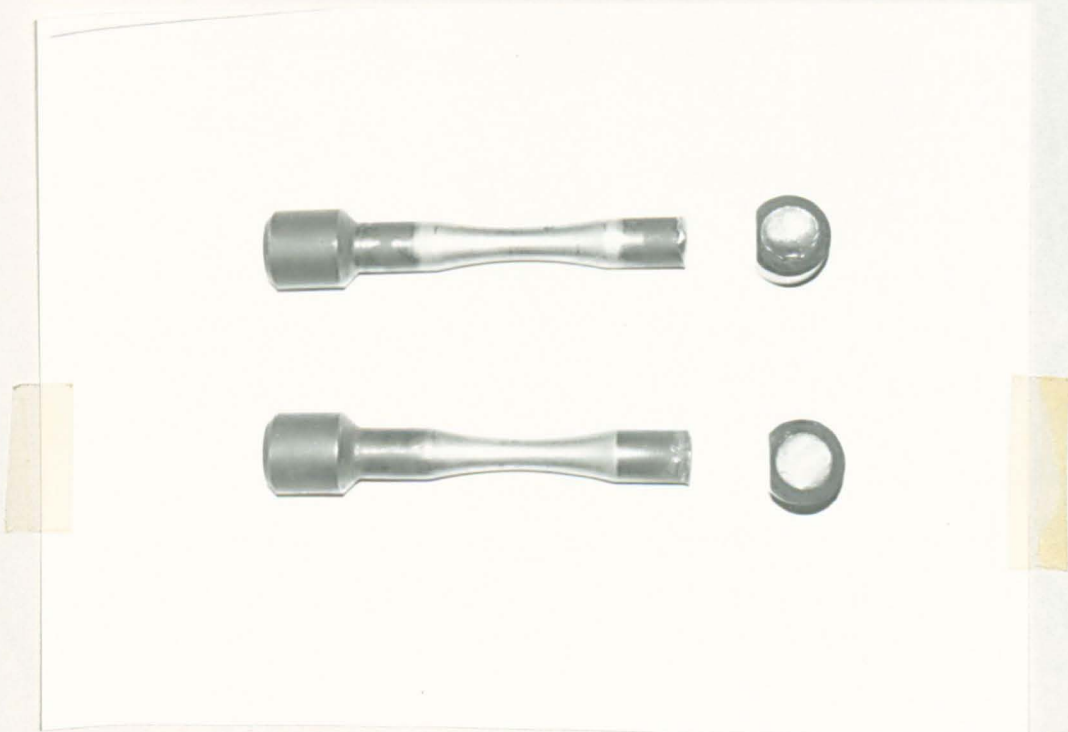
c) specimen for cyclic stress-strain tests

Fig.2.5 Design of Specimens



(a) Close-up (1.72 \times)

5 mm



(b) specimens (0.64 \times)

15 mm

Figure 2.6 Photograph of the Failures at Head

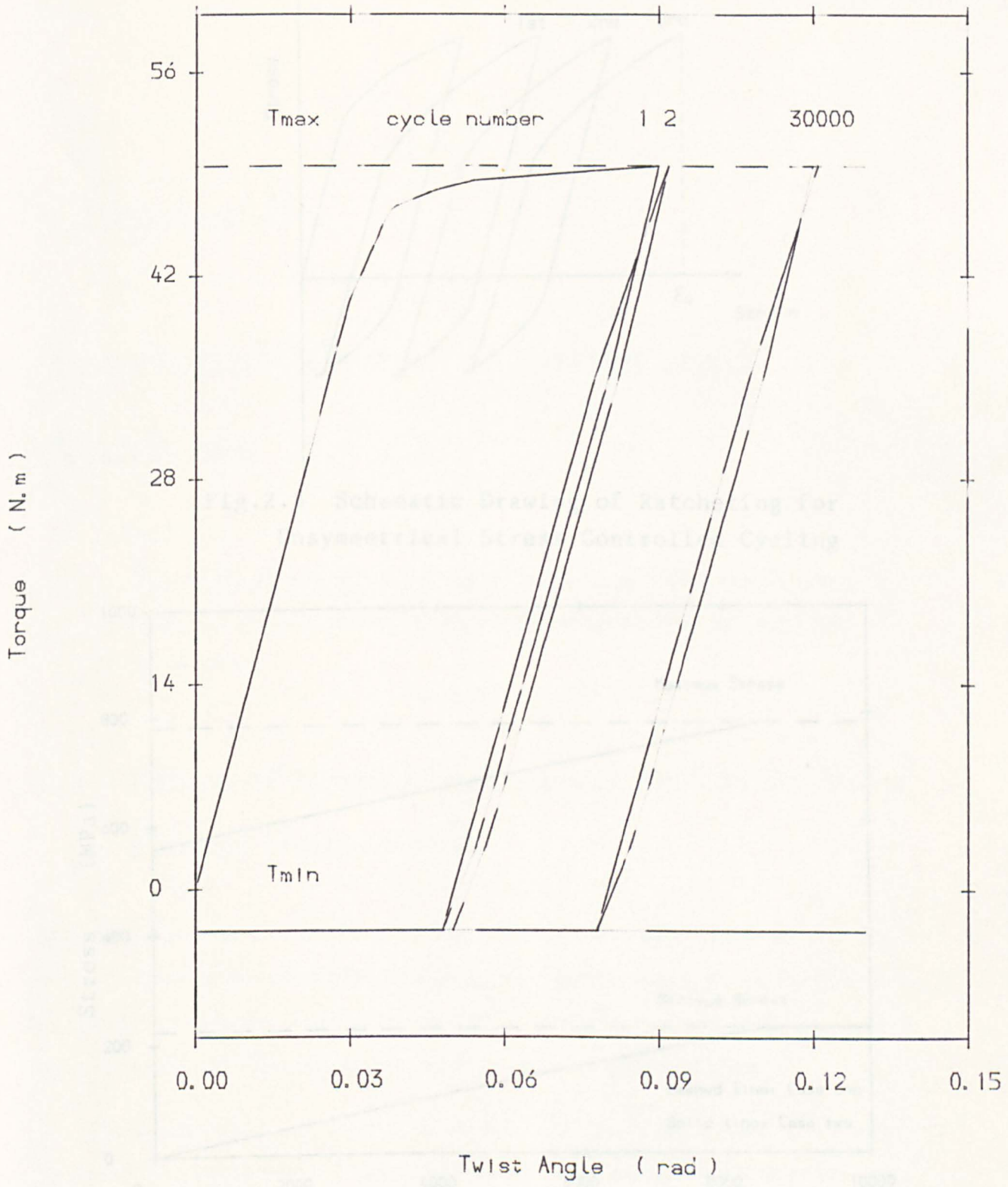


Figure 2.7 Recorded Torque-Twist Angle Curve

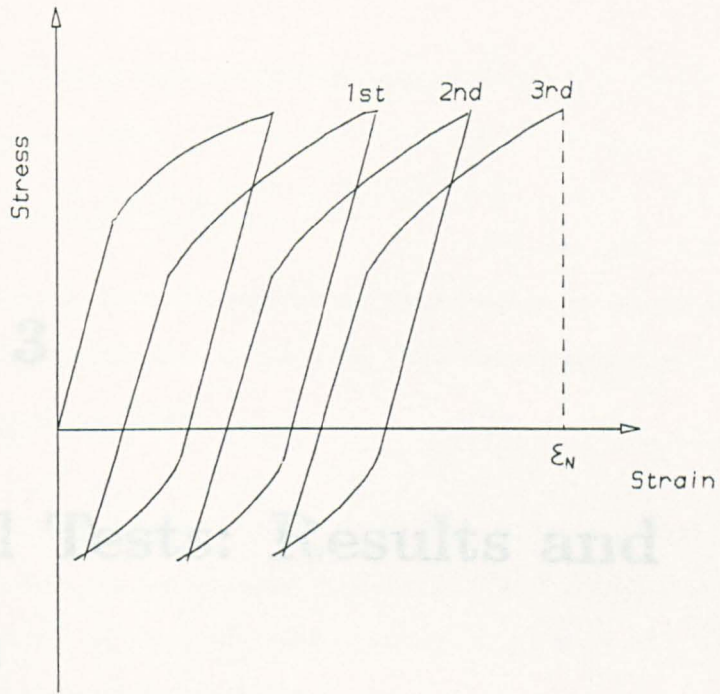


Fig.2.8 Schematic Drawing of Ratcheting for Unsymmetrical Stress-Controlled Cycling

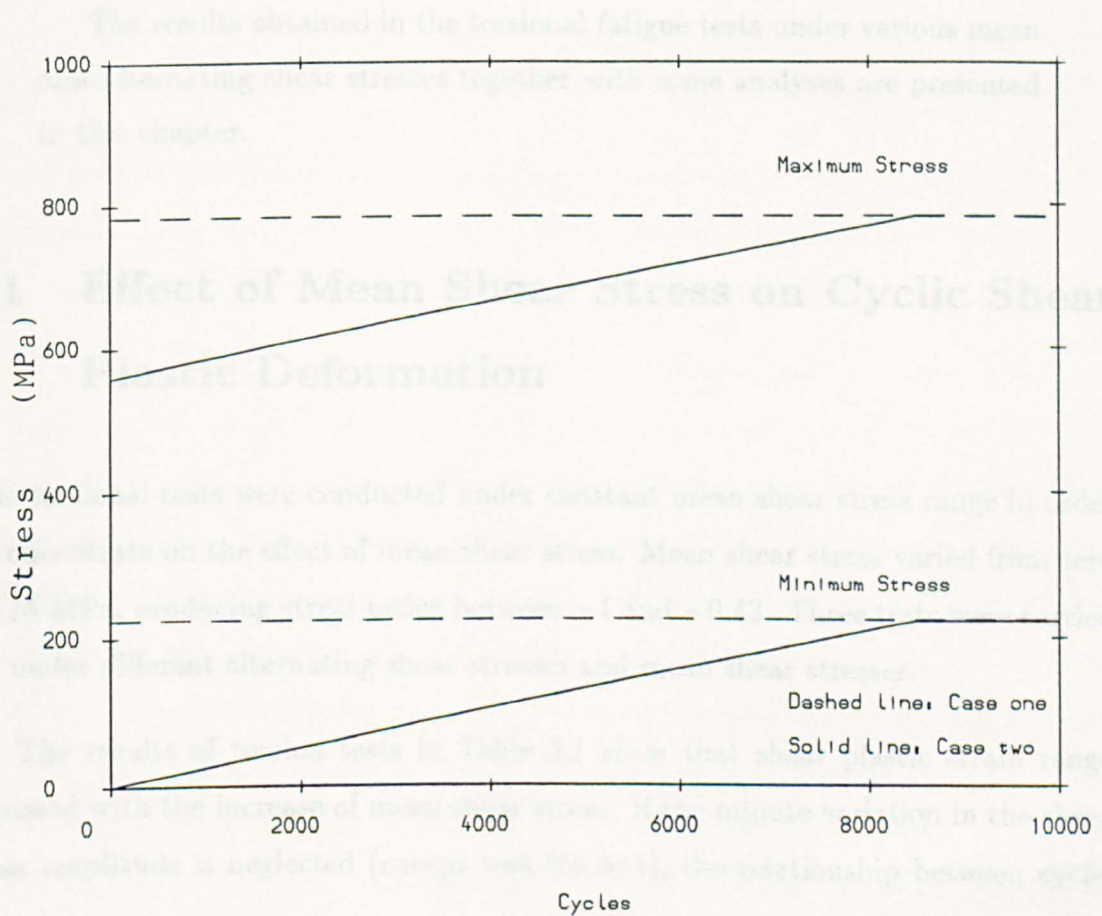


Fig.2.9 Loading Paths of uniaxial Tests

Chapter 3

Torsional Tests: Results and Analyses

The results obtained in the torsional fatigue tests under various mean and alternating shear stresses together with some analyses are presented in this chapter.

3.1 Effect of Mean Shear Stress on Cyclic Shear Plastic Deformation

Nine torsional tests were conducted under constant mean shear stress range in order to concentrate on the effect of mean shear stress. Mean shear stress varied from zero to 115 MPa, producing stress ratios between -1 and -0.43 . Three tests were carried out under different alternating shear stresses and mean shear stresses.

The results of torsion tests in Table 3.1 show that shear plastic strain range increased with the increase of mean shear stress. If the minute variation in the shear stress amplitude is neglected (except test No.A11), the relationship between cyclic

shear plastic strain and mean shear stress can be expressed as:

$$\Delta\gamma_p = 6.72 \times 10^{-5} e^{\tau_m/71.1} \quad (3.1)$$

Fig.3.1 shows the data along with Eq.3.1.

The relationship between the shear stress range and the cyclic plastic strain range can also be obtained by means of correlating the data using power law relationship,

$$\Delta\gamma_p = 1.07 \times 10^{-41} (\Delta\tau)^{13.39} \quad (3.2)$$

If we assume that the cyclic plastic strain range $\Delta\gamma_p$ can be expressed in the form: $\Delta\gamma_p = A(\Delta\tau)^\alpha f(\tau_m)$ then the combination of the Eq.3.1 and Eq.3.2 shown as below will provide the prediction of the cyclic plastic strain range under any combination of the alternating and mean shear stresses,

$$\Delta\gamma_p = 1.07 \times 10^{-41} (\Delta\tau)^{13.39} e^{\tau_m/71.1} \quad (3.3)$$

The validity of Eq.3.3 is supported by the satisfactory prediction of the datum of test No.A2 (the actual value of $\Delta\gamma_p$ is 5.3×10^{-4} and the predicted value is 6.22×10^{-4}).

Due to the inherent inaccuracy in the measurement and calculation of the diminutive plastic strain amplitude, the rigour of the above relationship is arguable. The indicated underlying trend, however, is believed to be reasonable.

In the literature, for instance in reference [1], mean stress was almost invariably assumed to have no effect on the cyclic plastic strain range. In other words, $\Delta\gamma_p$ is only dependent on $\Delta\tau$. This conclusion is frequently drawn from strain-controlled experiments whereas some stress-controlled tests reported in the literature show that cyclic plastic strain range does depend on the mean stress level. For example, Philips and his co-workers [2] have verified that the yield surface not only translates in the direction of mean stress, but also shrink in size during loading and unloading which implies a dependence of the size of the cyclic yield surface on the level of mean stress. The work by Kliman and Bily [3] on 0.4% Carbon steel also demonstrated that mean stress level could significantly influence the cyclic plastic strain amplitude for a given alternating stress.

From the viewpoint of the motion of dislocations under cyclic loading, mean shear stress can increase the irreversibility in dislocation motion by preventing them moving back to their previous position while the stress range tends to drive dislocations to move to-and-fro around a pinning point and to set up a path for reversible slip. Thus it is plausible that the existence of mean shear stress can alter the irreversibility of the motion of dislocations and the pattern of dislocation structure.

In addition, perhaps of more importance, mean shear stress would facilitate the localization of plasticity. Under monotonic loading, the stress necessary to cause plasticity is the yield stress of the material τ_y . For the cyclic loading condition, an alternating stress level around the fatigue limit τ_{fl} is enough to cause cyclic plasticity at least within one grain to produce one critical crack without the presence of mean shear stress. For an asymmetrical cycle (with an amplitude equal to τ_a), the increase in mean shear stress will induce the required conditions for yielding in several surface grains producing several possible crack localizations due to the extensive plasticity. Hence a lower alternating stress level may well provoke the plasticity localization required for the fracture process.

3.2 Tests Results

The failure of specimens was defined as when the surface cracks were three millimetres long. Some tests were left running until final failure, and some were stopped to preserve the fracture surface. These specimens were then pulled apart in order to make SEM observations. The results are presented in Table 3.1 and crack growth results are presented in Figs.3.2, 3.3 and 3.4.

From Table 3.1, it can be seen that mean shear stress dramatically reduced the fatigue lives for a given constant stress range. This point is revealed more explicitly

in Fig.3.5. The effect of mean shear stress can be divided into two zones. For low mean stress levels ($\tau_m \leq 90$ MPa, $\tau_{max} \leq 370$ MPa), the effect can be expressed as,

$$N_f = 1.13 \times 10^6(1 - 0.01 \tau_m) ; \tau_m \leq 90 \text{ MPa} \quad \tau_a = 280 \text{ MPa} \quad (3.4)$$

As the mean shear stress level was further increased, i.e. above 90 MPa fatigue life decreased but at a lower rate than for $\tau_m \leq 90$ MPa. For this regime the effect of mean shear stress on fatigue life can be expressed as,

$$N_f = 4.67 \times 10^5(1 - 0.007 \tau_m) ; 90 \text{ MPa} \leq \tau_m \leq 140 \text{ MPa} \quad (3.5)$$

when $\tau_a = 280$ MPa.

A relatively large scatter in the results was observed for high mean stress tests. When a high mean shear stress was active, a greater degree of cyclic creep occurred which relaxed the mean shear stress. Although the technique used in the present work could well maintain the mean shear stress level, a slight relaxation was inevitable if ratcheting was to be avoided (high cyclic creep straining might considerably influence crack growth).

Examinations of the fracture surfaces revealed that all dominant fatigue cracks were initiated from the surface. The initial crack growth (stage I mode II) showed a crystallographic pattern with fracture surfaces composed of small smooth facets. Cracks eventually branched to mode I, growing perpendicularly to the maximum tensile stress. Fig.3.6a shows the fracture surface with both the transverse and longitudinal cracks. This can also be recognized in an early stage of the life of the same specimen; see Fig.3.6b.

3.3 Stage I Crack Growth

Cracks were found to initiate and propagate either on the transverse or axial planes. One characteristic of this stage of crystallographic growth is that no rubbing effects can be observed; as shown in Fig.3.7. Rubbing is due to the friction between the flanks

of the mode II cracks. This effect has been offered as one reason for the termination of mode II fatigue crack growth [5] [6]. Other workers have also shown that pre-cracked specimens tested in mode II show evidence of surface rubbing and wear [7]. This phenomenon was not found for short mode II cracks in the present work, possibly due to the following reasons:

(1) Crack morphology. Smooth surface cracks are initiated in the relatively large grains (or from inclusions), lying on the maximum shear stress plane. Rubbing is invariably assisted by crack face irregularities generated by different slip systems. Due to the constraint of normally elastic deformation in the immediate surrounding material, cracks tend to grow in a coplanar manner involving a single slip system. This process covers the initial two or three grains.

(2) Small slipping and closing displacement. The BCS theory can be applied to estimate the relative displacement between crack faces [8]. At the centre of the crack, the relative crack slip displacement, CSD, for a mode II crack can be expressed as,

$$\begin{aligned} CSD &= \frac{4a\tau_u(1-\nu)}{\pi G} \cosh^{-1}\left[\sec\left(\frac{\pi}{2} \frac{\tau}{\tau_u}\right)\right] \\ &= 6.26 a \times 10^{-3} \end{aligned} \quad (3.6)$$

where $\tau = 280$ MPa, $\tau_u = 420$ MPa, $G = 77$ Gpa.

Surface observations show that the surface crack trajectory is not perfectly axial and minor angular deviations occur but invariably less than 30° ; see Fig.3.8. The relative closing displacement COD between the facets will be $CSD \times \sin 30^\circ = 0.313a$. If the surface crack length is $200 \mu\text{m}$, $a = 100 \mu\text{m}$, $CSD = 0.63 \mu\text{m}$, then $COD = 0.313 \mu\text{m}$. Since a gap of $0.5 \mu\text{m}$ or more between crack faces was observed for naturally initiated short cracks, cracks slip freely.

The initiation of cracks occurred in those grains whose slip plans lie on the maximum resultant shear stress. The localization of plasticity was more severe in these grains. If the neighbouring grain or grains were oriented towards the same direction or at a small angle, cracks would easily penetrate the boundaries and propagate into the next grains, experiencing very little retardation. Otherwise, the crack growth

would decrease with the increase of crack length, as typically shown in Fig.3.9. Obviously the deceleration is only restricted for crack length less than $150\ \mu m$. Therefore the dominant barriers to stage I growth were the prior austenite grains, or in a 3-dimensional sense, the packet of grains surrounding the crack tip. The boundaries between bundles also act as major barriers but their effect can be considered as the effect of the substructure, or a second order effect because the average distance between bundles was only $10\ \mu m$.

The delay periods of cracks at barriers decreased with the increase of the crack length, because the crack tip driving force was increasing, as shown in Fig.3.10. An important conclusion can be drawn from these results: the shorter the distance between barriers, the stronger is the resistance of microstructure to short crack growth.

Mean shear stress enhances the ability of cracks to overcome microstructural barriers which can be attributed to the maximum shear stress's effect on the crystallographic structure [4] and the maximum plastic zone produced due to the increase in maximum shear stress. In the extreme case, when the stress amplitude approaches zero, the damage is only due to the maximum stress, or mean shear stress.

3.4 Effects of Inclusions

Two types of inclusions have been found in the present material, sulphide inclusions (MnS) and oxide inclusions. While the former has a high index of deformability ($\nu \cong 1.0$) and can deform plastically with the steel, the later type is a hard spherical particle with a very low index of deformability ($\nu \cong 0$) and remains undeformed and in a spherical state. During the manufacture process, sulphide inclusions have deformed to ellipsoids and elongated along the longitudinal direction which is also the axis of specimens. The sizes of the sulphide inclusions are from $10\ \mu m$ to $80\ \mu m$ in length, $3\ \mu m$ to $13\ \mu m$ in width and $3\ \mu m$ to $13\ \mu m$ in depth. The second type of inclusions are about 2 to $5\ \mu m$ in diameter.

Most cracks were found to have originated from either sulphide inclusions or the base matrix, only a few cracks started from hard particle inclusions (less than $5\mu\text{m}$). After the initiation from inclusions, cracks still propagated in mode II with a decelerating speed up to a length of about 160 to 280 μm and then changed to stage II, see also Fig.3.11(a). The crack growth pattern can be seen in Figs.3.3, 3.4 and 3.5. Although inclusions started fatigue crack propagation and shortened the time for stage I crack growth, they did not affect transient behaviour to stage II and stage II crack growth. This indicates that inclusions, although they control the stress levels required to acquire specific crack growth rates do not affect the torsional fatigue limit itself. The overall effect of the present inclusions when compared to clear steels with respect to finite fatigue life is not substantial since it was the transition and stage II propagation phases which played a major part of fatigue life in torsion.

3.5 Transient and Stage II Growth

3.5.1 Transient behaviour

Two kinds of crack growth path were found on each specimen after cracks had grown about 200 to 300 μm in mode II. The first kind bifurcated at stage I crack tips and grew in mode I as shown in Fig.3.6b. This mode is preferred at high cyclic stress levels. The bifurcation behaviour is dependent on the mean stress level, as can be seen from Fig.3.6(b) and Fig.3.11(b), this will be further discussed in Section 3.6. The second kind were the majority and these cracks grew along a zig-zag path as shown in Fig.3.11(a). Here each microscopic segment of crack growth was at 90 degrees to the maximum tensile stress. This indicated that cracks were growing in a limited distance in mode I. This mode is a transition between stage I and stage II growth. The photos in Fig.3.11(a) and Fig.3.11(b) were taken from the same specimen, and hence at the same stress level, illustrating the transient behaviour to stage II crack growth. At the stress level $\tau = 280 \text{ MPa}$, 80% of cracks longer than 250 μm were of

the form shown in Fig.3.11(a) with only 20% of cracks of the form shown in Fig.3.6b.

The zig-zag crack path was due to only one slip system being active thereby tending to keep the overall crack growth direction parallel to the maximum shear strain. Even for some branched cracks, after some growth under the influence of mode I, they still tended to propagate at a small angle (less than 45 degrees) to the stage I crack plane, indicating a mixed-mode character.

The reversed and the forward plastic zone size at the transient length can be obtained by the of BCS theory (see Section 1.6). Here cracks are considered to be non- rubbing and the effect of microstructure is ignored,

$$r_{p,rev} = a \left[\sec\left(\frac{\pi}{2} \frac{\Delta\tau}{2\tau_u}\right) - 1 \right] \quad (3.7)$$

$$r_{p,max} = a \left[\sec\left(\frac{\pi}{2} \frac{\tau_{max}}{\tau_u}\right) - 1 \right] \quad (3.8)$$

where $a = a_s/2$.

Several researchers consider that for fully reversed cycling, the transient from stage I to stage II can be rationalized by $r_p = d$ where d is the average grain size. This does not hold for the present material in torsion. The average transient crack length for the zero mean shear stress case was $277 \mu m$ ($a = 138 \mu m$). At this crack length, the reversed plastic zone size is,

$$r_{p,rev} = 138 \times \left[\sec\left(\frac{\pi}{2} \frac{280}{420}\right) - 1 \right] = 138 \quad (\mu m) \quad (3.9)$$

but the average size of the prior austenite grains is $50 \mu m$ in the present material. The transient behaviour must be controlled by the stress and plastic deformation conditions at crack tips. For example, the 'maximum tangent (hoop) tensile stress' is considered as a good criterion for predicting crack bifurcation. For the present situation, the maximum reversed tangent tensile stress and the maximum tensile stress are both at 45° to the stage I crack plane.

What is interesting here is that the mean shear stress has been found to have no recognizable influence on the bifurcation crack length as shown in Fig.3.12. The

average length is 244 μm . This indicates that the maximum plastic zone size does not affect the transient crack length. If the change to stage II crack growth is the limiting condition between finite and infinite fatigue life, then it could be expected that mean shear stress would not significantly affect the torsional fatigue limit but some work would be required on studies of non-propagating cracks to be sure if this hypothesis is correct.

3.5.2 Stage II growth and theoretical modelling

Most of the dominant cracks were found to be those bifurcated at the Stage I crack tip and propagated in Mode I under the influence of a parallel tensile stress. In order to determine the plasticity condition of crack tips under complex-mode loading, a straight crack under biaxial loading condition is considered as a simple representation for stage II crack growth as shown in Fig.3.13.

For the low-stress, long crack case ($\sigma_1 \ll \sigma_y$, $\sigma_2 \ll \sigma_y$) Brown and Miller [9] have acquired a solution for cracks in a cruciform specimen on the basis of Dugdale-Barenblatt model (see also Section 1.6), which is not applicable to this case. In the present work a dislocation method is used to obtain the plastic zone size and crack tip opening displacement. Two shear bands are assumed to represent the plastic deformation at one crack tip, see Fig.3.14 in a manner similar to the BCS theory [10]. The difference is that a biaxial stress state is considered. Due to the extreme complexity of the problem, only the simplified equilibrium equation is presented,

$$\int \frac{f(S)}{S - S_0} g(\theta, S, S_0) dS = P(S_0)/A \quad (3.10)$$

here the integration is over the crack and four shear bands, and the term S is a complex variable referred to an arbitrary point within the crack or one shear band while S_0 is the complex number for a specific point within the crack or shear band. The function $g(\theta, S, S_0)$ is the orientation factor for the stress components by a dislocation at point S . The complex function $P(S_0)$ is given by,

$$P(S_0) = \begin{cases} \sigma_1 & S_0 \text{ is within the crack} \\ (\sigma_1/2 - \sigma_2/2 - \tau_u)(\frac{\sqrt{2}}{2} + \frac{\sqrt{2}}{2}i) & S_0 \text{ is within the shear band BC} \end{cases}$$

here the crack is simulated as a continuous distribution of infinitesimal dislocations which are not affected by the normal stress parallel to the crack plane. If the term $(\frac{1}{2}\sigma_2 + \tau_u)$ is replaced by τ_u^* , the above equation for a straight crack under biaxial loading will be the same as a tensile crack under uniaxial loading. Thus the solution for Eq.3.10 can be directly obtained by replacing τ_u by $(\tau_u + \sigma_2/2)$ in the BCS theory. This implies that the stress component parallel to the crack will decrease or increase the effective flow stress when the stress system is pure shear loading ($\lambda = -1$) or equal-biaxial loading ($\lambda = +1$), respectively, this conclusion is in agreement with the work by Brown and Miller [9] for the case of low stresses.

For shear loading for which, $\sigma_1 = \tau_m + \tau_a$, $\sigma_2 = -\tau_m - \tau_a$. It follows that,

$$\lambda = \frac{\sigma_2}{\sigma_1} = -1 \quad (\text{pure shear loading}) \quad (3.11)$$

$$R_{\sigma_1} = \frac{\tau_m - \tau_a}{\tau_m + \tau_a} \quad (\text{stress ratio of } \sigma_1) \quad (3.12)$$

$$R_{\sigma_2} = \frac{-\tau_m - \tau_a}{-\tau_m + \tau_a} \quad (\text{stress ratio of } \sigma_2) \quad (3.13)$$

Here no closure effect is assumed (closure stress level is related to the maximum stress level or the maximum plastic zone size) in order to obtain some approximations. The reversed plastic zone size can be obtained by replacing σ and σ_y in Eq.1.25 with τ_a and $(2\tau_u - \tau_a)$, respectively. The maximum plastic zone size can be obtained through substituting σ and σ_y by $\tau_a + \tau_m$ and $(2\tau_u - \tau_a - \tau_m)$ respectively, and so

$$r_{p,rev} = a \left[\sec\left(\frac{\pi}{2} \frac{\tau_a}{2\tau_u - \tau_a}\right) - 1 \right] \quad (3.14)$$

$$r_{p,max} = a \left[\sec\left(\frac{\pi}{2} \frac{\tau_a + \tau_m}{2\tau_u - \tau_a - \tau_m}\right) - 1 \right] \quad (3.15)$$

Obviously the reversed plastic zone size does not depend on the mean shear stress level while the maximum plastic zone size does as shown in Fig.3.15. It is clear from

the figure that the effect of mean stress on the maximum plastic zone size is small at low mean shear stress. However the effect becomes discernible when mean shear stress increases. Fatigue lives for the ten specimens can be well correlated by this parameter. Fig.3.15 is a reflection of the mean shear stress effect on the fatigue limit; see also Fig.1.6.

Since $R_{\sigma_2} < R_{\sigma_1}$, the branching of cracks would have shown an asymmetrical pattern had mean shear stress been present. When mean shear stress was present, at each crack tip one branch crack tended to grow faster than the other and the trend became more prominent with the increase of mean shear stress. This is in good agreement with experimental results for tests No.A4, A5 and A7 in which bifurcations were asymmetrical about the stage I crack plane and symmetrical bifurcations were observed in tests No.A8, A10.

Thus the effect of biaxial stress state and the nature of the biaxial mean stress levels influence the development of one dominant branch.

3.6 Polarities of Mean Shear Stress

Section 1.2.2 presented some experimental results from the literature, which showed the present stage of confusion about the polarity of mean shear stress. In the case of uniaxial fatigue, there are two different mean stresses, mean tensile stress (positive) and mean compressive stress (negative). It is known that the two stresses have different effects on fatigue endurance (see Section 1.2 and Chapter 4). Therefore it is important to clarify the stress states for the present asymmetrical torsion tests.

According to the results reported by Smith (see Section 1.2.2), mean shear stress in one direction appears to be more detrimental than mean shear stress in another direction. This is not explainable from elastic-plastic mechanics considerations since the different directions of mean shear stress should not give rise to differences in deformation and static failure process in isotropic materials.

Consider two specimens subjected to the same shear stress range and mean shear stresses but in different directions as shown in Fig.3.16 (a_1 and a_2). The two specimens are presumed to have identical mechanical properties. As the range of mean shear stress is the same in both cases, the following discussion is concentrated on the mean shear stress effect. One important aspect is the orientation of cracks, particularly with respect to the surface. The variations in stress-strain states that occur as the crack propagates are also important. As shown in Fig.3.16, the shear stress states in both cases have different relations with respect to the free surface. Hence strictly speaking, the two stress states are different and may have dissimilar effects on fatigue crack growth behaviour.

In the initial phase of life, cracks are designated stage I (mode II) and are on the planes of maximum shear strain, as shown in Fig.3.16 c_1 and c_2 . In this stage, cracks grow in shear mode. The different orientations of mean shear stresses with respect to the surface plane does not alter the effect of mean shear stress on crack growth. In other words, mean shear stresses with different polarities have the same effect on stage I crack growth. This is in agreement with the present experimental results, as shown in Table 3.1 and Appendix A, two pairs of tests No.A1 and A4, No.A6 and A7 had opposite mean shear stresses but Stage I crack growth behaviour was identical when the scatter of the growth data is taken into account.

At the transition to stage II, at each end of the crack bifurcation into two mode I cracks can occur under the same driving force if there is no mean shear stress. However, the presence of mean shear stress greatly affects the crack growth behaviour for such branch cracks. As can be seen in Fig.3.16 the growth of only one branch crack is favoured by the tensile mean stress (itself generated by the mean shear stress) acting upon it, whereas for the other one, a mean compressive stress contrives to close it and to terminate its growth. This is actually confirmed by the present experimental results as shown in Fig.3.6(b) and Fig.3.11(b). As a result, two different fracture surfaces are developed. Consequently, mean shear stresses with two different polarities produce dissimilar fracture surface orientation with respect to the twisting direction. However

this has the same effect on fatigue life if the material is isotropic and without any texture.

However, if the material exhibits a particular anisotropic behaviour and a texture which tends to prevent crack growth in one direction and facilitate crack growth in another direction, then the fatigue lives in case 1 and case 2 of Fig.3.16 are no longer the same. In other words, the material will show different resistances to mean twists applied in different directions.

In conclusion, for isotropic materials such as most engineering steels, effect of mean shear stress should be independent of the polarities. In present work, in tests A1 and A4 mean shear stresses were applied in opposite directions, so were the mean shear stresses in tests A6 and A7. The fatigue lives were well within the a scatter band and conformed the above analyses. Therefore for normally isotropic materials, unlike the effect of mean axial stresses which are sensitive to the polarities, mean shear stresses with different polarities do not affect the fatigue life and fatigue limit.

3.7 Discussion and Conclusions

In this chapter we have studied the effect of mean shear stress on torsion fatigue strength and short crack growth. Torsional fatigue lifetime has been found to be significantly affected by mean shear stress. For example, the lifetime may be reduced by an order when an mean shear stress of 110 MPa in magnitude is active.

Stage I cracks invariably grow in shear mode, the experimental results showed that mean shear stress plays a fundamental role in promoting shear crack growth. The dominant Stage II cracks under torsional loading has been idealized as a straight crack under biaxial loading, and a dislocation simulation technique has been applied to obtain the sizes of the plastic zones. The solution of the associated equilibrium equation can be obtained in analogy with the BCS approach. The results as shown in Eq.3.14 and Eq.3.15 reveal that the applied mean shear stress has significantly

intensified the effect of load biaxiality, viz the maximum plastic zone size increases rapidly with the mean shear stress as shown in Fig.3.15.

The analyses about the polarity of mean shear stress as shown in Section 3.6 have shown that mean shear stress does not show any preference towards its polarity in promoting shear mode crack growth, but can alter the Stage II crack growth path in relation to the free surface and the stress states. In terms of the surface crack growth rate, however, the polarity of mean shear stress has no effect in the case of isotropic material, but may not be the case for anisotropic material.

Therefore in this thesis, the shear stress ratio R_τ is defined as the follows since the polarity of mean shear stress has no effect on the fatigue behaviour of the present material,

$$R_\tau = \frac{|\tau_m| - \tau_a}{|\tau_m| + \tau_a} \quad (\geq -1) \quad (3.16)$$

the results of the eleven tests are shown in Table 3.1.

References

1. Tomkins, B. (1968) Fatigue Crack propagation—An Analysis, *Philosophical Magazine*, Vol.18 , 1968, pp.1041.
2. Philips, A. and Lu, W. Y. (1984) An Experimental Investigation of Yield Surfaces and Loading of Pure Aluminium with Stress-Controlled and Strain-Controlled Paths of Loading, *Journal of Engineering Materials and Technology*, Vol.106, pp.349-354.
3. Kliman, V. and Bily, M. (1980) Influence of Mode Control, Mean Value and Frequency of Loading on the Cyclic Stress Strain Curve, *Material Science and Engineering*, Vol.44, pp.73-79.
4. Gough, H. J. (1949) Engineering Steels under Combined Cyclic and Static Stresses, *Proceedings of Institute of Mechanical Engineering*, Vol.160, pp.472.
5. Smith, M. C. and Smith, R. A. (1988) Toward an Understanding of Mode II Fatigue Crack Growth, *Basic Questions in Fatigue: ASTM STP 924*, J. T. Fong and K. J. Fields Eds., American Society for Testing and Materials, Philadelphia, pp.260-280.
6. Otsuka, A., Moris, K., Ohshima, T. and Tsnyama, S. (1980) Mode II Fatigue Crack Propagation in Aluminium Alloys and Mild Steel, *Proceedings of 5th International Conference on Fracture*, Cannes, France, Vol.4.
7. Smith, M. C. and Smith, R. A. (1982) The Formation of Spherical Wear-Debris in Mode II Fatigue Cracks, *Wear*, Vol. 76, pp. 105–128.
8. Bilby, B. A. and Swinden, K. H. (1965) Representation of Plasticity at Notches by Linear Dislocation Arrays, *Proceedings of Royal Society of London, A*, 285, pp. 22–33.
9. Brown, M. W. and Miller, K. J. (1985) Mode I Fatigue Crack Growth Under Biaxial Stress at Room and Elevated Temperature, *Multiaxial Fatigue: ASTM STP 853*, K. J. Miller and M. W. Brown Eds., American Society for Testing and Materials, Philadelphia, pp. 135–152.
10. Bilby, B. A., Cottrell, A. H. and Swinden, K. H. (1963) The Spread of Plasticity from a Notch, *Proceedings of Royal Society of London, A272*, pp. 272–304.

Table 3.1: Torsion Test Results

Test Number	Shear Stress Amplitude (MPa)	Mean Shear Stress (MPa)	Cyclic Plastic Strain $\Delta\gamma_p$ (%)	Fatigue Life (cycles)	Test Frequency (Hz)	Stress Ratio R_τ
A1	288	-79	0.020	196500	2	-0.57
A2	293	+118	0.053	43787	1	-0.43
A3	280	+52	0.015	530000	3	-0.69
A4	278	+84	0.020	255150	2	-0.54
A5	277	+90	0.026	171902	2	-0.51
A6	280	-112	0.033	126792	2	-0.43
A7	284	+116	0.034	134600	2	-0.42
A8	280	0.0	0.006	1200000	3	-1.0
A9	280	+20	0.008	900000	3	-0.87
A10	282	0.0	0.008	1080000	3	-1.0
A11	330	0.0	0.060	84529	2	-1.0

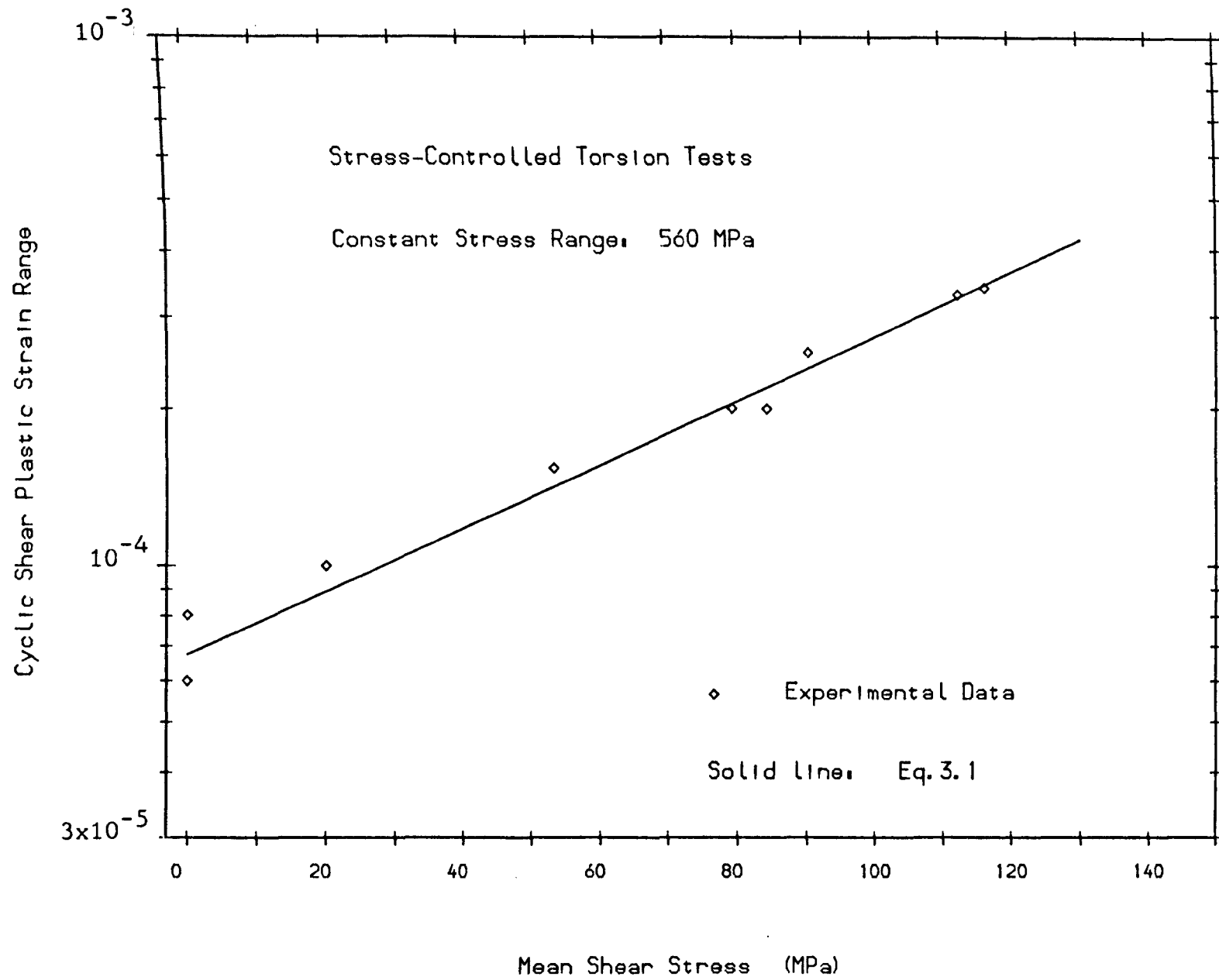


Fig. 3.1 Effect of Mean Shear Stress on Cyclic plastic Strain

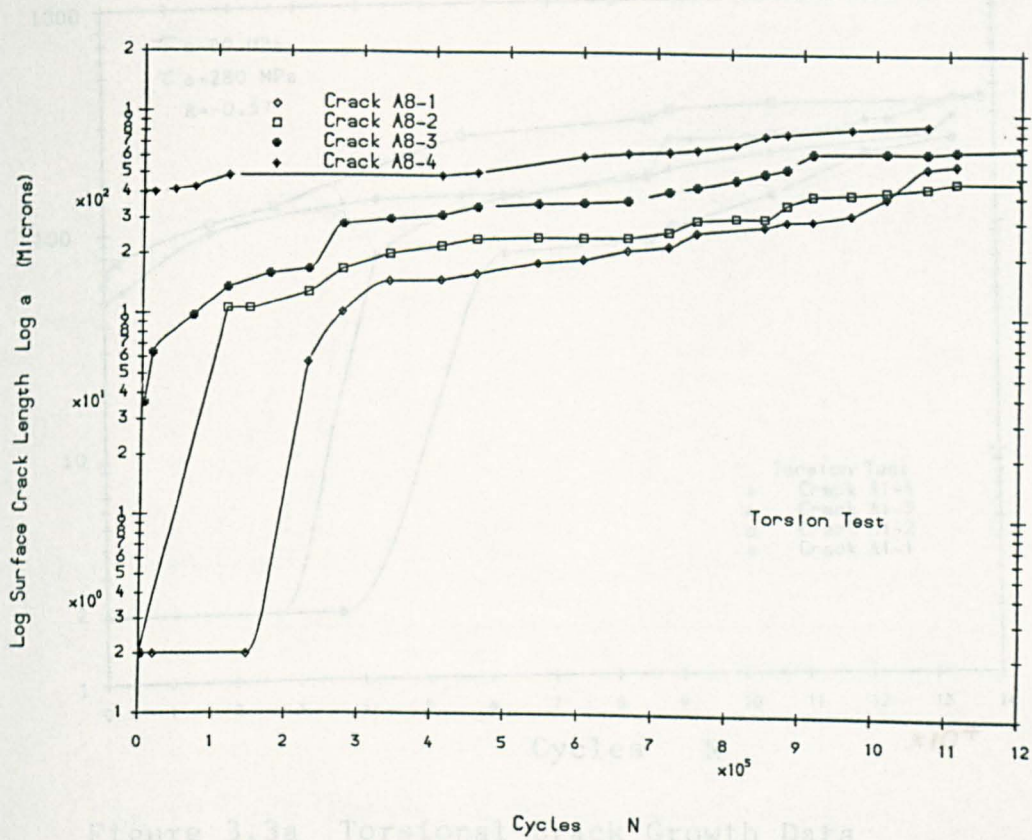


Figure 3.2a Torsional Crack Growth Data ($\tau_m = 0$, $\tau_a = 280$ MPa)

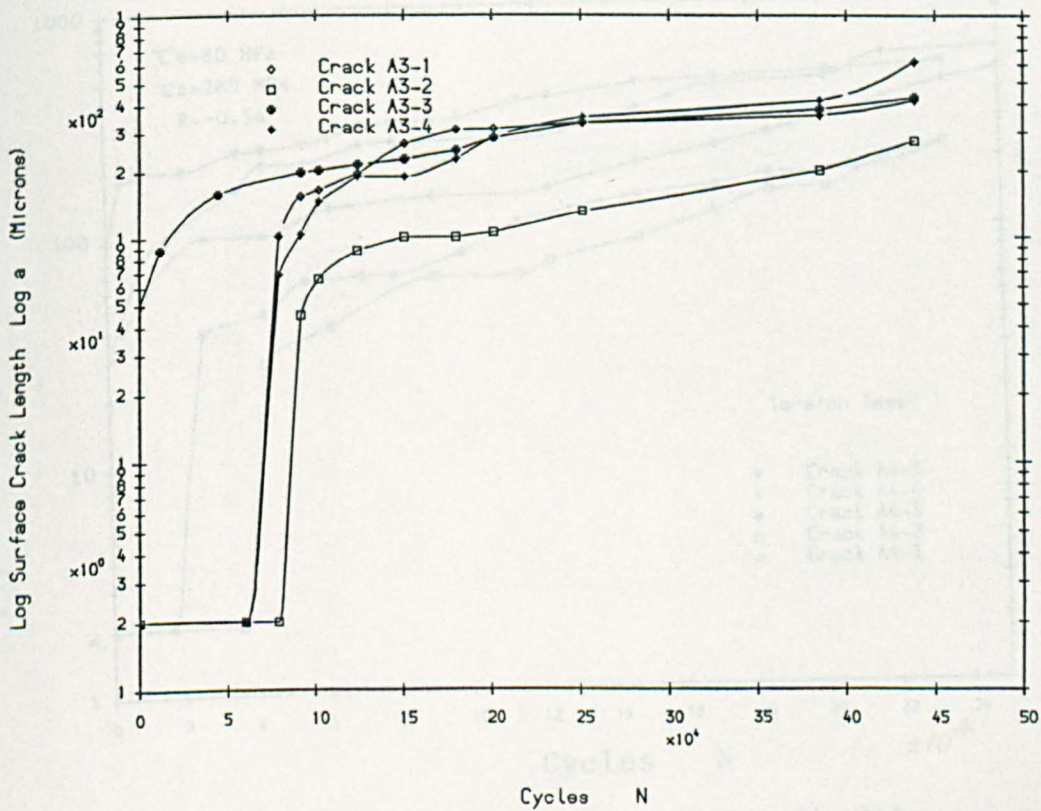


Figure 3.2b Torsional Crack Growth Data ($\tau_m = 52$ MPa, $\tau_a = 280$ MPa)

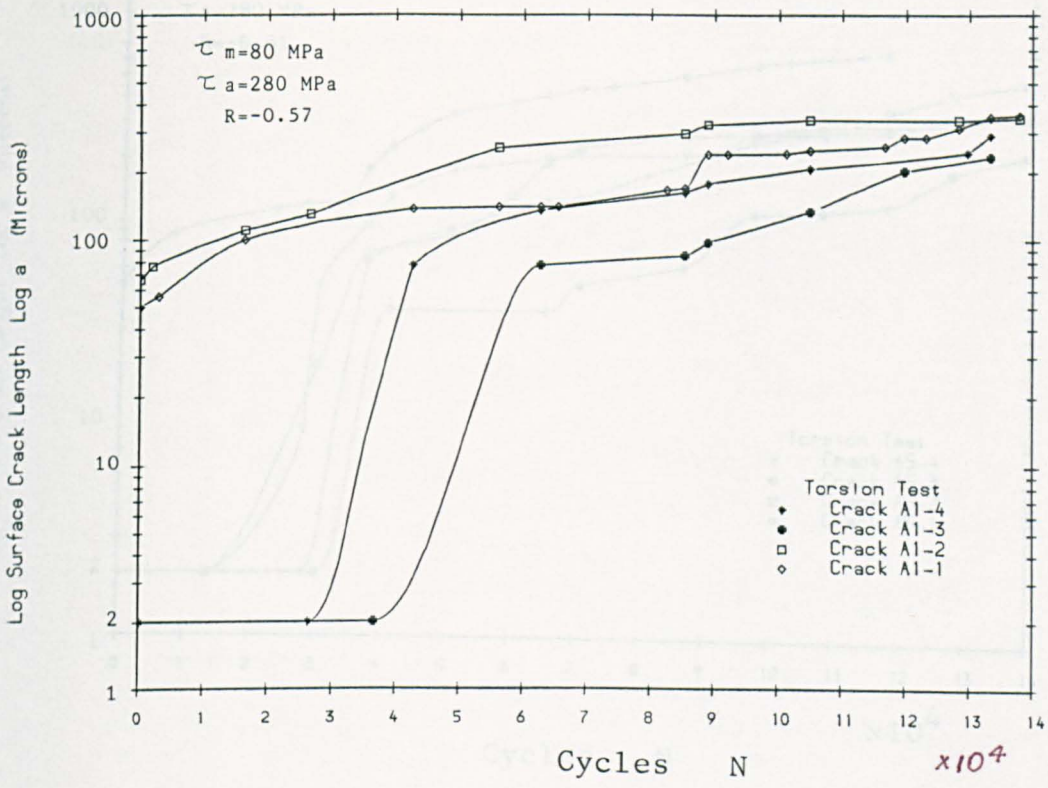


Figure 3.3a Torsional Crack Growth Data

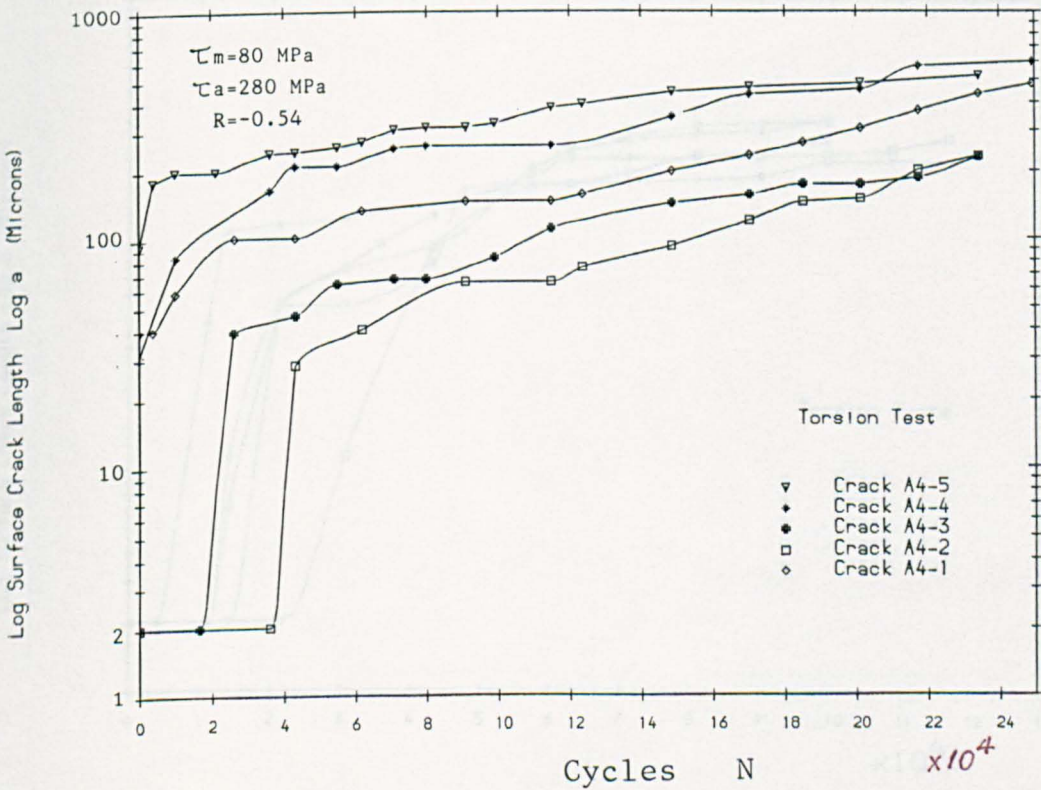


Figure 3.3b Torsional Crack Growth Data

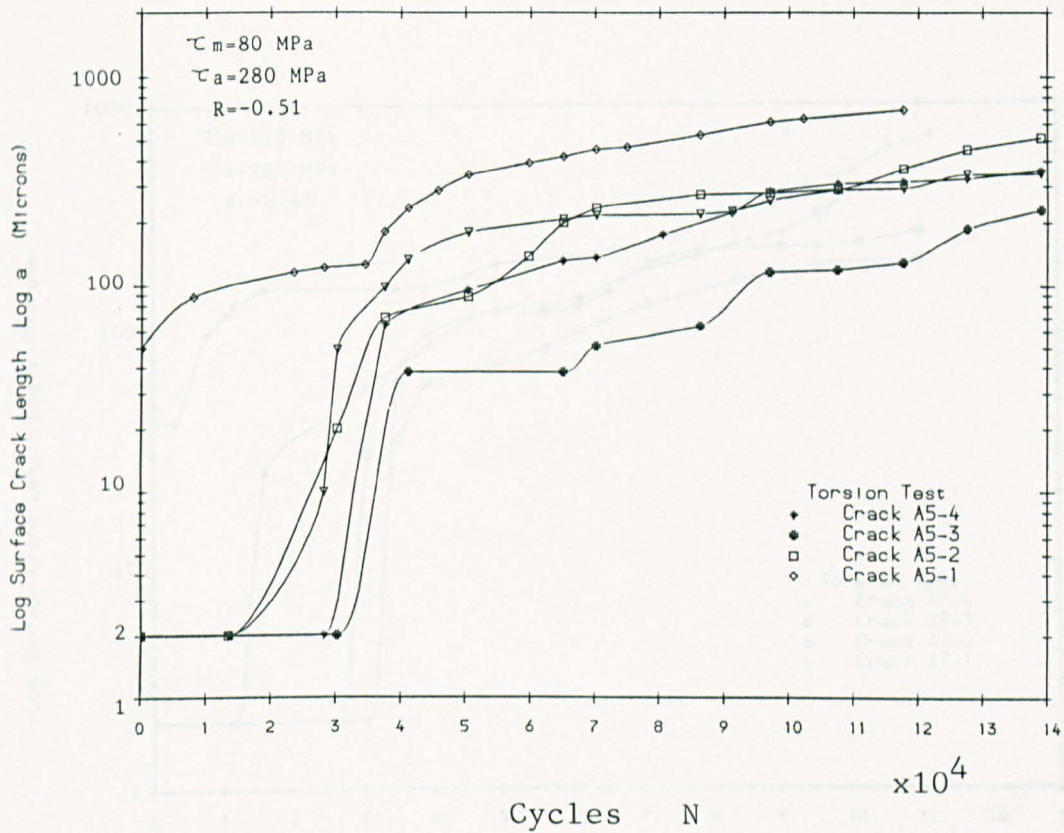


Figure 3.3c Torsional Crack Growth Data

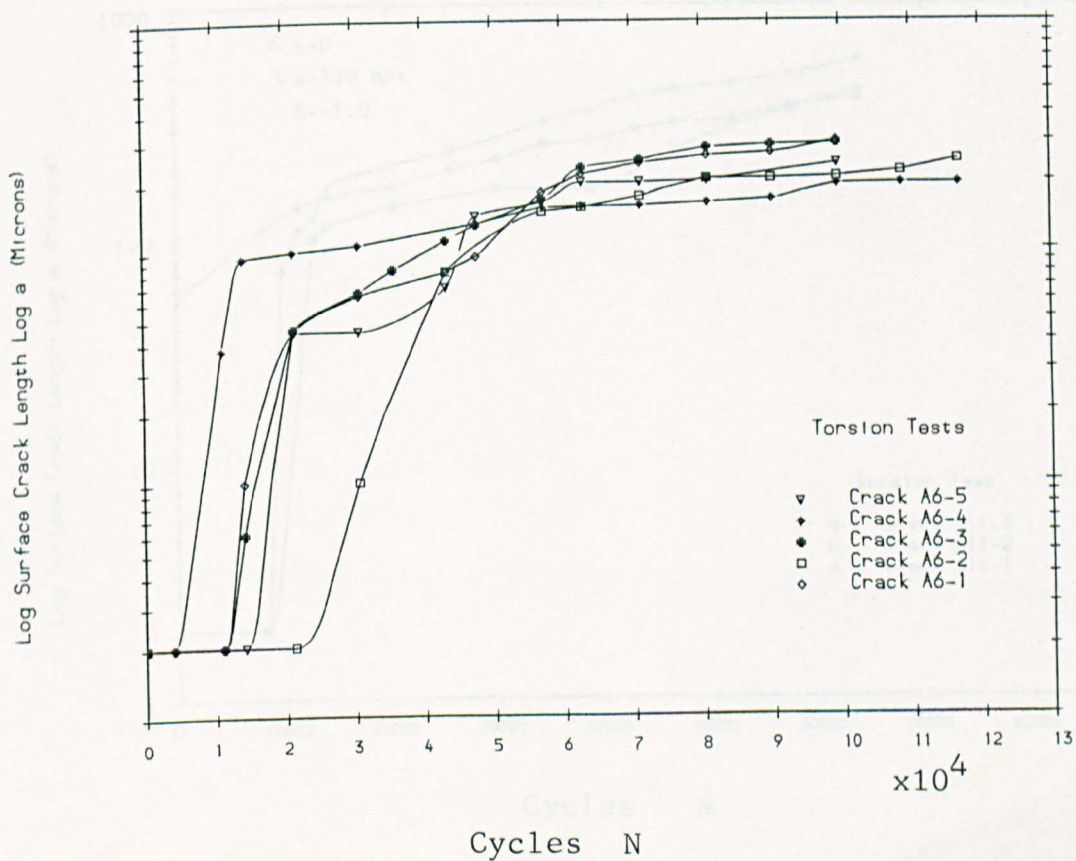


Figure 3.4a Torsional Crack Growth Data

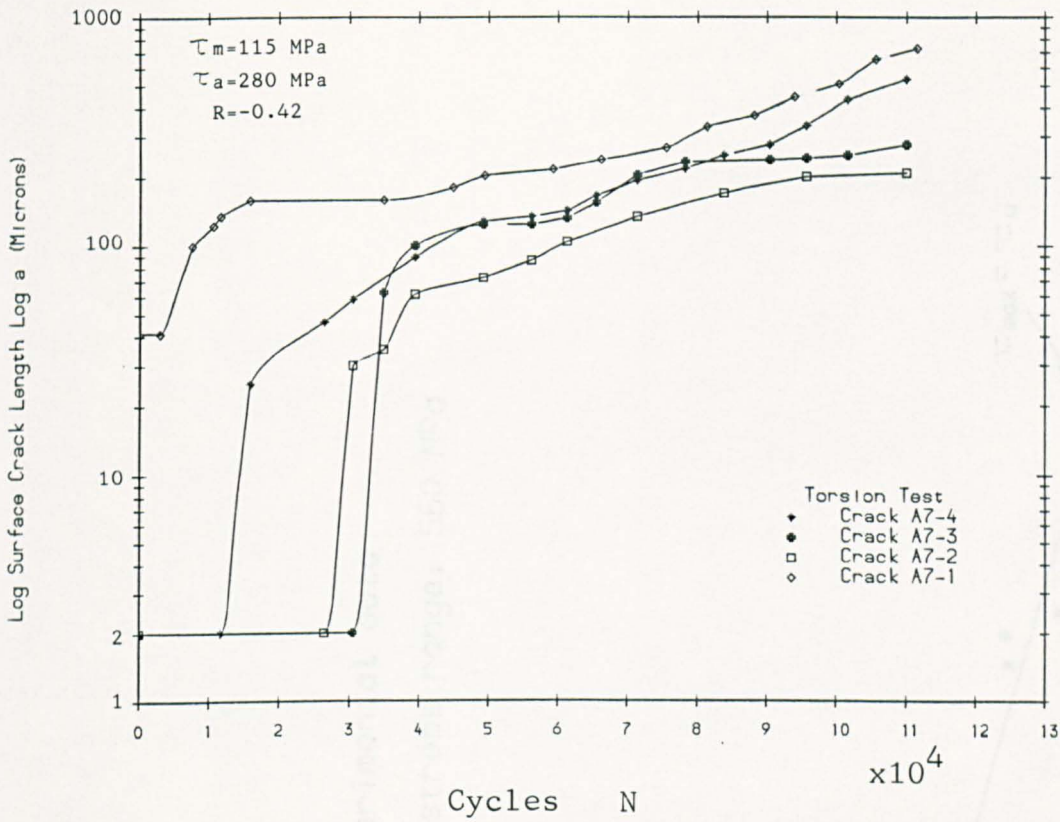


Figure 3.4b Torsional Crack Growth Data

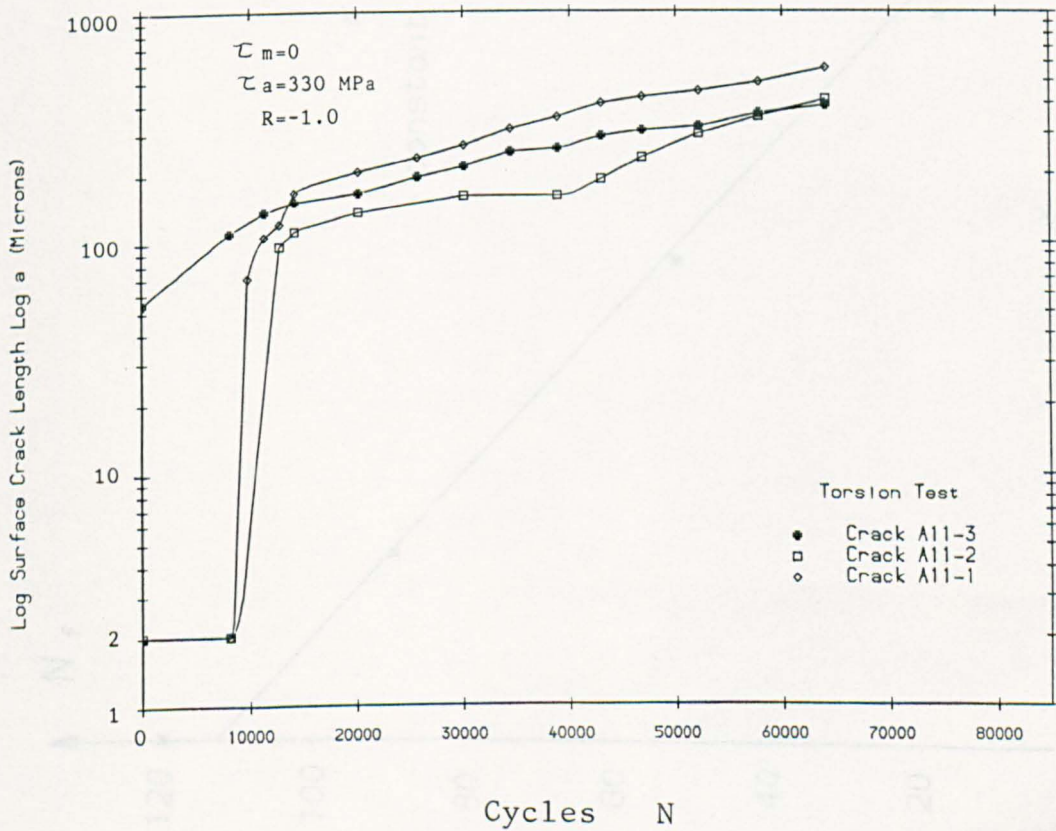


Figure 3.4c Torsional Crack Growth Data

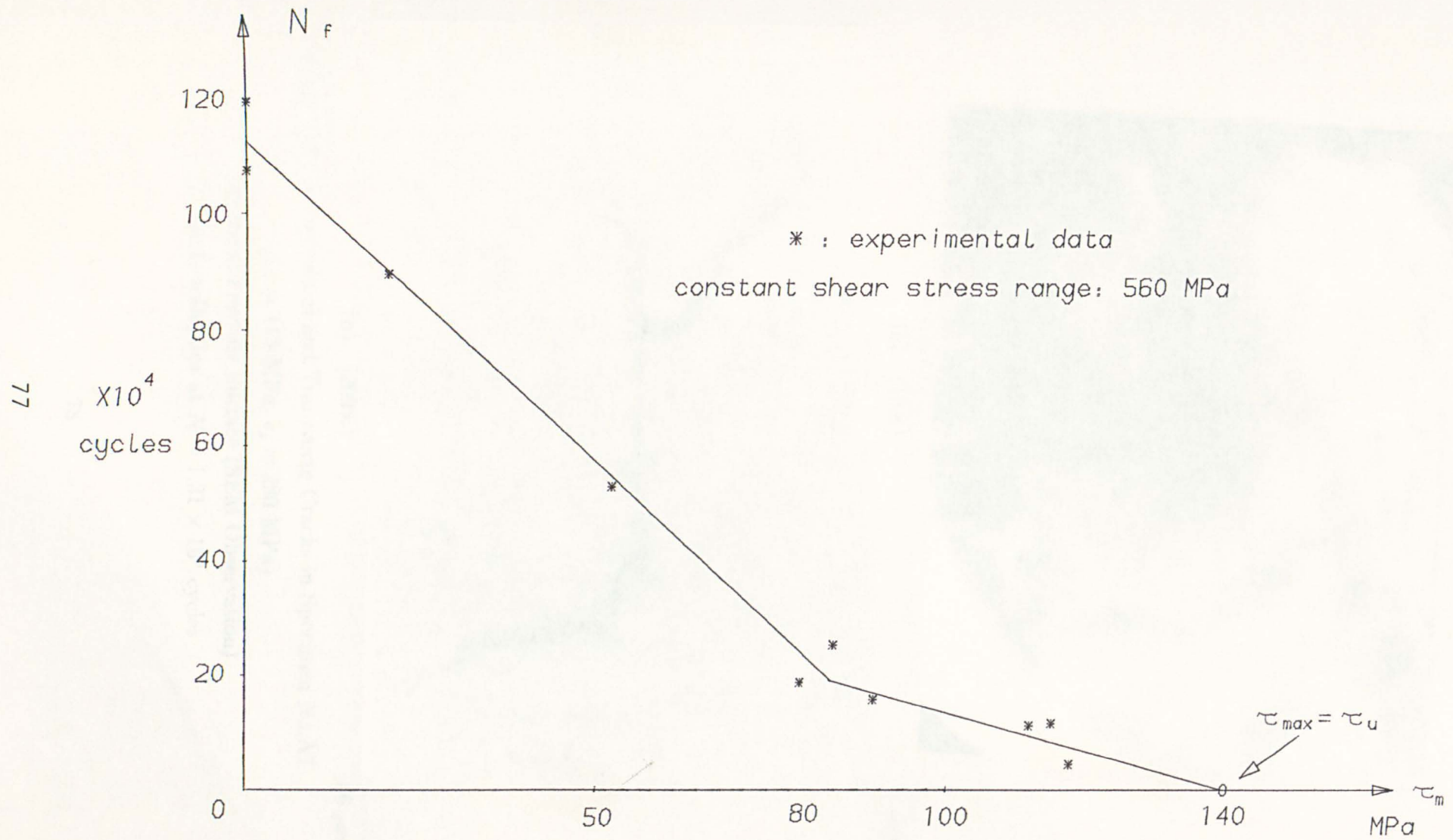
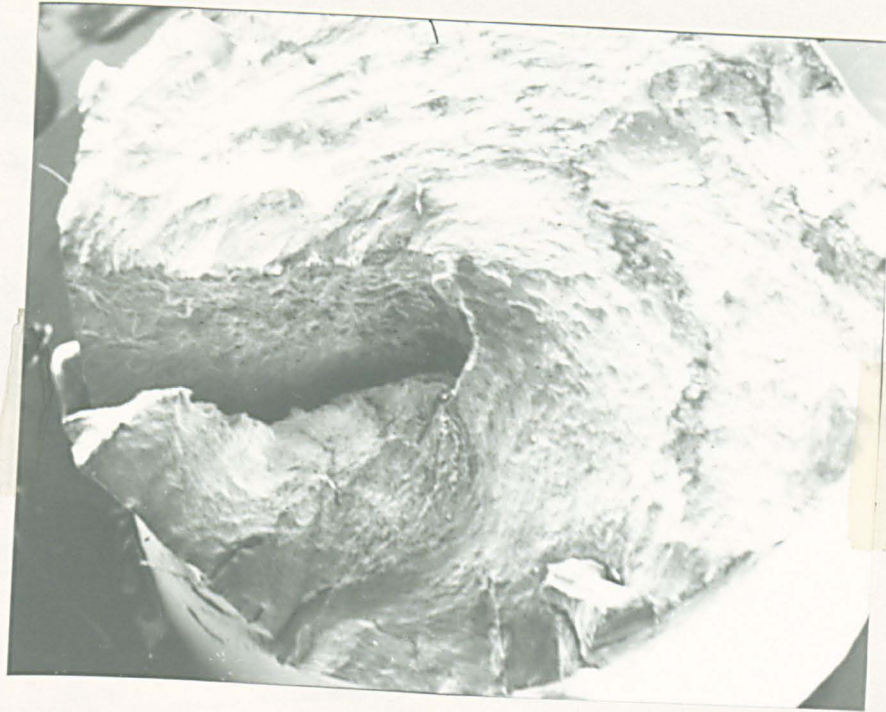
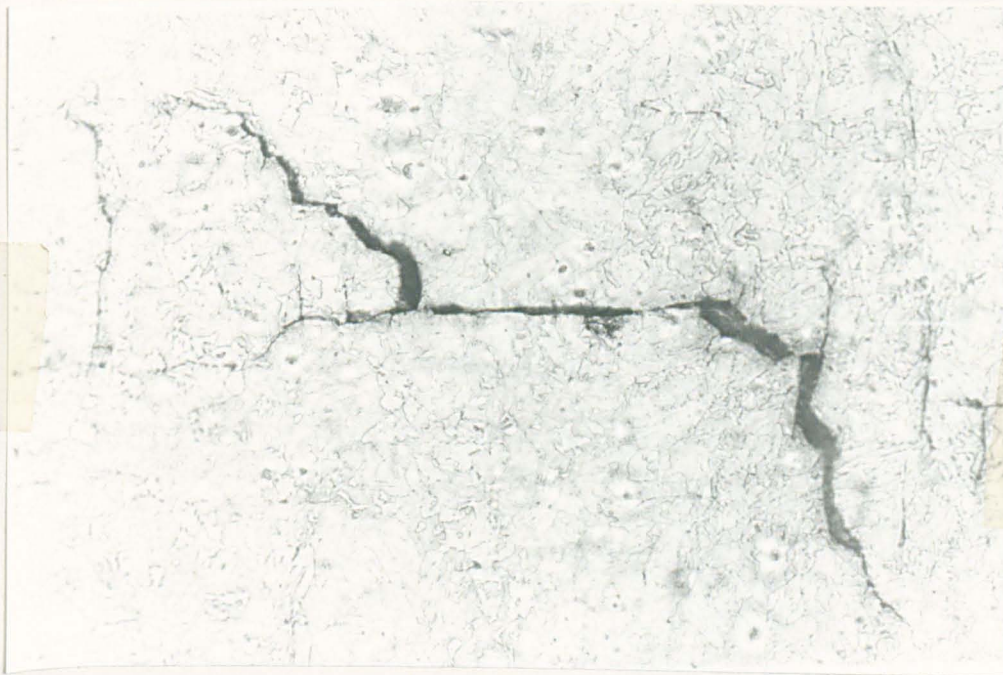


Fig.3.5 Effect of Mean Shear Stress on Torsional Fatigue Life



(a) (10×)

1 mm



(b) (200×)

50 μm

Figure 3.6 Longitudinal and Transverse Cracks in Specimen No.A7

($\tau_m = 115$ MPa, $\tau_a = 280$ MPa)

(a) Final Fracture Surface (SEM Observation)

(b) Surface Replica at $N = 1.31 \times 10^5$ cycles

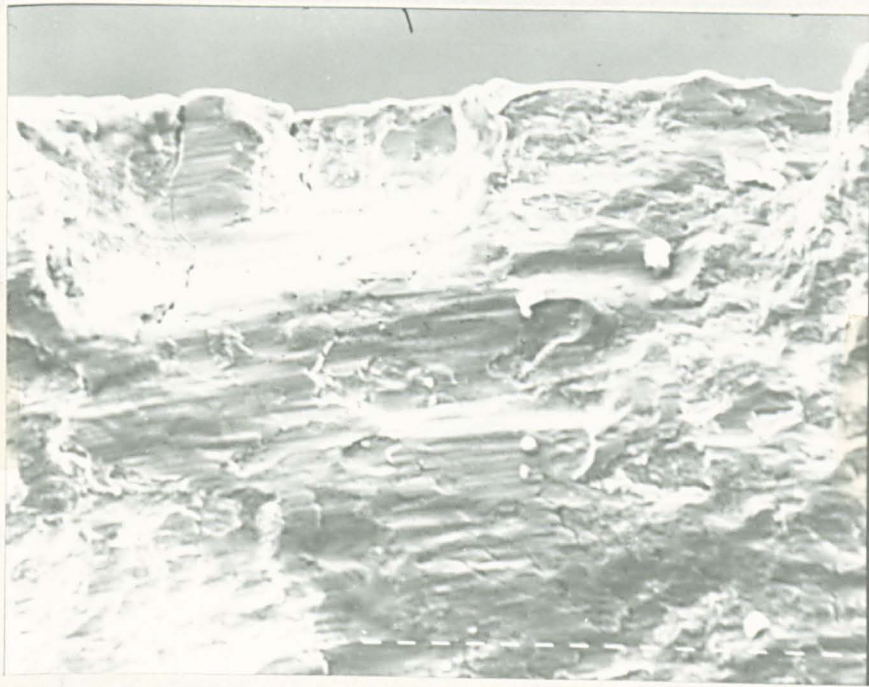


Fig.3.7 SEM Photograph of Specimen No.A2 ($\tau_m = 118$ MPa, $\tau_a = 293$ MPa)

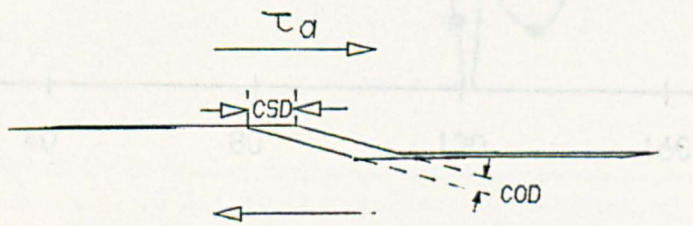
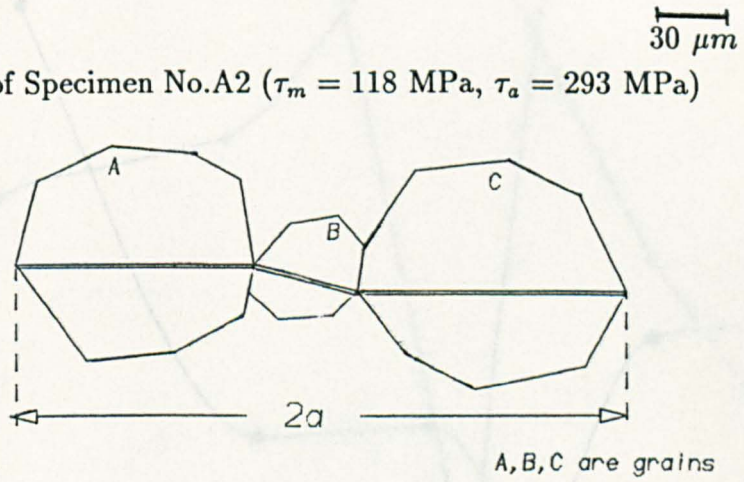


Fig. 3.9 Crack Growth Data of Tests No. 15 & 11

Fig.3.8 Schematic Drawing of the Deflection of Stage I Crack in Torsion

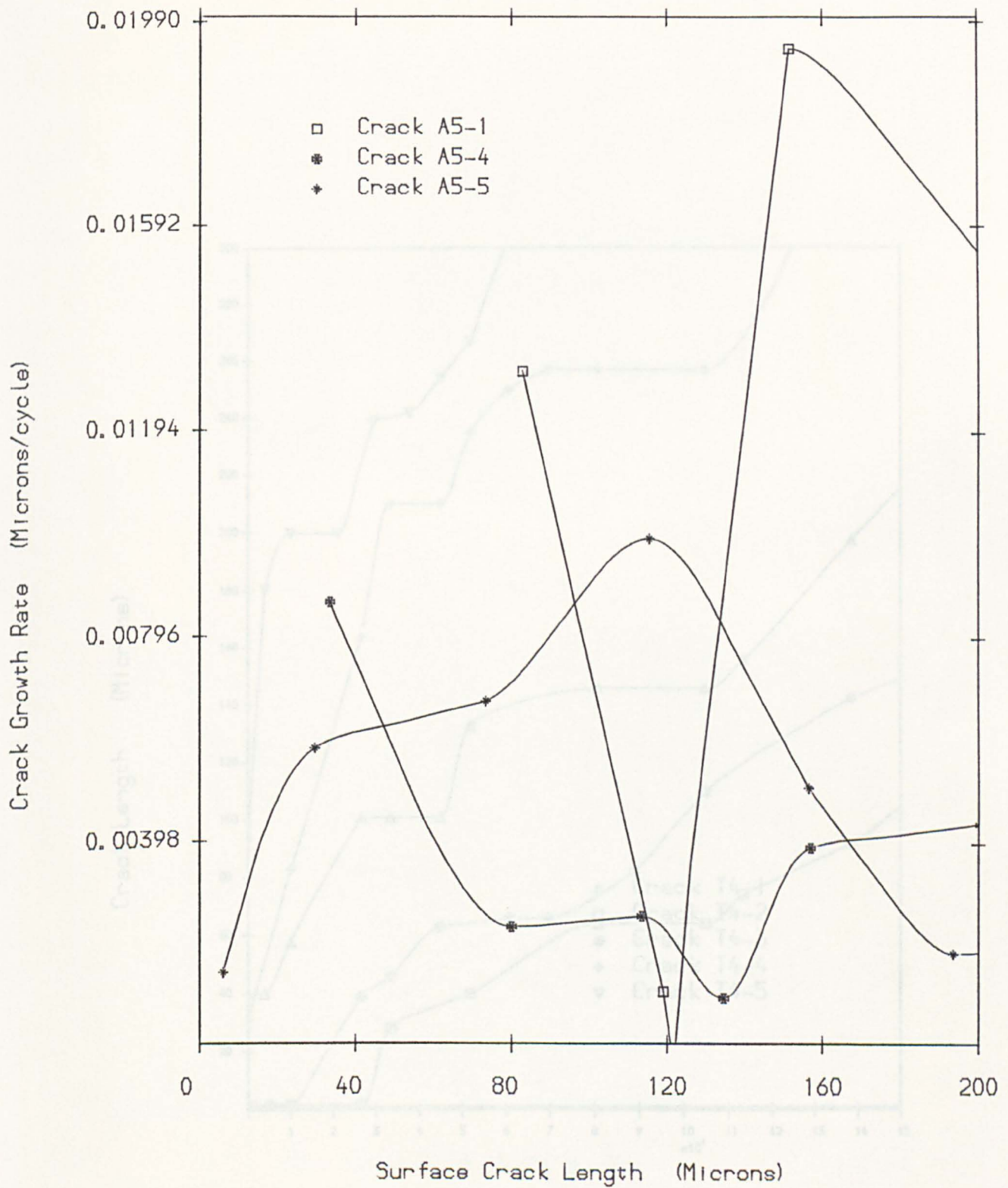


Fig. 3.9 Crack Growth Data of Tests No. A5 & A1

Fig. 3.10 Different Cracks in Specimen A4 ($\tau_m = 90$ MPa, $\tau_c = 200$ MPa) Showing Crack Retardation at Various Crack Lengths

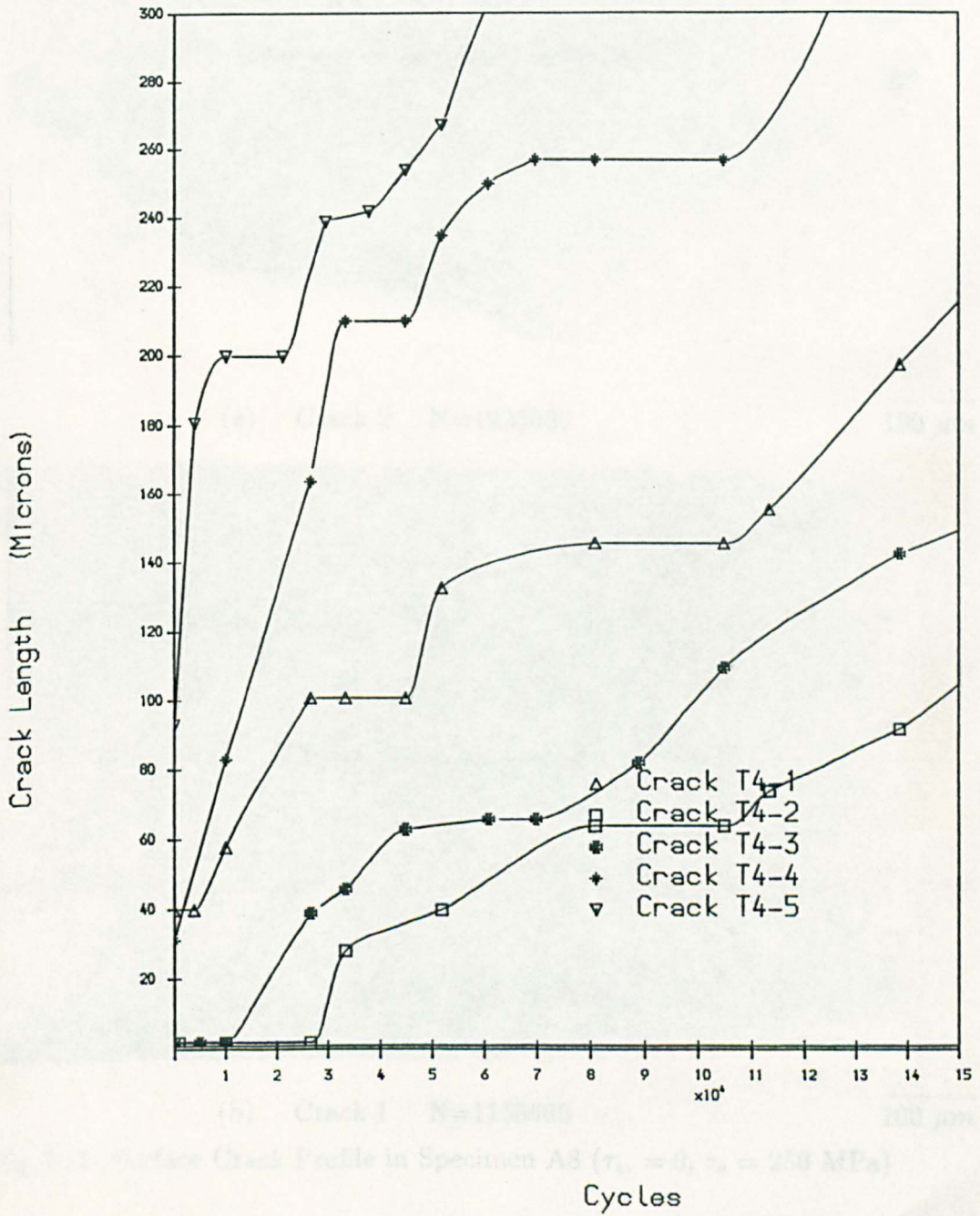
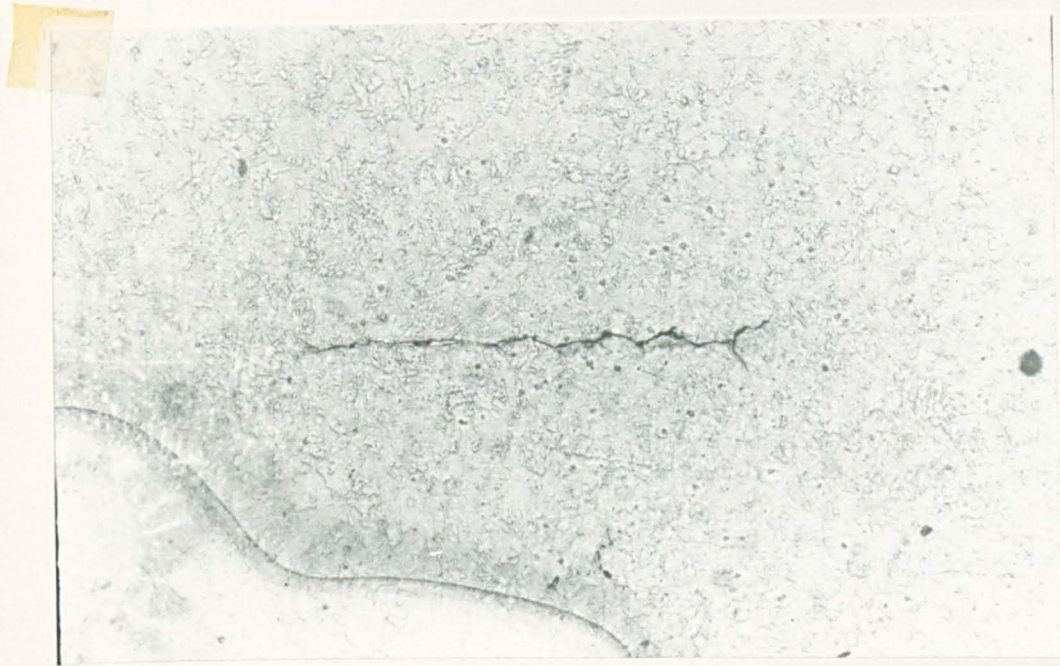
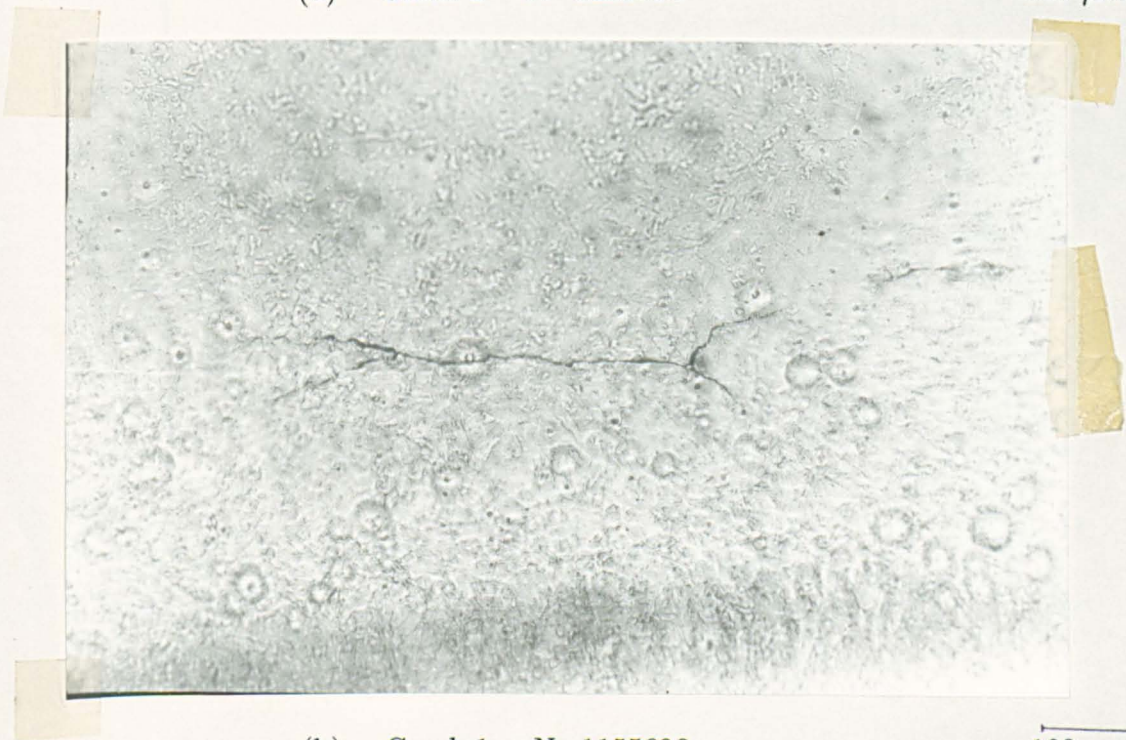


Fig.3.10 Different Cracks in Specimen A4 ($\tau_m = 90$ MPa, $\tau_a = 280$ MPa) Showing Crack Retardation at Various Crack Length



(a) Crack 2 N=1225030

100 μm



(b) Crack 1 N=1155600

100 μm

Fig.3.11 Surface Crack Profile in Specimen A8 ($\tau_m = 0$, $\tau_a = 280$ MPa)

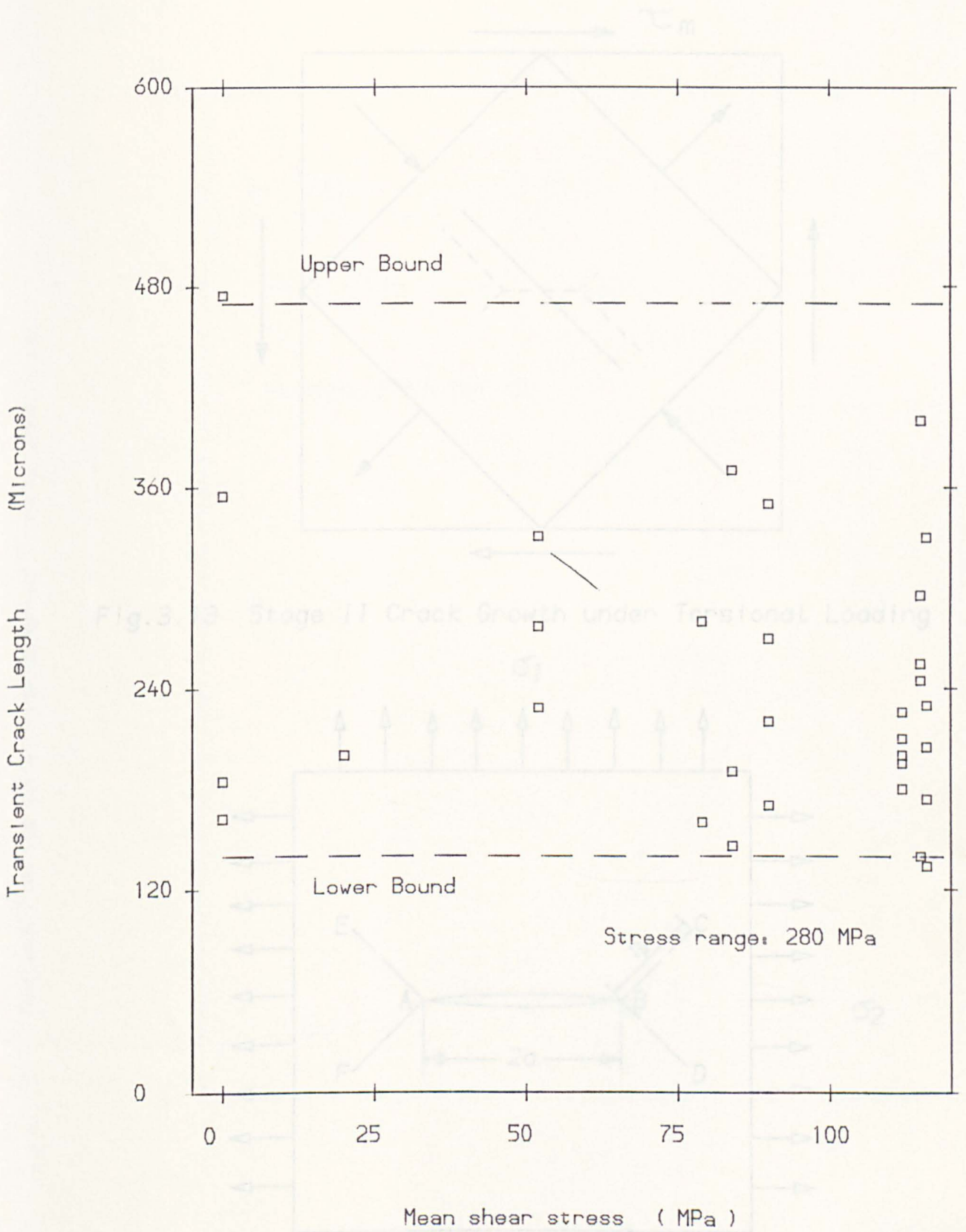


Fig.3.12 Effect of Mean Shear Stress on the Crack Length at Transition between Stage I and Stage II Growth

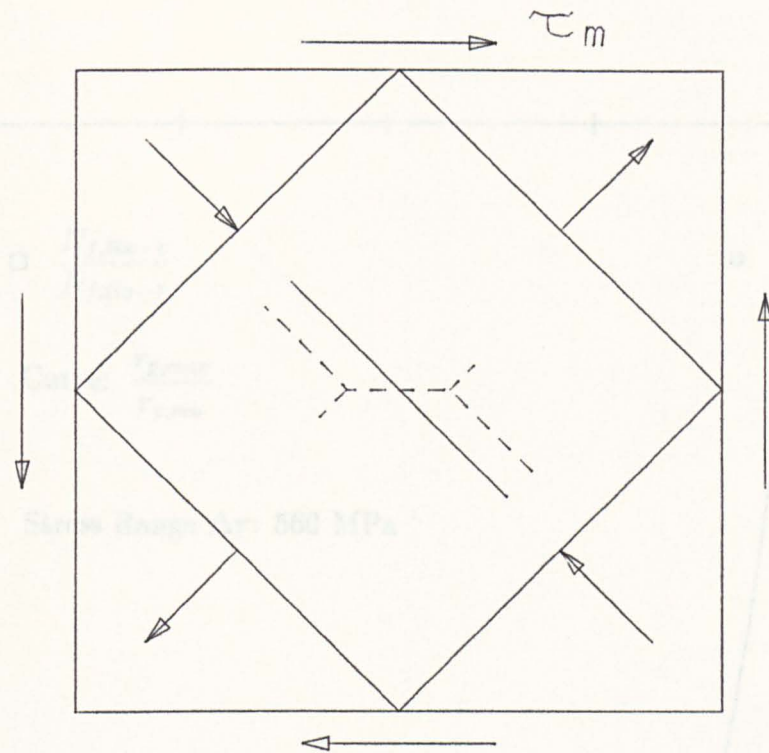


Fig.3.13 Stage II Crack Growth under Torsional Loading

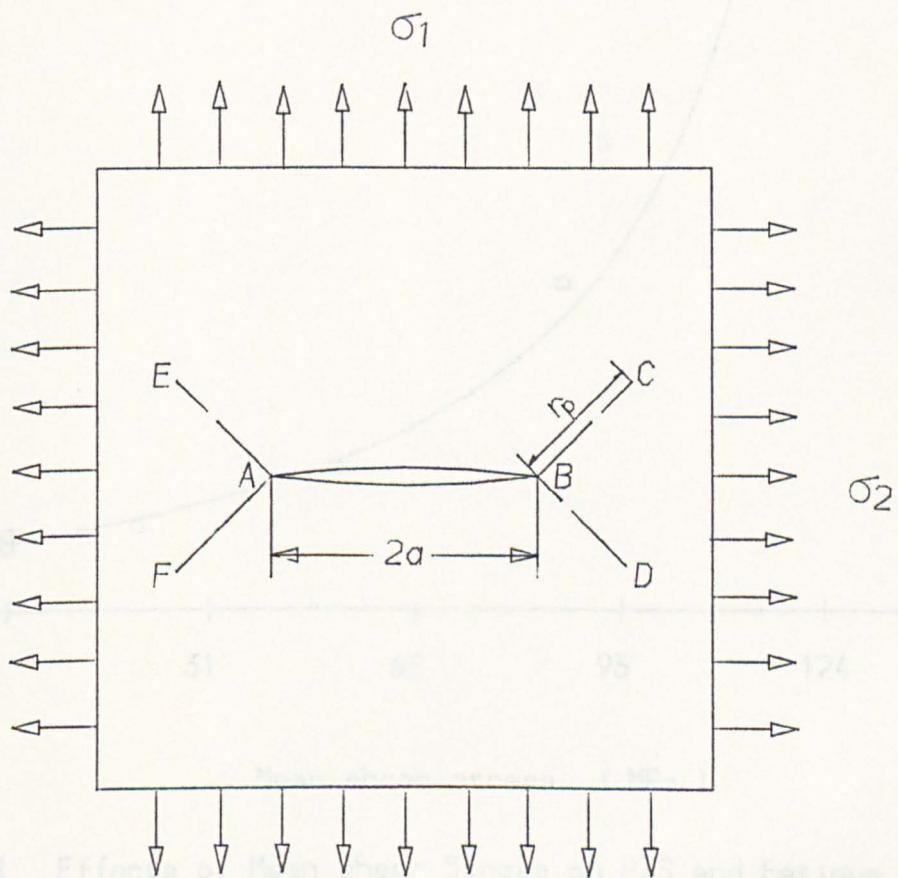


Fig.3.14 Elastic-Plastic Crack Loading for BCS Analysis

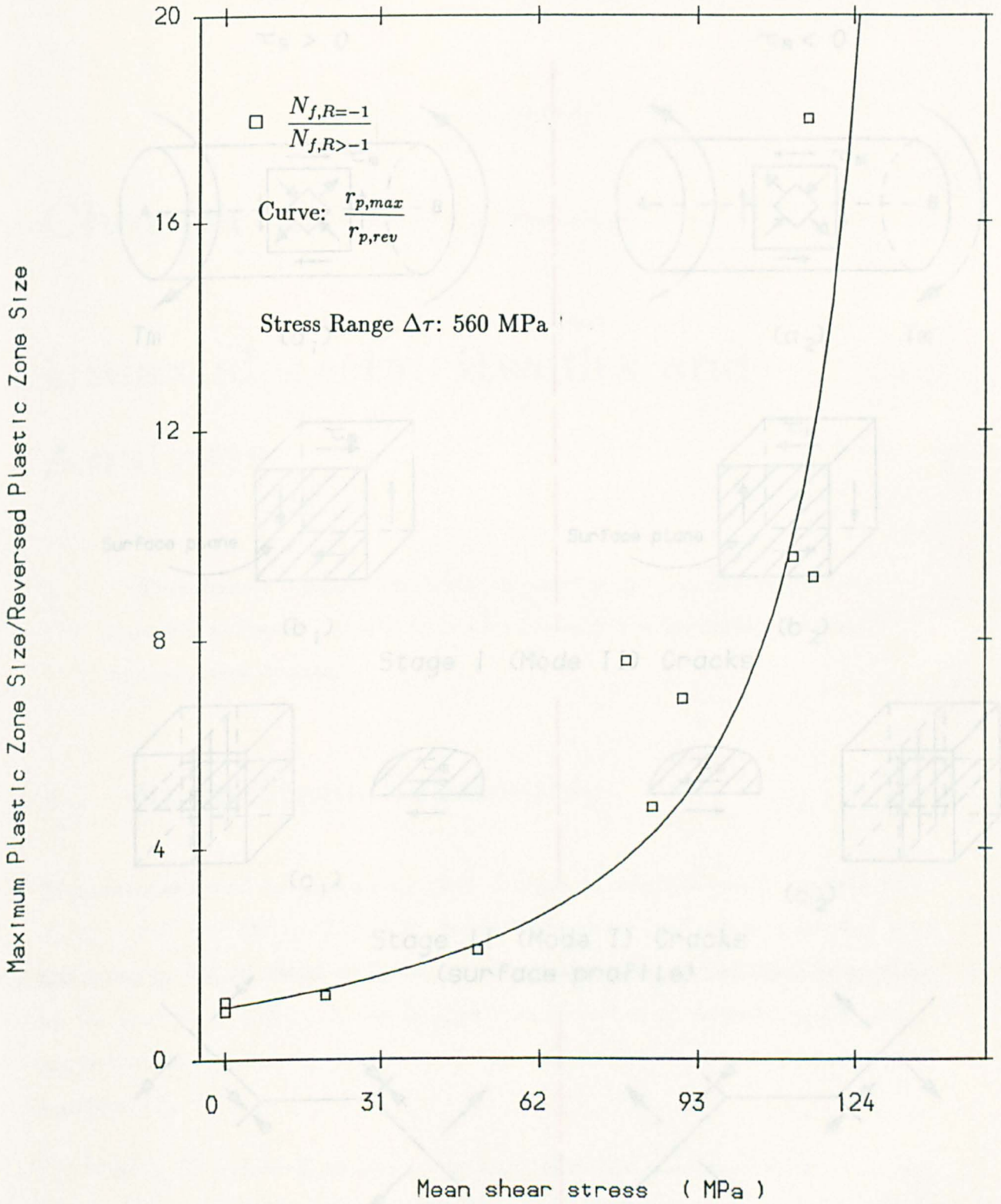


Fig. 3.15 Effects of Mean Shear Stress on PZS and Fatigue Life

Fig. 3.16 Effect of Mean Shear Stress on Fatigue Crack Growth Under Torsion

Case 1

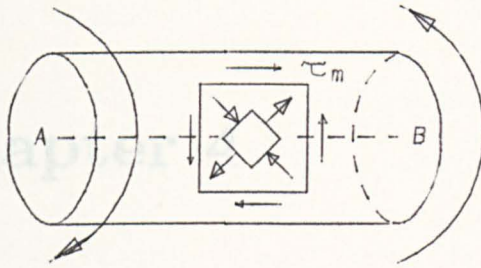
$$T_m > 0$$

$$\tau_m > 0$$

Case 2

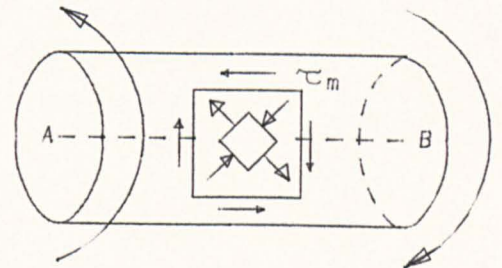
$$T_m < 0$$

$$\tau_m < 0$$



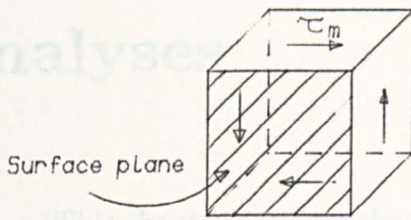
T_m

(a₁)

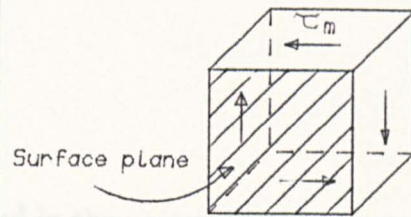


T_m

(a₂)

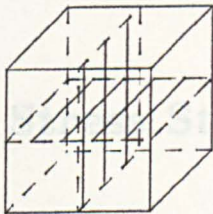


(b₁)

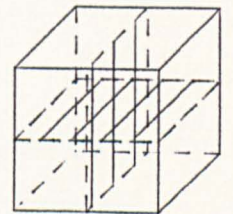
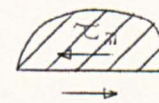
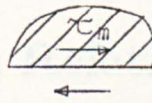


(b₂)

Stage I (Mode II) Cracks

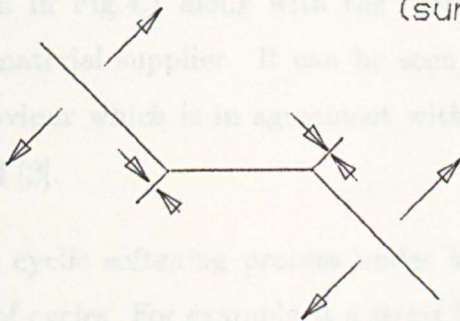


(c₁)

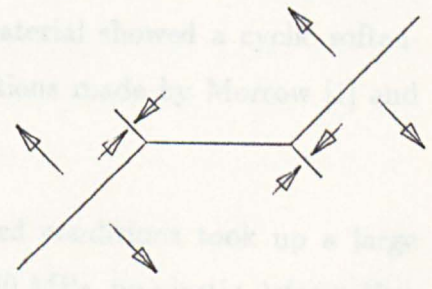


(c₂)

Stage II (Mode I) Cracks
(surface profile)



(d₁)



(d₂)

Fig.3.16 Effect of Mean Shear Stress on Fatigue Crack Growth Under Torsion

Chapter 4

Uniaxial Tests: Results and Analyses

This chapter presents the results obtained in the uniaxial fatigue tests and some analyses. Uniaxial tests were conducted under various alternating and mean stresses.

4.1 Stress Strain Relationship

The material tested exhibits a high yield strength to ultimate tensile strength ratio, $\sigma_y/\sigma_u = 0.85$ (see Section 2.1). The results of the strain- and stress- controlled tests are given in Fig.4.1 along with the monotonic stress-strain relationship provided by the material supplier. It can be seen that the material showed a cyclic softening behaviour which is in agreement with the predictions made by Morrow [1] and Landgraf [2].

The cyclic softening process under load-controlled conditions took up a large number of cycles. For example at a stress level $\sigma_a = 600$ MPa, no plastic deformation could be detected until $N = 120$ cycles. Fig.4.2 shows the resulting stress range

and the saturated plastic strain range plotted on a logarithmic scale. A best fit relationship to the data is given by the following,

$$\Delta\sigma = 1988.0 (\Delta\epsilon_p)^{0.075} \quad (4.1)$$

where stress is in MPa. The cyclic strain range can be expressed as

$$\Delta\epsilon = \frac{\Delta\sigma}{E} + \left(\frac{\Delta\sigma}{1988}\right)^{13.33} \quad (4.2)$$

where $E = 210$ GPa.

The effect of mean stress on the cyclic stress–strain relationship is difficult to assess, due to the ratcheting induced by a mean stress and the limit of the experimental technique in measuring diminutive plastic strain, especially in the case of low stress ranges. In a constant stress range test, the change in cyclic plastic strain would be too small to be detected by routine techniques if a low mean stress (tensile or compressive) is superimposed. However if a high mean stress is active, a large amount of cyclic creep strain would be introduced, which might possibly be of the same order as that of the cyclic plastic strain amplitude. One example is from test No.A39 ($\sigma_a = 280$ MPa, $\sigma_m = 504$ MPa) and failure was due to ratcheting rather than fatigue.

As discussed in Section 3.1, the mean stress could affect the cyclic plastic deformation behaviour. The hysteresis loop would not only be shifted in the direction of mean stress, but its width will also be increased. In terms of the fatigue process, plasticity localization is one of most important phases which control the birth of early cracks. Such an effect can be related to the resistance of materials to the yielding. In a monotonic loading mode, the yield stress of the material characterises the materials' maximum resistance to yielding whereas for cyclic loading, the fatigue limit at zero mean stress characterises the maximum stress amplitude below which no significant plasticity localization would occur. When a mean stress is active, the alternating stress level required for plasticity localization decreases as a result of an increase in the maximum stress level in a cycle (see also Chapter 3).

4.2 Fully Reversed Uniaxial Fatigue Tests

4.2.1 Conventional fatigue results

Fig.4.3a is the $S - N$ curve obtained under load- controlled conditions. As mentioned in Section 2.3, failure was defined as the instant of rupture. The best fit relationship as shown in Fig.4.3a is,

$$\Delta\sigma N_f^{0.051} = 1815 \quad (4.3)$$

where N_f is the number of cycles to failure. Here the effect of test frequency (see Section 2.3) and the error between different test machines are neglected. In terms of plastic strain, the Coffin-Manson relationship for the present material can be expressed as,

$$\Delta\epsilon_p N_f^{0.68} = 0.297 \quad (4.4)$$

Fig.4.3b presents the experimental data together with the above equation.

The application of the Coffin-Manson relationship to high cycle fatigue, however, is doubtful, since in the low-stress high-cycle fatigue regime, the macroscopic plastic strain is almost negligible comparing with the total strain and is difficult to be accurately measured.

The failure of one test carried out at high stress level ($\sigma_a = 650$ MPa) showed a mixture of fatigue and ratcheting failure, which may be ascribed to the following reasons:

1. Quasi-static failure mode (high $\Delta\sigma$).
2. The slight stress concentration ($K_t = 1.04$) at the minimum section of the hour glass specimen could lead to a large degree of plasticity localization at the minimum section.

From the previous study, this stress level ($\sigma_a = 650$ MPa) is approximately the cyclic yield stress level ($\epsilon_{p,a} = 0.2\%$). Examination of the replicas revealed that only a few cracks and a large number of shear bands were initiated at $N = 200$ cycles, while at $N = 550$ cycles a high density of short cracks were formed. But all cracks were of lengths less than $70 \mu m$, see Fig.4.4. Final failure happened within a further 50 cycles as a result of the increase in net section stress (due to a reduction in net section area) and coalescence of short cracks.

Fatigue results are presented in Table 4.1. The results from the specimens whose final cooling rate was $10^\circ C$ per minute are presented in Table 4.2.

4.2.2 Crack growth data

Crack growth results for four different stress levels ($\sigma_a = 460$ MPa, 500 MPa, 550 MPa and 600 MPa) are presented in Figs.4.5 to 4.8. Initial crack length is taken as the average surface roughness of $2 \mu m$, the roughness level could be produced by slight etching in the present work.

Cracks less than $20 \mu m$ were very difficult to measure, especially when they were obscured by other microstructural features. Therefore the determination of the earliest stages of cracks by the present measurement technique was not accurate. The criterion used in the present work is based on the change in the contrast on the replicas between the 'crack-like' feature and its surrounding microstructure. For instance, the 'future-to-be' crack would become more dark than its vicinity in comparison to the previous replication stage. Such changes, which resulted from an increase of crack length and depth, is constrained to a very small region (about $70 \mu m$ in diameter) and is moderately independent of the overall impression of replicas.

Examinations of the replicas revealed that initial cracks (about $50 \mu m$ in size) were inclined at any angle between 0° to 45° to the loading direction. This is understandable if the plane of crack growth is inclined at 45° to the direction of applied

stress, irrespective of the orientation of the surface crack. This has been confirmed by SEM observations in the present work.

From the crack growth results, it can be seen that once cracks have grown to a clearly detectable stage, they rarely show any significant slowing down in growth rate. This shows that for the present material, the dominant microstructural barrier to fatigue crack growth is the first grain boundary, which dictates the fatigue resistance of this material. Here it is worth pointing out that cracks were found originating from grain boundaries, packet boundaries and matrix material. Therefore the major effect of microstructures was due to the mis-orientation between different grains or bundles and it is the orientation factor rather than the absolute boundary strength that causes the temporary arrest of cracks at boundaries.

Some portion of fatigue life was spent before any crack could be detected. For example, 25%, 10%, 14%, 20%, and 8% of fatigue life elapsed before cracks became detectable for tests with $\sigma_a = 500$ MPa, $\sigma_a = 550$ MPa, $\sigma_a = 600$ MPa, and $\sigma_a = 650$ MPa respectively. This phenomenon is partially attributable to the fine grain size and the completely bainitic structure and partially to the cyclic softening behaviour. The plasticity localization can require a number of cycles to complete after which time a specific dislocation structure is formed [4]. One example is that at a high stress level ($\sigma_a = 600$ MPa); no cyclic plasticity was detected until $N = 80$ cycles. Initiation of cracks is known to be due to the creation of plasticity, consequently for cyclic softening materials, fatigue undergoes a transient from the high cycle fatigue stage to the low cycle fatigue stage during the continuation of load cycling. Fig.4.9 shows the effect of such cyclic softening. Therefore, cyclic softening tends to be more dangerous than cyclic hardening as more plasticity can be produced for a constant load range. However cyclic softening is more difficult to detect especially at the early stage of fatigue.

The end of cyclic softening or the localization of plasticity is defined here (Fig.4.9) as when the cyclic plastic strain range becomes greater than one third of the saturated cyclic plastic strain range. The end of stage I growth is defined as when the length of

the longest crack reaches 40 μm . Fig.4.9 suggests that the data for the end of cyclic softening and the end of stage I growth appear to have the same slope as that of the final failure $S - N$ curve. The end of the plasticity localization and the end of stage I growth can be expressed respectively as,

$$N_0 = \left(\frac{782}{\sigma_a}\right)^{19.61} \quad (4.5)$$

$$N_1 = \left(\frac{867}{\sigma_a}\right)^{19.61} \quad (4.6)$$

As presented in Section 4.2.1, the relationship between fatigue life and stress amplitude is,

$$N_f = \left(\frac{908}{\sigma_a}\right)^{19.61} \quad (4.7)$$

The total percentages of the time spent in plasticity localization and stage I crack initiation are easy to obtain,

$$\frac{N_0}{N_f} = \left(\frac{782}{908}\right)^{19.61} = 5.3 \quad (\text{percentage}) \quad (4.8)$$

$$\frac{N_1}{N_f} = \left(\frac{867}{908}\right)^{19.61} = 41.3 \quad (\text{percentage}) \quad (4.9)$$

It can be seen here that a large proportion (over forty per cent) of fatigue lifetime was spent in initiating and propagating very short cracks (less than 40 microns). Compared to the work by Hobson [5] on 0.4C steel, in which short cracks were found to have initiated in the first few cycles (less than 5% of fatigue life time), this alloy steel shows a stronger resistance to crack initiation and initial crack growth than the ferrite-pearlite material.

No significant coalescence of short cracks was found except in the low cycle fatigue regime ($N_f < 4000$ cycles). At low stress levels, fatigue failures were mainly due to the initiation and propagation of a dominant crack which might join with other cracks at a the very late stage close to final failure. In this case, the coalescence had no substantial effect on fatigue life.

4.3 High Cycle Unsymmetrical Uniaxial Fatigue Tests

4.3.1 Conventional fatigue results

Most of the tests were conducted within the high cycle fatigue regime, except that a few tests had slight excursions into the low cycle regime. Fatigue $S-N$ curves for different mean stress levels are presented in Fig.4.10, which suggests that mean tensile stress and mean compressive stress have disparate effects. The region in which LEFM is valid will be discussed in Section 6.1.

Mean tensile stress

Tensile mean stress decreased lifetime and reduced the fatigue endurance (for a constant mean stress level) from 444 MPa to 270 MPa when a 500 MPa mean tensile stress was superimposed. To rationalise the effects of mean stress, a $R-M$ diagram is constructed for the fatigue endurance and finite fatigue life at $N_f = 2 \times 10^5$ as shown in Fig.4.11a. The fatigue endurances for various mean stresses are obtained by extrapolating $S-N$ curves to $N_f = 2 \times 10^6$ as there is no significant change in the slope of $S-N$ curves in the high cycle regime.

Asymmetrical fatigue is likely to be linked with ratcheting failure as there is no clear-cut demarcation between these two types of failure. In the present work, $\sigma_a = 650$ MPa characterizes the boundary between fatigue failure and ratcheting failure under load control for $R = -1$. With the increase of mean stress, the alternating stress level required to induce ratcheting failure should drop off to zero when a mean stress of 840 MPa is superimposed; the maximum stress level of 840 MPa (or the room temperature creep strength) should be used here which is equal to the UTS of the material. A simple linear relationship is adopted here to evaluate the maximum

stress level,

$$\begin{aligned}\sigma_{max}^t &= 650 + C \cdot \sigma_m = 650 + \frac{840 - 650}{840} \cdot \sigma_m \\ &= 650 + 0.226 \sigma_m\end{aligned}\tag{4.10}$$

hence the alternating stress is,

$$\sigma_a^t = \sigma_{max}^t - \sigma_m = 650 - 0.774 \sigma_m\tag{4.11}$$

The curve representing the possibility of ratcheting together with Goodman curve, Gerber's parabola and a constant SWT (Smith, Waston and Topper [6]) parameter curve are drawn in Fig.4.11a.

It is worth pointing out that (i) mean stress is still effective beyond the point where the maximum stress level exceeds the yield stress since the fatigue endurance is further reduced. (ii) no failure can occur even when the maximum stress is higher than the yield stress provided the alternating stress is below a certain level, which means that a substantial alternating stress is necessary to cause fatigue failure even under high mean stress. However, as the maximum stress level in a cycle approaches the ultimate tensile strength, additional ratcheting might dominate the deterioration of the material. Thereafter it is ratcheting failure rather than fatigue failure that occurs for extremely high mean stress in the present case.

It can also be seen that the Goodman line is too conservative and Gerber's parabola provides a non- conservative prediction of the effect of mean stress. The effect of mean stress almost follows a linear relationship up to the highest allowable mean stress. For the fatigue endurance, the two best fit curves for endurance of 2×10^5 cycles and 2×10^6 cycles are,

$$\sigma_a = 503 - 0.36 \sigma_m \quad (\text{MPa}) \quad \text{for } N_f = 2 \times 10^5\tag{4.12}$$

$$\sigma_a = 441 - 0.30 \sigma_m \quad (\text{MPa}) \quad \text{for } N_f = 2 \times 10^6\tag{4.13}$$

The iso-fatigue life curves are almost parallel to each other in the high cycle regime; see Fig.4.12.

A good correlation between the SWT parameter and the constant fatigue life has been observed over the whole range of tensile mean stress. The constant SWT parameter curve lies between the Goodman curve and Gerber's parabola except when the mean stress level approaches the U.T.S of the material. Good correlations have also been reported in other references, e.g. [6] [7]. However the disadvantage of this approach is that it lacks physical meaning, especially in regard to the mechanism of fatigue crack propagation processes and the non-propagation (fatigue limit) condition. Additionally, the following discussions demonstrate that this approach is incapable of predicting the effect of compressive mean stress.

Compressive mean stress

While it is evident that mean tensile stress reduces the fatigue lives and fatigue endurance, compressive mean stress is frequently thought to be beneficial and tends to extend fatigue lives and raise the fatigue endurance. However, the present results show that compressive mean stress (less than 200 MPa in magnitude) has no recognizable benefit to both fatigue life and the fatigue endurance. For high values of compressive mean stress (e.g. great than 200 MPa in magnitude), there is tendency to change the failure mode from fatigue to ratcheting and to reduce fatigue lives (test No.A50). Fig.4.10 shows that the $S - N$ curves for compressive mean stresses almost retrace that for zero mean stress.

Fig.4.11b presents the effects of compressive mean stress upon the fatigue endurance and finite fatigue life. Obviously the Goodman relationship is much more non- conservative (for tensile mean stress, it is conservative!), and so is the constant SWT parameter criterion. Gerber's parabola seems to fit the experimental data quite well. However, this criterion cannot explain the differences in the effects of mean stresses, especially the marked transition at zero mean stress.

The Goodman Diagram is frequently used by engineers and is interpreted such that for a small negative mean stress, σ_a increases for a given life time, which is not

unreasonable since the effective value of the cyclic stress range $2\sigma_a$ is reduced due to crack closure for a mode I (stage II) crack. It is understandable therefore that compressive mean stress might cause longer fatigue lives and give a higher fatigue endurance. However, for some materials and certain surface finishes, the fatigue endurance and the majority of life time are not controlled by stage II mode I crack growth. In these cases, the above assumption or conventional extrapolation may be inappropriate since the growth of stage I cracks is governed by the shear stress or shear strain: both amplitude and maximum level, see Section 3.3. The normal stress or strain only modifies the crack growth rate and such modification is relatively small for a low compressive mean stress.

In addition, the maximum shear stress level will increase with the superposition of compressive mean stress (mean shear stress does not exhibit any direction discrimination for mode II crack growth, see Section 3.6), which might cancel the beneficial effect of a compressive mean normal stress acting upon the crack plane.

Now consider the stress system acting upon a stage I crack, which is inclined 45° to loading axis; see also Section 1.4. Here Case 1, Case 2 and Case 3 denote the cases of tensile mean stress, zero mean stress and compressive mean stress, respectively.

$$\Delta\tau_n = \frac{1}{2}(\sigma_{max} - \sigma_{min}) \quad (4.14)$$

$$\tau_{n,max} = \frac{1}{2}\sigma_{max} \quad (4.15)$$

$$\Delta\sigma_n = \frac{1}{2}(\sigma_{max} - \sigma_{min}) \quad (4.16)$$

$$\sigma_{n,max} = \frac{1}{2}\sigma_{max} \quad (4.17)$$

It is clear that when the applied stress range $\sigma_{max} - \sigma_{min}$ is maintained constant and a tensile mean stress is superimposed, the differences between Case 1 and Case 2 are in the parameters $\sigma_{n,max}$ and $\tau_{n,max}$,

$$\sigma_{n,max} \text{ Case 1} > \sigma_{n,max} \text{ Case 2} \quad (4.18)$$

$$\tau_{n,max} \text{ Case 1} > \tau_{n,max} \text{ Case 2} \quad (4.19)$$

these two effects are both detrimental and tend to enhance the fatigue crack growth. Therefore the effect of mean tensile stress is that it always tends to reduce fatigue lives and the fatigue limit.

However when a compressive mean stress is active while the applied stress range $\sigma_{max} - \sigma_{min}$ is maintained constant, the differences between Case 2 and Case 3 are in the parameters $\sigma_{n,max}$ and $\tau_{n,max}$,

$$\sigma_{n,max} \text{ Case 2} > \sigma_{n,max} \text{ Case 3} \quad (4.20)$$

$$\tau_{n,max} \text{ Case 2} < \tau_{n,max} \text{ Case 3} \quad (4.21)$$

these two effects can be equalised if the fatigue crack growth in the material is equally sensitive to the effect of maximum shear stress and maximum tensile stress. For the present material, torsional tests proved that mean shear stress does enhance short crack growth (see Section 3.3). The counteraction of these two opposing effects could lead to an insensitivity to compressive mean stress. This is why for the present material compressive mean stress has no beneficial effect on fatigue life and the fatigue endurance.

The maximum shear stress effect will intensify when mean stress (tensile or compressive) increases in magnitude. In the extremity, ratcheting failure or creep failure can occur when the maximum shear stress approaches the ultimate shear strength and the dominant crack is in mode II with fracture surface inclined at 45° . The boundary between fatigue failure and ratcheting failure in the case of compressive mean stress can be expressed as,

$$\sigma_a^t = 650 - 0.774 |\sigma_m| \quad (4.22)$$

The competition between the maximum shear stress and maximum tensile stress will determine the influence of compressive mean stress. If materials show different behaviour towards the sensitivities of maximum shear stress and normal stress, or

the fatigue lives are dominated by stage II (mode I) crack growth, compressive mean stress may be beneficial and cause longer fatigue lives.

An overall diagram showing the effects of tensile and compressive mean stresses is presented as Fig.4.12.

A more detailed analysis of the effect of mean compressive stress will be presented in Chapter 6 together with a new model proposed in the present work in relation to crack growth mode.

4.3.2 Fractographic studies

A Philip 500 Scanning Electron Microscopy was used to make fractographical observations. Seven specimens were selected from tests of $R = -1.7, -1.0, -0.28, 0.04$ and 0.25 . Generally cracks started from the surface without any observable surface flaws such as inclusions, which confirms the conclusion drawn from the observation on replicas. Three distinct regions on fracture surfaces existed for all stress ratios: initial crystallographic growth, stage II (mode I) crack growth and final slant fracture.

Stage I growth

Fig.4.13(a) shows the surfaces of initial crack growth for fully reversed ($R = -1.0$) high cycle fatigue ($N_f = 2.2 \times 10^5$). Crack growth is in the shear mode with the crack plane inclined at about 30° to specimen axis. Some evidence of crack closure could also be found on crack surfaces, which was due to the deformation induced by the contact between crack faces during cyclic loading. Part of the surfaces had been smeared and squashed. Referring to the observations on replicas in Section 2.4.3 that cracks did not close at zero stress level, it can be concluded that crack closure happens at a stress level between zero and the minimum stress level,

$$\sigma_{min} \leq \sigma_{op} \leq 0 \quad (4.23)$$

With the increase of stress ratio, less indication of crack closure was observed. Fig.4.13(b), (c), (d) show the appearance of the fracture surfaces at stress ratios of -0.25 , 0.04 and 0.25 respectively (high cycle fatigue). For a stress ratio equal to zero, no indication of crack closure was spotted and neither was there for the case of the highest stress ratio 0.25 . In these cases stage I crack growth shows a highly crystallographic pattern and the small facets produced by the change in crack growth path were well preserved.

Clearly short cracks under fully reversed loading do in fact close up at stress levels above the minimum stress. Mean uniaxial tensile stress greatly affects crack closure stress level and reduces closure under asymmetrical loading.

The fracture surfaces for compressive mean stress shown in Fig.4.13(e) ($R = -1.7$) presents a different appearance to those of tensile mean stresses. The Stage I growth phase seems to be more distinct and the length of stage I crack growth appears to be longer than in the cases of zero or positive mean stresses. There are more deviations along crack growth path revealing that extra mean shear stress enhances stage I growth. Evidence of crack closure is more prominent than for high stress ratios and the crystallographic growth feature for stage I growth has been erased by the smearing of crack faces.

Stage II growth

Figure 4.14(a) (b) (c) (d) (e) shows the stage II crack surfaces for stress ratios of -1.0 , -0.28 , 0.04 , 0.25 and -1.7 respectively. Manifestations of crack closure were also found for fully reversed loading. Such phenomena tend to disappear with the increase of the stress ratio. For a zero stress ratio only some smearing marks could be found at the peaks and valleys while the flat areas were found intact. When the stress ratio was further raised, no signs of crack closure were found except in some very limited areas. For example in Fig.4.14(d) a spot of about 5 microns radius was found to be squashed. This poses a different feature for short fatigue cracks as opposed to

long fatigue cracks. As it has been frequently proved that for a zero stress ratio, the closure stress level is well above zero stress level for LEFM type of crack.

The effect of compressive mean stress, as shown in Fig.4.14(e), was easy to observe since much more smearing and squashing between crack faces had occurred. In fact some of the fracture surface was totally deformed rather than just being smeared as in the case of zero mean stress. There were more deviations of crack path all the way to the final failure region. This effect may be ascribed to the fact that the combination of high shear stress amplitude and maximum shear stress enables cracks to grow in the shear mode. Such a stress system can set up a predominant single slip system rather than a multi-slip system thereby facilitating mode II crack growth.

Secondary cracks were also found, as shown in Fig.4.14(a) where ample secondary cracks are seen on the crack growth path, suggesting that at this stage striation formation is not the only mechanism responsible for crack growth, since secondary cracking might also enhance crack growth. Additionally more crack growth might occur due to the combination of the shear mode and secondary cracking. In another words, due to the high ratio of the yield stress to the U.T.S of the material, secondary cracks might have been formed within shear bands in front of the crack tip and it was the rate of the growth and formation of such secondary cracks that controlled the crack growth rate, see also reference [8].

4.3.3 Crack growth results

All fatigue failures under unsymmetrical cycling are due to the propagation of cracks started from surfaces. Figures 4.15 to 4.18 present the crack growth data for different stress ratios, viz $R = -1.7, -0.28, 0.06, 0.25$. More data are presented in Appendix B. Since the fatigue failure mode may be compromised by the ratcheting mode, see Fig.4.12, the experimentally achievable stress ratios ranged from -2.0 to 0.30 , and no crack growth data could be obtained at stress ratio beyond this range.

It can be seen that all the cracks exhibit three phases as in fully reversed fatigue: (i) localization of plasticity, (ii) slowing down from a high speed and (iii) increase of growth rate in proportion to crack length. One interesting feature is that for all high cycle fatigue, the major part of the life time was consumed in the short crack phase (less than 100 microns) of growth. As it has been shown by SEM observations, such short cracks grow predominantly in the shear mode with distinct crystallographic features. It can be concluded that the high cycle fatigue is controlled by the shear deformation of the bulk and that induced by the crack itself. This indicates that the conventional wisdom which states that fatigue life is dominated by cracks growing in mode I, and the associated concepts invoking a crack closure argument to rationalise the stress ratio effect on the fatigue endurance should be re-assessed.

References

1. Morrow, J. D. (1965) Cyclic Plastic Strain Energy and Fatigue of Metals, *ASTM ST 378*, pp.45.
2. Landgraf, R. W. (1970) The Resistance of Metals to Cyclic Deformation, *ASTM STP 467*, pp.3.
3. Tomkins, B. (1968) Fatigue Crack Propagation—An Analysis, *Philosophical Magazine*, 18, 1968, pp.1041.
4. Brown, M. W. and Miller, K. J. (1979) Biaxial Cyclic Deformation Behaviour of Steels, *Fatigue of Engineering Materials and Structures*, Vol.1, pp.93–106.
5. Hobson, P. D. (1985) The Study of Short Fatigue Crack Growth in a Carbon Steel, *Ph.D Thesis*, Sheffield University.
6. Smith, K. N., Watson, P. and Topper, T. M. (1970) A Stress Strain Function for the Fatigue of Metals, *Journal of Materials*, Vol.5, pp.767-787.
7. Koh, S. K. and Stephens, R. I (1990) Mean Stress Effects on Low Cycle Fatigue for a High Strength Steel, to be published in *Fatigue & Fracture of Engineering Material and Structures*.
8. Tomkins, B. (1971) Fatigue Failure in High Strength Metals, *Philosophical Magazine*, 1971, pp.687- 703.

Table 4.1: Uniaxial Fatigue Results (furnace cooled)

Test Number	Minimum Radius (mm)	Stress Amplitude (MPa)	Mean Stress (MPa)	Fatigue Life (cycles)	Test Frequency (Hz)	Stress Ratio
A31	3.627	510	0	1.90×10^5	150	-1
A32	3.625	520	0	2.02×10^5	150	-1
A33	3.630	490	0	2.23×10^5	150	-1
A34	3.633	378	400	2.03×10^5	150	+0.03
A35	3.607	369	407	3.03×10^5	150	+0.05
A36	3.630	358	400	2.02×10^5	150	+0.05
A37	3.644	355	401	6.32×10^5	150	+0.06
A38	3.708	405	232	1.42×10^5	150	-0.27
A39	3.656	280	504	Ratcheting	150	+0.29
A40	3.620	405	228	2.04×10^5	150	-0.28
A41	3.623	600	0	3345	1	-1
A42	3.635	550	0	2.88×10^4	1	-1
A43	3.627	500	0	1.31×10^5	2	-1
A44	3.627	600	0	3571	1	-1
A45	3.623	650	0	600	1	-1
A46	3.630	Cyclic	Stress	Strain	Measurement	
A47	3.736	Cyclic	Stress	Strain	Measurement	
A48	3.638	550	-150	1.60×10^4	1	-1.75
A49	3.638	460	0	2.23×10^5	150	-1
A50	3.628	500	-200	1.12×10^5	2	-2.33
A51	3.653	464	100	3.91×10^5	150	-0.64
A52	3.661	460	0	1.15×10^6	150	-1
A53	3.639	456	0	1.06×10^6	150	-1
A54	3.683	500	-80	1.37×10^5	150	-1.38
A55	3.652	464	-120	8.79×10^5	150	-1.73
A56	3.645	490	-120	2.98×10^5	150	-1.65
A57	3.629	315	471	9.23×10^5	150	+0.20
A58	3.640	310	504	3.73×10^5	150	+0.28
A59	3.655	500	-120	2.16×10^5	150	-1.63
A60	3.639	295	504	8.42×10^5	150	+0.23

Table 4.2: Uniaxial Fatigue Results (Type B heat treatment)

Test Number	Minimum Radius (mm)	Stress Amplitude (MPa)	Mean Stress (MPa)	Fatigue Life (cycles)	Test Frequency (Hz)	Stress Ratio
B12	3.992	360	0	broke at head	150	-1
B15	3.641	340	100	9.72×10^5	150	-0.55
B16	3.984	380	0	broke at head	150	-1
B17	3.983	400	0	broke at head	150	-1
B18	3.989	various	amplitude	—	150	
B19	3.608	389	0	9.52×10^5	150	-1
B20	3.671	315	262	7.02×10^5	150	-0.09
B21	3.654	389	0	9.61×10^5	150	-1
B22	3.636	205	542	Ratcheting	150	0.45
B23	3.680	395	0	3.02×10^5	150	-1
B24	3.700	285	285	3.61×10^5	150	0.0
B25	3.647	286	266	1.32×10^6	150	-0.04
B26	3.609	various	amplitude	—	150	
B27	3.656	280	504	Ratcheting	2	+0.29
B28	3.501	500	0	1.69×10^4	0.33	-1
B29	3.597	various	amplitude	—	150	
B30	3.627	400	0	2.72×10^5	2	-1

Note: Tests B18, B26 and B29 were carried out with the aim to obtain crack growth data for $N_f > 1.0 \times 10^6$, however it turned out to be extremely difficult for this material.

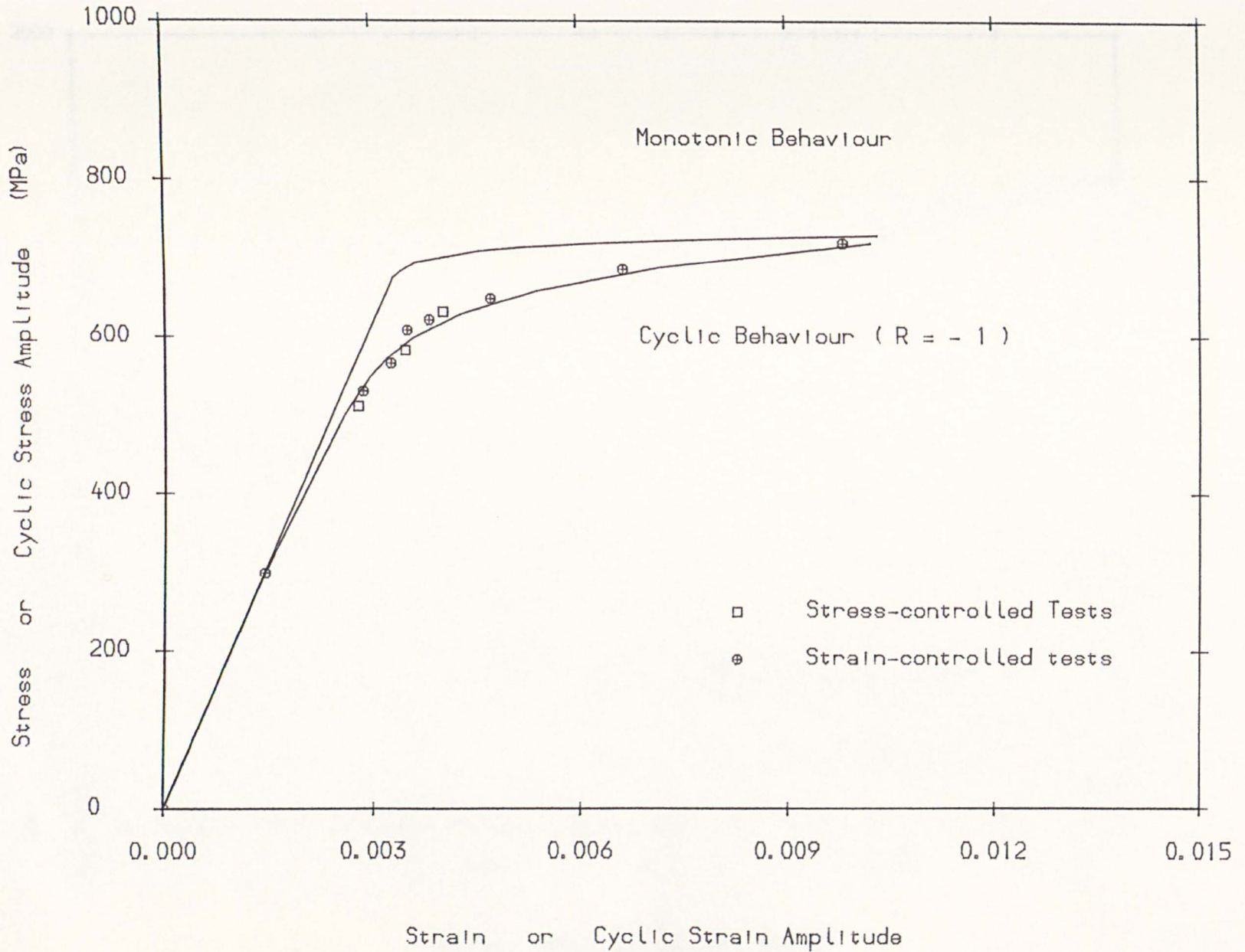


Fig. 4.1 Uniaxial Stress versus Strain

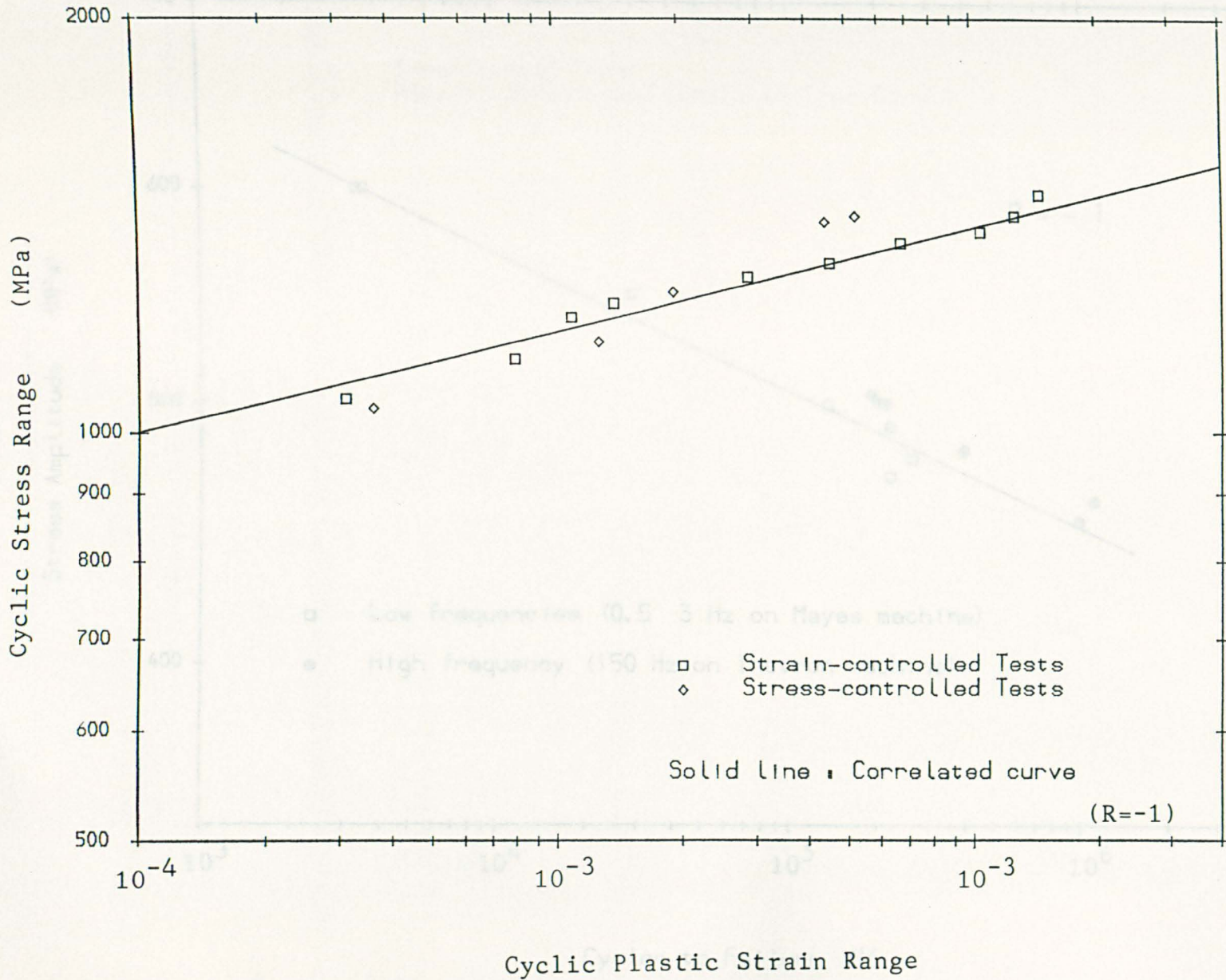


Fig.4.2 Cyclic Plastic Strain Range .vs. Cyclic Stress Range

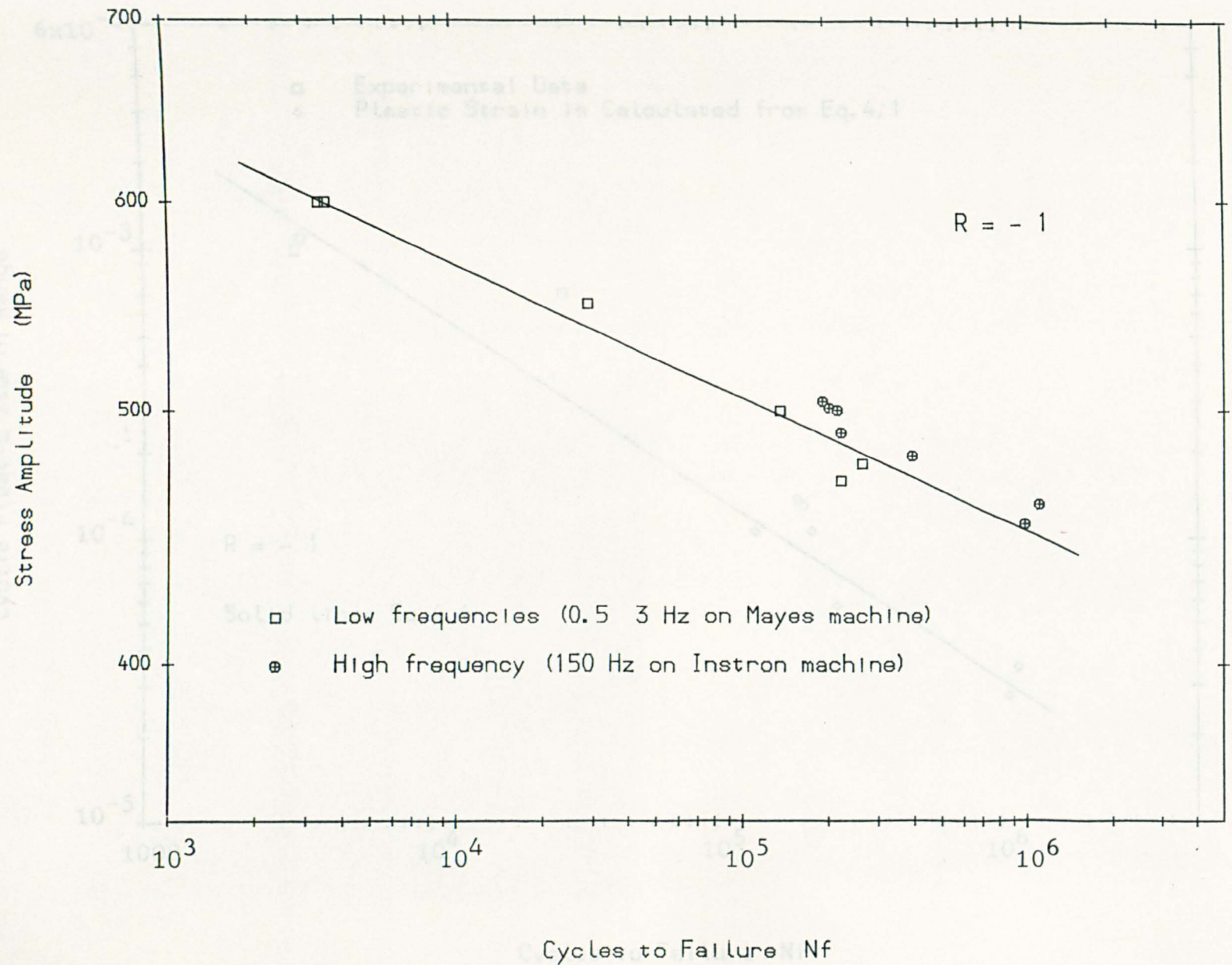


Fig. 4.3a Uniaxial Fatigue S-N Curve

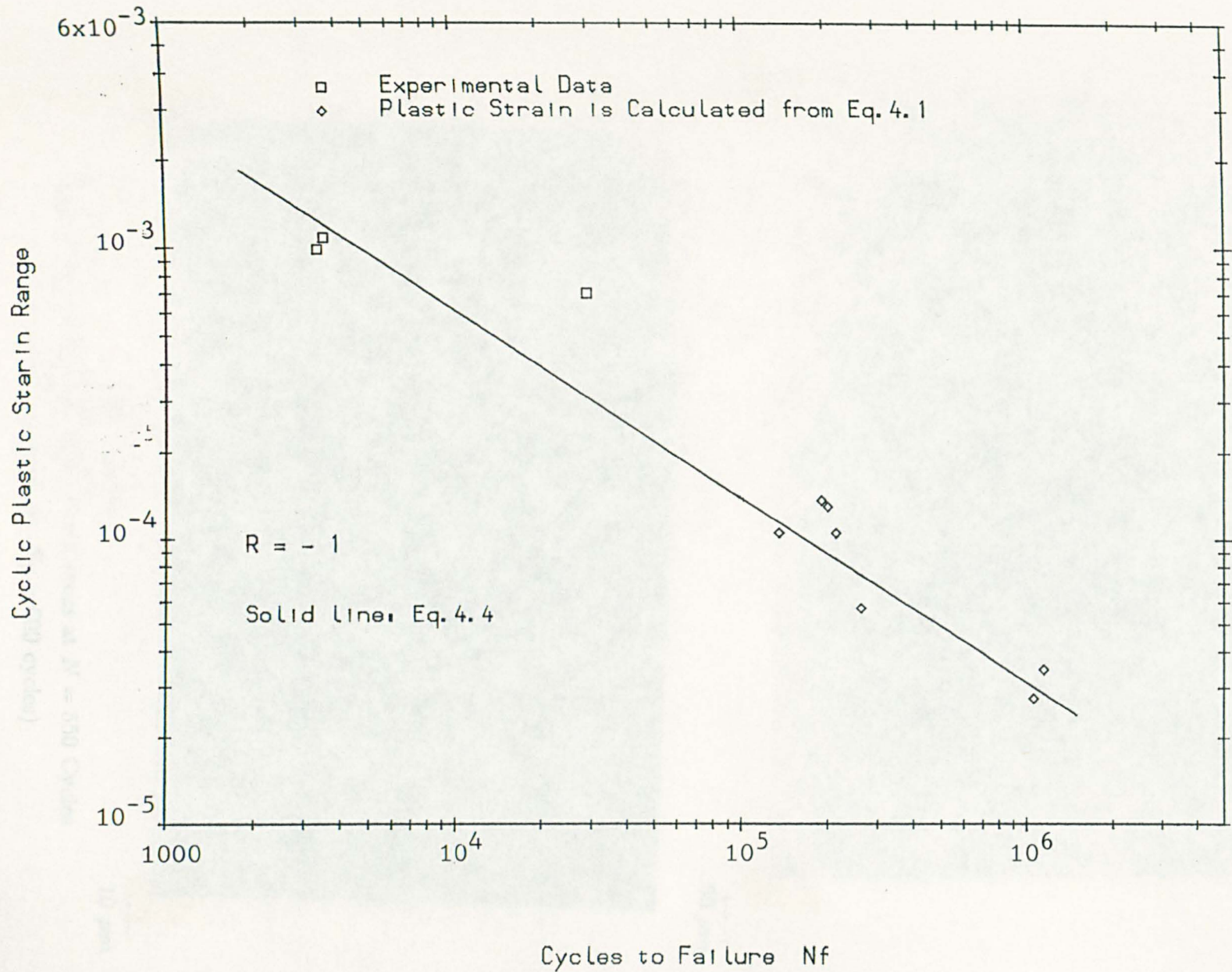
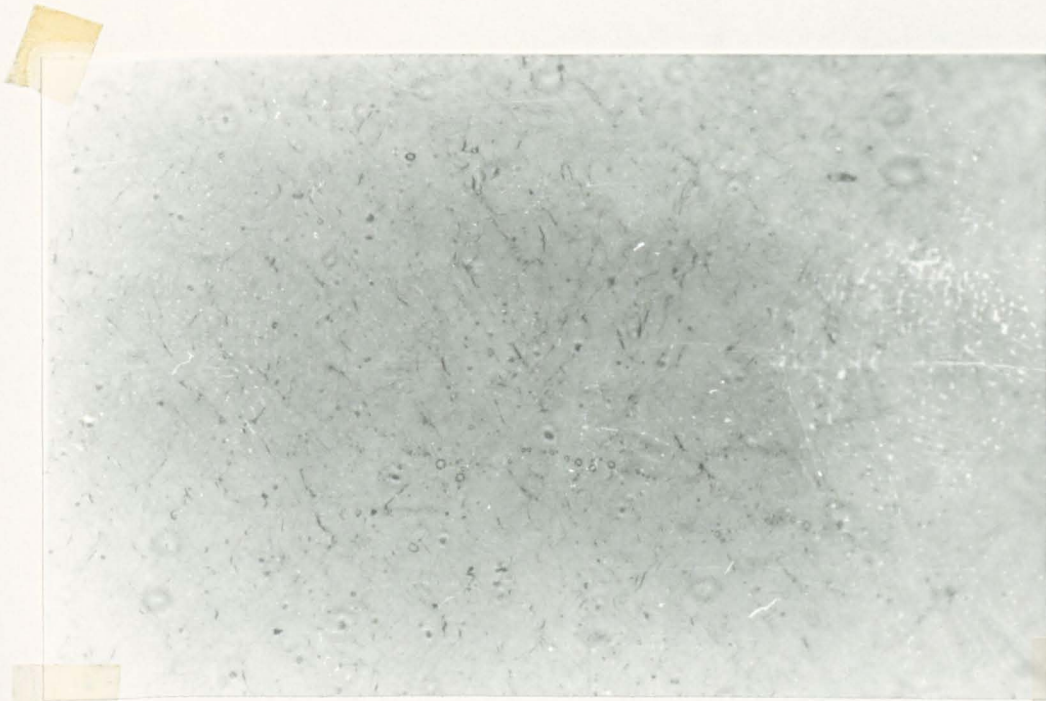
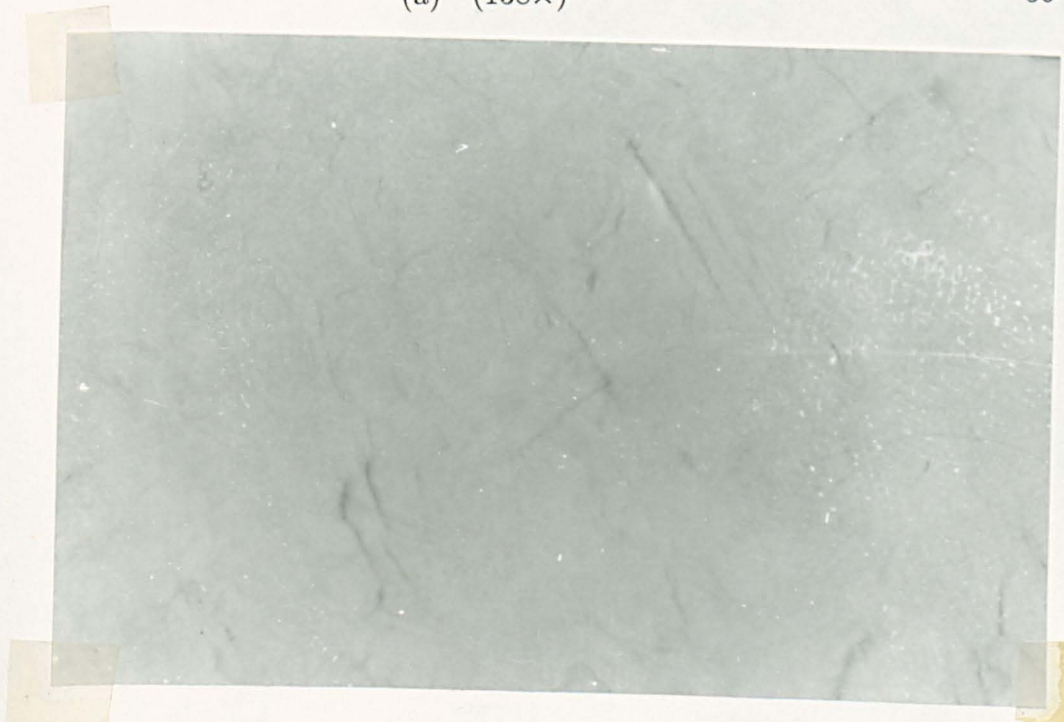


Fig. 4.3b Uniaxial Fatigue Life versus Cyclic Plastic Strain Range



(a) (138×)

50 μm



(b) (600×)

10 μm

Figure 4.4 Distribution of Surface Cracks at $N = 550$ Cycles
($\sigma_a = 650$ MPa, $R = -1$, $N_f = 600$ cycles)

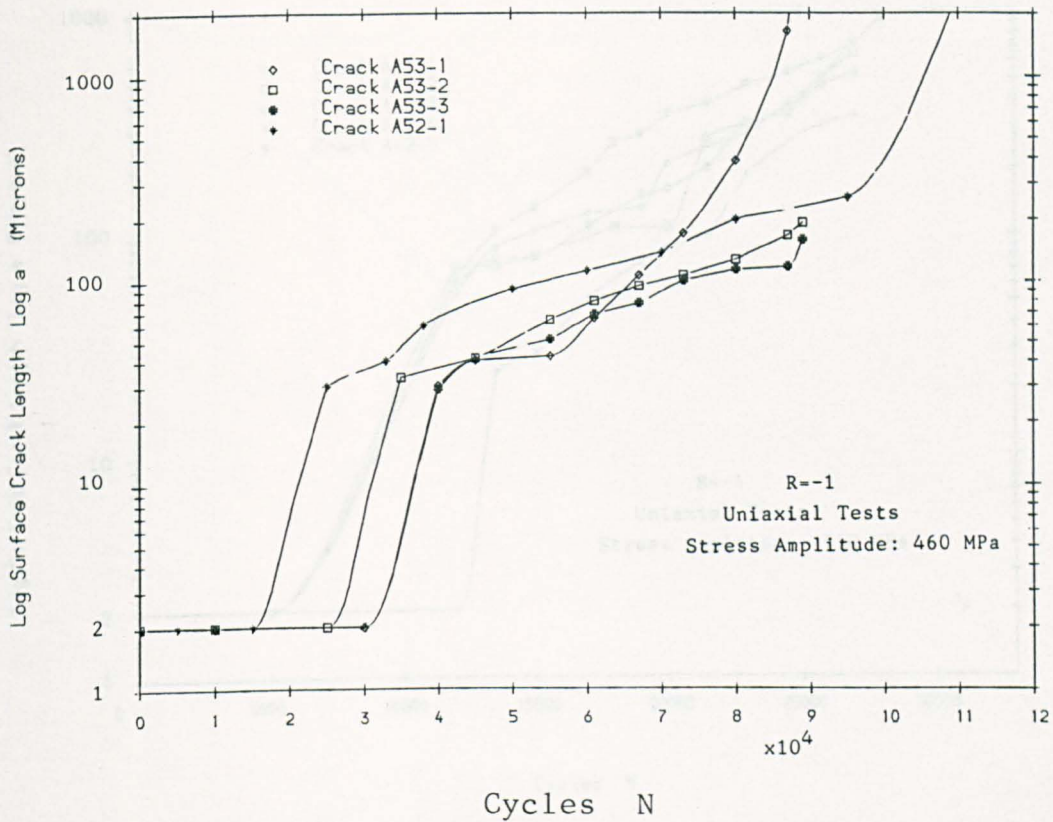


Figure 4.5 Push-Pull Crack Growth Data

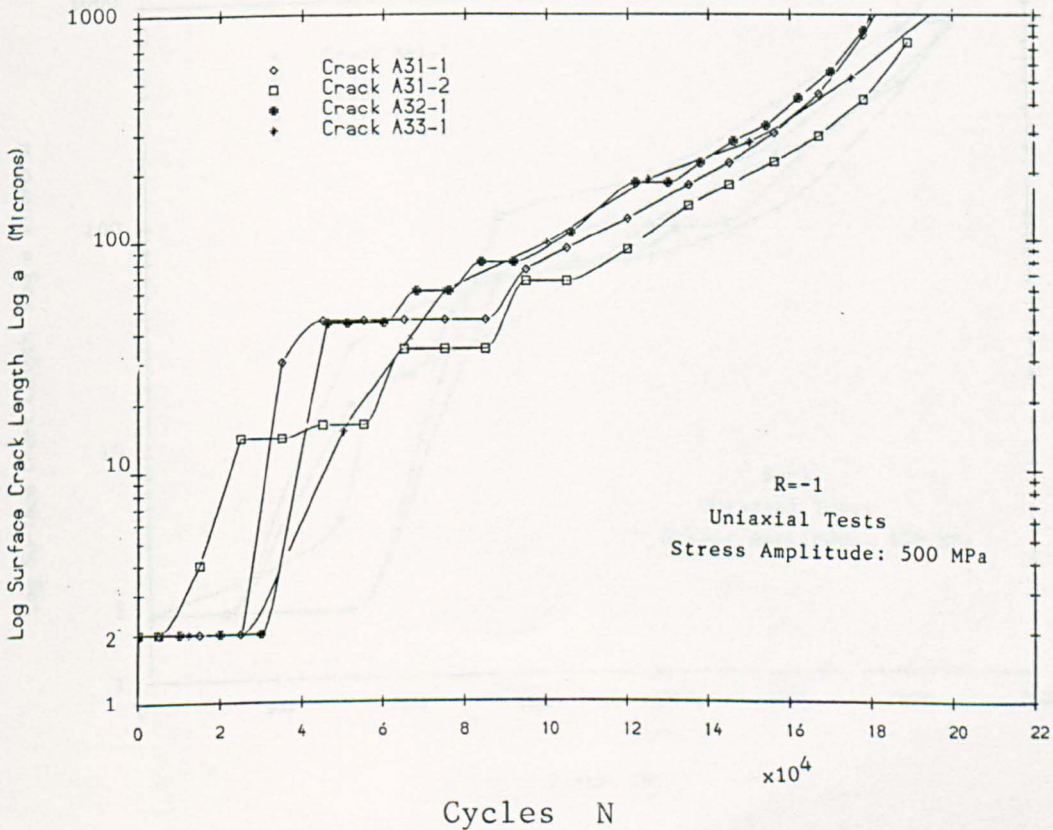


Fig.4.6 Push-Pull Crack Growth Data

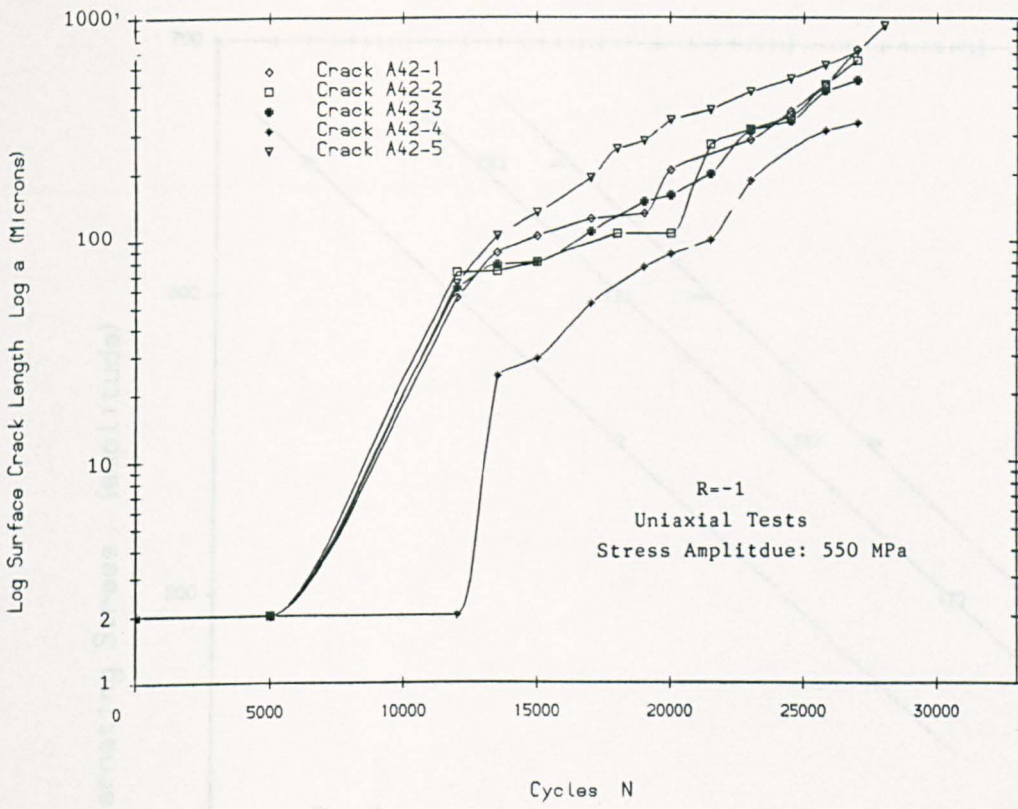


Figure 4.7 Push-Pull Crack Growth Data

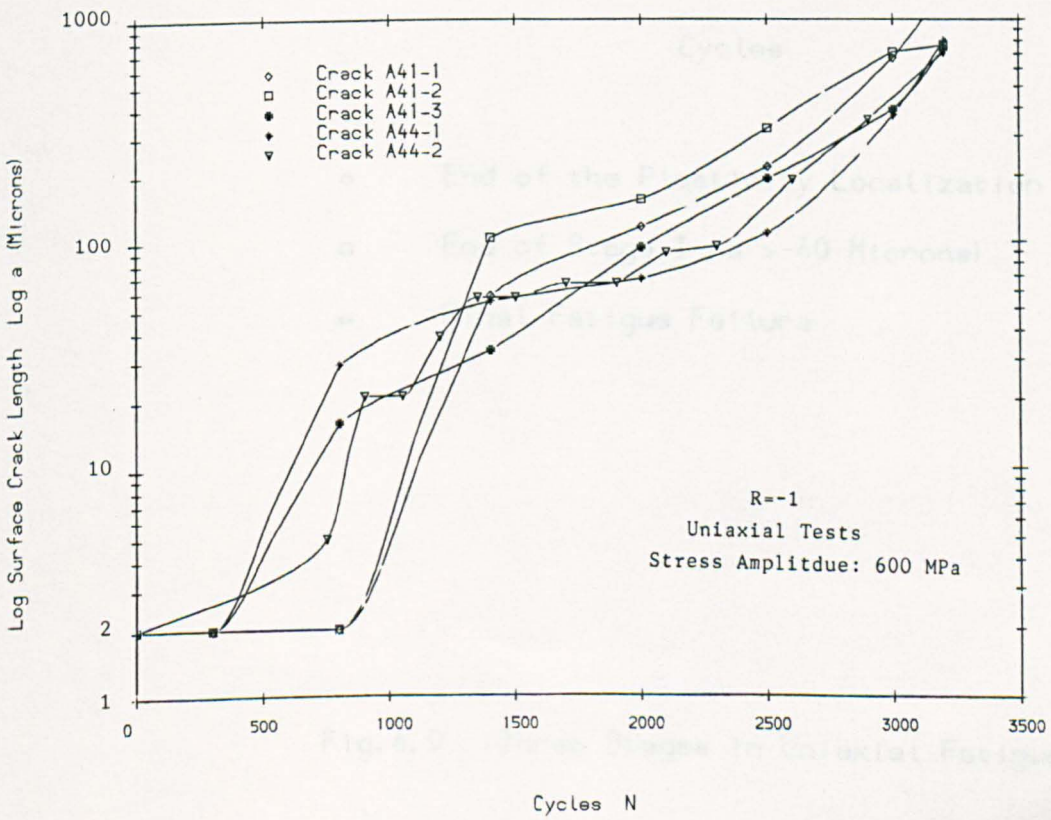
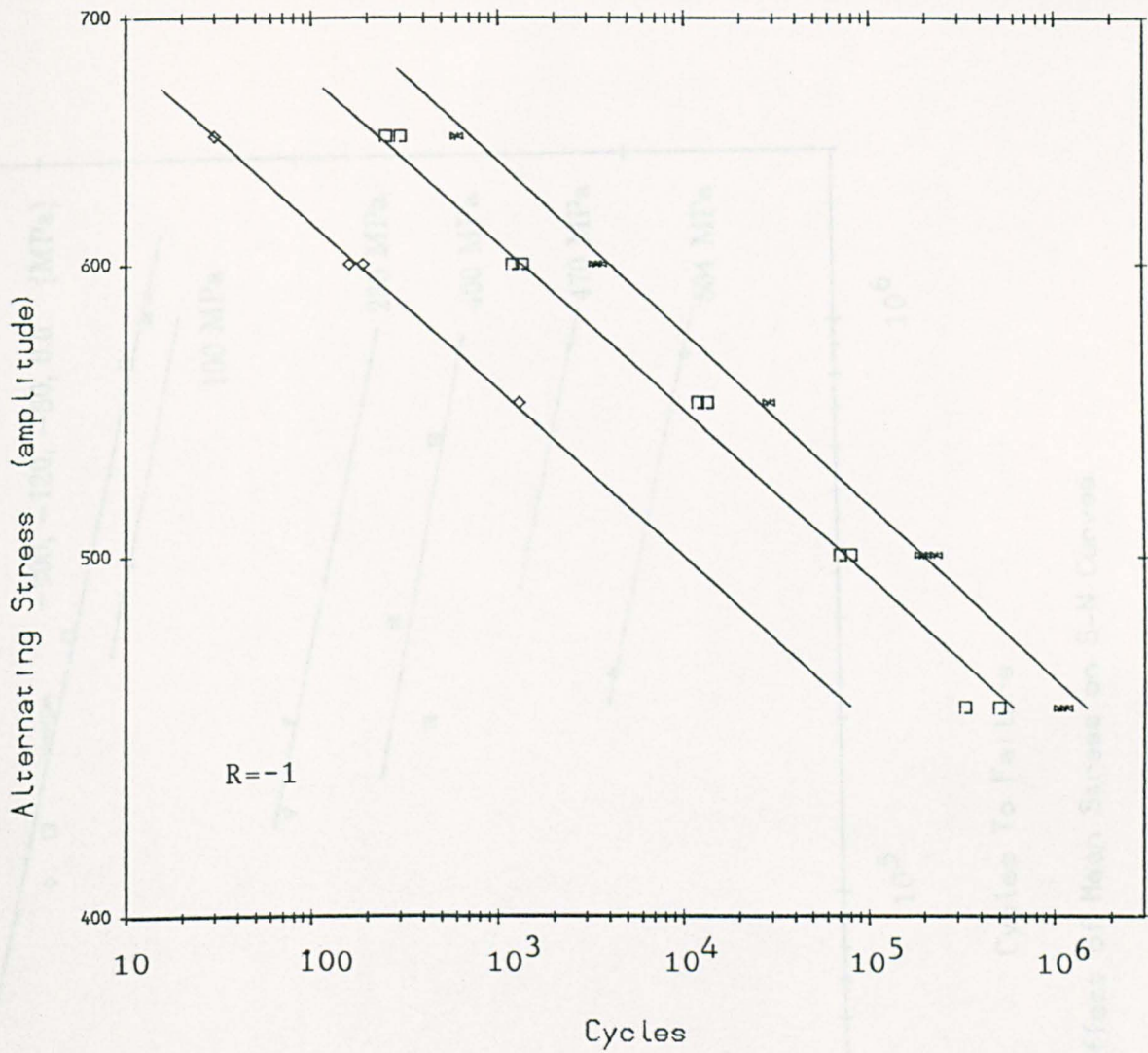


Figure 4.8 Push-Pull Crack Growth Data



- ◇ End of the Plasticity Localization
- End of Stage I (a > 40 Microns)
- # Final Fatigue Failure

Fig. 4.9 Three Stages in Uniaxial Fatigue

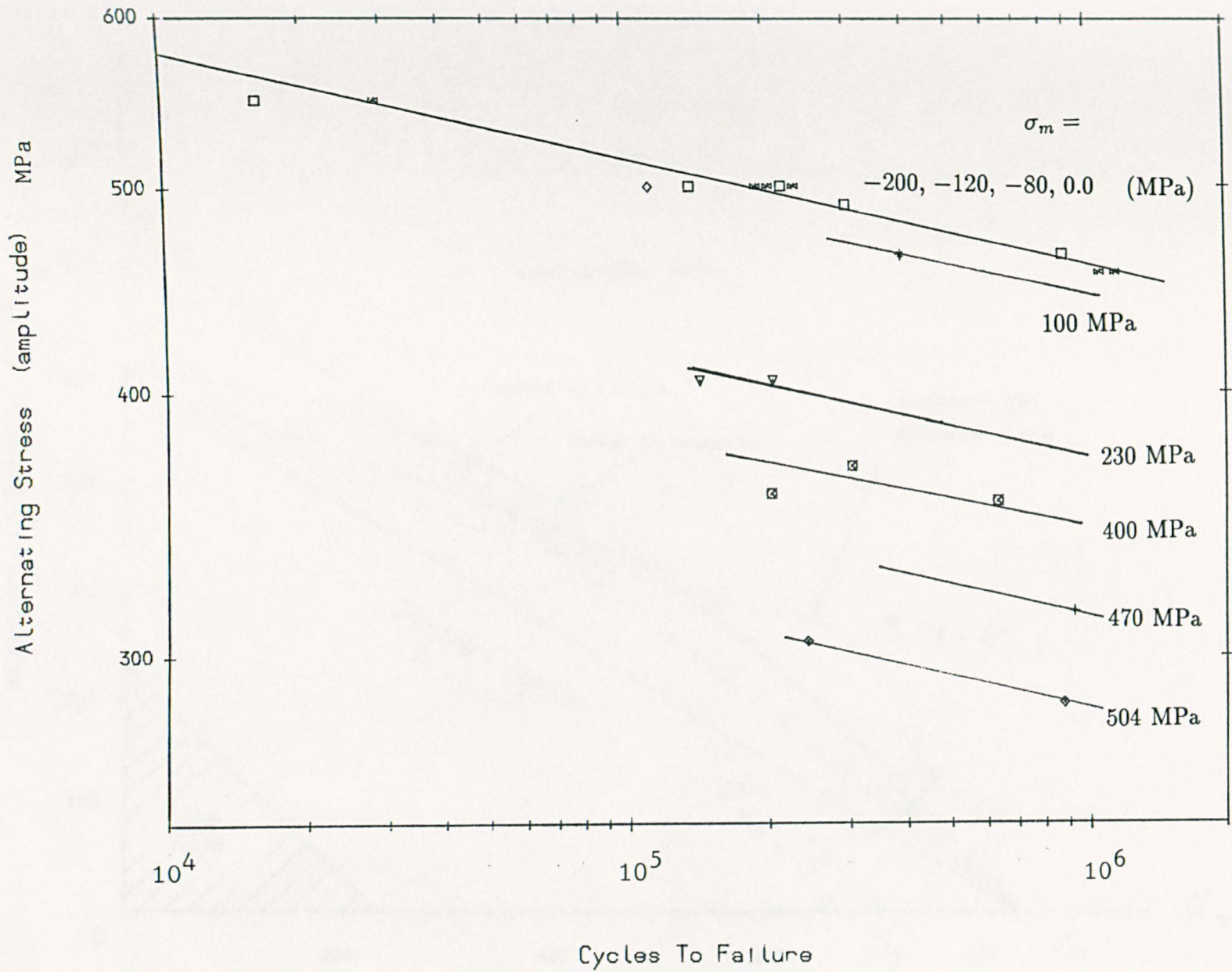


Fig.4.10 Effect of Mean Stress on S-N Curves

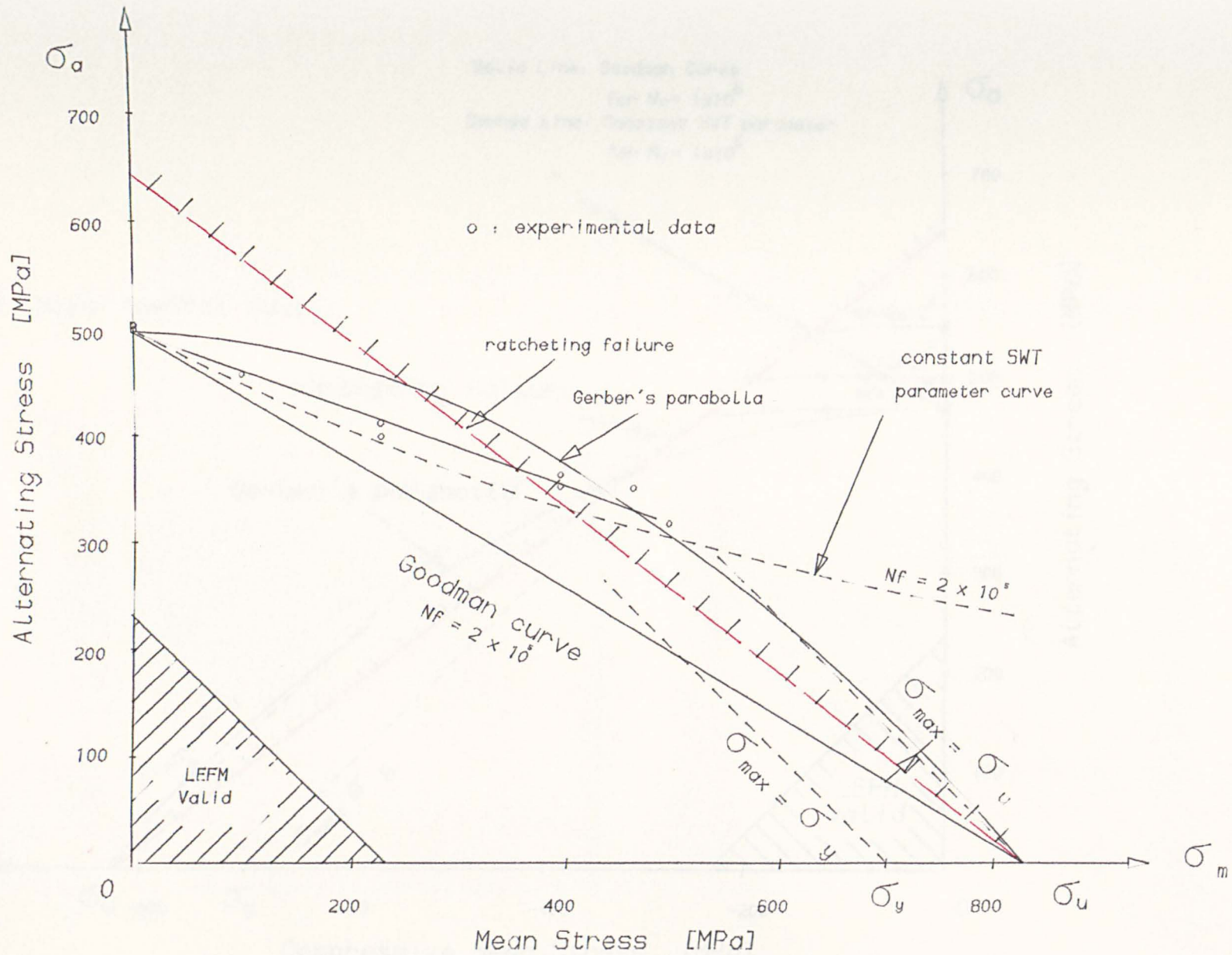


Fig.411a R-M Diagram for Uniaxial Fatigue

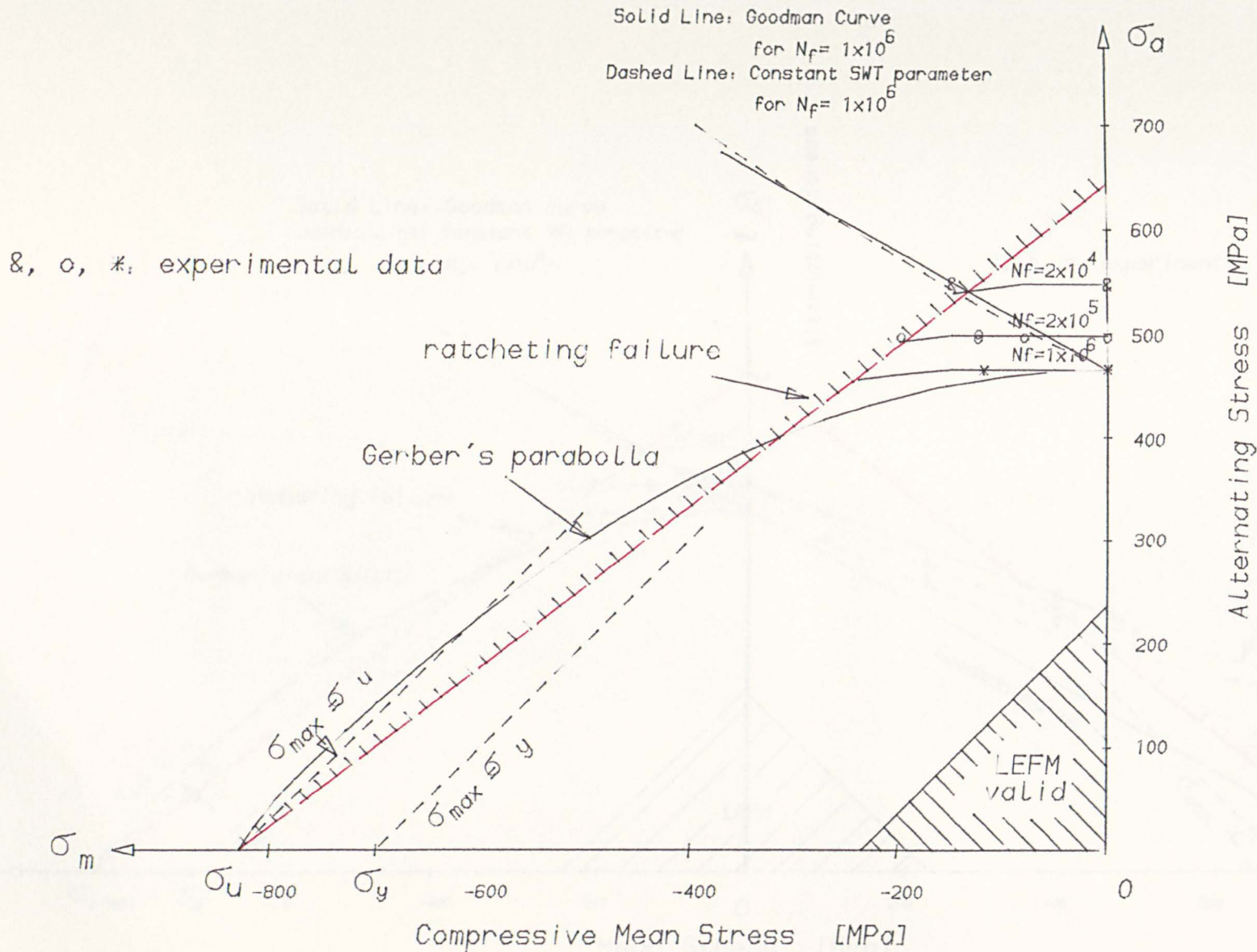


Fig.4-11b R-M Diagram for Uniaxial Fatigue

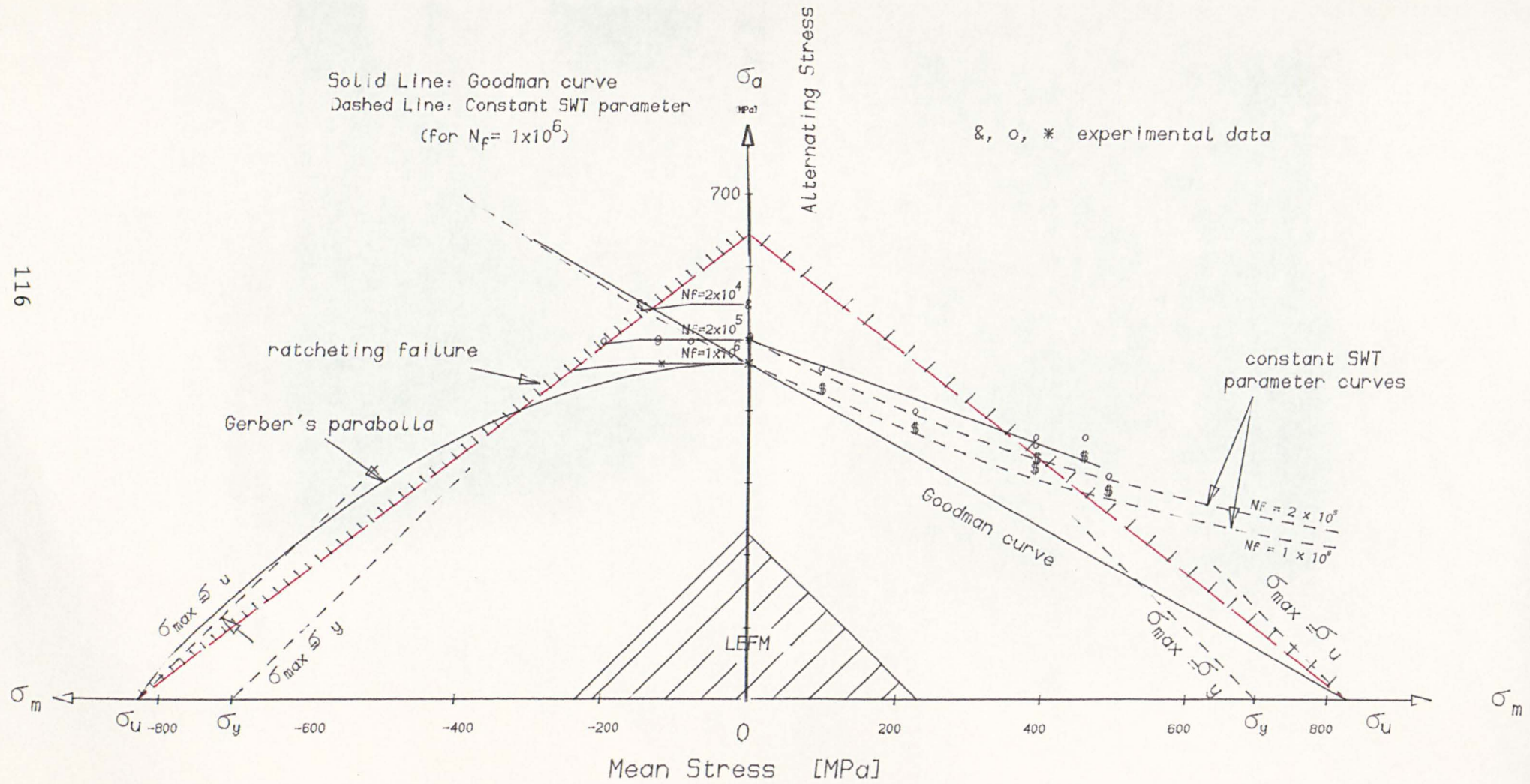


Fig.4.12 R-M Diagram for Uniaxial Fatigue



(a)

Test A32 $N_f = 2.02 \times 10^5$, $R = -1.0$ (250 \times)

40 μm



(b)

Test A40 $N_f = 2.04 \times 10^5$, $R = -0.28$ (800 \times)

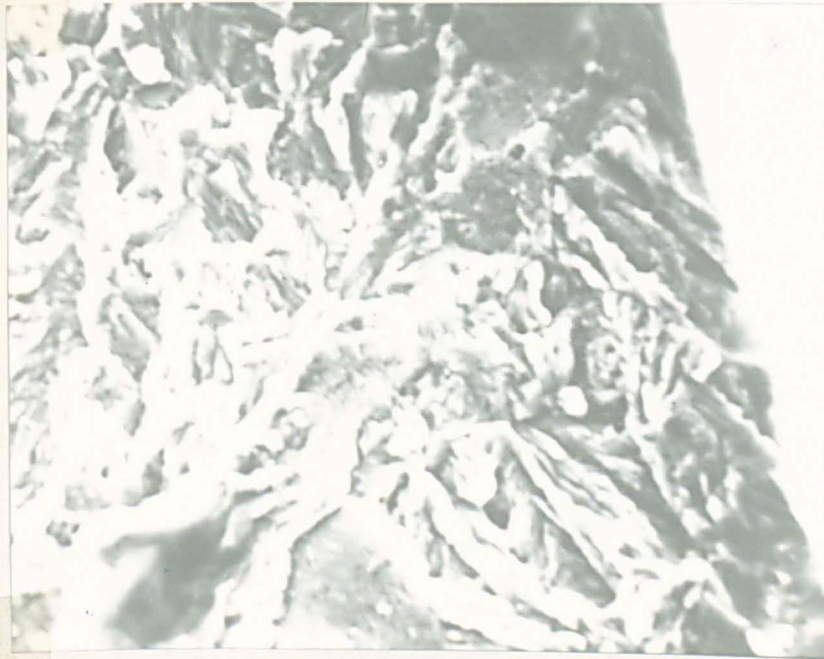
10 μm

Fig.4.13 Stage I Cracks in Uniaxial Tests



(c) Test A36 $N_f = 2.02 \times 10^5$, $R = 0.05$ (250 \times)

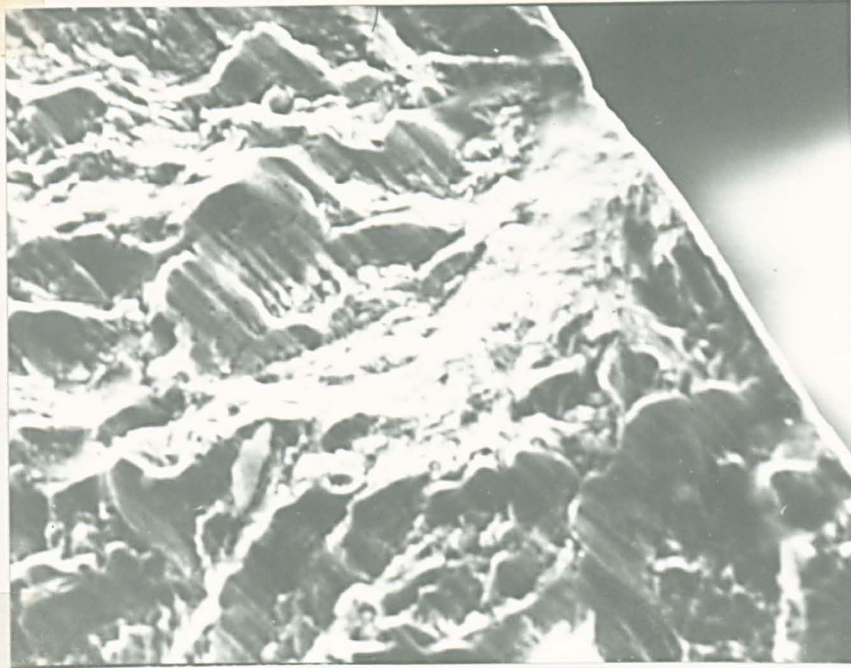
$\overleftarrow{40\mu m}$



(d) Test A58 $N_f = 3.73 \times 10^5$, $R = 0.28$ (800 \times)

$\overleftarrow{10\mu m}$

Fig.4.13 Stage I Cracks in Uniaxial Tests

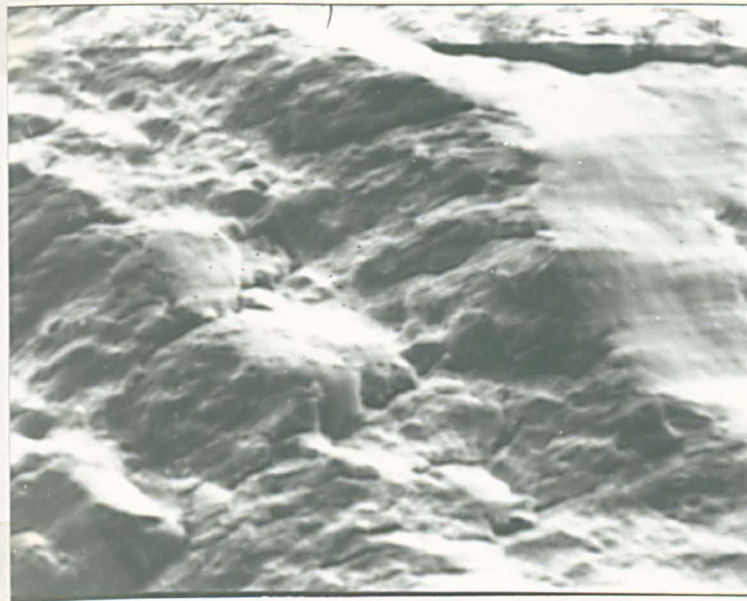


(e)

Test A55 $N_f = 8.79 \times 10^5$, $R = -1.7$ (500 \times)

Fig.4.13 Stage I Cracks in Uniaxial Tests

20 μm

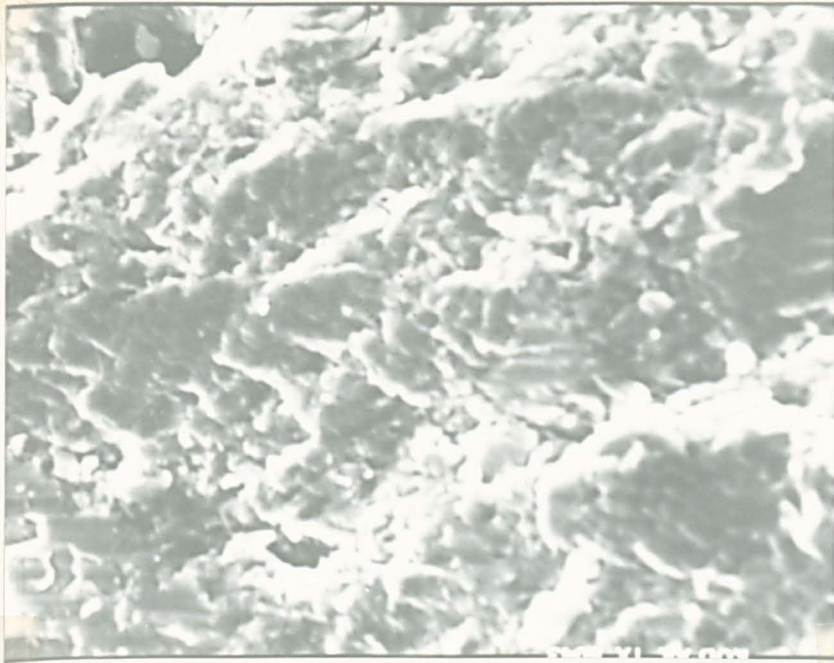


(a)

Test 41 $N_f = 3345$, $R = -1.0$ (250 \times)

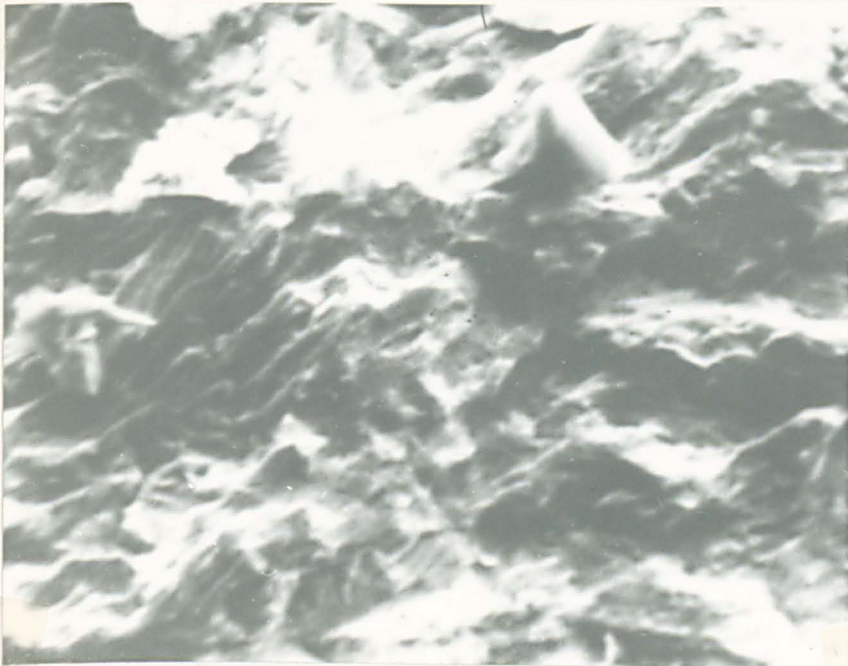
Fig.4.14 Stage II Cracks in Uniaxial Tests

40 μm



(b) Test A40 $N_f = 2.04 \times 10^5$, $R = -0.28$ (800 \times)

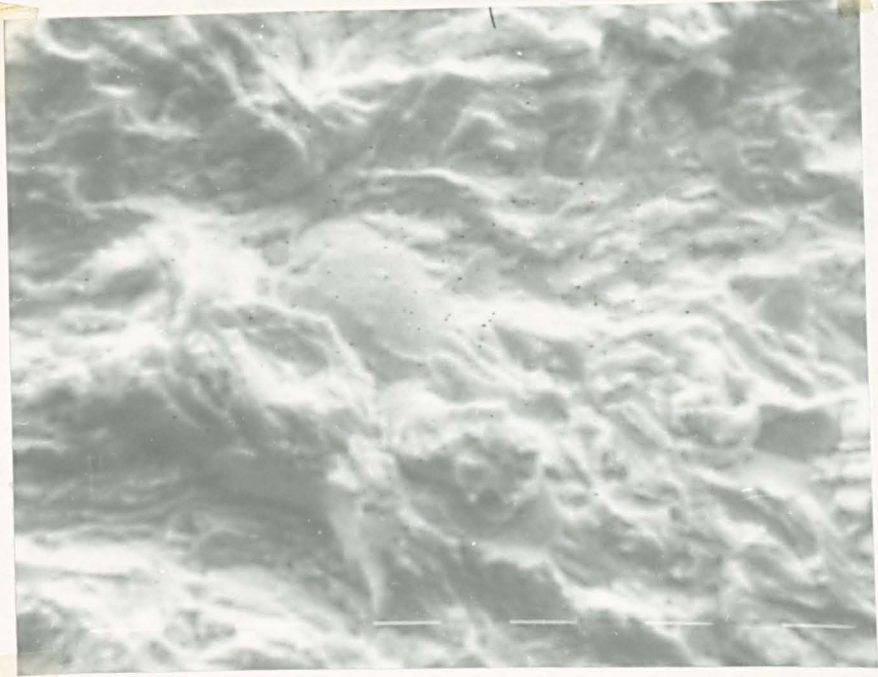
$\overline{10\mu m}$



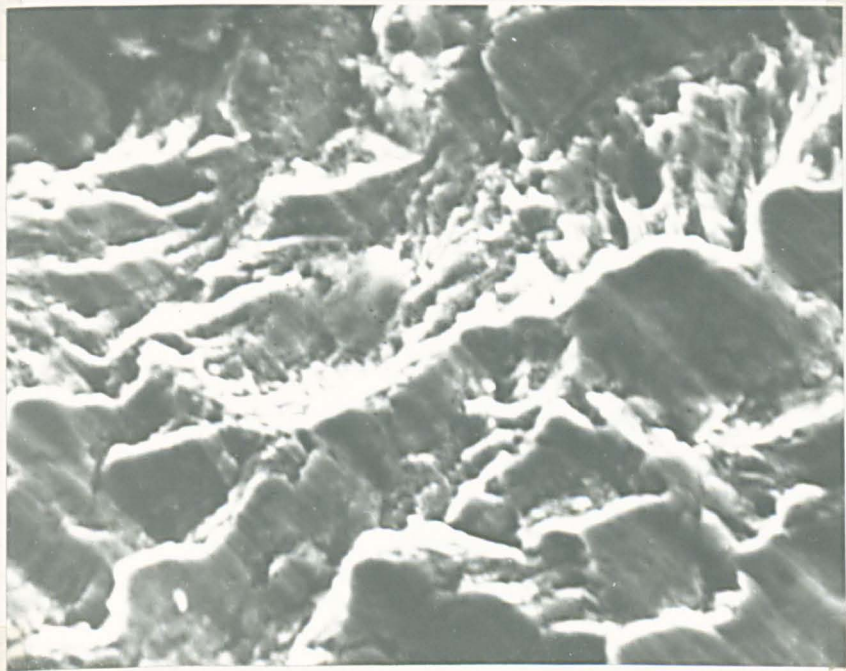
(c) Test A36 $N_f = 2.02 \times 10^5$, $R = 0.05$ (500 \times)

$\overline{20\mu m}$

Fig.4.14 Stage II Cracks in Uniaxial Tests



(d) Test A57 $N_f = 9.23 \times 10^5$, $R = 0.20$ (800 \times) $\overline{10\mu m}$



(e) Test A55 $N_f = 8.79 \times 10^5$, $R = -1.73$ (800 \times) $\overline{10\mu m}$
Fig.4.14 Stage II Cracks in Uniaxial Tests

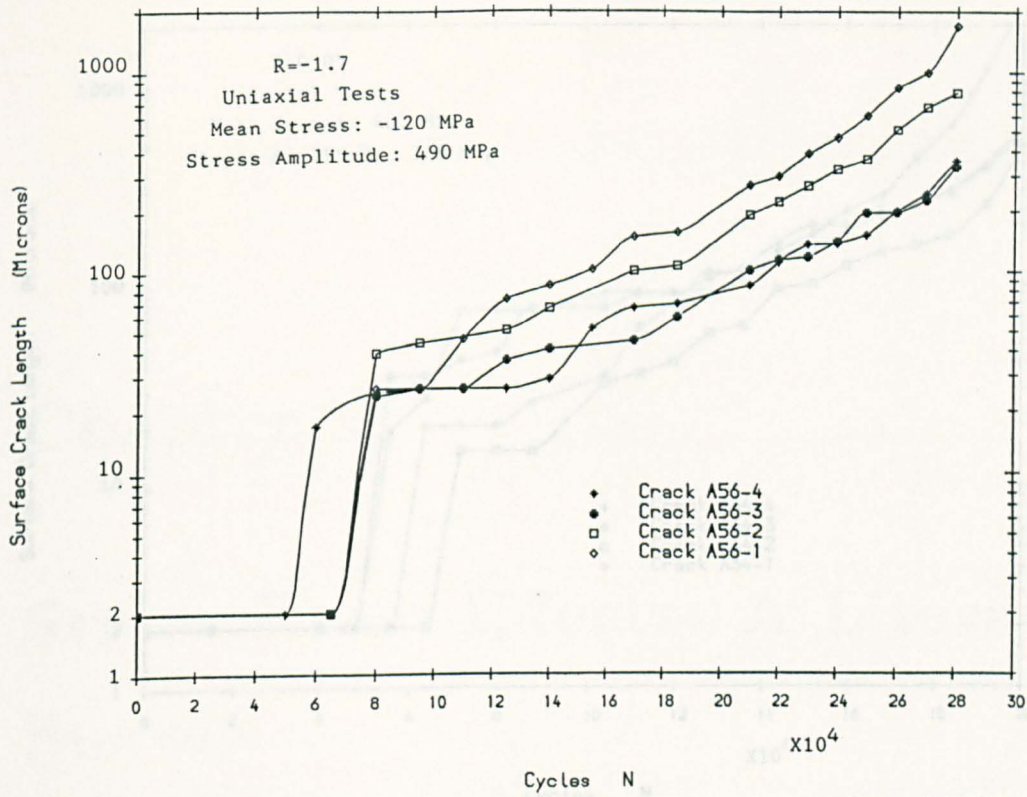


Figure 4.15 Crack Growth under Uniaxial Loading (R=-1.7)

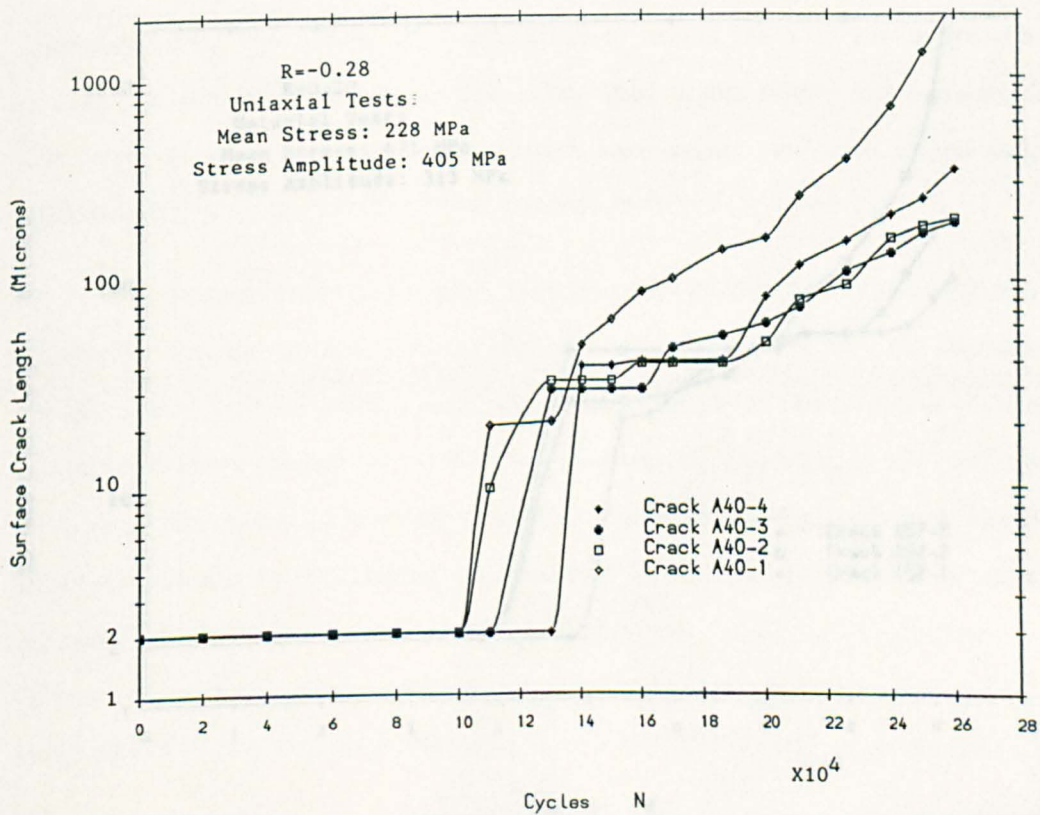


Figure 4.16 Crack Growth under Uniaxial Loading

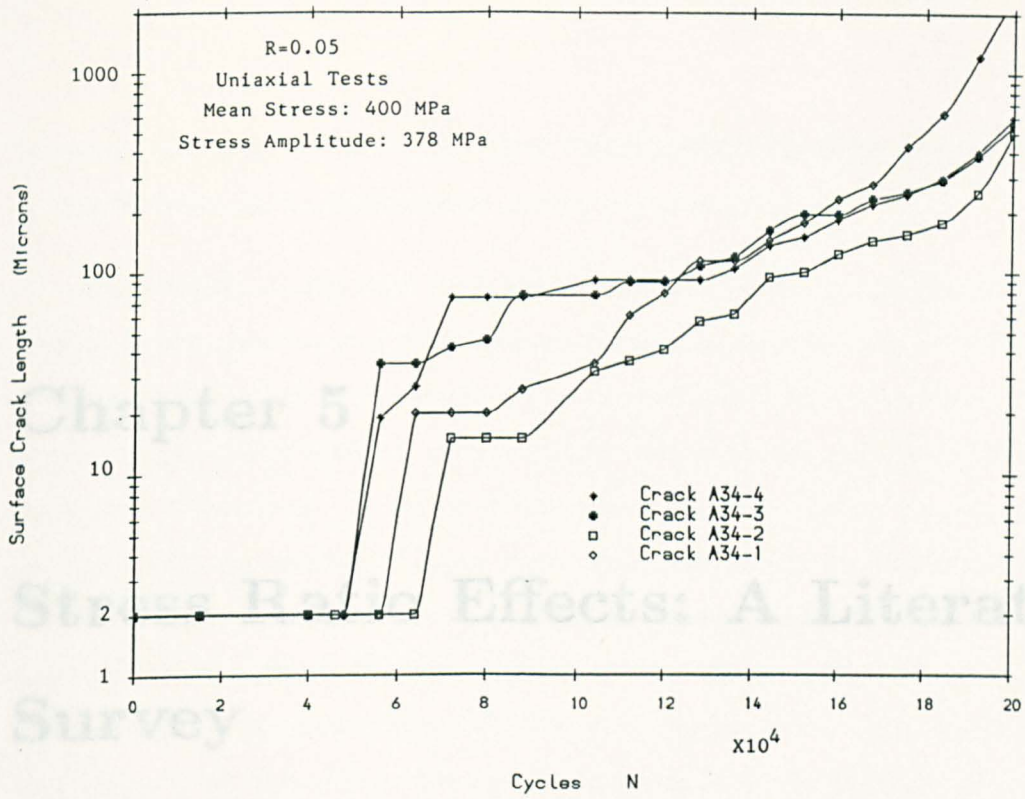


Figure 4.17 Crack Growth under Uniaxial Loading

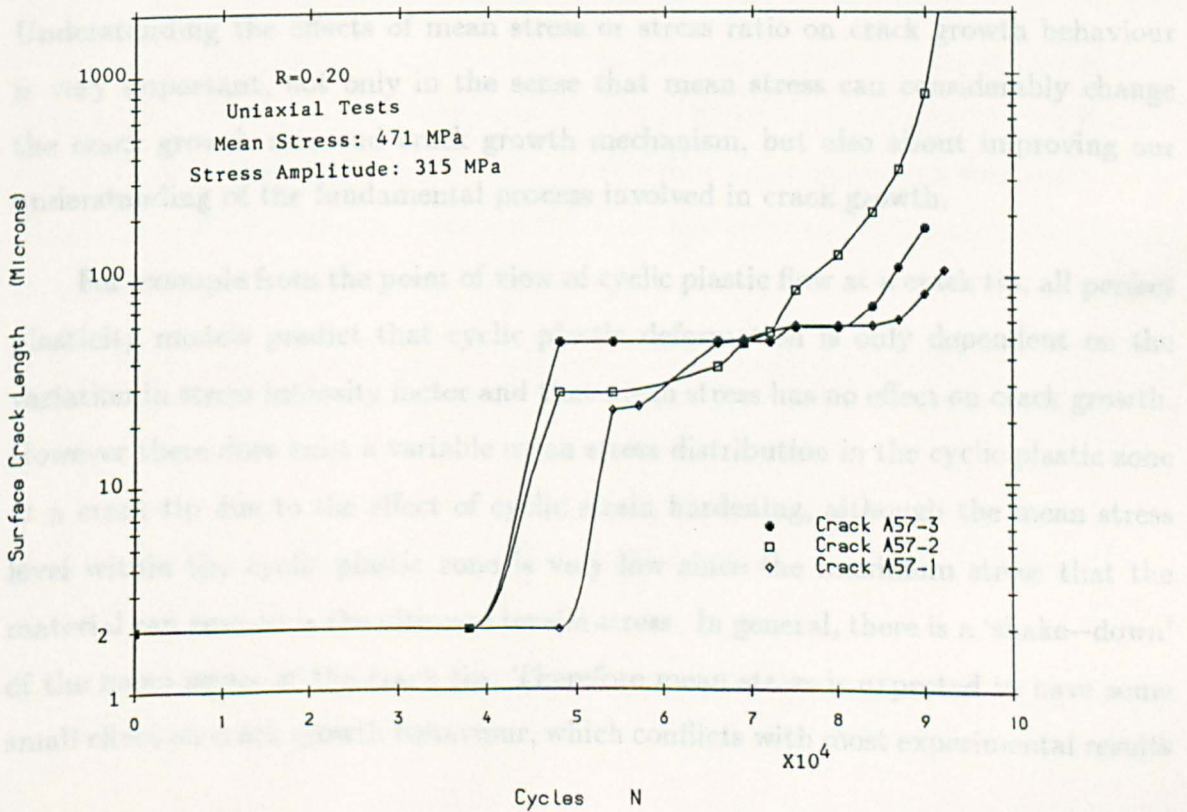


Figure 4.18 Crack Growth under Uniaxial Loading

Chapter 5

Stress Ratio Effects: A Literature Survey

5.1 Introduction

Understanding the effects of mean stress or stress ratio on crack growth behaviour is very important, not only in the sense that mean stress can considerably change the crack growth rate and crack growth mechanism, but also about improving our understanding of the fundamental process involved in crack growth.

For example from the point of view of cyclic plastic flow at a crack tip, all perfect plasticity models predict that cyclic plastic deformation is only dependent on the variation in stress intensity factor and that mean stress has no effect on crack growth. However there does exist a variable mean stress distribution in the cyclic plastic zone at a crack tip due to the effect of cyclic strain hardening, although the mean stress level within the cyclic plastic zone is very low since the maximum stress that the material can sustain is the ultimate tensile stress. In general, there is a 'shake-down' of the mean stress at the crack tip. Therefore mean stress is expected to have some small effect on crack growth behaviour, which conflicts with most experimental results

for most materials tested in air, which indicate that the crack growth rate and the threshold level are both dependent on the mean stress level.

Historically, studies have been carried out within the framework of LEFM. Various theories, models, and explanations have been proposed to explain the effects of mean stress. Most of the models can be classified into two categories. The first is that tensile mean stress is considered to increase crack growth by increasing the maximum stress level. In terms of the stress intensity factor, the maximum value increases with an increase of mean stress when the amplitude of stress intensity factor is maintained constant, and so cracks are more prone to propagate. An earlier example is Forman's modification [1] to the Paris–Erdogan law. The second category is based on the experimental observation that cracks can be closed during unloading at a stress level higher than the minimum stress level. In the light of fatigue crack growth mechanisms, the two models are totally different.

The crack closure argument implies that the effective range of the stress intensity factor is the only controlling factor and the applied mean stress intensity factor level does not affect crack growth behaviour if the effective stress–intensity factor range is the same. Experimental results, however, have shown that the crack closure level is intimately related to the mean stress intensity factor level. In other words, $K_{max} - K_{op} = Function(K_{max}, K_{mean})$. This reveals that mean stress or stress ratio is the direct cause of the change in closure level. It is impossible to bring about two different stress states (same ΔK , different R) but which give the same value of $K_{max} - K_{op}$. Hence both models are generally accepted but most of the experiments are performed under a positive stress ratio and only a few are under a negative stress ratio.

5.2 Mean Stress Effect on Long Crack Growth

In the first category of models, one of the earliest modifications to the Paris–Erdogan law was made by Forman *et al* [1], in which the crack growth rate was suggested

to become infinite when the maximum stress intensity factor reaches the fracture toughness of the material,

$$\frac{da}{dN} = \frac{C(\Delta K)^m}{K_c - K_{max}} = \frac{C(\Delta K)^m}{(1-R)K_c - \Delta K} \quad (5.1)$$

Obviously this modification predicts a slope change in the crack growth diagram, but only for high stress intensity factor levels.

The Japan Welding Engineering Society (WES) Standard 2805 offers a formula [6] as an alternative to Paris–Erdogan law when mean stress effects are significant in all regions,

$$\frac{da}{dN} = C \left(\frac{1+R}{1-R} \right) (\Delta K)^m = \frac{C}{2} \cdot K_{mean} \cdot (\Delta K)^{m-1} \quad \text{for } 0 \leq R \leq 1 \quad (5.2)$$

This formula indicates a strong dependence of crack growth rate on the mean value of K .

One interesting ‘effective stress’ (σ_{ef}) parameter was proposed by Smith, Watson and Topper [3] the so-called SWT parameter based on Walker’s parameter [4] for the correlation of $R - M$ curves (see Section 1.2), which predicts the effect of mean stress in the following manner,

$$\sigma_{ef} = (\sigma_{max} \epsilon_a)^{\frac{1}{2}} \quad (5.3)$$

$$\Delta K_{ef} = \frac{\Delta K}{[2(1-R)]^{\frac{1}{2}}} \quad (5.4)$$

According to this equation, the ratio of effective stress intensity factor range at $R = 0$ and $R = -1$ is $\sqrt{2}$. If $m = 2$ and for the same range of K , crack growth rate at $R = 0$ is twice that of the growth rate at $R = -1$. This is in good agreement with some experimental data [7] and finite element analyses [8].

5.3 Closure of Long Cracks

The second category of models focuses on an ‘effective stress intensity factor range’ which was first proposed by Elber [5] in 1970 on the basis of his experimental observa-

tions. Cracks were found to be closed at a stress level higher than the minimum stress level. Since the contact of crack faces during unloading stops the reversed yielding at crack tip, the subsequent loading portion does not contribute to crack advance until crack opening occurs. Hence an 'effective range of K ' was used instead of the whole range of K as in the Paris–Erdogan law.

$$\Delta K_{eff} = K_{max} - K_{op} = U \times \Delta K \quad (5.5)$$

where, $U = (K_{max} - K_{op}) / (K_{max} - K_{min})$ is the fraction of the cycle during which the crack is fully open. Elber from his data proposed the relationship:

$$U = 0.5 + 0.4R \quad -0.1 \leq R \leq 0.7 \quad (5.6)$$

This formula predicts an independence of U on K_{max} and ΔK . Tanaka and Matsuoka [11] discussed the inter-relationship between C and m on the basis of the crack closure concept and pointed out that U is a function of stress range. They further concluded that albeit experimental da/dN vs. ΔK relationships depend on material and mean stress level, the calculated da/dN vs. ΔK_{eff} relationships are independent of material and stress ratio, i.e.

$$\frac{da}{dN} = C_1 (\Delta K_{eff})^{m_1} \quad (5.7)$$

where C_1 and m_1 are material constants independent of stress ratio.

Experimental data however have shown that U is dependent on the ratio of K_{max} to ΔK and the ratio of maximum stress level (σ_{max}) to yield stress (σ_y) of the material.

The factors generally considered to be responsible for crack closure are:

1. The elastic recovery response of materials in the wake of the crack.
2. Roughness of the crack surface due to the nature of the crack path which itself is influenced by microstructure features (e.g. grain size), crack deflection, etc.
3. Corrosion-debris induced closure.

The first factor, crack wake plasticity induced closure, is of primary importance in many cases. The other two factors may be either insignificant or not present. In the sense of continuum mechanics, closure in plane stress arises as a result of the lateral contraction of material in the plastic zone at the crack tip. This lateral contraction involves the transport of material from the original surface into subsurface regions. As a result, when the crack passes through a previous cyclic plastic zone, these compressive stresses are relaxed and the material behind the tip expands. Under plane strain conditions, both experimental results and numerical calculations are conflicting. For example, the work by Ritchie *et al* [20] showed that closure can occur for plane strain condition, but the predicted normalized closure values K_{cl}/K_{max} were approximately 3 times larger for plane stress conditions. McEvily [14], on the contrary, proposed that under a plain strain condition, because the factors that promote plane stress closure are greatly reduced, the extent of closure under plane strain conditions should be small, or not occur at all.

The work of Ritchie *et al* [20] also showed that under both plane stress and plane strain conditions, the predictions from finite element analysis were lower than the measured closure level, indicating that the primary contributions to closure near threshold levels originate from a wedge shielding mechanism resulting from the deflected crack path itself caused by the effect of microstructure. This implies that the theoretical modelling of crack closure should also incorporate the effect of microstructure. This is clearly more difficult.

The experimental techniques available for routine monitoring of long cracks employ either a compliance method using, for example, strain gauges, or non-compliance methods using, for example, electrical resistance measurements, acoustic emission, or ultrasonics. Some disagreements between different methods have been reported, for example by Frandson *et al* [9].

Crack closure and the introduction of the concept of effective stress-intensity factor range ΔK_{eff} have been one of the most controversial aspects of fatigue crack

growth. Some work justified this approach for explaining such apparently diverse phenomena as the influence of overloads on crack retardation, and the influence of mean stress on the level of threshold for fatigue crack growth. For instance, Kang *et al* [10] reported that when the opening stress levels were measured via an unloading elastic compliance technique, both crack growth rate data and threshold stress intensity factors under stress ratio values from -2 to 0.4 can be correlated on the basis of an effective range of stress intensity factor. However, discrepancies between the correlation of fatigue data with ΔK_{eff} are also reported in the literature. e.g. the work by Minakawa *et al* [12]. This is because crack growth is also affected by fracture toughness, crack growth mode, etc. Crack closure involves a ‘double slip’ system to be operative and if a mode II component is present, it can be expected that the crack closure argument will not be able to explain Stage I crack growth behaviour.

Considerable efforts have been made to estimate the closure stress level, which is widely believed to be vital for correlating constant–amplitude applied stress crack growth with that under variable–loading, especially in aeronautical structures. On the basis of the empirical relationship proposed by Elber, which can only account for the effect of positive R . (for negative R values, the equation predicts an increasing σ_{op} with decreasing R ratios for a given value of σ_{max}) Schijve [15] proposed the following empirical equation,

$$\frac{\sigma_{op}}{\sigma_{max}} = 0.45 + 0.22R + 0.21R^2 + 0.12R^3 \quad (5.8)$$

This equation does not include the effect of the ratio of maximum stress to yield stress. Ibrahim [16], based on his experimental data, proposed an unusual set of formulae implying a strong influence of the values of σ_{max}/σ_y ,

$$\sigma_{op}/\sigma_{max} = 0.5(1 - \sigma_{max}/\sigma_y)^{1/2} \quad \text{when } R = 0 \quad (5.9)$$

$$\sigma_{op}/\sigma_{max} = (\sigma_{op}/\sigma_{max})_{R=0} \cdot (1 - R)^2 + R \quad \text{when } R \geq 0 \quad (5.10)$$

$$\sigma_{op}/\sigma_{max} = (\sigma_{op}/\sigma_{max})_{R=0} \cdot [1 - (\sigma_{op}/\sigma_y)^2]^2 \quad \text{when } R \leq 0 \quad (5.11)$$

where σ_y is the yield stress of the material. Even so the above equations still predict a positive closure stress level for $R = -1$.

It is worthwhile to point out that the assumption frequently adopted for the case of $K_{min} < 0$, i.e.,

$$\Delta K = K_{max} \quad \text{and} \quad R = 0 \quad \text{for} \quad K_{min} \leq 0 \quad (5.12)$$

leads to a non-conservative estimate of the crack growth rate when crack growth rate at $R = 0$ is taken as the reference; see Crooker [17] which reports that the compressive portion of the stress cycle contributes considerably to crack growth. This assumption illustrated by Eq.5.14 predicts no effect of mean stress on the stress intensity factor threshold for negative stress ratio when $R = 0$ is taken as a reference.

5.4 Effect of Stress Ratio on Threshold

There exists a critical value of cyclic stress intensity factor range ΔK_{th} below which LEFM characterized fatigue cracks do not propagate. For a particular material, stress ratio, and environment, the value is independent of crack length. In practice, this threshold is defined as the ΔK value corresponding to an extremely low fatigue crack growth rate of the order of 10^{-11} m per cycle. To achieve this threshold condition, either extensive $S - N$ curves for pre-cracked specimens should be produced, or a 'load shedding' method is employed on a single specimen so as to approach the undetectable crack growth condition. The later method is widely used, but the unloading must be carefully controlled to eliminate the possible overload effect of the preceding high level of stress intensity factor. For instance, the American Society for Testing and Materials, ASTM [18] have recommended that during unloading, the stress ratio R and the normalised ΔK gradient of $(1/\Delta K)(d\Delta K/da)$ are maintained constant.

It is clear that the measured threshold value is associated with a certain level of crack closure. Schmidt and Paris [19] first proposed that the R dependency of the

threshold value is due to the crack closure,

$$\Delta K_{th} = \Delta K_{eff} + (K_{op} - RK_{max}) \quad R < R_{cl} \quad (5.13)$$

$$\Delta K_{th} = \Delta K_{th} \quad R > R_{cl} \quad (5.14)$$

where ΔK_{eff} is the effective stress intensity range at the threshold, R_{cl} is the stress ratio at which the closure (or opening) stress intensity factor, K_{op} is zero. This simple formula implies that, firstly, there exists an intrinsic threshold value for a high stress ratio, and secondly, the stress ratio effect on the threshold is fully attributable to the effect of crack closure. Some experiments have confirmed this. For example, Kang [10] recently demonstrated that the threshold value under stress ratios ranging from -2 to 0.4 can be well correlated on the basis of ΔK_{eff} .

At near-threshold, the plastic wake at the crack tip is not fully developed as in the steady growth region due to the low level of stress intensity factor. Moreover, crack tip opening displacements are smaller and cracks tend to follow a microstructurally sensitive or crystallographic crack path, hence crack closure is induced primarily by corrosion debris, fracture surface roughness, and combined wedging and bridging [20], whereas the plasticity induced mechanism is less important. As a result, Mode II crack growth will occur at the near-threshold region, e.g. the work by Otsuka *et al* [21] indicates that Mode II (shear mode) is significantly involved in the crack growth mechanism close to the threshold region, but the ΔK_{eff} approach tacitly assumes that the crack growth is a Mode I (opening mode) mechanism. Hence different crack growth paths and mechanisms prevent a correlation on the basis of ΔK_{eff} at near threshold level, which is also confirmed by Minakawa, Levan and McEvily [12] who showed that ΔK_{eff} at threshold decreases with the decrease of stress ratio, implying that the portion of the cycle after crack closure also affects crack growth behaviour, however no further attempts were made to clarify the influence of Mode II growth. Beevers [22] pointed out that crack closure cannot explain the threshold for both air and vacuum conditions.

From the above discussion, the effects of mean stress on the threshold seem to be

very complicated. Only when the crack growth path and mechanism are not affected by stress ratio, is the ΔK_{eff} approach able to explain and correlate the mean stress effect. Therefore empirical correlations between ΔK_{th} and R is also of importance. In this respect, Klesnil and Lukas [23] proposed the following relationship,

$$\Delta K_{th} = \Delta K_{th(R=0)}(1 - R)^\gamma \quad (5.15)$$

thereby suggesting that ΔK_{th} and R are related by a simple power-law. Determination of γ still needs more information about the way in which the threshold level varies with K_{max} and R . Also the formula does not indicate precisely the relative effects of K_{max} and R on ΔK_{th} . Fig.5.1 shows some experimental results of the dependence of the threshold value on stress ratio and it appears that a relationship which is best able to correlate most data is,

$$\frac{\Delta K_{th(R)}}{\Delta K_{th(R=0)}} = 1 - BR \quad (5.16)$$

where B for is a material and environment dependent parameter, For most metallic and non-metallic materials, B has a value between 0 and 1.0.

5.5 Effects of Mean Stress on Short Crack Growth

In contrast to the extensive experimental and theoretical work on the effects of mean stress upon long crack growth, no systematic studies could be located in the literature on the closure of short cracks and the effect of mean stress on short crack growth. Only a few papers refer to crack closure argument in relation to short crack growth behaviour.

It is generally accepted that there is no essential difference in the mechanism by which long and short cracks propagate in mode I (stage II). The observation of fatigue striations on fracture surfaces resulting from short crack growth has provided evidence and support for this belief, which could lead to the consideration that the effective stress range $\Delta\sigma_{eff} = \sigma_{max} - \sigma_{op}$ is also able to unify short crack growth rates under

different stress ratios but no experimental results have confirmed this. Conversely, the work by James and Sharpe [24] showed that for both the materials they investigated, the crack growth rates cannot be correlated by $\sigma_{max} - \sigma_{op}$, indicating that the portion of the cycle after crack closure does contribute to the crack growth.

It is expected that short cracks, which leave behind a limited wake, are subject to less closure. However, there are difficulties in experimental techniques to measure the crack closure level of short cracks, because the measurement requires extremely high spatial resolution. In addition, the location of crack opening displacement has also been shown to influence the results significantly [25]. So far no quantified data can be found in the literature and neither can any theoretical modelling of crack closure and opening levels for short cracks under high stress cycling be located.

Many workers have suggested that the LEFM effective stress intensity factor range, $\Delta K_{eff,th}$, should be substituted for ΔK_{th} on the basis of crack-closure arguments and therefore they modify the Kitagawa-Takahashi diagram to correlate short crack growth at the near-fatigue limit stress level [26] [27], see Fig.5.2. Such arguments are not acceptable close to the MSC regime and only partially acceptable to the LEFM boundary. From the previous discussion, it is clear that the crack closure argument by itself is not sufficient to extend LEFM closure analysis to the fatigue limit stress level [20]. Hence although closure may occur at the interface between PSC and LEFM zones, it will not be a major effect at the interface between MSC/PSC regimes, nor at high mean stress levels and high growth rate. For instance, in their work [8], Newman and Beevers showed that short cracks did not display any evidence of crack closure at crack lengths up to $250 \mu m$ (note: in their tests the stress ratio R was 0.1).

5.6 Comments

Although extensive studies have been carried out to explore the effects of mean stress on long crack growth and the involved mechanisms, the exploration of mean stress effects upon short crack growth is far from extensive. Actually no work could be located in the literature in regard to the short crack growth behaviour under mean stresses, possibly due to the following reasons,

- (i) Invalidity of LEFM to quantify short crack growth.
- (ii) Difficulties in the measurement of crack closure level for short cracks.
- (iii) A lack of the understanding of the effect of microstructural on crack growth.

From the forgoing discussion, the effect of mean stress on long crack growth behaviour is considered to be due to the change in crack closure stress level, and short cracks are subjected to less closure due to their limited plastic wake, this seems to suggest that the short crack growth should be less sensitive to mean stress level than long cracks.

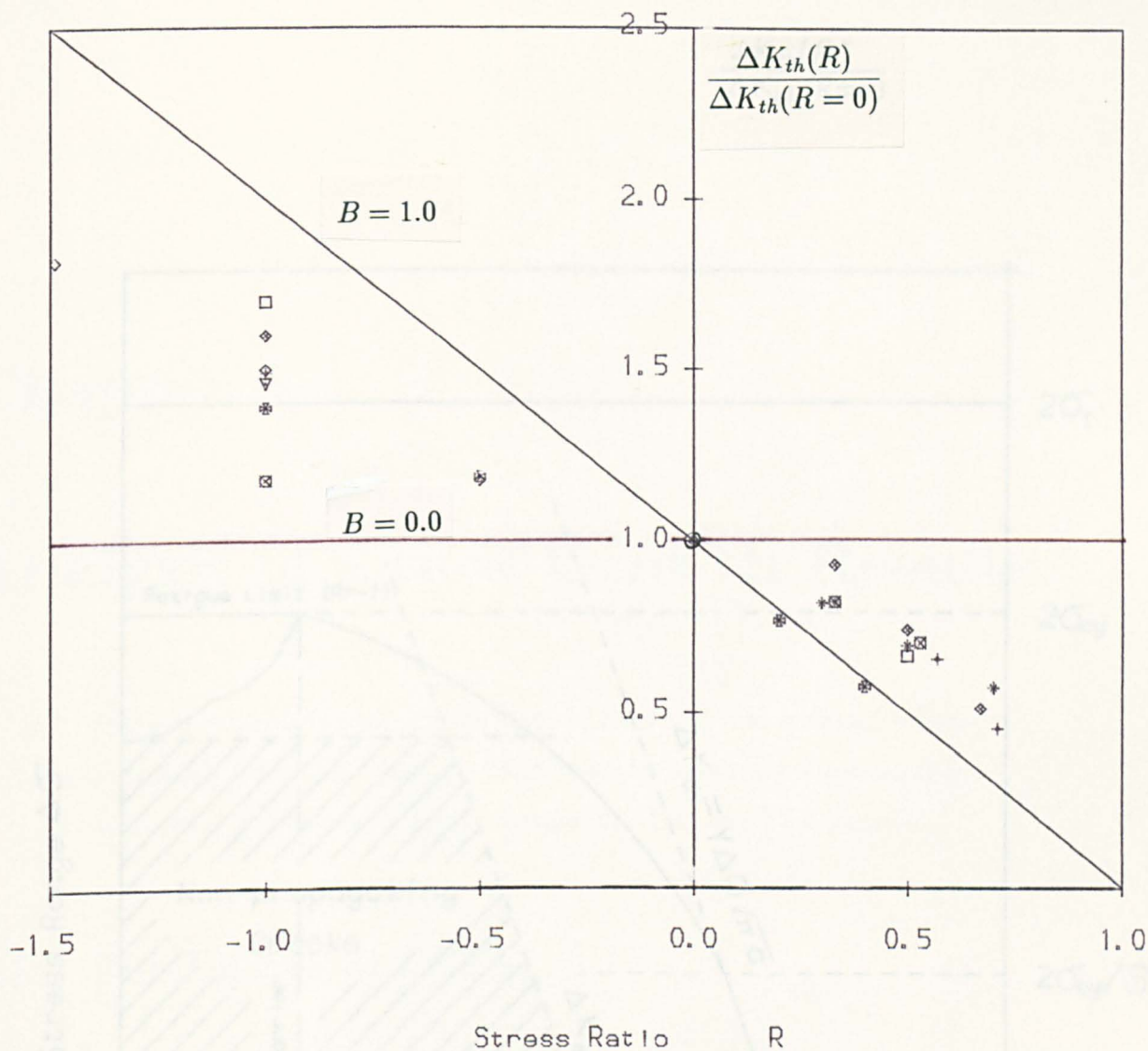
Crack growth, under push–pull loading, can be divided into two stages: Stage I (shear mode) and Stage II (opening mode). Obviously crack closure argument cannot explain the effects of mean stress upon Stage I crack growth, which is of primary importance because the early fatigue life can be dominated by shear mode Stage I crack growth. Fatigue limit has been interpreted as the transition from Stage I growth to Stage II growth. So far there is no published experimental data about the effects of mean stresses on the Stage I and II crack growth. Thus one of the main aims of this thesis is to study the effects of mean shear stress and mean uniaxial stress upon the short fatigue crack growth which will enable the prediction of the fatigue strength of materials under various mean stresses and the evaluation of residual fatigue life of components under asymmetrical loading.

References

1. Forman, R. G., Kearney, V. E. and Engle, R. H. (1967) Numerical Analysis of Crack Propagation in Cyclic Loading Structures, *Transactions of ASME (ser. D) 69*, pp.459–463.
2. Maddox, S. J. (1972) The Effect of Mean Stress on Fatigue Crack Propagation: A Literature Review, *International Journal Fracture, Vol. 11, No. 3*, pp.389–408.
3. Smith, R. N., Watson, and Topper, T. H. (1970) A Stress–Strain Function for the Fatigue of Metals, *Transactions of ASME, Journal of Materials, Vol. 5, No. 4*, pp. 767–778.
4. Walker, K. (1970) The Effect of Stress Ratio During Crack Propagation and Fatigue for 2024–T3 and 7075–T6 Aluminium; Effects of Environment and Complex Load History on Fatigue Life, *ASTM STP 462*, pp.1.
5. Elber, W. (1970) The Significance of Crack Closure, *Damage Tolerance in aircraft Structures, ASTM STP 486*, pp.230–242.
6. Allen, R. J. (1980) Fatigue Crack Growth Characterization by LEFM – Part II, *Fatigue and Fracture of Engineering Materials and Structures, vol. 11, No. 2*, pp.71–108.
7. Qingzhi, H. (1984) A Model for Calculating the Fatigue Crack Opening Load and its Applications, *Fatigue of Engineering Materials and Structures, vol. 7*, pp.41–53.
8. Newman, J. C. Jr. (1976) A Finite Element Analysis of Fatigue Crack Closure, *ASTM STP 590*, pp.281–300.
9. Frandson, J. D., Inman, R. V. and Buck, O. (1975) A Comparison of Acoustic and Strain Gauge Techniques for Crack Closure, *International Journal of Fracture, Vol. 11*, pp.345–348.
10. Kang, K. J., Song, J. H. and Earmme, Y.Y. (1989) Fatigue Crack Growth and Closure through a Tensile Residual Stress Field under Compressive Applied Loading, *Fatigue and Fracture of Engineering Materials and Structures, Vol. 12, No. 5*, pp.363–367.
11. Tanaka, K. and Matsuoka, S. (1977) A Tentative Explanation for Two Parameters, C and m , in Paris Equation of Fatigue Crack Growth, *International Journal of Fracture, Vol. 13, No. 5*, pp.563–583.

12. Minakawa, K., Levan, G. and McEvily, A. J. (1986) The Influence of Load Ratio on Fatigue Crack Growth in 7090-T6 and IN9021-T4 Aluminium Alloys, *Metallurgical Transactions, Vol. 17A*, pp.1787-1795.
13. Ritchie, R. O., Yu, W., Blom, A. F., and Holm, D. K. (1987) An Analysis of Crack Tip Shielding in Aluminium Alloy 2124: A Comparison of Large, Small, Thorough-Thickness and Surface Fatigue Cracks, *Fatigue and Fracture of Engineering Materials and Structures, Vol. 10, No. 5*, pp. 343-362.
14. McEvily, A. J. (1989) Discussion, *Fatigue and Fracture of Engineering Materials and Structures, Vol. 12, No. 1*, pp. 71-72.
15. Schijve, J. (1981) Some Formulae for the Crack Opening Stress Level, *Engineering Fracture Mechanics, Vol. 14*, pp.461-465.
16. Ibrahim, F. K. (1989) The Effect of Stress Ratio, Compressive Peak Stress and Maximum Stress Level on Fatigue Behaviour of 2024 - T3 Aluminium Alloy, *Fatigue and Fracture of Engineering Materials and Structures, Vol. 12, No. 1*, pp.1 - 8.
17. Crooker, T. W. (1971) Effect of Tension-Compression Cycling on Fatigue Crack Growth in High Strength Alloys, *Transactions of ASME, Journal of Engineering Industry, 93*, pp.893-896.
18. ASTM (1981) Appendix II, Fatigue Crack Growth Measurement and Data Analysis, *ASTM STP 738*.
19. Schmidt and Paris (1973) *ASTM STP 536*, pp.79.
20. Ritchie, R. O. (1986) Short Crack Effects in Fatigue: A Consequence of Crack Tip Shielding. *Small Fatigue Cracks*, edited by R. O. Ritchie and J. Lankford, A Publication of the Metallurgical Society Inc. pp.167-189.
21. Otsuka, A., Mori, K. and Miyata, T. (1975) The Condition of Fatigue Crack Growth in Mixed Mode Condition, *Engineering Fracture Mechanics, Vol.7*, pp.427.
22. Beevers, J. (1977) Fatigue Crack Growth Characteristics at Low Stress Intensity Factor for Metals and Alloys, *Metal Science, Vol. 11*, pp.362-367.
23. Klesnil, M. and Lukas, P. (1972) The Effect of Stress Cycle Asymmetry on Fatigue Crack Growth, *Materials Science & Engineering, Vol.9*, pp.231.
24. James, M. N. and Sharpe, W. N. Jr. (1989) Closure Development and Crack Opening Displacement in the Short Crack Regime for Fine and Coarse Grained A533B Steel, *Fatigue and Fracture of Engineering Materials and Structures, Vol. 12 No. 4*, pp. 347-367.

25. Macha, D., Corby, D. M. and Jones, J. W. (1979) The Variation of Fatigue Crack Opening Load with Measurement Location, *Experimental Mechanics*, Vol. 19, pp.213.
26. Miller, K. J., "The behaviour of Short Fatigue Cracks and Their Initiation Part I—A Review of Two Recent Books", *Fatigue Fracture of Engineering Materials and Structures*. Vol.10, No.1, 1987, pp. 75-91.
27. Miller, K. J., "The behaviour of Short Fatigue Cracks and Their Initiation Part II—A General Summary", *Fatigue Fracture of Engineering Materials and Structures*. Vol.10, No.2, 1987, pp.93-113.
28. Bu, R. and Stephens, R. I. (1986) Comparison of Short and Long Fatigue Crack Growth in 7075-T6 Aluminium, *Fatigue & Fracture of Engineering Materials and Structures*, Vol.19, No.1, pp.35-48.
29. Pook, L. P. and Smith, R. A. (1979) in *Fracture Mechanics—Current Status, Future Prospects*, edited by R. A. Smith, Pergamon Press, London.



- ◇ Carbon Steel (M. Klesnil & P. Lukas, 1972)
- 7075-T6 Al Alloy (R. Bu & R. I. Stephens, 1986)
- * SM50A Steel (K. J. Kang et al, 1989)
- + SAE1010 Steel (F. K. Ibrahim, 1989)
- ▽ 1.99CrMoV Steel (GEC, communication)
- ⊠ Aluminium (R. A. Smith)
- + Nickel Alloy (R. A. Smith)
- ◇ Monel Alloy (R. A. Smith)

Figure 5.1 Effect of Stress Ratio on Fatigue Threshold

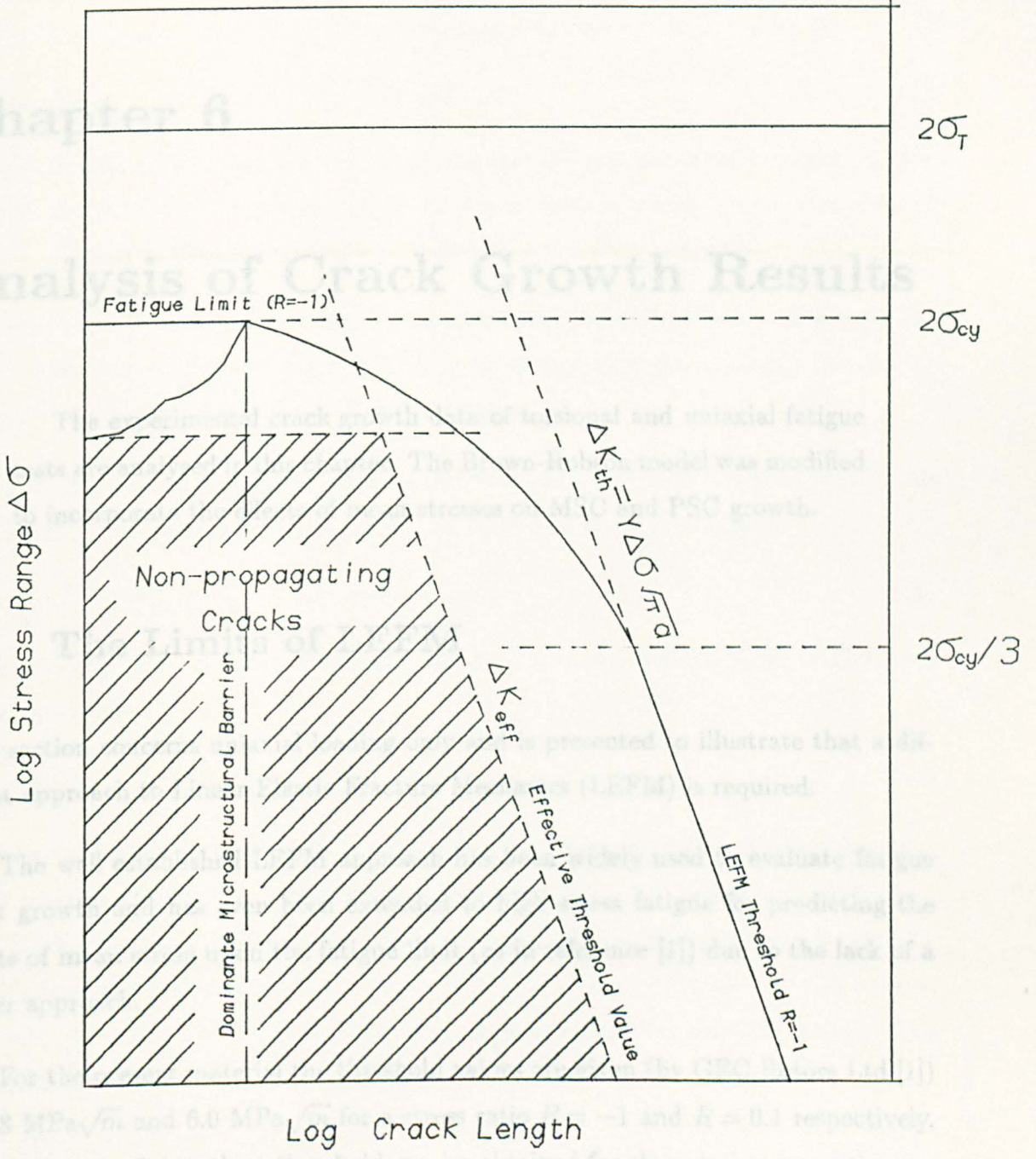


Fig.5.2 Schematic Drawing for the Effect of Stress Level and Stress Ratio

Chapter 6

Analysis of Crack Growth Results

The experimental crack growth data of torsional and uniaxial fatigue tests are analysed in this chapter. The Brown-Hobson model was modified to incorporate the effects of mean stresses on MSC and PSC growth.

6.1 The Limits of LEFM

This section concerns uniaxial loading only and is presented to illustrate that a different approach to Linear Elastic Fracture Mechanics (LEFM) is required.

The well established LEFM approach has been widely used to evaluate fatigue crack growth and has even been extended to high stress fatigue for predicting the effects of mean stress upon the fatigue limit (as in reference [1]) due to the lack of a better approach.

For the present material the threshold values are given (by GEC Rotors Ltd [1]) as $8.8 \text{ MPa}\sqrt{m}$ and $6.0 \text{ MPa}\sqrt{m}$ for a stress ratio $R = -1$ and $R = 0.1$ respectively. The surface crack length at threshold can be obtained for these two stress ratios,

$$a_{s,th(R)} = 2a_{th(R)} = \frac{1}{\pi} \left(\frac{\Delta K_{th(R)}}{Y \Delta \sigma} \right)^2 \quad (6.1)$$

where Y equals 0.64 for a surface semi-circular crack (assume that $a=0.5 a_s$). Hence

for $R = -1$ and $\sigma_a = 500$ MPa the non-propagating surface crack length is

$$a_{s,th(R=-1)} = \frac{2}{\pi} \left(\frac{8.8}{0.64 \times 1000} \right)^2 = 120 \text{ } \mu m \quad (6.2)$$

and for $R = 0.1$, $\sigma_a = 360$ MPa the non-propagating surface crack length is

$$a_{s,th(R=0.1)} = \frac{2}{\pi} \left(\frac{6.0}{0.64 \times 720} \right)^2 = 108 \text{ } \mu m \quad (6.3)$$

It can be seen that LEFM significantly over-estimates the non-propagating crack size for all stress ratios since, as presented in Chapter 4, surface cracks longer than $60 \text{ } \mu m$ tend to propagate at an increasing speed and do not become arrested.

While much work has been done to analyse the limits of LEFM and to estimate the limiting stress level for fully reversed cyclic loading (see reference [2]) the case of mean stress cycling has not been fully explored.

The requirement for the small scale yielding condition to be satisfied is that the maximum plastic zone size be less than one fiftieth of the crack length, i.e.

$$\frac{1}{6\pi} \left(\frac{K_{I,max}}{\sigma_y} \right)^2 \leq \frac{a}{50} \quad \text{for plane stress} \quad (6.4)$$

For a crack with a geometry factor, Y , equal to unit, the validity limit of LEFM is approximately,

$$\frac{\sigma_{max}}{\sigma_y} \leq \frac{1}{3} \quad (6.5)$$

Once this maximum stress level is exceeded, the values of $\sigma\sqrt{\pi a}$ derived from the stress intensity factor will significantly deviate from the real values and be dangerous. Therefore the application of LEFM to mean stress cycling should be strictly constrained below this level as shown in Fig.4.12. Whereas for the case of surface semi-circular cracks and $Y = 0.64$, the limiting peak stress level may be up to one-half of the yield stress,

$$\frac{\sigma_{max}}{\sigma_y} \leq \frac{1}{0.64} \frac{1}{3} = 0.52 \quad (6.6)$$

Even so LEFM cannot be used to evaluate fatigue crack growth under high maximum stress levels as illustrated by the above calculations.

Now the diagram presented by Kitagawa and Takahashi [3] has been cited in many technical papers to exemplify the applicability of LEM to the evaluation of non-propagating cracks and the effect of defect size on the fatigue limit. This diagram, however, does not consider the effect of mean stress as previously discussed. However some workers have suggested relating the fatigue limit to the fatigue threshold value obtained under a high stress ratio. This is now seem not to be appropriate; it has no physical meaning since the fatigue limit itself is also affected by stress ratio (or more precisely mean stress). By taking into account the above considerations, the Kitagawa-Takahashi diagram can be modified as shown in Fig.6.1.

6.2 Generation of Crack Growth Rate Data

A secant method was adopted in the present work to calculate the crack growth rate using the crack length data obtained from replicas. It has been demonstrated by many workers that short cracks, especially microstructurally short cracks (MSCs), do not exhibit a simple monotonic relationship to crack length as do LEM cracks. The disadvantage of the secant method is that compounded errors may be borne by the errors coming from the measurement of the short crack length.

Crack growth rate was taken as the average growth rate between two successive replica stages. The terms $a_{s,i}$ and $a_{s,i+1}$ are defined as crack length at two successive replication stages. The corresponding crack length was taken as the mean value of crack length during the cyclic interval, i.e.

$$a_{s,mean} = \frac{a_{s,i} + a_{s,i+1}}{2} = a_{s,i} + \frac{\delta a_s}{2} \quad (6.7)$$

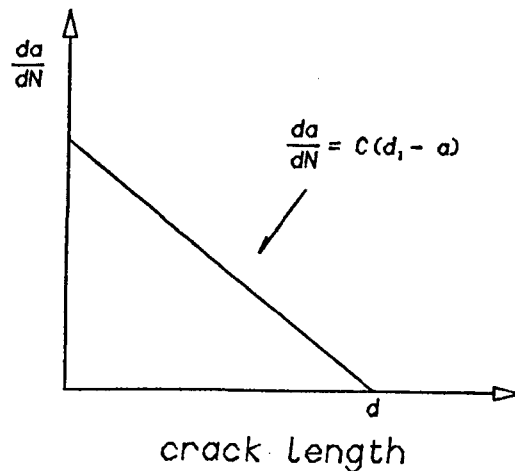
Finally the crack growth rate is as follows,

$$\frac{da_s}{dN} = \left(\frac{\delta a_s}{\delta N} \right)_{a_s = a_{s,mean}} \quad (6.8)$$

6.3 Microstructurally Short Crack Growth in Torsion

6.3.1 Introduction

In this section the MSC growth behaviour in torsion under various alternating and mean shear stresses will be examined. The diagram shown below illustrates the basic principle of MSC growth phase, hence this is what this section explores in order to



determine the parameters C_1 and A_1 in the equation,

$$\frac{da_s}{dN} = C_1 (d_1 - a_s) = A_1 \tau_a^\alpha (d_1 - a_s) \quad (6.9)$$

here C_1 is dependent on the applied stress, and A_1 may be a constant for constant mean stress. The shear stress amplitude τ_a ($= \Delta\tau/2$) is used instead of $\Delta\gamma_p$ or $\Delta\gamma_t$ because it is more reliably determined in experiments. However since $\Delta\tau$ can be related to the cyclic plastic strain or total strain range, then it is a simple matter to do the translation to strain parameters.

6.3.2 MSC Growth under Various Mean stress Torsional Loading

Crack growth rates were calculated by means of the secant method discussed in Section 6.2. Crack growth data have been presented in Chapter 3. While some cracks started promptly from inclusions, these being the dominant cracks, requiring no initiation, others were initiated in the base matrix probably due to micro-plasticity localization. If the plasticity localization phase is ignored then the fatigue process may be considered to be composed wholly of crack propagation, and one may be tempted to accept the extrapolation that the crack growth rate whilst zero at zero crack length, increases rapidly to a maximum level which is followed by a deceleration, as proposed by Lankford [4] for an aluminium alloy. It follows that for torsion N_0 (initiation) is assumed to be zero which is a reflection of the fact that cracks invariably started at inclusions which were favourably aligned to the direction of maximum shear stress. This will not be the case for push-pull loading.

The use of such models is appropriate should the plasticity localization period be removed by cycling at stress levels below the fatigue limit which may create non-propagating cracks. Therefore in the present work only the crack growth rates at crack lengths longer than $10 \mu m$ were analysed.

Crack growth rate data are presented in Figs.6.2 to 6.6, from which it can be seen that the majority of the cracks exhibited a slowing down in growth rate with an increase of crack length. Only a few cracks seemed to have grown at an increasing speed at the beginning and then started to decelerate possibly due to the fact that these cracks started from very small grains but eventually encountered grains with unfavourable orientations.

A "least squares" fit calculation was performed on those experimental points, where da_s/dN was decreasing for increasing crack length, in order to obtain both the values of slope C_1 and d_1 (Eq.6.9). Here d_1 was the value of a_s where the extrapolated "least square" equation intersected the crack length axis. Appendix 1 presents the

data and values of C_1 and d_1 for a total of 42 cracks. Considerable scatter exists which points to the fact that the MSC growth is strongly influenced by microstructure and texture.

The alternating stress level poses a strong influence upon short crack growth as shown in Fig.6.7a. A power law relationship is assumed between the alternating stress level and the values of C_1 when τ_m equals zero, i.e. $A_1 = 3.68 \times 10^{-52}$ and

$$C_1 = 3.68 \times 10^{-52} \tau_a^{19.07} \quad (\tau_m = 0) \quad (6.10)$$

The value of the exponent of 19.07 on shear stress amplitude is equivalent to an exponent of only 1.49 on plastic shear strain amplitude (see Eq.3.2 in Chapter 3).

The plot of the C_1 values as a function of mean shear stress level is shown in Fig.6.7b. An upper bound solution is chosen since fatigue life is dependent on the fastest growth rate. The best fit relationship is

$$C_1 = 1.715 \times 10^{-5} e^{\tau_m/62.6} \quad (\tau_a = 280 \text{ MPa}) \quad (6.11)$$

For an arbitrary combination of mean and alternating stress, the dependence of C_1 on the mean and alternating stress level can be obtained as follows, assuming the effects of the mean and alternating stress can be uncoupled, that is the parameter A_1 does not vary with alternating stress level. Therefore

$$C_1 = 3.68 \times 10^{-52} e^{\tau_m/62.6} \tau_a^{19.07} \quad (6.12)$$

The above modelling is supported by the data for test A2 in which $\tau_a = 293$ MPa, $\tau_m = 118$ MPa, the maximum value of C_1 is 29.8×10^{-5} and the prediction from the above equation is 25.3×10^{-5} .

Eq.6.12 can be rewritten as

$$C_1 = 3.68 \times 10^{-52} (\tau_a e^{\tau_m/1194})^{19.07} \quad (6.13)$$

Considering Eq.6.10, the term $(\tau_a e^{\tau_m/1194})$ can be designated as the 'effective shear stress amplitude' since it incorporates the effect of mean shear stress.

The above results reveal that mean shear stress enhances the crack growth rate. Since little or no friction between crack faces or crack closure is involved for shear type cracks in torsion (see Section 3.3), this detrimental effect of mean shear stress cannot be accounted for by the crack closure argument and hence cannot be correlated on the basis of an 'effective stress range' proposed from the push-pull or axial loading crack closure concept. The mechanisms involved must be different and need to be examined in more detail, particularly in relation to the effect of microstructure.

The decelerating growth pattern of MSCs is attributable to the effect of microstructure. The term d_1 is the distance between two strong microstructural barriers for a specific crack. Due to the random nature of the grain structure, d_1 values vary from crack to crack as shown in Figs.6.8a and 6.8b. For a total 43 cracks, d_1 values range from 48 μm to 310 μm . However, these two figures suggest that neither the mean shear stress level nor alternating stress level modifies the upper and lower bound of d_1 values. This confirms that d_1 is a measure of the degree of misorientation between the surrounding grains and is not affected by stress level (stress ratio and alternating stress level). Therefore the average of all d_1 values can provide an average measure of the resistance of a specific microstructure to the growth of short fatigue cracks. For the present material, the average distance between barriers $d_{1,average}$ equals 167 μm with a standard deviation of 67 μm .

The conclusion therefore of this section is that in terms of the simple Brown-Hobson model the microstructurally short crack growth phase is expressed by

$$\frac{da}{dN} = 3.68 \times 10^{-52} e^{\tau_m/62.6} \tau_a^{19.07} (d_1 - a) \quad \mu m/cycle \quad (6.14)$$

here $d_1 = 167\mu m$. This equation illustrates the importances of d_1 , τ_m and τ_a in the MSC growth phase.

6.4 Analysis of Physically Short Crack Growth in Torsion

6.4.1 Derivation of the crack growth equation

The previous section was concerned with cracks where microstructure played an important role, i.e. via the term d_1 in Equation 6.15.

This section concerns the condition of growth where microstructure is no longer a major consideration according to the Brown-Hobson model, i.e.

$$\frac{da_s}{dN} = B a_s - D = B_1 \tau_a^\beta a_s - D \quad (6.15)$$

Here B is a function of the alternating and mean shear stress level, and B_1 may be constant for constant mean stress.

However the microstructure continues to have a role (but a rapidly decreasing role) as depicted in the Navarro-de los Rios model [6]. The crack growth rate data in Figs.6.2 to 6.6 show such an effect beyond about $167 \mu m$. However, the two basic assumptions in the Navarro-de los Rios model need to be re-examined and modified to enable its application to the case of mean stress loading. This will be a part of further work following this project.

In the following analysis the Brown-Hobson Model is adopted and modified to take into account the effect of mean stress. The advantages of this model are its simplicity and possible use by designers. Its empirical nature is derived from experimental results.

As shown in Figs.6.2 to 6.6, albeit that the crack growth rate increases with crack length, the oscillation of the growth rates renders the successful application of the 'least squares' fit approach inappropriate. The considerable scatter in the crack growth rate can be ascribed to two reasons; Firstly, the microstructure of the material can seriously perturb the crack growth. As discussed in Chapter 3, one of two possible (mutually perpendicular) slip systems is favoured under torsional

loading. Additionally the periodic spread of the shear band at the crack tip is a result of the mis-orientation between grains, although the increase in crack length tends to increase the crack growth rate. Secondly, errors can be introduced during measurements, since cracks are very narrow, especially at locations close to crack tips and can be obscured by microstructural features. This makes it difficult to ascertain the position of a crack tip. As a result, cracks do not exhibit monotonically increasing growth rate against crack length as is suggested in the Brown-Hobson model although not in the Navarro-de los Rios model.

However, Figs.3.2 to 3.6 suggest that the logarithm of the surface crack length ($\log a_s$) shows a good linearity with respect to the cycles (N) when cracks are longer than certain lengths which are dependent on the mean and alternating stress level. For example about $167 \mu\text{m}$ for zero mean shear stress with a shear stress amplitude of 280 MPa.

$$\log a_s = A_0 + B_0 N \quad \text{for a certain stress state}$$

It follows that the overall crack growth rate can be obtained by differentiating the above equation,

$$\frac{d \log a_s}{d N} = \frac{1}{a_s} \frac{d a_s}{d N} \quad (6.16)$$

so

$$\frac{d a_s}{d N} = \frac{d \log a_s}{d N} \times a_s = B_0 a_s \quad (6.17)$$

and it is not unreasonable to adopt the fracture mechanics approach to simplify the analysis with the assumption that crack growth rate increases in proportion to crack length. In order to simulate the fatigue limit and non-propagating cracks, a threshold crack length is also introduced as in the Brown-Hobson model leading to

$$\frac{d a_s}{d N} = B (a_s - a_{s,th}) = B a_s - D \quad (6.18)$$

where B and $a_{s,th}$ are dependent on both τ_a and τ_m .

Difficulties have arisen in obtaining the values B and $a_{s,th}$ directly from the crack growth rate data since the results obtained using the 'least squares' fit method show

a vast scatter. A new approach is therefore required here which should at least offer a reasonable prediction to the crack growth data.

The fatigue process can be divided into three phases, (i) plasticity localization which induces, by cyclic softening, the creation of a fatigue crack. This period is denoted by N_0 , (ii) a crack propagation phase which is concerned with both the MSC growth phase and the PSC growth phase; the joint period of crack propagation will be denoted by N_p . In other words,

$$N = N_0 + N_p \quad (6.19)$$

where N_p can be obtained by integrating the two crack growth equations Eq.6.9 and Eq.6.17.

$$\begin{aligned} N_p &= N - N_0 = \int_{a_{s,0}}^{a_{s,1}} \frac{d a}{C_1 (d_1 - a)} + \int_{a_{s,1}}^{a_s} \frac{d a}{B (a - a_{s,th})} \\ &= \frac{1}{C_1} \log \frac{d_1 - a_{s,0}}{d_1 - a_{s,1}} + \frac{1}{B} \log \frac{a_s - a_{s,th}}{a_{s,1} - a_{s,th}} \end{aligned} \quad (6.20)$$

where $a_{s,1}$ is the crack length when the two lines represented by Eq.6.9 and Eq.6.17 intersect with each other, viz,

$$C_1 (d_1 - a_{s,1}) = B (a_{s,1} - a_{s,th}) \quad (6.21)$$

Hence,

$$a_{s,1} = \frac{C_1 d_1 + B a_{s,th}}{C_1 + B} \quad (6.22)$$

Inserting the above equation into Eq.6.17, give

$$\begin{aligned} \log(a_s - a_{s,th}) &= B(N - N_0) + \log \frac{C_1(d_1 - a_{s,th})}{C_1 + B} - \frac{B}{C_1} \log \frac{(C_1 + B)(d_1 - a_{s,0})}{B(d_1 - a_{s,th})} \\ &= B(N - N_0) + Y(B, a_{s,th}, C_1, d_1) \end{aligned} \quad (6.23)$$

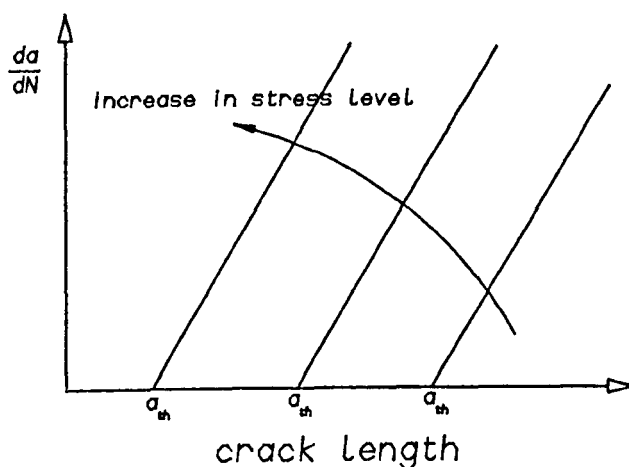
where

$$Y(B, a_{s,th}, C_1, d_1) = \log \frac{C_1(d_1 - a_{s,th})}{C_1 + B} - \frac{B}{C_1} \log \frac{(C_1 + B)(d_1 - a_{s,0})}{B(d_1 - a_{s,th})} \quad (6.24)$$

Here the values of C_1 and d_1 are obtained for a specific crack from the calculations carried out in Section 6.3.1. As the value of a_{th} is almost impossible to determine

directly from crack growth data, a simplified analysis is developed here to rationalise the crack growth rate.

To illustrate simply what this analysis is attempting to do is to find satisfactory curves such as those shown below but it requires putting in values for the zero crack growth rate, i.e. the parameter $a_{s,th}$.



The threshold crack length $a_{s,th}$ was taken as zero to obtain a first order approximation. A “least squares” fit calculation was performed for every crack at those points where a crack is longer than the length read from Figs.3.2 to 3.6 after which a linearity between $\log(a_s)$ and N is observed. The results are shown in Table 6.1.

The first order results may become more inaccurate at low stress levels and the fatigue limit is unexplainable because Eq.6.9 and Eq.6.17 predict a finite fatigue life at any stress level if $a_{s,th}$ is assumed to be zero. Therefore an improved attempt has been made in the above model by incorporating a specific threshold value.

Since the fatigue limit corresponds to the condition when $a_{th} = d_1$ (see also reference [2]), an increase in mean stress will assist in accelerating the removal of the microstructural barrier effect and reduce the fatigue lifetime for a constant alternating stress level. This means that the presence of mean stress can reduce the threshold crack size $a_{s,th}$ for a constant alternating stress. Due to the competition between the increase in B and the reduction in $a_{s,th}$, it can be a good approximation to assume

that $B a_{s,th}$ is constant. It has been reported in the literature [2] that the threshold D value is independent of the stress range for fully reversed loading, in which LEFM was applied for want of a better approach. In the present work the use of LEFM becomes even more doubtful as there has been no study on the effect of mean shear stress upon the stress intensity factor threshold which is unknown under torsional loading.

In the case of a low stress level and long fatigue life, the value of $a_{s,th}$ must be very close to the value of d_1 . For simplicity, $a_{s,th}$ was taken to be equal to $(d_1 - 15\mu m)$ and Eq.6.23 was used to calculate B for the six cracks in specimens A8 and A10 ($\tau_m = 0$ MPa). Fig.6.2 shows that the derived value provides a reasonable correlation to the experimental crack growth rate data. The average value of $B a_{s,th}$ was then considered as the constant for any mean and alternating shear stress level. Therefore all other crack growth data were normalised as below and a repeated calculation was carried out for every crack in which $a_{s,th}$ increased from zero to a certain value at which the value of D equals the average value of D derived from the results of zero mean stress tests. Table 6.1 presents the results for all the cracks.

6.4.2 Effect of mean shear stress on PSC growth and its modelling

Table 6.1 shows that the values of B and B_1 are dependent on both the mean and alternating shear stress level. A power-law relationship is assumed between B and τ_a as $B = B_0 \tau_a^\alpha$ where B_0 is constant for a certain mean shear stress but varies with mean shear stress.

For the data from fully reversed loading tests, the maximum and mean value of B are given by

$$B_{max} = 1.09 \times 10^{-34} \tau_a^{11.712} \quad (6.25)$$

$$\bar{B} = 3.94 \times 10^{-37} \tau_a^{12.65} \quad (6.26)$$

The values of B_{max} and \bar{B} for non-zero mean shear stress tests are plotted against mean shear stress as in Fig.6.9 (a) and (b), respectively. The upper bound of the maximum value of B and best fit relationships are

$$B_{max} = 4.47 \times 10^{-6} e^{\tau_m/66.5} \quad (6.27)$$

$$\bar{B} = 2.82 \times 10^{-6} e^{\tau_m/64.6} \quad (6.28)$$

Here B_{max} corresponds to the fastest growing crack whereas \bar{B} presents an average measurement of the PSC growth behaviour in the material. In order to predict the fatigue lifetime which is invariably dictated by the fastest growing crack, B_{max} will be used in the following discussions.

Following the same argument used in Section 6.3 the above two equations can be combined to provide a general equation for the value of B_{max} assuming that B_{max} can be expressed as $B_{max} = A h(\tau_m) \tau_a^\alpha$. Here the function $h(\tau_m)$ equals unit for $\tau_m = 0$ and so $A = 1.09 \times 10^{-34}$ and $\alpha = 11.712$. Thus,

$$B_{max} = 1.09 \times 10^{-34} e^{\tau_m/66.5} \tau_a^{11.712} \quad (6.29)$$

From the analysis in this section it can be concluded that for the PSC growth phase

$$\frac{d a_s}{d N} = 1.09 \times 10^{-34} e^{\tau_m/66.5} \tau_a^{11.712} a_s - D \quad \mu m/cycle \quad (6.30)$$

here $D = 5.1 \times 10^{-4} \mu m/cycle$. Figs.6.2 to 6.6 show that the present model with the above derived values of B_{max} and D provides satisfactory correlation to the experimental crack growth rate data.

Thus we now have a complete set of equations (Eq.6.14 and Eq.6.30) for which fatigue lifetime can be calculated by the addition of the integrated equation, this of course assumes that N_0 is zero for the failure or dominant crack although this need not to be so for other cracks monitored on the specimen; see Table 6.1. Fig.6.10 schematically shows the changes in crack growth behaviour with the change in the mean or alternating shear stress.

6.5 Torsional Fatigue Lifetimes Prediction

Following the procedure explained in Section 6.3, the total fatigue lifetime is the summation of the plasticity localization period, the MSC propagation period and the PSC propagation period.

The boundary between the later two periods is the intersecting point ($a_{s,th}$) of the two lines represented by Eq.6.9 and Eq.6.15 (see Section 6.4.1). The period of plasticity localization is significantly dependent on surface finish and the material microstructure. For example, the material used in the present investigation has a high population of inclusions aligned to the maximum shear plane. Therefore dominant cracks are easy to start from inclusions and for these cracks, the plasticity localization period can be neglected as these cracks started promptly at the beginning of a test.

Therefore the total predicted fatigue life can, on the conservative side, be expressed as the summation of two periods, ie. the MSC propagation period and the PSC propagation period,

$$\begin{aligned} N_f &= \int_{a_{s,0}}^{a_{s,1}} \frac{d a}{C_1 (d_1 - a)} + \int_{a_{s,1}}^{a_f} \frac{d a}{B a - D} \\ &= \frac{1}{C_1} \log \frac{d_1 - a_{s,0}}{d_1 - a_{s,1}} + \frac{1}{B} \log \frac{a_f - a_{s,th}}{a_{s,1} - a_{s,th}} \end{aligned} \quad (6.31)$$

here $a_{s,0}$ should be taken as the size of the largest inclusion. As only a very short period is required to propagate a crack from $2 \mu m$ to the size of inclusions, $a_{s,0}$ is taken to be $2 \mu m$ for simplicity. The threshold crack size $a_{s,th} = D/B$. The value of $a_{s,1}$ is given by Eq.6.22. For each stress state (ie. different values of alternating and mean shear stress), the values of C_1 and B are given by Eq.6.13 and Eq.6.27 or Eq.6.28.

The two individual periods together with the total predicted lifetime and actual lifetime are given in Table 6.2. Fig.6.11(a) shows the actual life and predicted life with two bounding lines, namely $\times 1.5$ (*safe*) and $\times 0.67$ (*unsafe*), indicating that the predictions can be accepted as satisfactory.

Therefore the fatigue lifetime under mean stress torsional loading can be obtained

by integrating the two crack growth equations (Eq.6.13 and Eq.6.32). Fig.6.11(b) presents the predictions of $S - N$ curves at four different mean shear stress level together with the experimental data.

6.6 MSC Growth under Uniaxial Loading

In this section the MSC growth behaviour under various mean stress uniaxial loading conditions will be examined in a similar manner to that used previously for torsion. However in uniaxial loading the size of the inclusions do not have the significance they had in torsional loading hence N_0 will not be zero.

6.6.1 Fully Reversed Loading

The simple model used in Section 6.3 was also adopted for the present case to simplify the analysis of the fatigue crack growth data under uniaxial loading with various alternating and mean stresses. Figs.6.12 (a) to (h) show some of the experimental crack growth data. In order to obtain the appropriate fit to crack growth rate, two models were examined in parallel. The first model is devoted to fitting the envelope of the crack growth rate i.e the upper bound to the crack growth rate. Obviously this model will only emphasize the effect of the prior austenite grain size which presents the largest microstructural barrier type feature in uniaxial loading. The second model gives the average growth rate, which may incorporate the effect of the sub-structure or bundles within the prior austenite grains upon the crack growth.

$$\frac{da_s}{dN} = C_{max} (d - a_s) \quad (6.32)$$

$$\frac{da_s}{dN} = \bar{C} (d - a_s) \quad (6.33)$$

here d is taken to be $50 \mu m$ providing a rationale for the initial Stage I crack growth. Fig.6.13 shows a typical plot of $d - a_s$ versus da/dN for several cracks in test A31. For each pair of data, a value of C can be calculated on the basis of the above equation.

Fig.6.13 also shows the enormous amount of scatter in the values of C . Here the two lines are corresponding to C_{max} and \bar{C} respectively, which are the envelope curve and the average growth rate curve. The values of C_{max} and \bar{C} for a total number of 75 cracks in some 21 specimens are presented in Table 6.3, in which the values have been classified into different groups of stress states.

The values of C_{max} and \bar{C} at four stress levels ($R = -1$) are then plotted against the relevant stress range as shown in Fig.6.14a and 6.14b. A power-law relationship seems to provide a good correlation,

$$C_{max} = 3.894 \times 10^{-78} \sigma_a^{27.2} \quad (6.34)$$

$$\bar{C} = 1.513 \times 10^{-64} \sigma_a^{22.06} \quad (6.35)$$

6.6.2 Effect of mean axial stress

Similar calculations can also be performed for mean stress loading tests and the results are summarised in Table 6.3. Here both the values of C_{max} and \bar{C} are presented.

The figures (Fig.4.9 and Fig.4.10) presented in Chapter 4 suggest that for low alternating stress, mean tensile stress can enhance the plasticity localization and reduce the fatigue endurance. With regard to the MSC growth rate, the effect of mean stress is more significant. For example, compare test A51 with A52 and A53. A mean tensile stress of 100 MPa increased the MSC growth rate by more than 3 times for a certain crack length, viz, C_{max} increased from 0.95×10^{-5} to 6.0×10^{-5} and \bar{C} increased from 0.85×10^{-5} to 2.10×10^{-5} (see Table 6.3). In this case the stress ratio changed from -1 to -0.645 . Such a significant effect of mean tensile stress on short crack growth is far beyond the predictions by traditional models developed in the frame work of LEFM.

In the present case, tests at high stress ratios were invariably under low alternating stress to avoid ratcheting failure. The combination of high mean stress level and relatively low alternating stress level produced similar crack growth rates to high σ_a

plus low σ_m conditions (see Table 6.3 and Fig.6.12). Generally, crack growth rate is a function of the alternating stress level and the mean stress level and any universal equation should be able to predict the crack growth rate in the case of fully reversed loading when mean stress is zero. Therefore, similar to Section 6.3, a simple equation can be expressed as follows (if the effects of alternating stress level and mean stress level can be uncoupled) which becomes identical to Eq.6.34 for zero mean stress,

$$C_{max} = 3.894 \times 10^{-78} [f_1(\sigma_m) \sigma_a]^{27.2} \quad (6.36)$$

$$\bar{C} = 1.513 \times 10^{-64} [f_2(\sigma_m) \sigma_a]^{22.06} \quad (6.37)$$

where f_1 and f_2 are two unknown functions of mean stress which will be derived by fitting the experimental data. These two equations imply that Eq.6.34 and Eq.6.35 can be extrapolated to the low stress region although this may not be rigorous considering that no crack initiation would occur at $\sigma_a = 300$ MPa and $R = -1$. However the above approach is supported by the present data. For example the values of C_{max} and \bar{C} for tests A57, A58, and A60 (see Table 6.3) suggest that for the stress states with a high mean stress level and a low alternating stress, the overall contribution of alternating stress and mean stress can be expressed as illustrated by Eq.6.36 and 6.40.

A calculation was performed as detailed below to determine the functions $f_1(\sigma_m)$ and $f_2(\sigma_m)$. For each stress state, the values of these two functions are computed using the following equations,

$$f_1(\sigma_m) = \frac{1}{\sigma_a} \left(\frac{C_{max}}{3.894 \times 10^{-78}} \right)^{\frac{1}{27.2}} \quad (6.38)$$

$$f_2(\sigma_m) = \frac{1}{\sigma_a} \left(\frac{\bar{C}}{1.513 \times 10^{-64}} \right)^{\frac{1}{22.06}} \quad (6.39)$$

The calculation was performed for all the data of C_{max} and \bar{C} presented in Table 6.3. The results are plotted against the mean stress level in Fig.6.15a and 6.15b which suggest that for tensile mean stress, $f_1(\sigma_m)$ and $f_2(\sigma_m)$ increase with mean tensile stress, but for compressive mean stress they appear to be constant.

The correlation between $f_1(\sigma_m)$ and $f_2(\sigma_m)$ with mean tensile stress are given by

$$f_1(\sigma_m) = 0.99 e^{\sigma_m/1171} \approx 1.0 + \sigma_m/1171 \quad \sigma_m > 0 \quad (6.40)$$

$$f_2(\sigma_m) = 0.98 e^{\sigma_m/1195} \approx 1.0 + \sigma_m/1195 \quad \sigma_m > 0 \quad (6.41)$$

The above two functions can be considered to be virtually identical since the error is far less than the scatter of the data. This suggests that mean tensile stress not only increases the upper bound of the crack growth rate but also the average growth rate.

Compressive mean stress, however, appears to have neither a detrimental effect nor a beneficial effect on short crack growth, the function $f(\sigma_m)$ being equal to unit. This is puzzling on the ground of the following two considerations: (1) Crack growth rate is traditionally believed to be lower when the stress ratio is reduced. (2) The crack closure consideration invariably leads to the conclusion that compressive mean stress reduces the effective stress when a crack is open and hence crack growth rate will be reduced. The conflicts between the present experimental results and the current understanding of crack growth mechanisms under mean stress loading votes for a new approach to be established to provide a better physical understanding and a theoretical modelling of crack growth behaviour. Further discussion will be presented in Chapter 7.

The conclusion therefore for this section is that the MSC growth phase (upper bound) under uniaxial loading can be expressed as the following by inserting Eq.6.40 and Eq.6.41 into Eq.6.36 and Eq.6.37,

the upper bound

$$\frac{da_s}{dN} = 3.894 \times 10^{-78} e^{\sigma_m/43.1} \sigma_a^{27.2} (d - a_s) \quad \text{when } \sigma_m \geq 0 \quad (6.42)$$

$$\frac{d a}{d N} = 3.894 \times 10^{-78} \sigma_a^{27.2} (d_2 - a) \quad \text{when } \sigma_m \leq 0 \quad (6.43)$$

the average rate

$$\frac{da_s}{dN} = 1.513 \times 10^{-64} e^{\sigma_m/54.1} \sigma_a^{22.1} (d - a_s) \quad \text{for } \sigma_m \geq 0 \quad (6.44)$$

here $d_2 = 50\mu m$ and the unit of the crack growth rate is $\mu m/cycle$.

6.7 PSC Growth under Uniaxial Loading

The crack growth rate data presented in Fig.6.12 suggest that, on log-log scale, the crack growth rate for crack lengths greater than 100 μm shows a linear relation to crack length. Therefore the crack growth rate can be expressed as,

$$\frac{da_s}{dN} = G_0 a_s^n \quad (\text{for a certain stress state}) \quad (6.45)$$

A regression line was fitted to data points obtained from replicas where crack length was greater than 150 microns to obtain the values of G_0 and n . The results are summarised in Table 6.3, indicating that G_0 is dependent on both the alternating and mean stresses. The majority of the values of n are within a range from 1.256 to 1.581 with an average value of 1.405, irrespective of the stress state. A single value of n required for further analysis was taken as the average of all the n values which provides a rationale for the correlation between crack growth rate and crack length, then the following equation is obtained,

$$\frac{da_s}{dN} = G(\sigma_a, \sigma_m) a_s^{1.405} \quad (\mu m/cycle) \quad (6.46)$$

where the exponential index 1.405 is the average of all n values shown in Table 6.3. The obtained values of G are also shown in Table 6.3.

6.7.1 Fully reversed loading

The function G (when $\sigma_m = 0$) follows a power-law relationship,

$$G(\sigma_a) = 2.346 \times 10^{-58} \sigma_a^{19.33} \quad (6.47)$$

Fig.6.16 shows the data points together with the curve of the above equation.

Since the crack growth rate where crack length is less than 50 microns is given by Eq.6.42, Eq.6.43 and Eq.6.44, it is important to determine the intersecting point where crack growth can start to be considered as having been taken over by PSC growth governed by Eq.6.47. The fatigue limit is related to the transition point. For

example, two cracks (30 and 39 microns respectively) were found in test B29 which did not propagate after 1.5×10^7 cycles. Therefore Eq.6.46 needs to be modified accordingly,

$$\frac{da_s}{dN} = G(\sigma_a) a_s^{1.405} - D \quad (6.48)$$

The determination of the value of D directly from crack growth data was found extremely difficult in the present case, due to the enormous scatter in the data (see also Section 6.4). Consequently a calculation was performed to estimate the value of D . The Integration of Eq.6.42 (or Eq.6.43 for compressive mean stress case) and Eq.6.48 plus N_0 should provide a best fit to $a - N$ curves as shown in Section 6.4.1, viz,

$$N - N_0 = \int_{a_0}^{a_1} \frac{d a_s}{C_{max}(d - a_s)} + \int_{a_1}^a \frac{d a_s}{G a_s^{1.405} - D} \quad (6.49)$$

where a_1 and D is related by

$$D = G a_1^{1.405} - C_{max} (d - a_1) \quad (6.50)$$

here the plasticity localization period (N_0) (see Table 6.3) decreases with an increase of stress level, the best fit relationship for the case of fully reversed loading is

$$N_0 = 2.97 \times 10^{66} \sigma_a^{-23} \quad (6.51)$$

An iterative computation was carried out by running a programme in which a convergence of values of a_1 was tried. The required a_1 was obtained when the two sides in Eq.6.49 were sufficiently close to each other. The results of the calculated D values are presented in Table 6.3.

The derived D values (see Table 6.3) are not constant for different alternating stress but increase with the stress level,

$$D = 2.76 \times 10^{-34} \sigma_a^{11.1} \quad (\mu m/cycle) \quad (6.52)$$

As a conclusion of this section, the PSC growth under fully reversed loading can be expressed as

$$\frac{d a_s}{d N} = 2.346 \times 10^{-58} \sigma_a^{19.33} a_s^{1.405} - D \quad (\mu m/cycle) \quad (6.53)$$

where D is given by Eq.6.52.

6.7.2 Uniaxial loading under mean stress

Following the same approach as in the previous section, the crack growth rate under mean stress loading can be expressed as,

$$\frac{d a_s}{dN} = G(\sigma_a, \sigma_m) a_s^{1.405} - D \quad (6.54)$$

In a similar to Sections 6.3 and 6.6, the value of G can be expressed as

$$G(\sigma_a, \sigma_m) = 2.346 \times 10^{-58} [f_3(\sigma_m) \sigma_a]^{19.33} \quad (6.55)$$

where the function f_3 was calculated from the following equation,

$$f_3(\sigma_m) = \left(\frac{G}{2.346 \times 10^{-58}} \right)^{\frac{1}{19.33}} \quad (6.56)$$

The calculated results are shown in Fig.6.17 together with the curve of the following regression relationship,

$$f_3(\sigma_m) = 0.99 e^{\sigma_m/1083} \approx 1.0 + \sigma_m/1083 \quad \text{when } \sigma_m > 0 \quad (6.57)$$

Fig.6.17 also suggests that the function $f_3(\sigma_m)$ equals unity for $\sigma_m < 0$ since compressive mean stress seems to have no significant effect on the value of $G(\sigma_a, \sigma_m)$ (when $-200 < \sigma_m < 0$).

If the term $f(\sigma_m) \sigma_a$ is denoted as the effective stress amplitude, which includes the contribution of mean stress, the parity between $f_1(\sigma_m)$, $f_2(\sigma_m)$ and $f_3(\sigma_m)$ suggests that the effect of mean tensile stress on both Stage I and Stage II crack growth rate could be unified by a single parameter ($f(\sigma_m)\sigma_a$).

Following the same approach as used in deriving C and G for mean stress loading conditions, the values of N_0 and D can be expressed as

$$N_0 = 2.97 \times 10^{66} e^{-\sigma_m/51.5} \sigma_a^{-23} \quad (\sigma_m \geq 0) \quad (6.58)$$

$$D = 2.76 \times 10^{-34} e^{\sigma_m/137} \sigma_a^{11.1} \quad (\mu\text{m}/\text{cycle}) \quad (\sigma_m \geq 0) \quad (6.59)$$

From the analysis in this section it can be concluded that for the PSC growth phase under uniaxial loading with tensile mean stress,

$$\frac{d a}{d N} = 2.346 \times 10^{-58} e^{\sigma_m/56.1} \sigma_a^{19.33} a^{1.405} - D \quad \mu\text{m}/\text{cycle} \quad (6.60)$$

where D is given by Eq.6.59. In the case of mean compressive stress, the crack growth rate is approximately identical to that of fully reversed loading.

Thus we now have a complete set of equations (Eq.6.42 and Eq.6.60) from which fatigue lifetime can be calculated by the addition of the integrated equations plus the plasticity localization period (N_0).

6.8 Uniaxial Fatigue Lifetime Prediction

Following the foregoing analyses, total fatigue life can be expressed as a summation of N_0 and N_p , i.e.

$$\begin{aligned} N_f &= N_0 + N_p = N_0 + \int_{a_0}^{a_1} \frac{d a}{C (d - a)} + \int_{a_1}^{a_f} a_f \frac{d a}{G a^{1.405} - D} \\ &= N_0 + \frac{1}{C} \log \frac{d - a_0}{d - a_1} + \int_{a_1}^{a_f} \frac{d a}{G a^{1.405} - D} \end{aligned} \quad (6.61)$$

where $d = 50\mu m$ for uniaxial loading and a_0 equals $2\mu m$ (surface roughness). The terms a_1 , C and G are given by Eq.6.50, Eq.6.34 and Eq.6.55, respectively.

A numerical computation was carried out to obtain the total predicted fatigue lifetime. The results are shown in Table 6.4. Fig.6.18 shows the actual life and predicted life with two bounding lines, namely $\times 2.0$ (*safe*) and $\times 0.5$ (*unsafe*). The predicted $S - N$ curves at five different mean stress levels together with some experimental data are shown in Fig.6.19. These two figures suggest that the present model provides a satisfactory prediction to fatigue lifetime curves at different mean stress levels.

6.9 Summary

The principal aim of this chapter is to study the effects of mean stresses on short fatigue crack growth in order to improve understanding of the effects of mean stresses on the fatigue strength of materials.

There are two distinct short crack growth phases: the MSC phase and the PSC phase. In the MSC phase, crack growth is strongly affected by microstructure while in the PSC phase the microstructural effect tends to diminish with the increase of crack length.

Mean shear stress has a significant effect on both MSC (growing in Mode II) and PSC growth rate under torsional loading as depicted in Eq.6.13 and Eq6.30 which can be rewritten as

$$\begin{aligned} \frac{da_s}{dN} &= C(\tau_a, \tau_m) (d_1 - a_s) \\ &= 3.68 \times 10^{-52} (e^{\tau_m/1194} \tau_a)^{19.07} (d_1 - a_s) \quad \text{for } (a_s \leq a_{s,1}) \end{aligned} \quad (6.62)$$

$$\begin{aligned} \frac{d a_s}{d N} &= B(\tau_a, \tau_m) a_s - D \\ &= 1.09 \times 10^{-34} (e^{\tau_m/779} \tau_a)^{11.712} a_s - D \quad \text{for } (a_s \geq a_{s,1}) \end{aligned} \quad (6.63)$$

here $d_1 = 167 \mu m$ and $D = 5.1 \times 10^{-4} \mu m/cycle$, with both terms being independent of the mean or alternating shear stress. In both equations τ_m and τ_a are expressed in MPa. The term $a_{s,1}$ is the crack length at which the two lines represented by the above equations intersect with each other.

Fig.6.20 shows the characteristic crack growth pattern under different combinations of the alternating and mean shear stresses.

In torsion tests, the polarity of the mean shear stress has no effect on MSC growth (although materials may be anisotropic) and PSC growth in isotropic materials. But mean shear stress can have a significant effect on PSC crack growth in anisotropic materials.

When considering push-pull tests, a mean uniaxial stress, however, shows strong preference towards its polarity in promoting MSC and PSC growth in isotropic materials: mean tensile stress increases short crack growth rate while mean compressive stress does not. The following equations characterise the crack growth behaviour under uniaxial loading for the present material:

Tensile mean stress ($\sigma_m \geq 0$)

$$\frac{d a_s}{d N} = C(\sigma_a, \sigma_m) (d_2 - a_s)$$

$$= 3.894 \times 10^{-78} (e^{\sigma_m/1172} \sigma_a)^{27.2} (d_2 - a_s) \quad \text{for } a_s \leq a_{s,1} \quad (6.64)$$

where $d_2 = 50 \mu m$

$$\begin{aligned} \frac{d a_s}{d N} &= G(\sigma_a, \sigma_m) a_s^n - D \\ &= 2.346 \times 10^{-58} e^{\sigma_m/56.1} \sigma_a^{19.33} a_s^{1.405} - D \quad \text{for } a_s \geq a_{s,1} \end{aligned} \quad (6.65)$$

where D is given by Eq.6.59 as $2.76 \times 10^{-34} (e^{\sigma_m/1521} \sigma_a)^{11.1}$. The term $a_{s,1}$ is the crack length at which the two lines represented by the above equations intersect with each other. One example of the different effects of mean and alternating stresses is shown in Fig.6.21

Compressive mean stress ($-200 \leq \sigma_m \leq 0$) In this case the MSC and PSC crack growth rates are the same as in the case of fully reversed loading ($\sigma_m = 0$). In other words, the crack growth rates are given by Eq.6.64 and Eq.6.64 in which the mean stress σ_m is taken to be zero.

References

1. Suhr, R. W. (1986) The Effect of Surface Finish on High Cycle Fatigue of a Low Alloy Steel, *The Behaviour of Short Fatigue Cracks*, EGF Publication No.1 (edited by K. J. Miller and E. R. de los Rios) pp.69-86.
2. Brown, M. W. (1986) Interfaces between Short, Long and Non-propagating Cracks, *The Behaviour of Short Fatigue Cracks*, EGF Publication No.1 (edited by K. J. Miller and E. R. de los Rios) pp.423-439.
3. Kitagawa, H. and Takahashi, S. (1976) Applicability of Fracture Mechanics to Very Small Cracks or the Cracks in the Early Stage, *Proc. 2nd Int. Conf. Mech. Behaviour of Metals, Boston*, pp.627-631.
4. Lankford, J. (1982) The Growth of Small Fatigue Cracks in 7075-T6 Aluminium Alloy, *Fatigue and Fracture of Engineering Materials and Structures, Vol.5*, pp.233-348.
5. Tomkins, B. (1968) Fatigue Crack Propagation—An Analysis, *Philosophical Magazine, 18*, 1968, pp.1041.
6. Navarro, A. and de los Rios, E. R. (1988) Short and Long Fatigue Crack Growth: A Unified Model, *Philosophical Magazine A, Vol.57, No.1*, pp.15-36.

Table 6.1:
Results of Torsional Tests

Stress τ_a MPa	Mean Stress MPa	No. of Crack	N_0 Cycles	C_1 $\times 10^5$	d_1 μm	B_0 $\times 10^5$	a_{th} μm	B $\times 10^5$	D $\mu m/cycle$ $\times 10^3$
280	0	A8-1	146740	0.474	217	0.233	202	0.512	1.07
		A8-2	132500	1.212	124	0.122	108	0.229	0.249
		A8-3	0	1.685	164	0.123	149	0.460	0.683
		A8-4	0	—	166	0.073	151	0.100	0.151
		A10-1	64571	1.27	120	0.278	105	0.463	0.486
		A10-2	64571	0.34	170	0.148	155	0.491	0.761
280	20	A9-1	44311	1.72	110	0.157	145	0.351	0.51
		A9-2	44311	2.39	167	0.161	150	0.339	0.51
280	52	A3-1	60050	3.50	211	0.124	151	0.293	0.51
		A3-2	79008	4.27	105	0.384	68	0.752	0.51
		A3-3	0	2.20	217	0.207	130	0.392	0.51
		A3-4	60050	1.88	251	0.283	121	0.423	0.51
280	79	A1-1	0	1.76	207	0.857	49	1.05	0.51
		A1-2	0	6.01	146	0.363	93	0.550	0.51
		A1-3	36617	2.26	170	0.253	100	0.509	0.51
		A1-4	26440	3.06	194	0.305	93	0.548	0.51
280	84	A4-1	0	5.29	111	0.747	51	1.00	0.51
		A4-2	36155	3.61	85	1.06	34	1.473	0.51
		A4-3	16516	5.85	73	0.655	46	1.092	0.51
		A4-4	0	3.11	223	0.544	73	0.698	0.51
280	90	A5-1	0	7.17	131	1.52	30	1.676	0.51
		A5-2	13504	2.15	290	1.84	25	1.996	0.51
		A5-4	28156	5.22	151	1.091	39	1.314	0.51
		A5-6	28156	2.84	346	1.563	27	1.860	0.51
280	112	A6-1	14123	7.86	85	1.829	23	2.788	0.51
		A6-2	21267	3.93	198	0.4856	69	0.740	0.51
		A6-3	0	—	—	0.704	55	0.9234	0.51
		A6-4	3980	7.34	154	0.533	59	0.862	0.51
280	115	A7-1	0	12.85	171	2.08	23	2.254	0.51
		A7-2	26492	7.98	88	1.456	28	1.844	0.51
		A7-3	30511	14.82	129	1.297	32	1.588	0.51
		A7-4	11627	15.73	48	2.544	18	2.903	0.51

(—continued)

Stress Amplitude MPa	Mean Stress MPa	No. of Crack	N_0 Cycles	C_1 $\times 10^5$	d_1 μm	B_0 $\times 10^5$	a_{th} μm	B $\times 10^5$	D $\times 10^3$
293	118	A2-1	4043	29.9	335	2.545	19	2.671	0.51
		A2-2	0	21.8	180	3.107	15	3.350	0.51
		A2-3	4634	18.4	160	—	—	—	—
		A2-4	11566	21.1	139	—	—	—	—
		A2-5	14230	15.77	222	—	—	—	—
330	0	A11-1	8132	38.66	143	2.446	19	2.641	0.51
		A11-2	8132	18.52	158	3.192	15	3.435	0.51
		A11-3	0	5.28	234	1.578	29	1.762	0.51

Table 6.2:
Comparison between Actual Fatigue Lifetime and Predicted Lifetime
 (Torsion Tests)

Specimen No.	Predicted MSC Growth	Predicted PSC Growth	Predicted Life	Actual Life
A1	20960	194774	215734	196500
A2	7076	61256	68332	43787
A3	47206	313297	36053	530000
A4	28347	186620	215167	255150
A5	26576	170142	196718	171902
A6	16461	118701	135162	126792
A7	13469	111262	124731	134600
A8	140932	811951	952883	1200000
A9	88233	548486	636719	900000
A10	140932	811951	952883	1080000
A11	7420	89204	96624	84529

Table 6.3:
Results of Uniaxial Tests

Stress Amplitude MPa	Mean Stress MPa	No. of Specimen	N_0 cycles	C_{max} $\times 10^5$	C $\times 10^5$	G_0 $\times 10^5$	n	G $\times 10^5$	D $\times 10^5$
464	-120	A55	300000	3.06	0.72	0.0165	1.66	0.094	15.6
490	-120	A56	65000	8.37	2.08	0.289	1.33	0.201	30
500	-120	A59	20000	9.83	2.77	0.315	1.42	0.321	54.24
500	-200	A50	10000	18.4	8.45	3.485	1.355	0.367	
460	0	A52	200000	0.82	0.823	0.001	1.57	0.0865	10.5
456	0	A53	300000	0.95	0.85				
500	0	A31	15000	8.66	1.97				
500	0	A32	30000	14.1	5.21	0.244	1.445	0.342	35
500	0	A33	25000	5.01	2.51				
550	0	A42	5000	88.9	38.2	13.95	1.00	1.356	101
600	0	A41	300	447	196	37.65	1.256	16.28	203
600	0	A44	750	1710	434				
464	100	A51	15000	6.0	2.10	0.0447	1.537	0.111	23
405	228	A40	10000	14.5	4.06	0.399	1.356	0.322	45.1
378	400	A34	48000	13.1	3.46				14.4
369	407	A35	170000	7.53	3.92	0.256	1.432	0.308	
360	400	A36	10000	6.3	2.63				24.9
355	400	A37	10000	5.45	0.83				
315	471	A57	380000	1.92	0.69	0.0598	1.581	0.206	34
310	504	A58	100000	4.96	3.19	0.1915	1.44	0.2618	43.6
295	504	A60	330000	0.79	0.68	0.056	1.39	0.057	

Note: The unit of D is $\mu m/cycle$.

Table 6.4:
Comparison between Actual Fatigue Lifetime and Predicted Lifetime
 (Uniaxial Tests)

Specimen No	Predicted N_0	Predicted Crack Growth	Predicted Life	Actual Life
A31	15799	107148	122947	190000
A32	10108	71560	81669	202000
A33	39650	252469	292119	223000
A34	6571	27807	34378	203000
A35	11437	45869	57306	303000
A36	22942	86603	109545	202000
A37	27841	103554	131396	632000
A38	35080	161134	196213	142000
A40	37913	174206	212118	204000
A41	376	3889	4265	3345
A42	2782	22452	25234	28800
A44	376	3889	4265	3571
A45	60	807	866	600
A48	2782	22452	25234	16000
A51	19936	114917	134852	391000
A54	24914	163232	188146	137000
A55	138945	851011	999956	879000
A56	39650	252469	292119	298000
A57	109680	342087	451767	923000
A58	83502	252533	336035	373000
A59	24914	163232	188146	216000
A60	261283	762815	1024098	842000

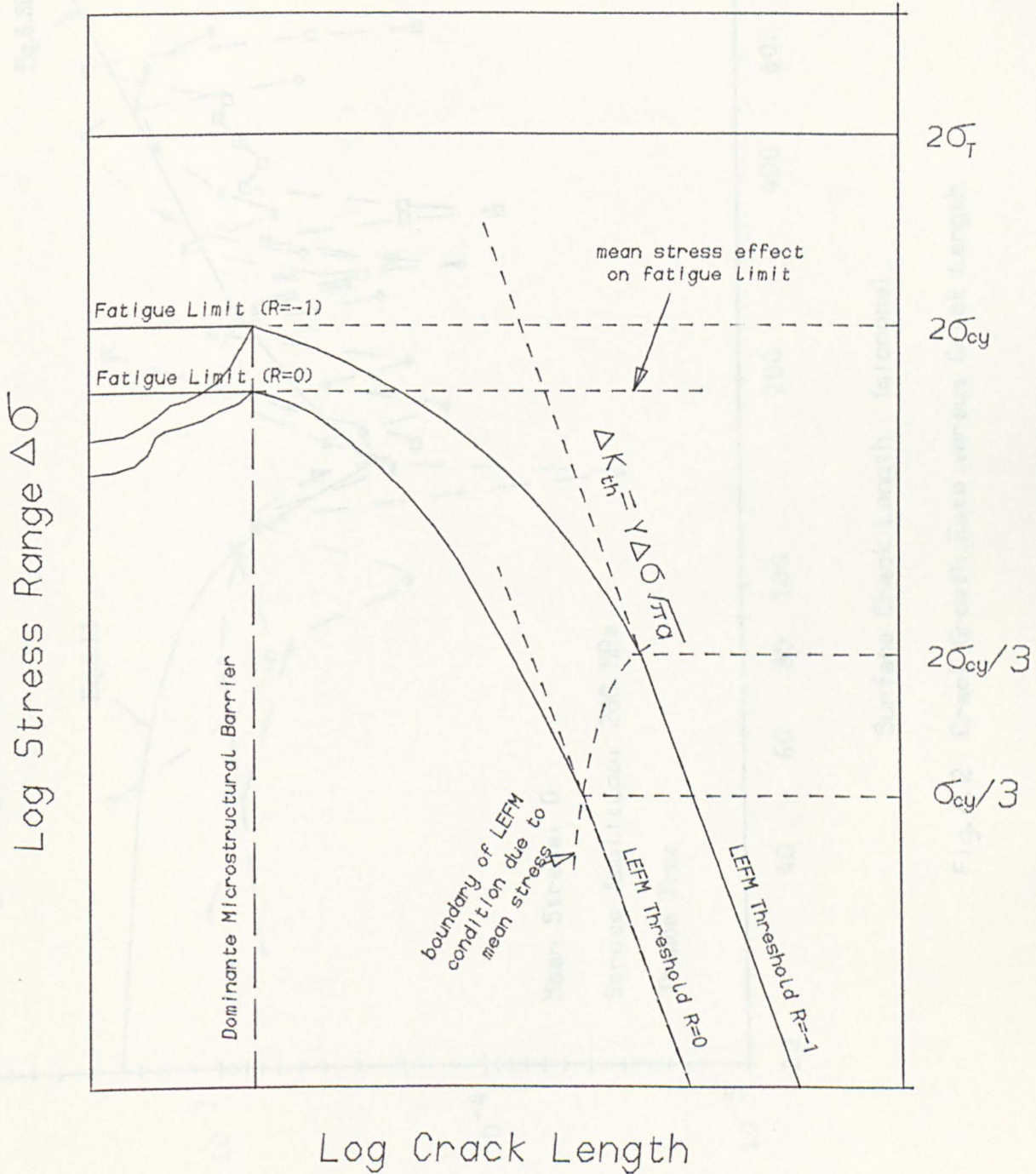


Fig.6.1 Schematic Drawing to Show the Effects of Stress Ratio and Defect Size on the Crack Growth Contour $da/dN = 0$

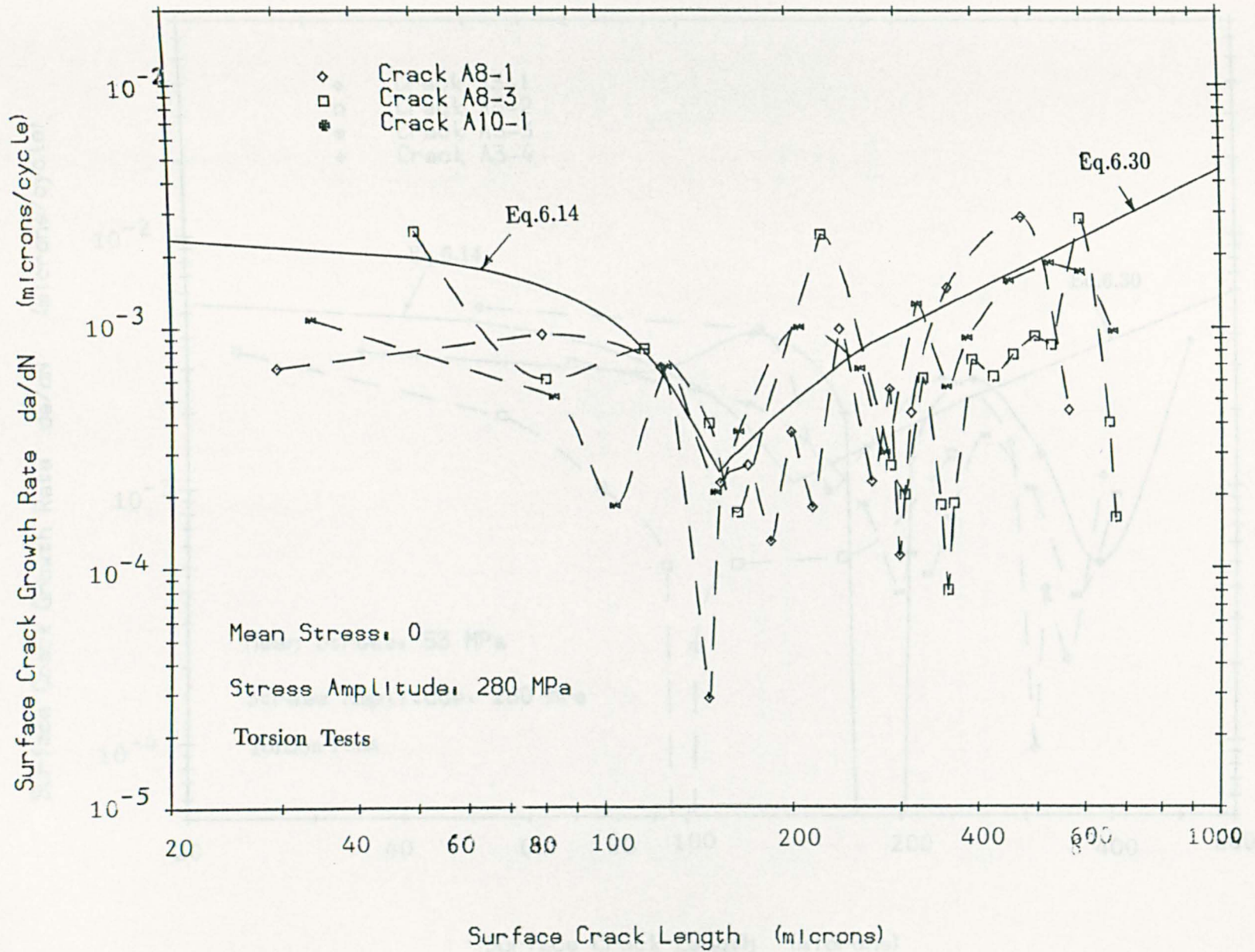


Fig. 6.2 Crack Growth Rate versus Crack Length

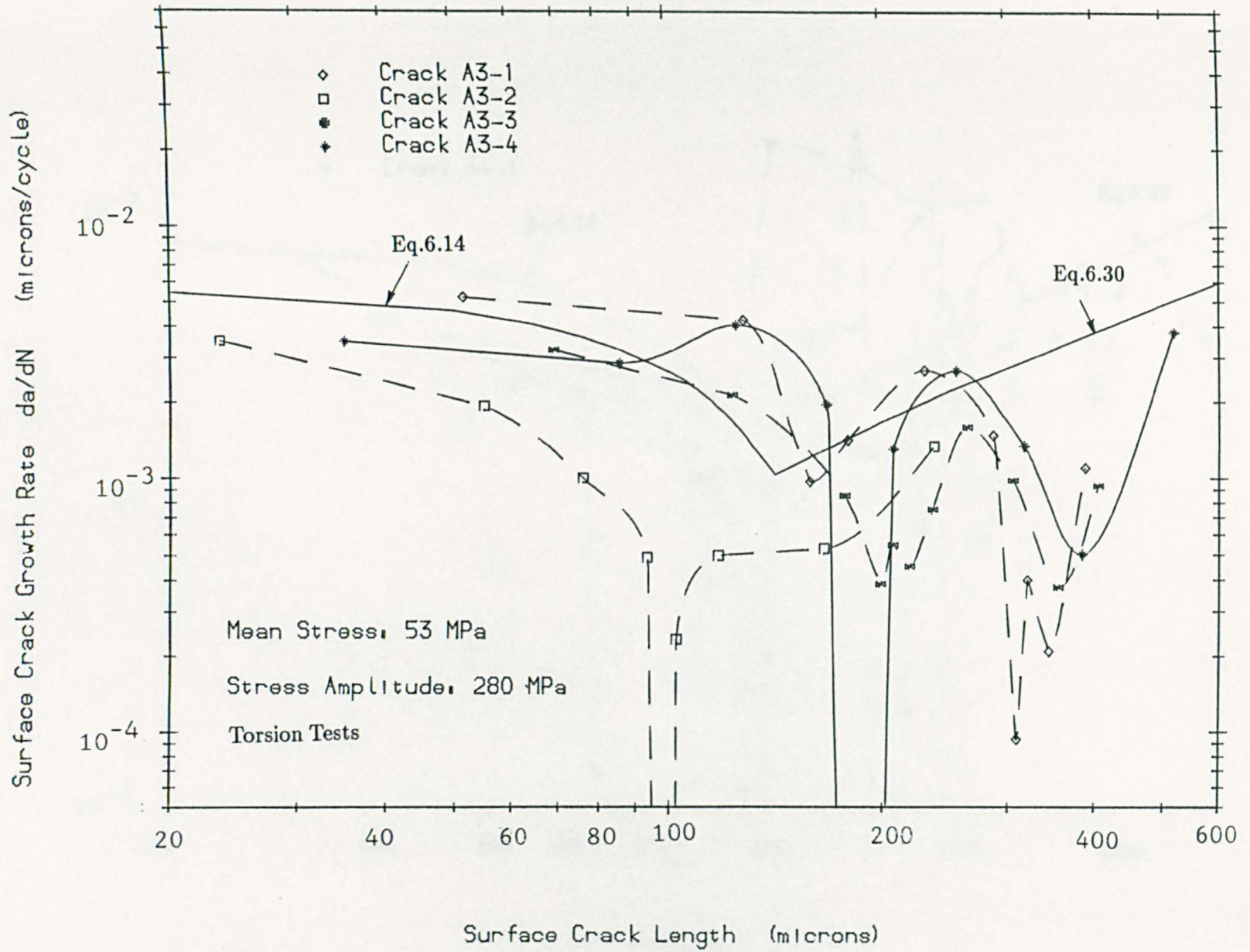


Fig. 6.3 Crack Growth Rate versus Crack Length

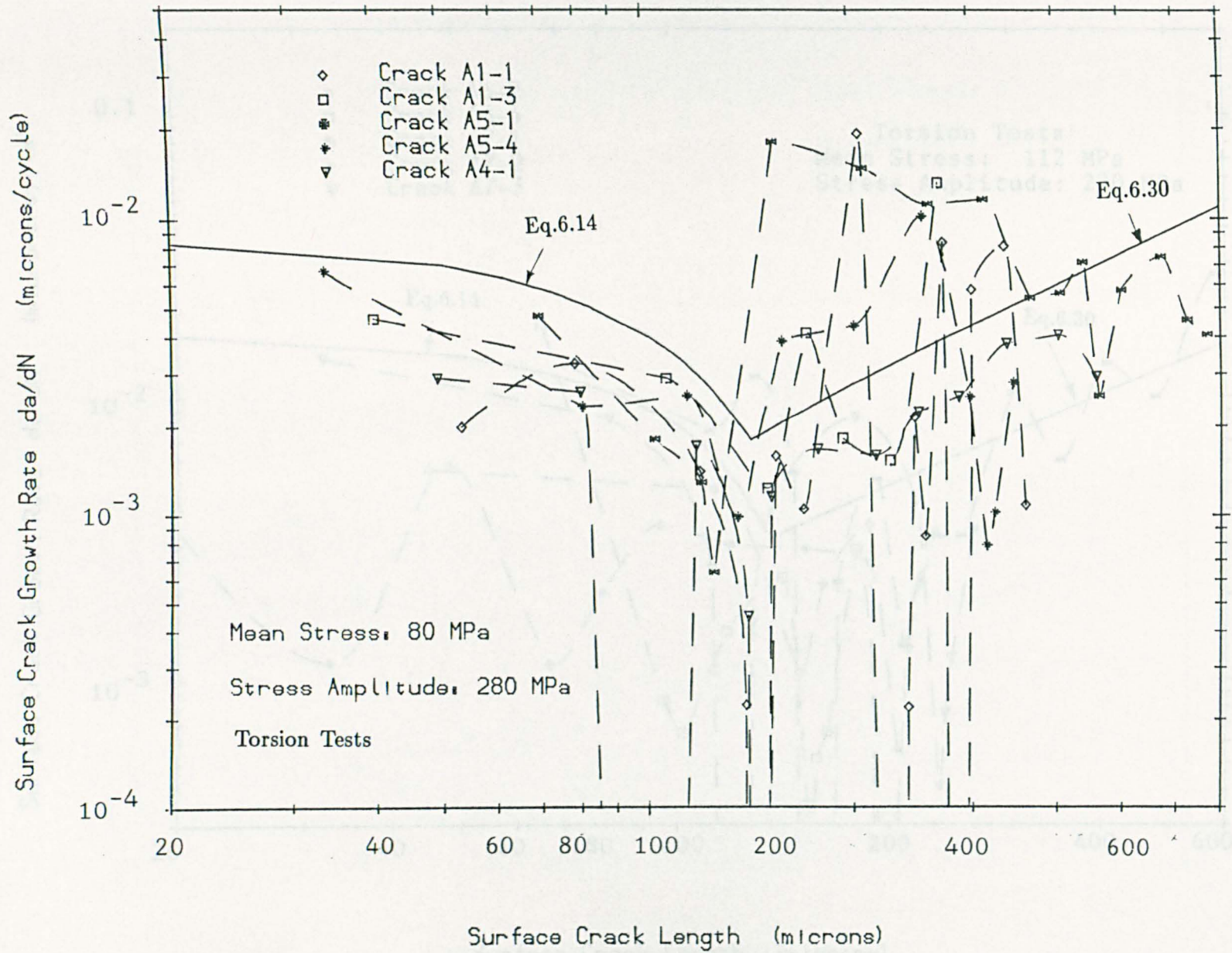


Fig. 6.4 Crack Growth Rate versus Crack Length

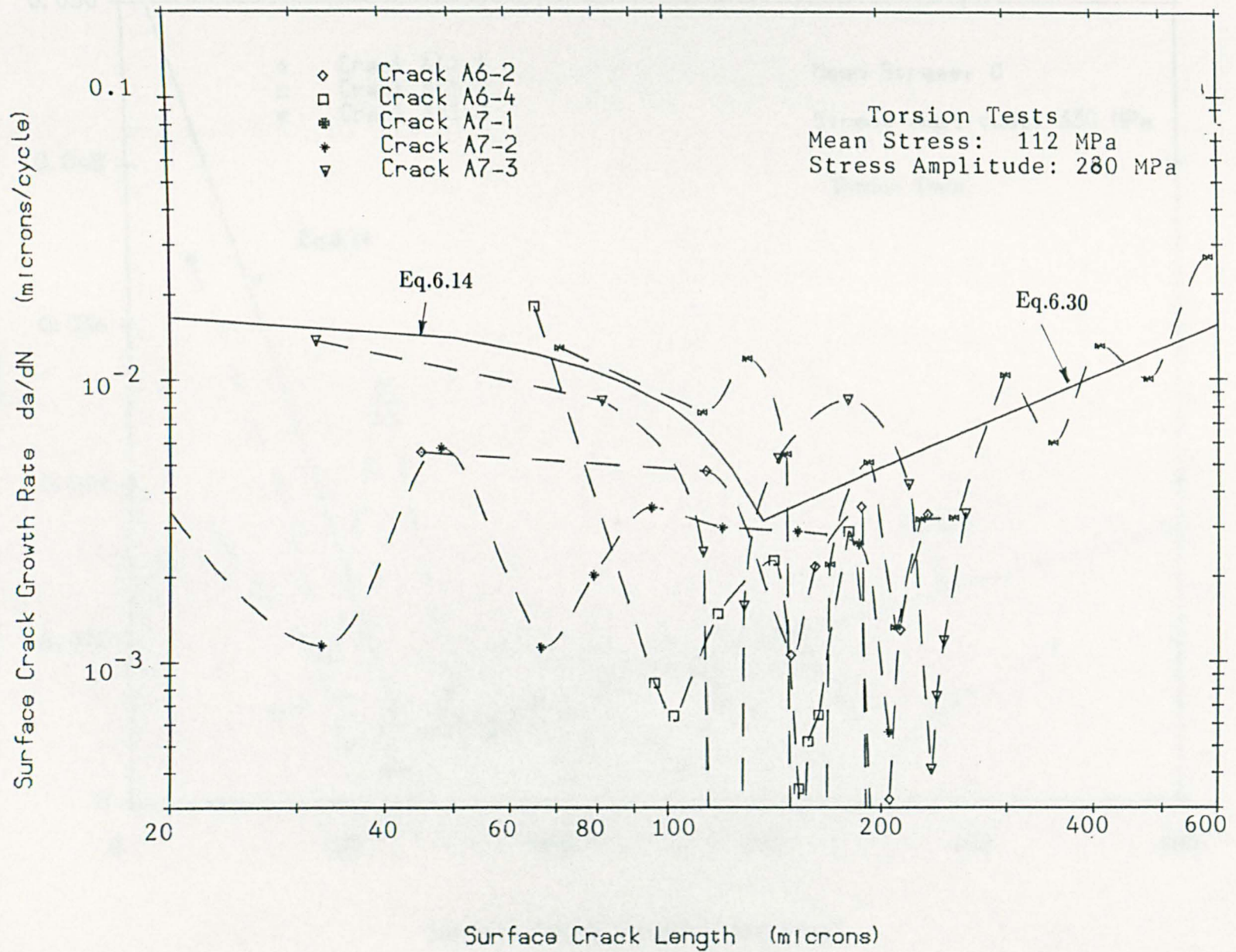


Fig. 6.5 Crack Growth Rate versus Crack Length

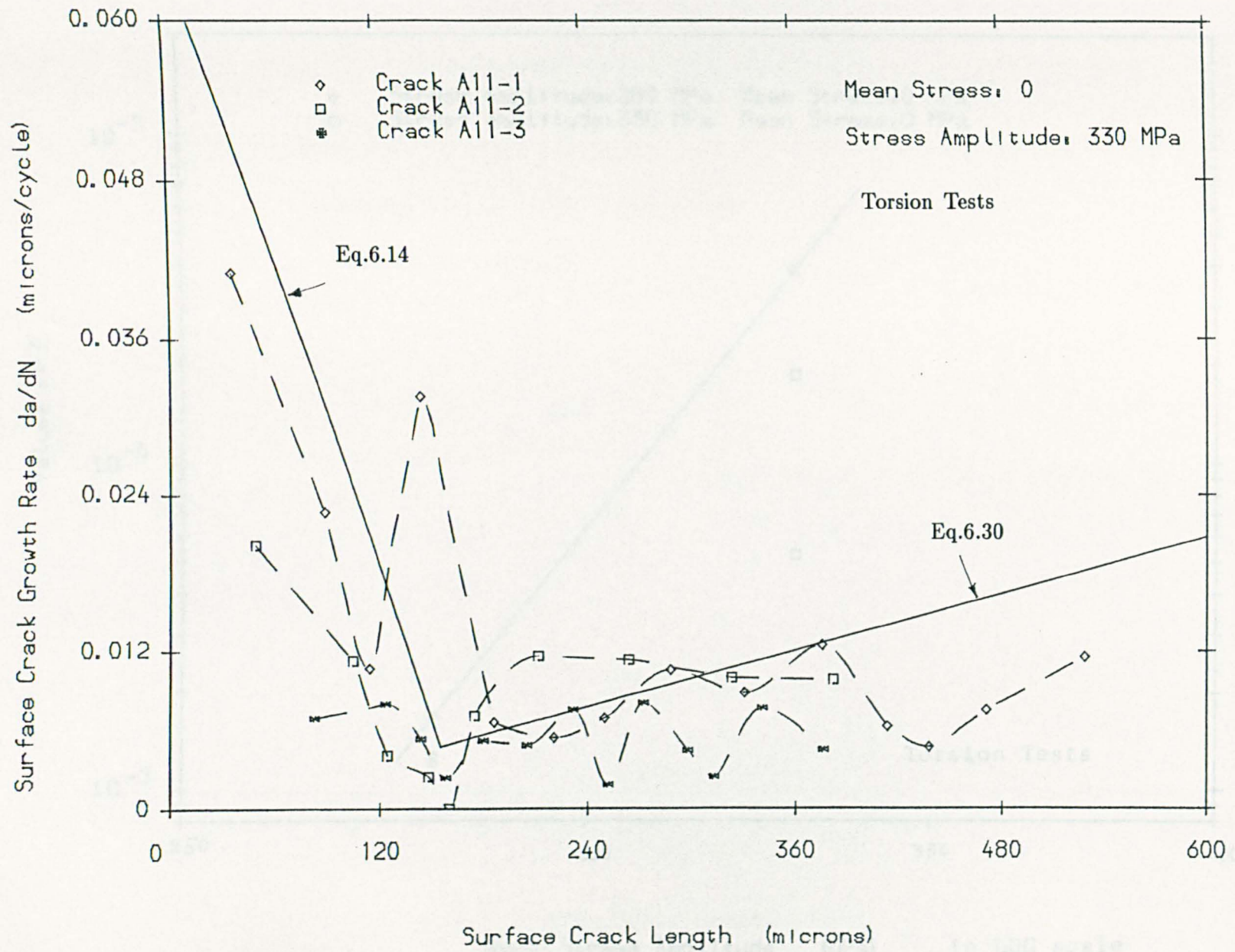


Fig. 6.6 Crack Growth Rate versus Crack Length

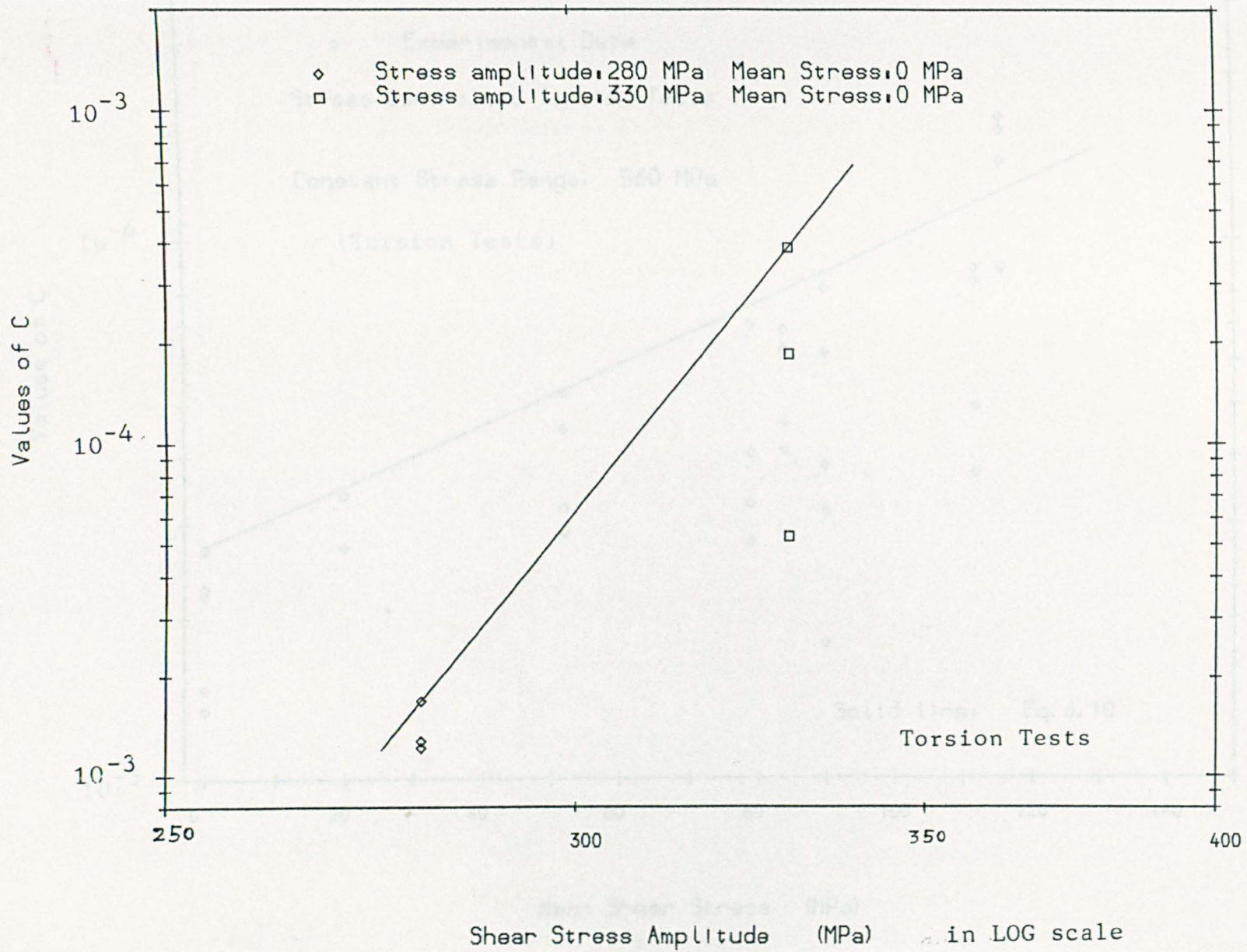


Fig. 6.7a Values of C versus Shear Stress Amplitude

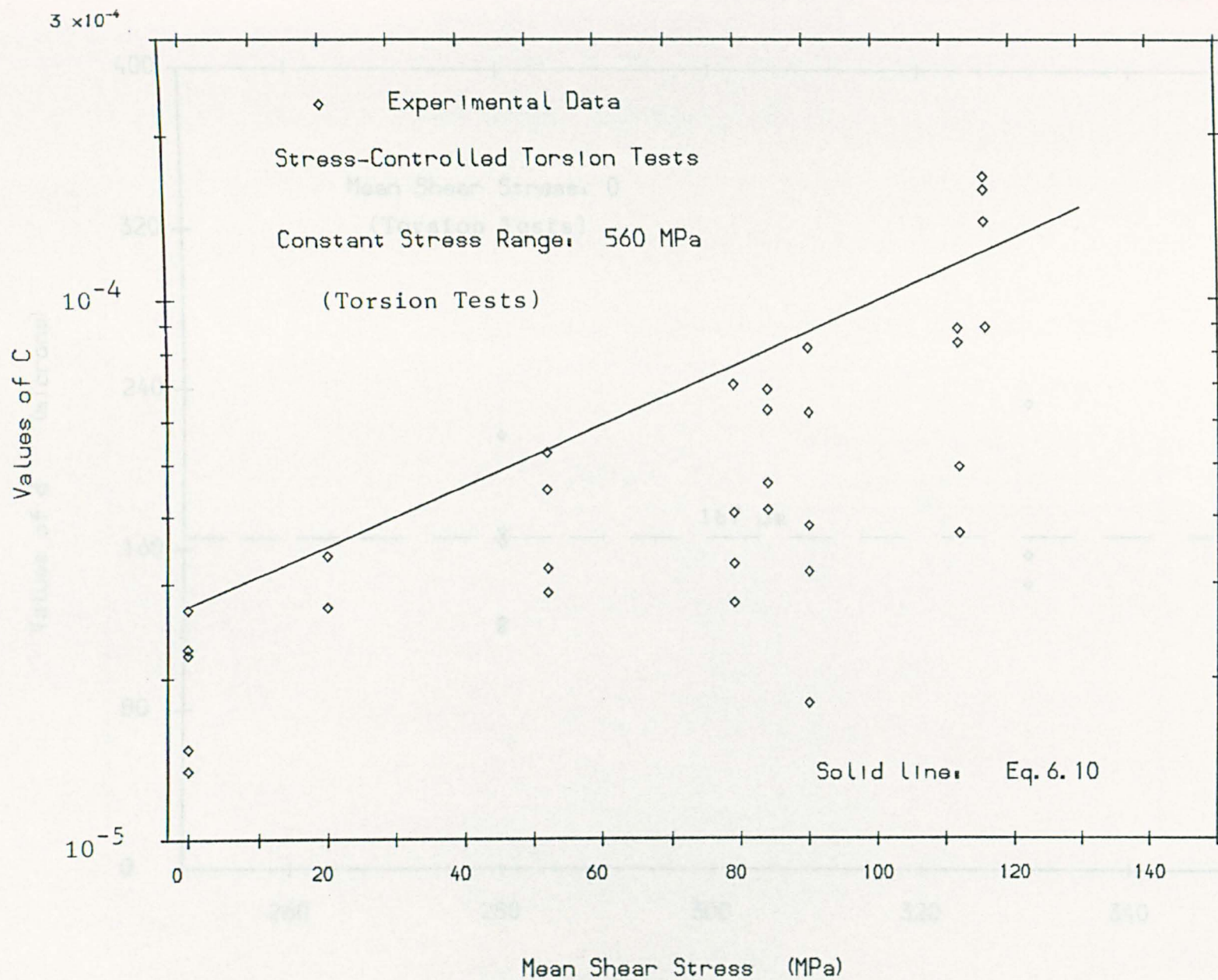


Fig. 6.7b Values of C versus Mean Shear Stress

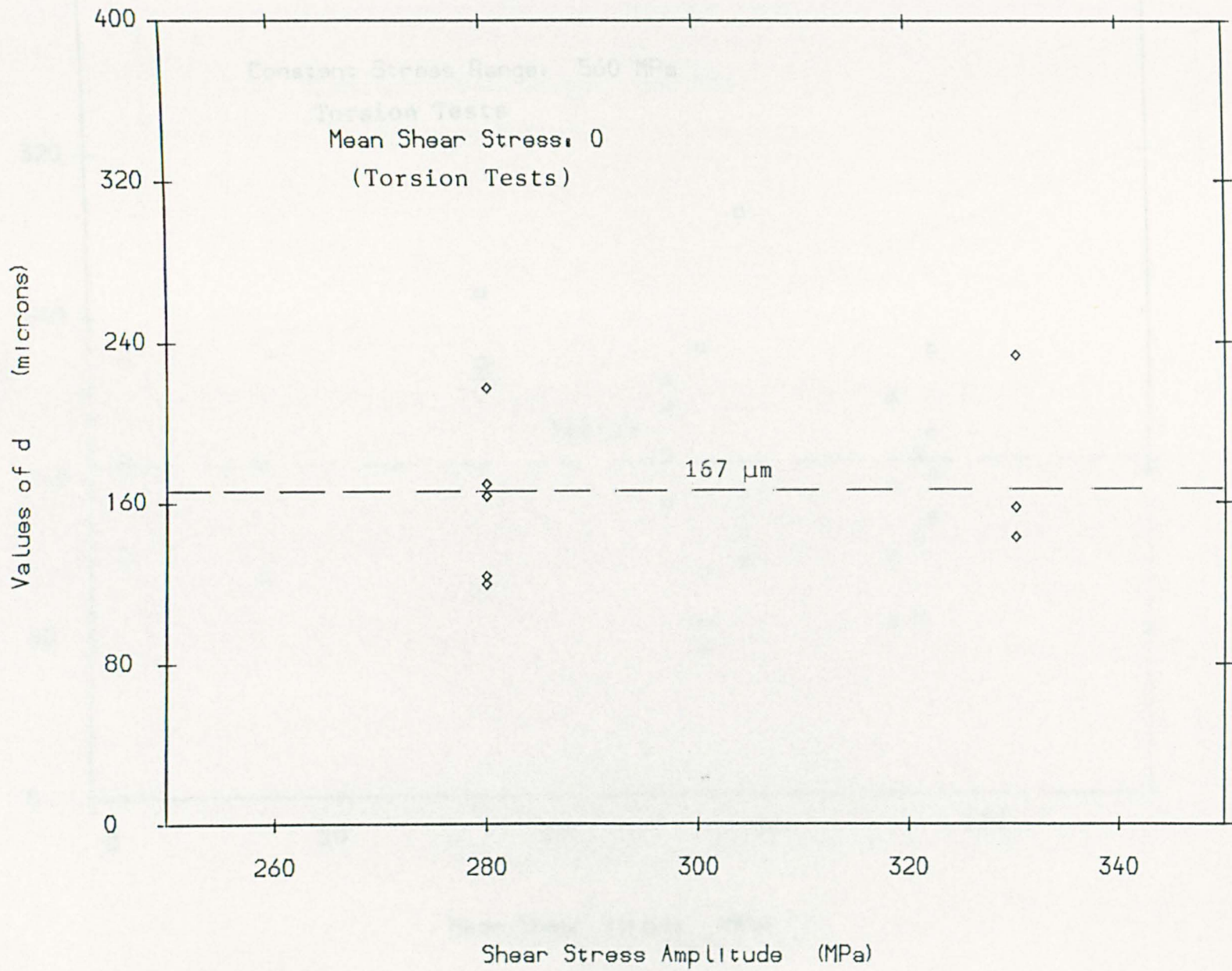


Fig. 6.8a Values of d versus Stress Amplitude

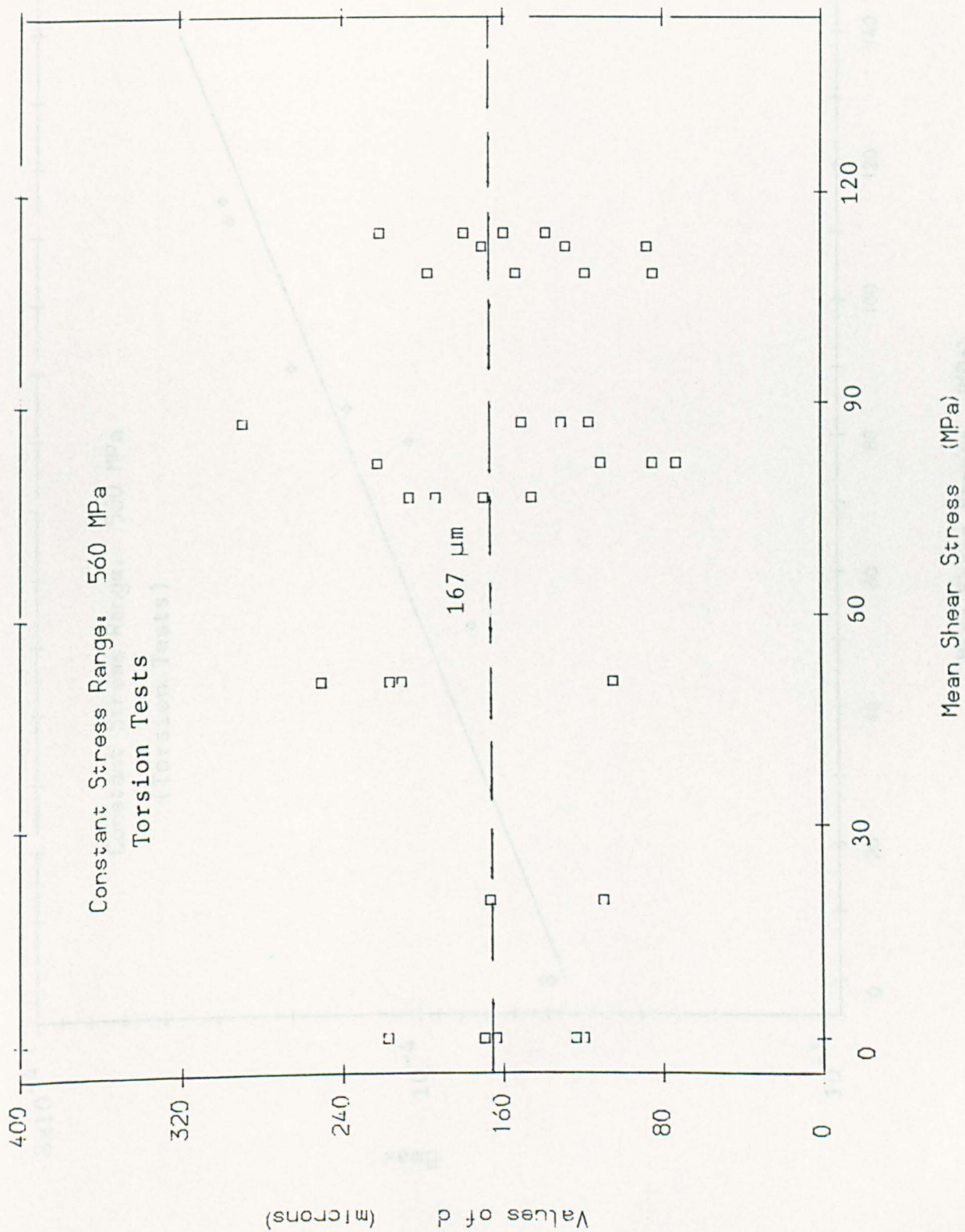


Fig. 6.8b Values of d versus Mean Shear Stress

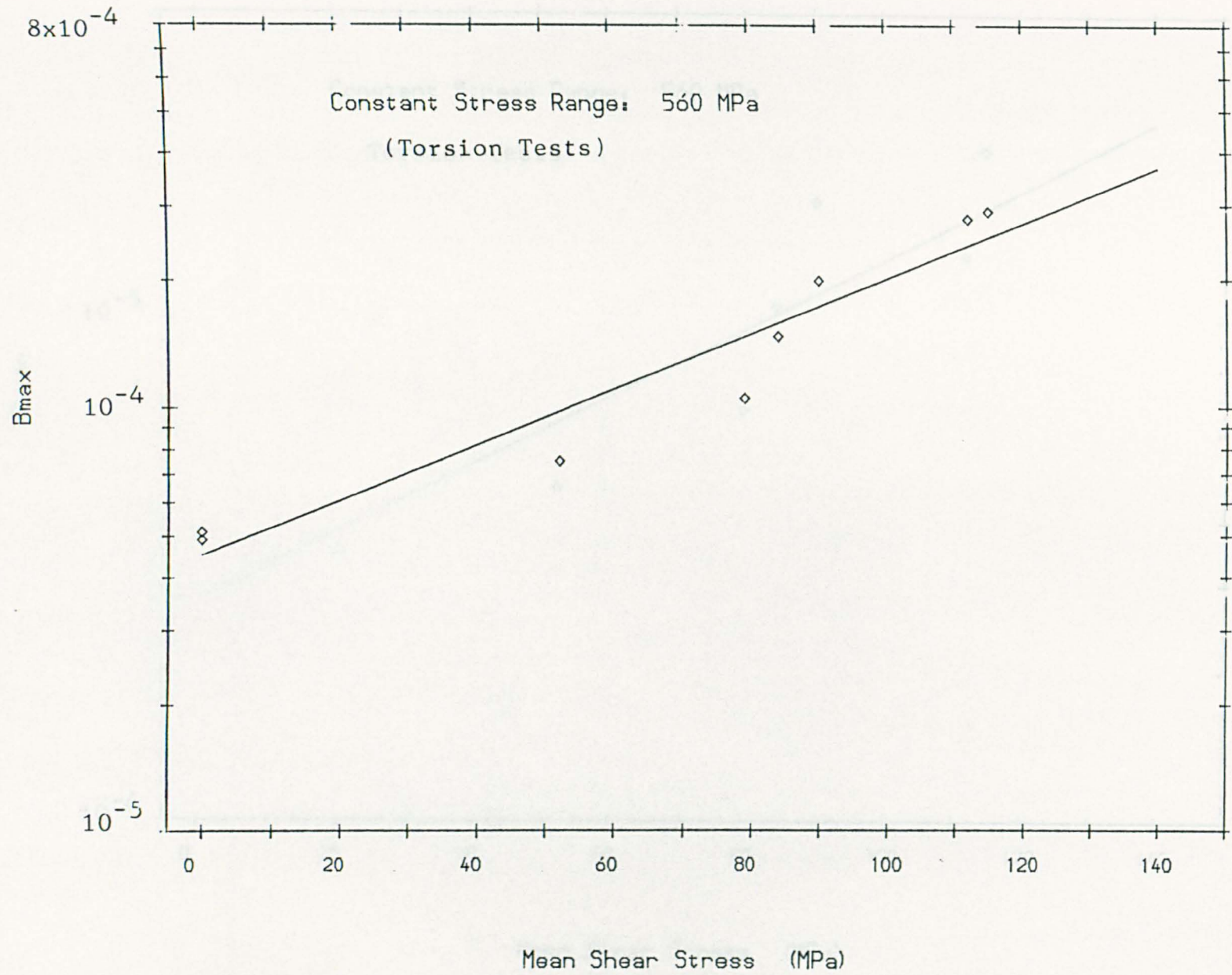


Fig. 6.9a Value of Bmax versus Mean Shear Stress

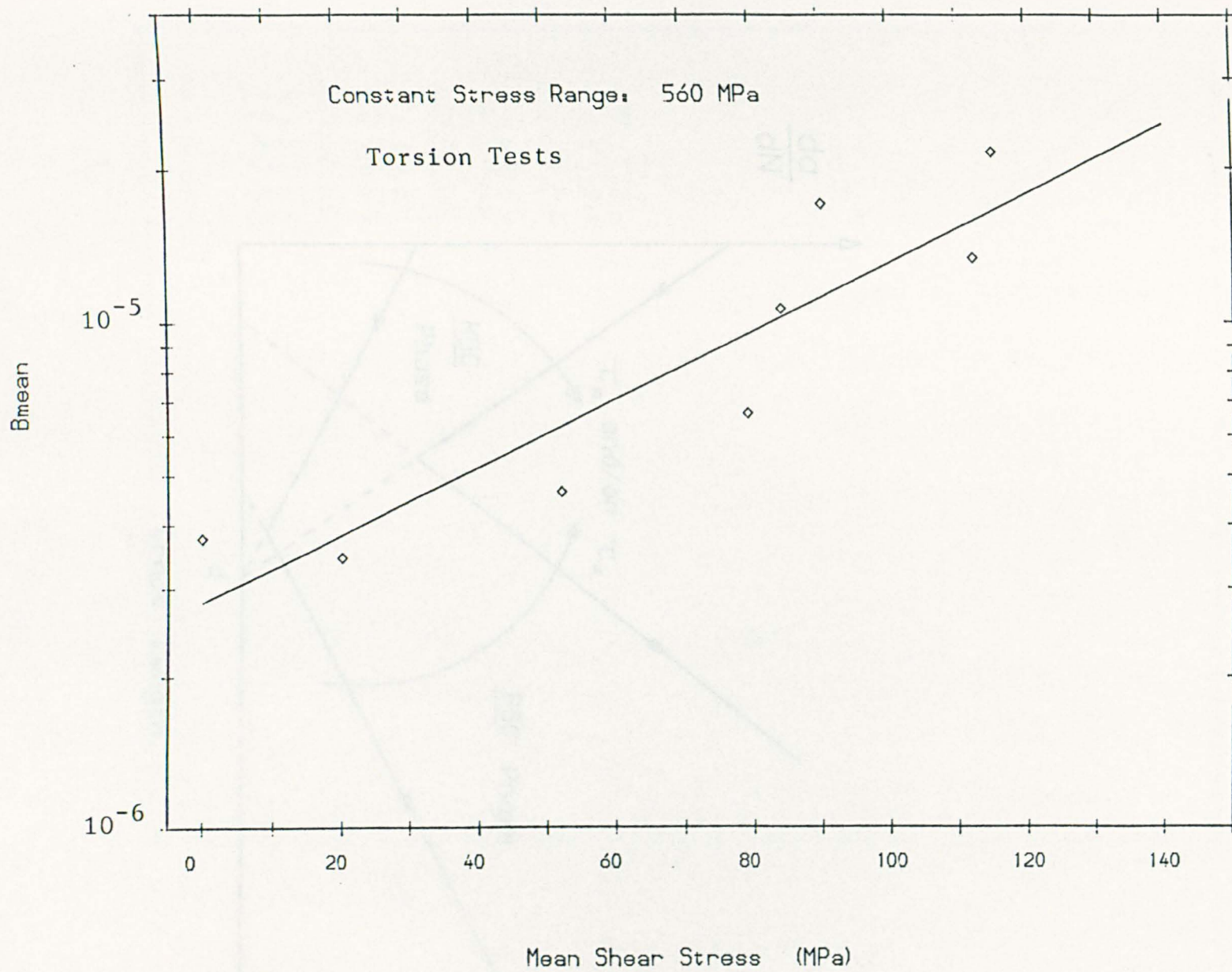


Fig. 6.9b Value of Bmean versus Mean Shear Stress

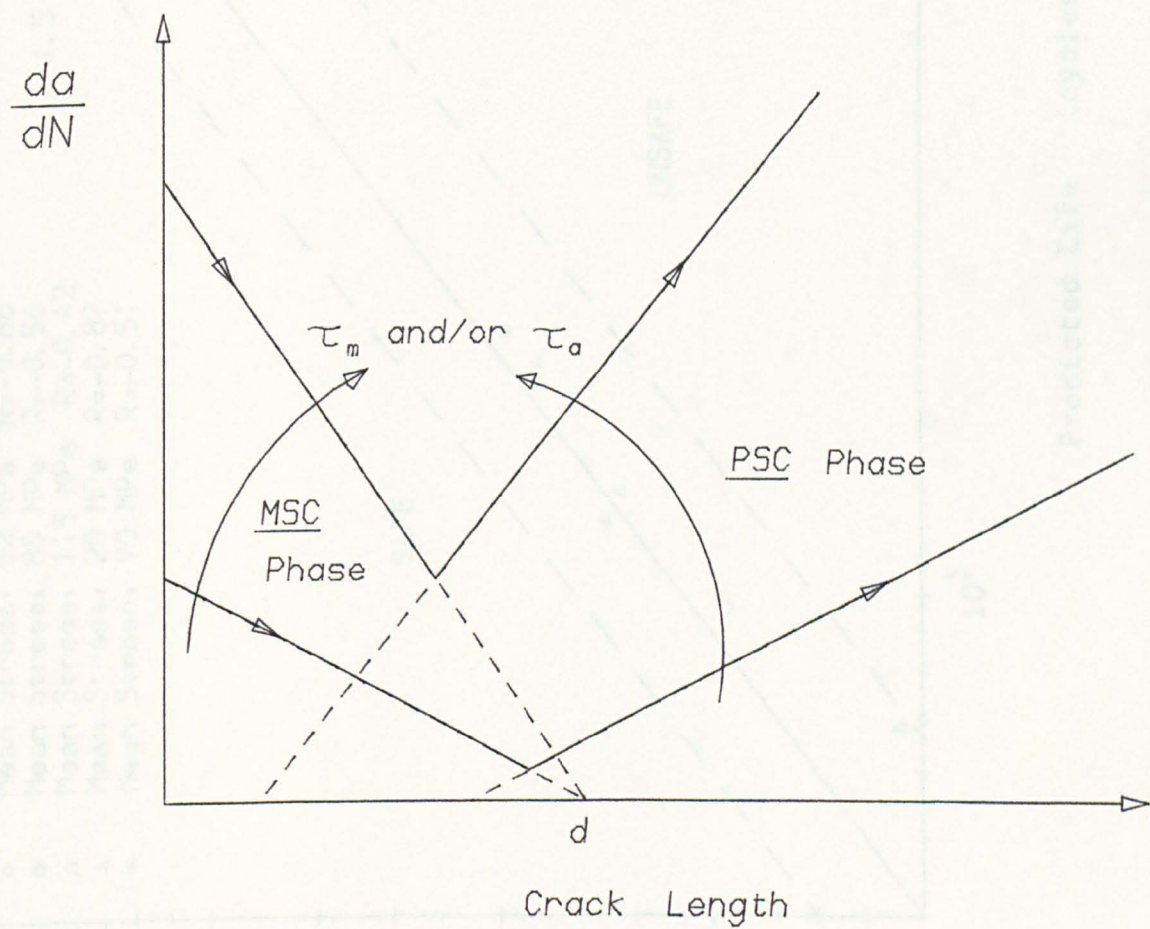


Fig.6.10 Schematic Showing the Effect of Stress Level on Crack growth

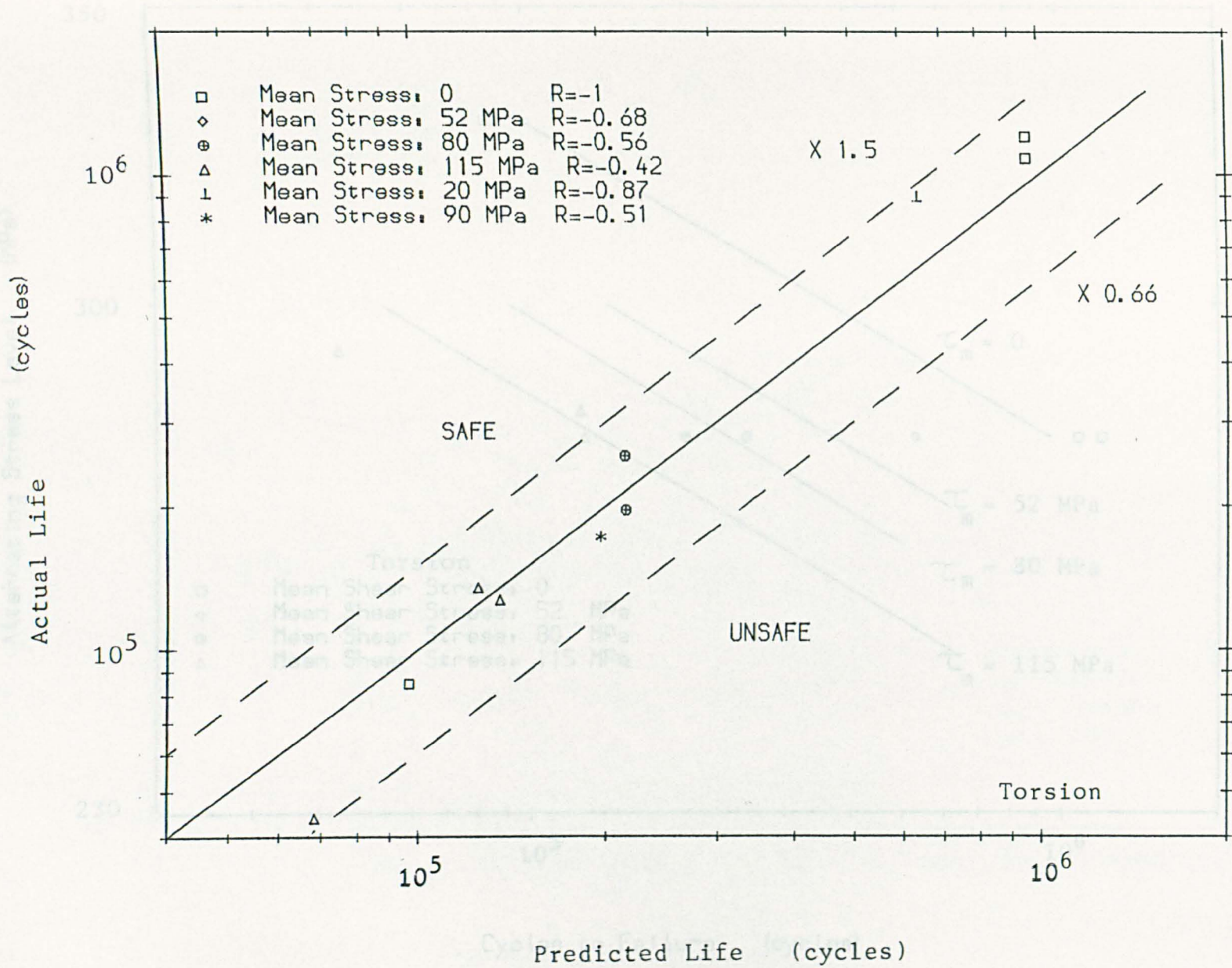


Fig. 6.11a Comparison between Actual Life and Predicted Life (torsion)

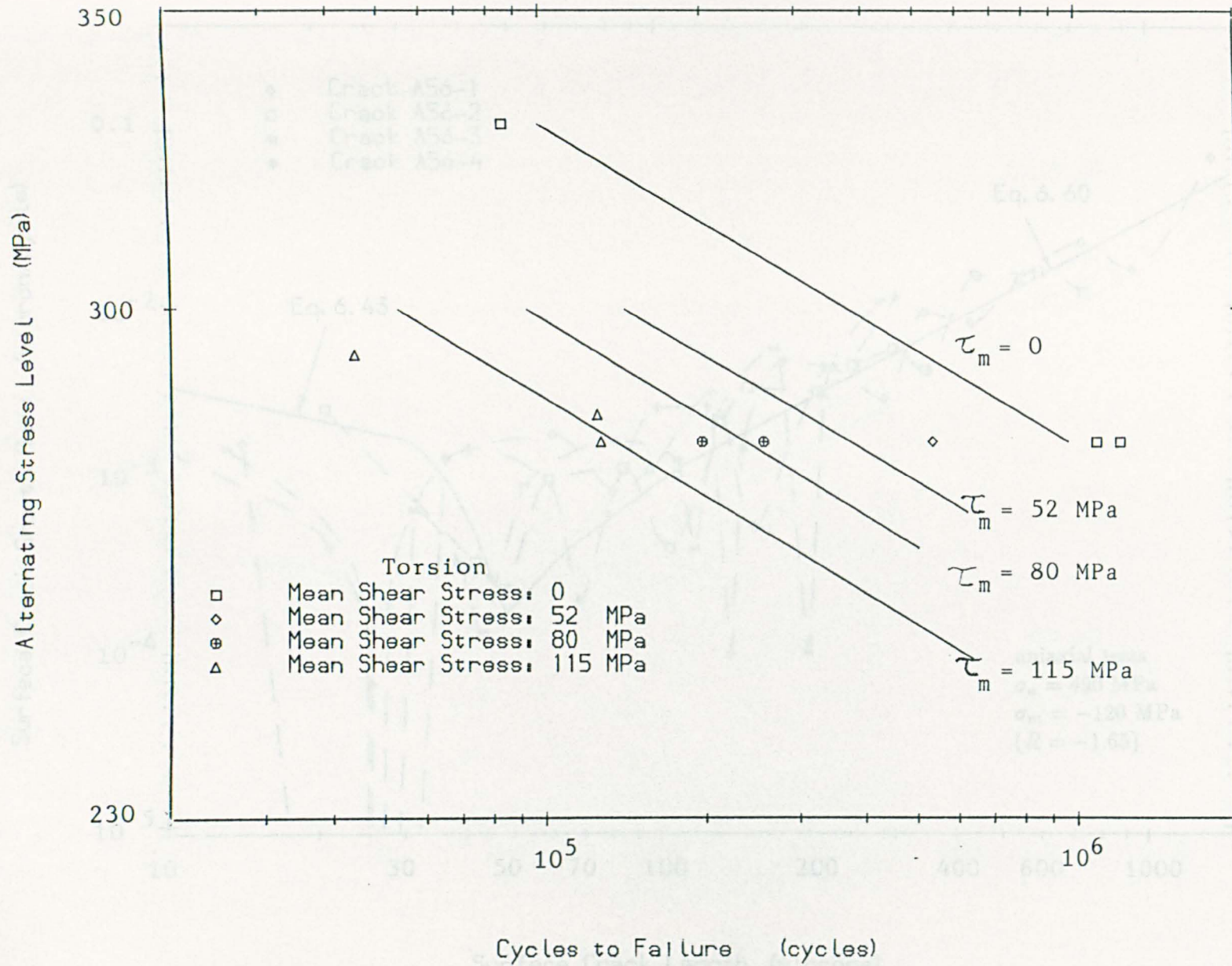


Fig. 6.11b Prediction of S--N Curves with Experimental Data (torsion)

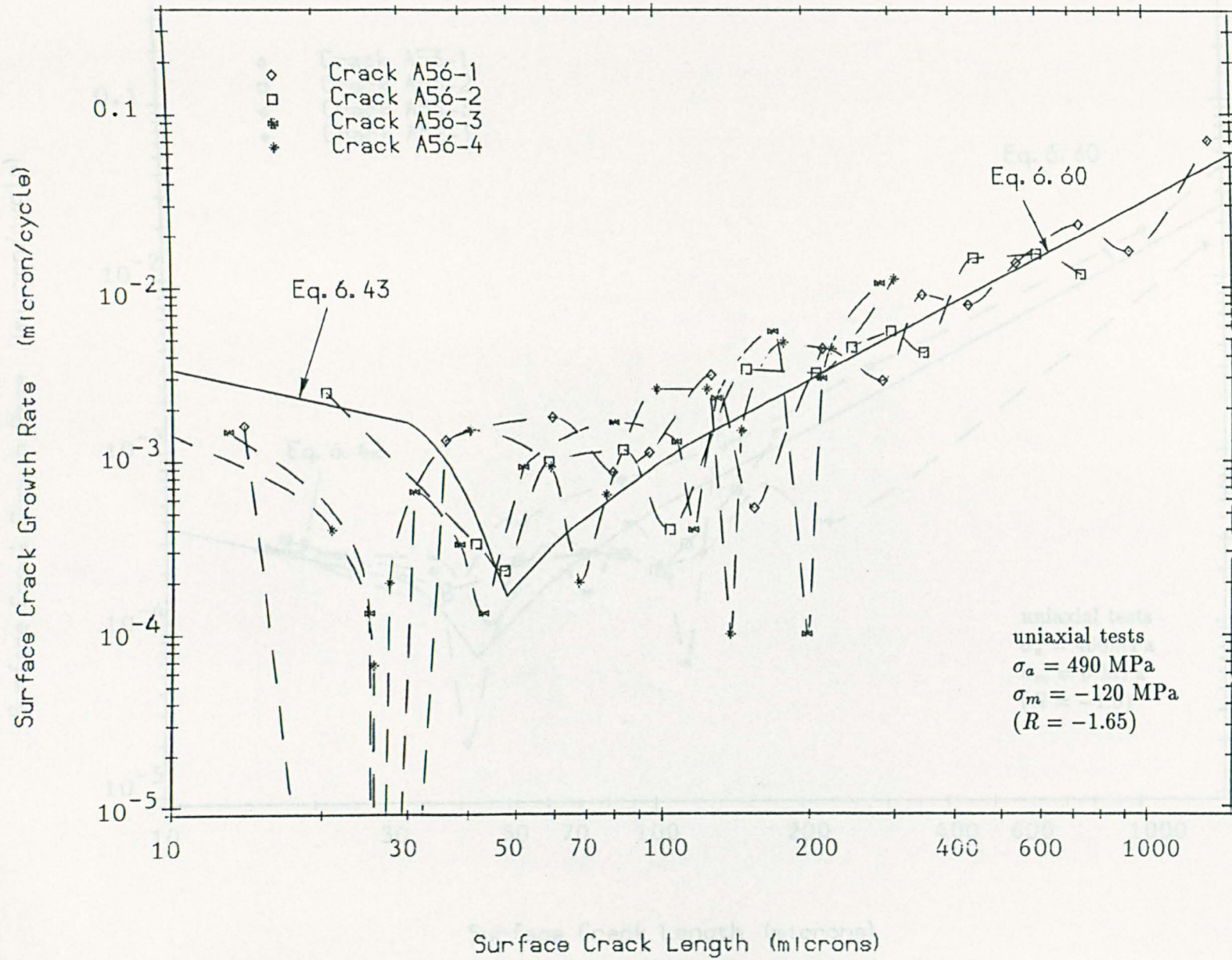


Fig. 6.12(a) Surface Crack Growth Rate versus Surface Crack Length

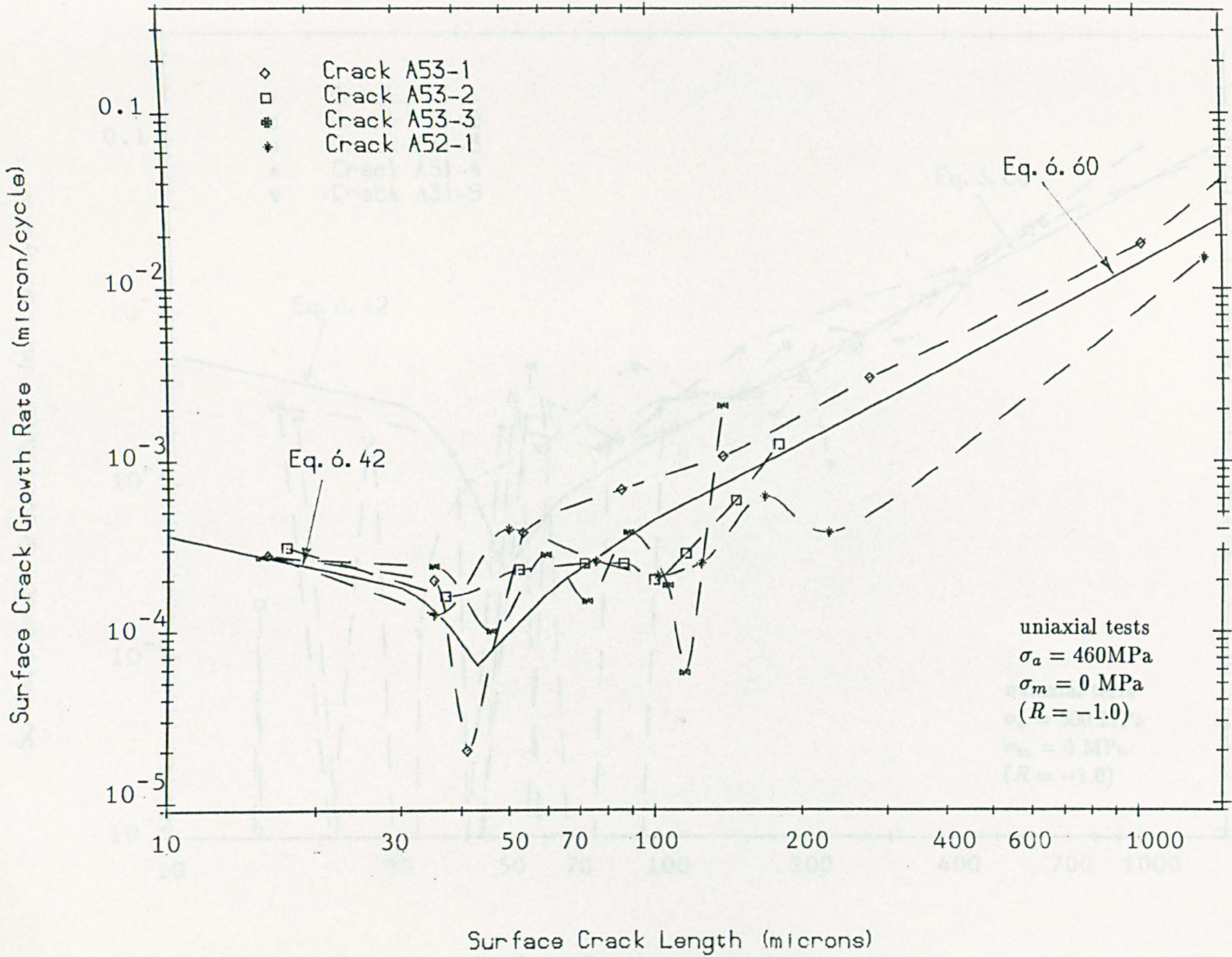


Fig. 6.12 (b) Surface Crack Growth Rate versus Surface Crack Length

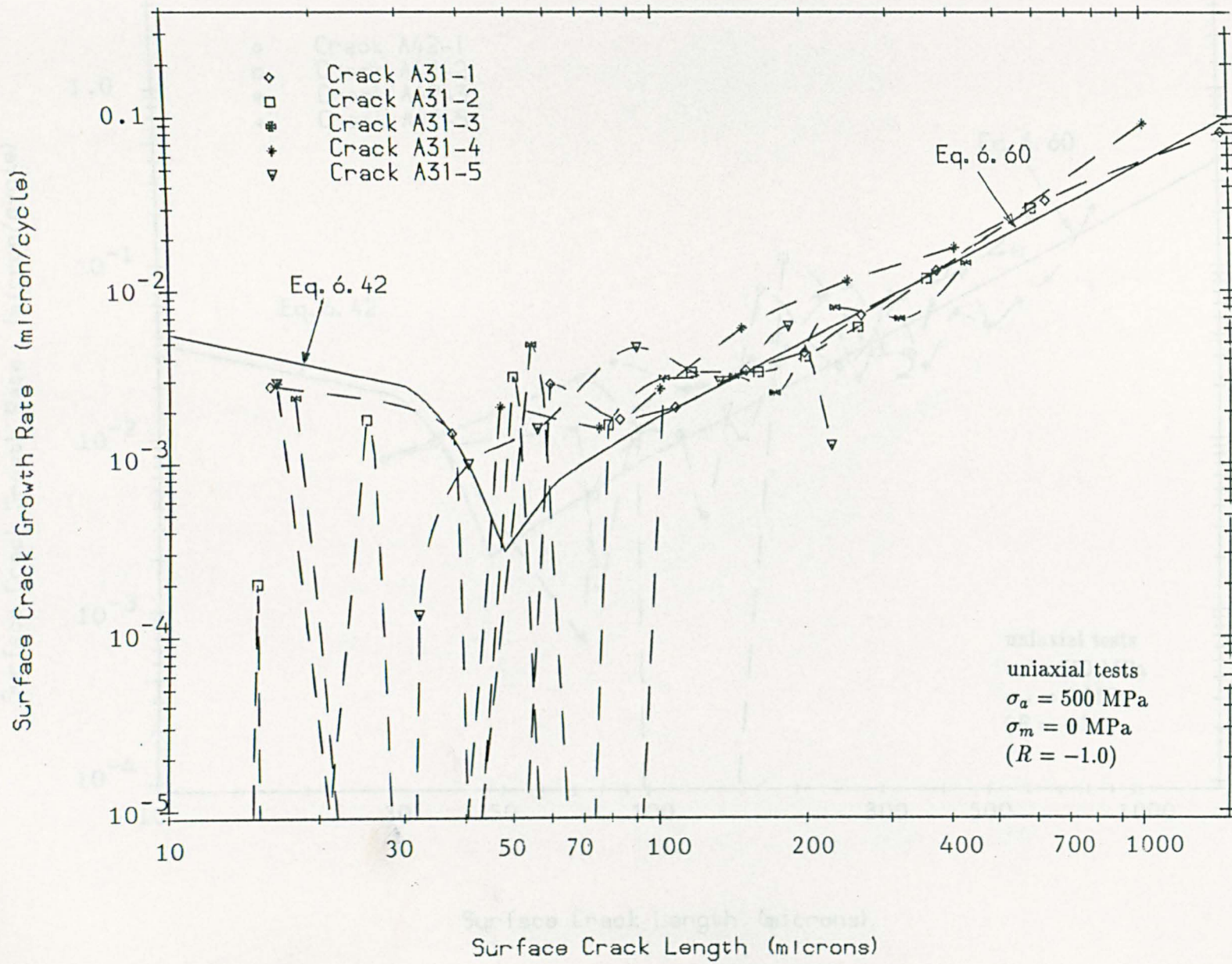


Fig. 6.12(c) Surface Crack Growth Rate versus Surface Crack Length

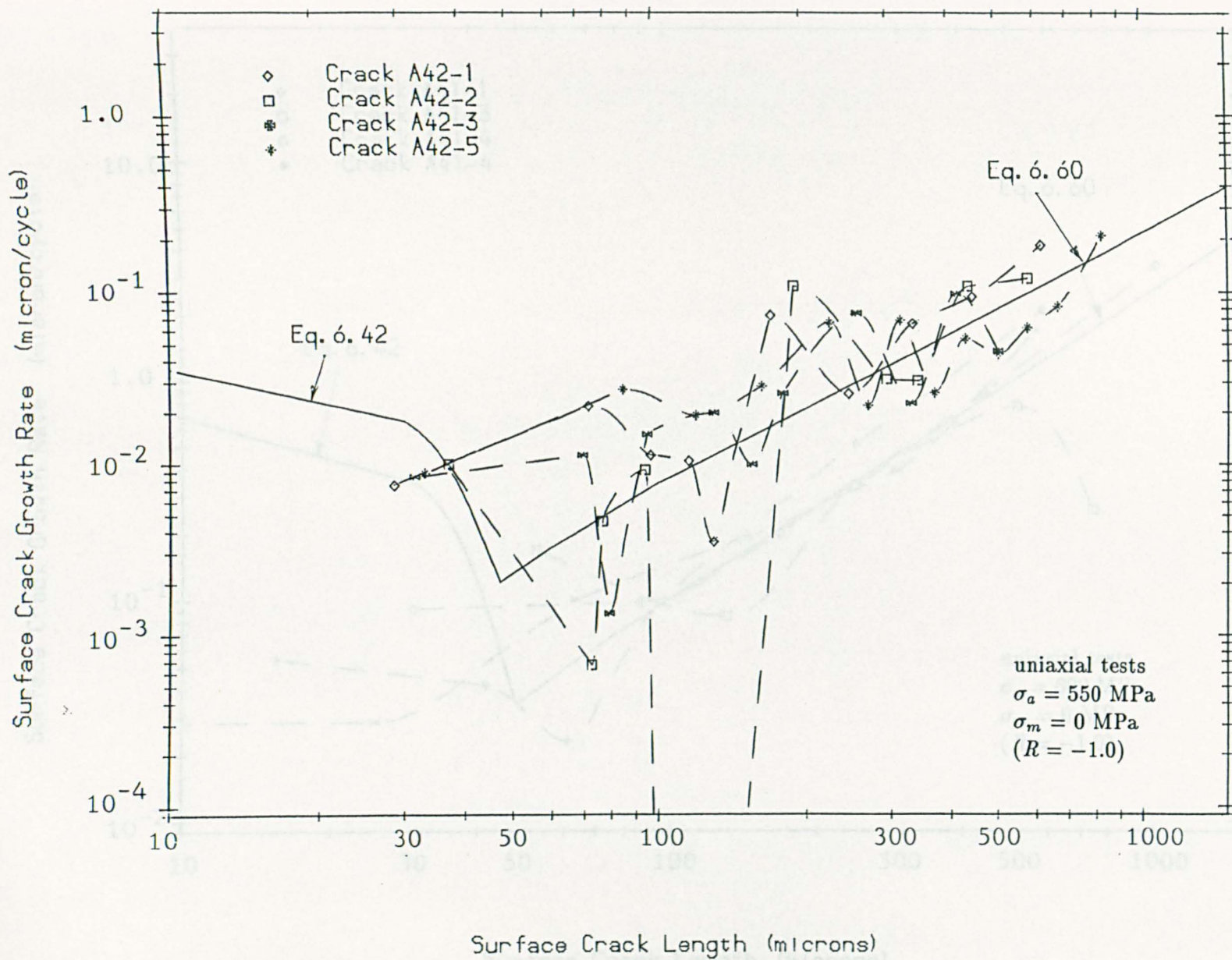


Fig. 6.12(d) Surface Crack Growth Rate versus Surface Crack Length

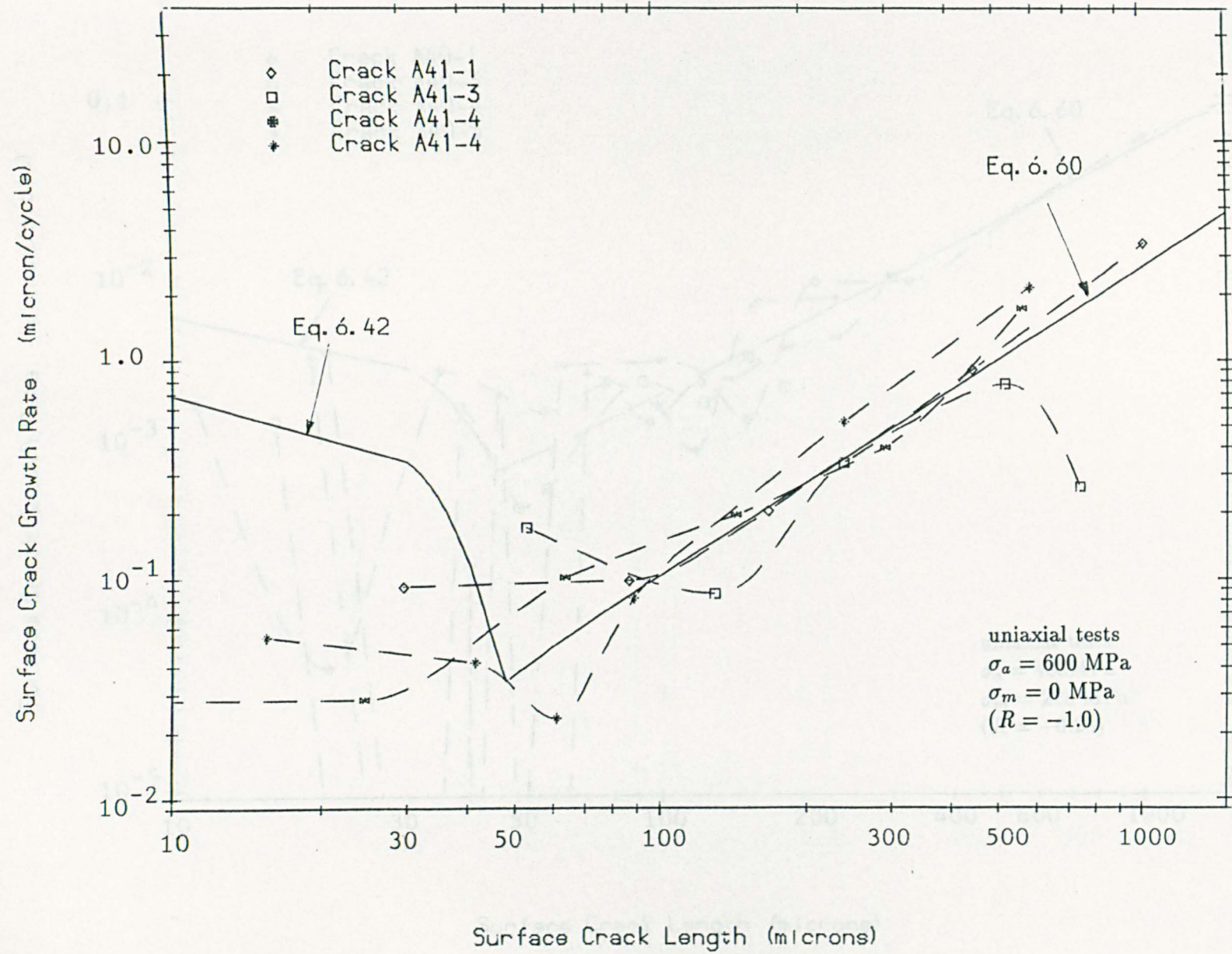


Fig. 6.12 (e) Surface Crack Growth Rate versus Surface Crack Length

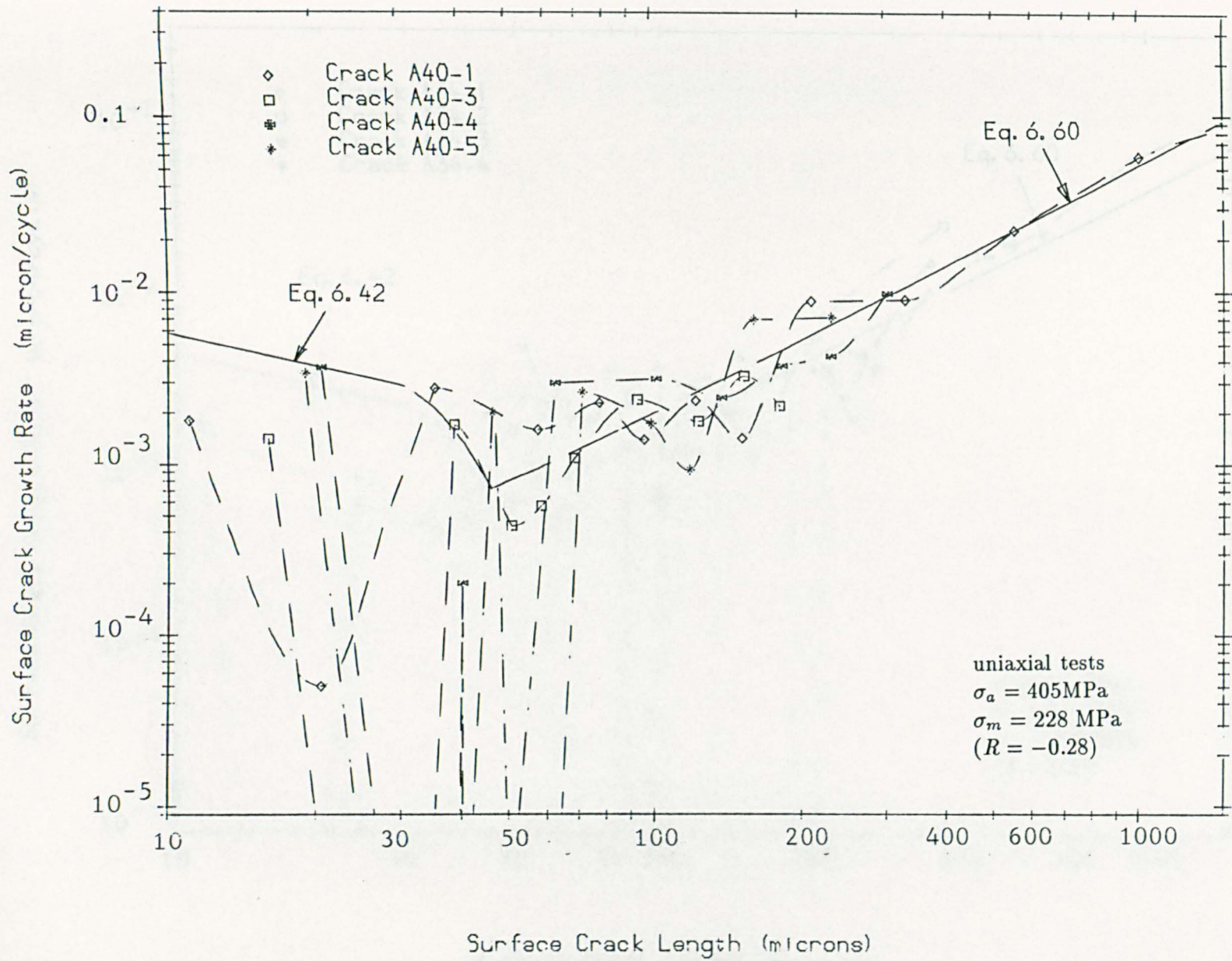


Fig. 6.12(f) Surface Crack Growth Rate versus Surface Crack Length

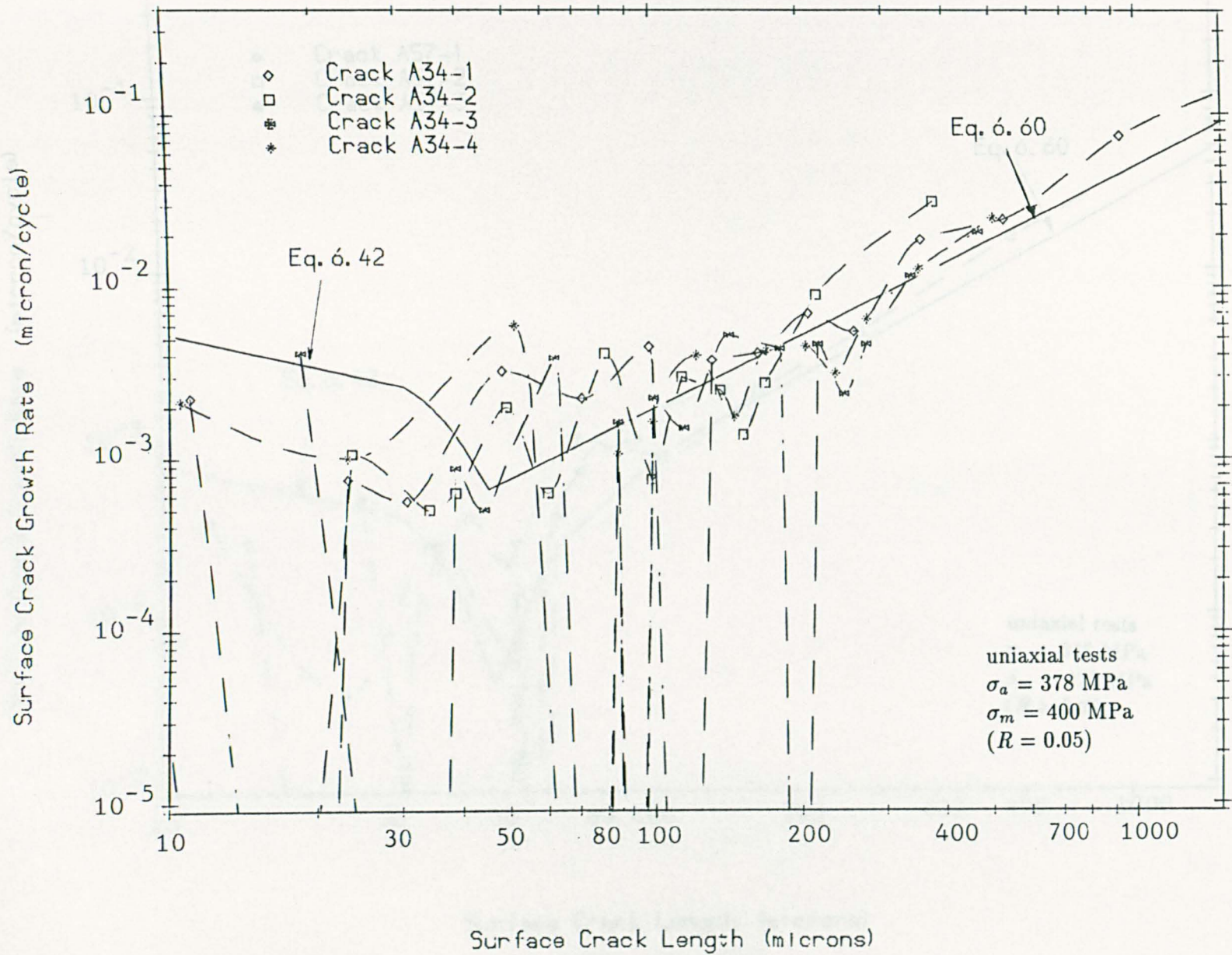


Fig. 6.12(g) Surface Crack Growth Rate versus Surface Crack Length

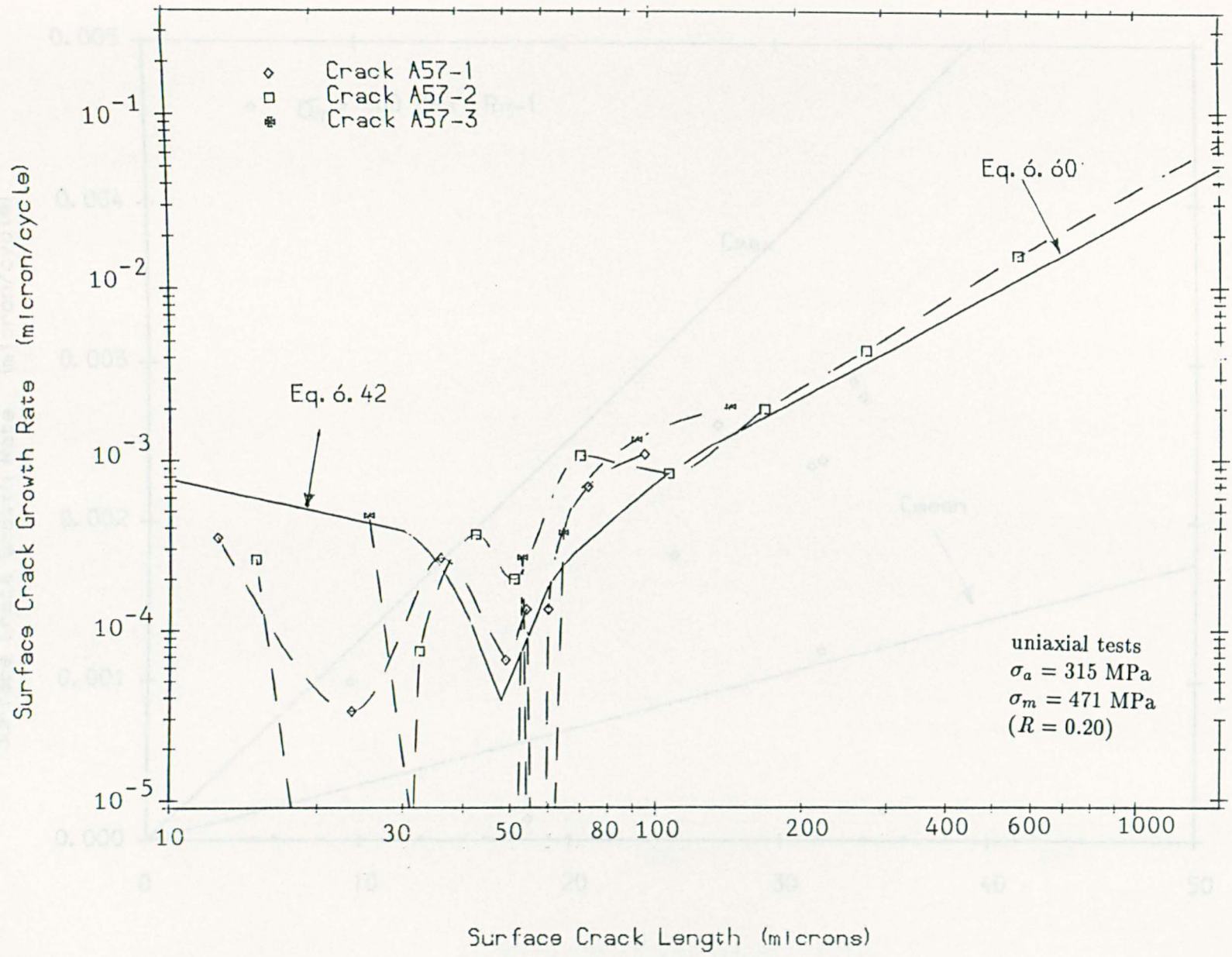


Fig. 6.12 (h) Surface Crack Growth Rate versus Surface Crack Length

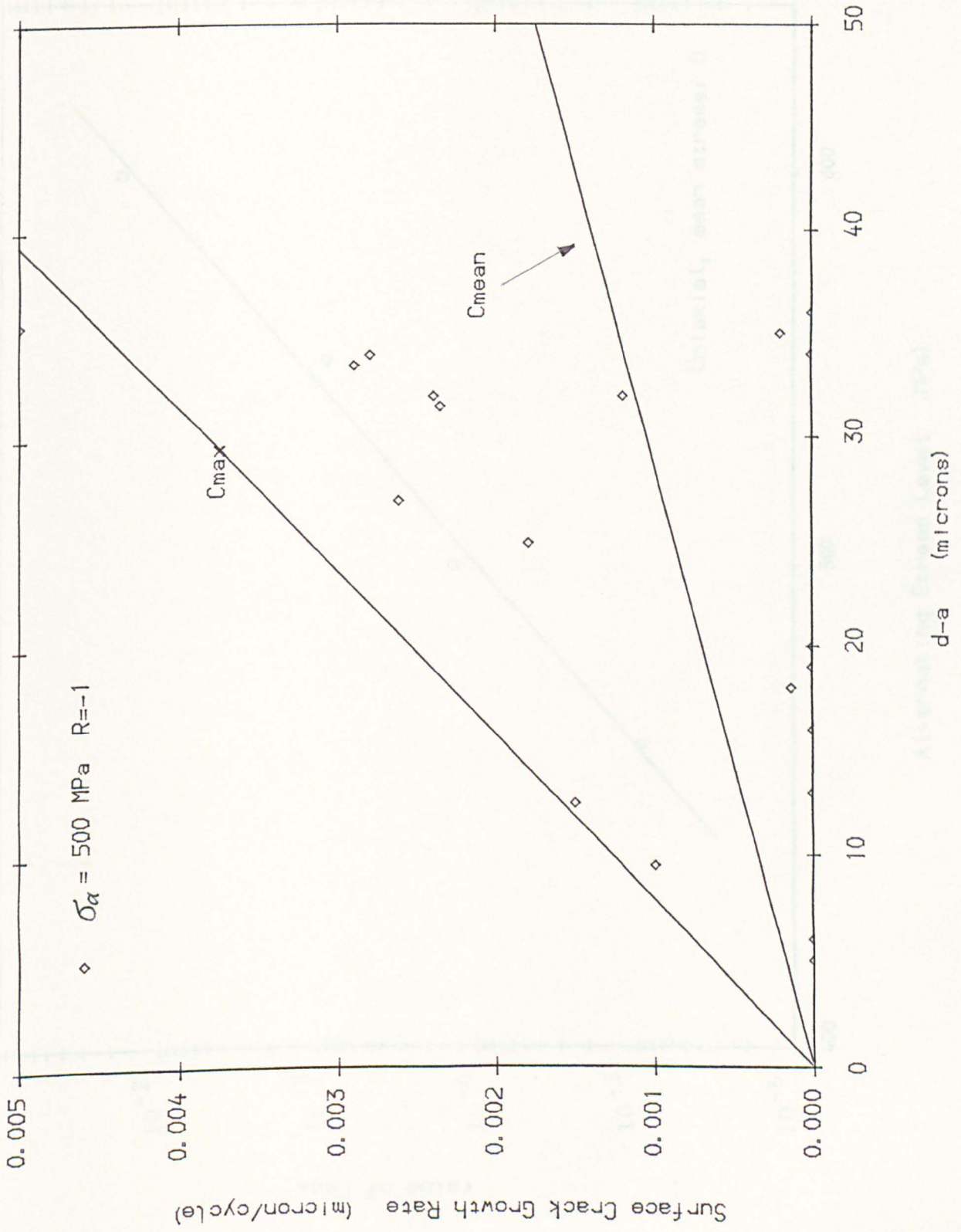
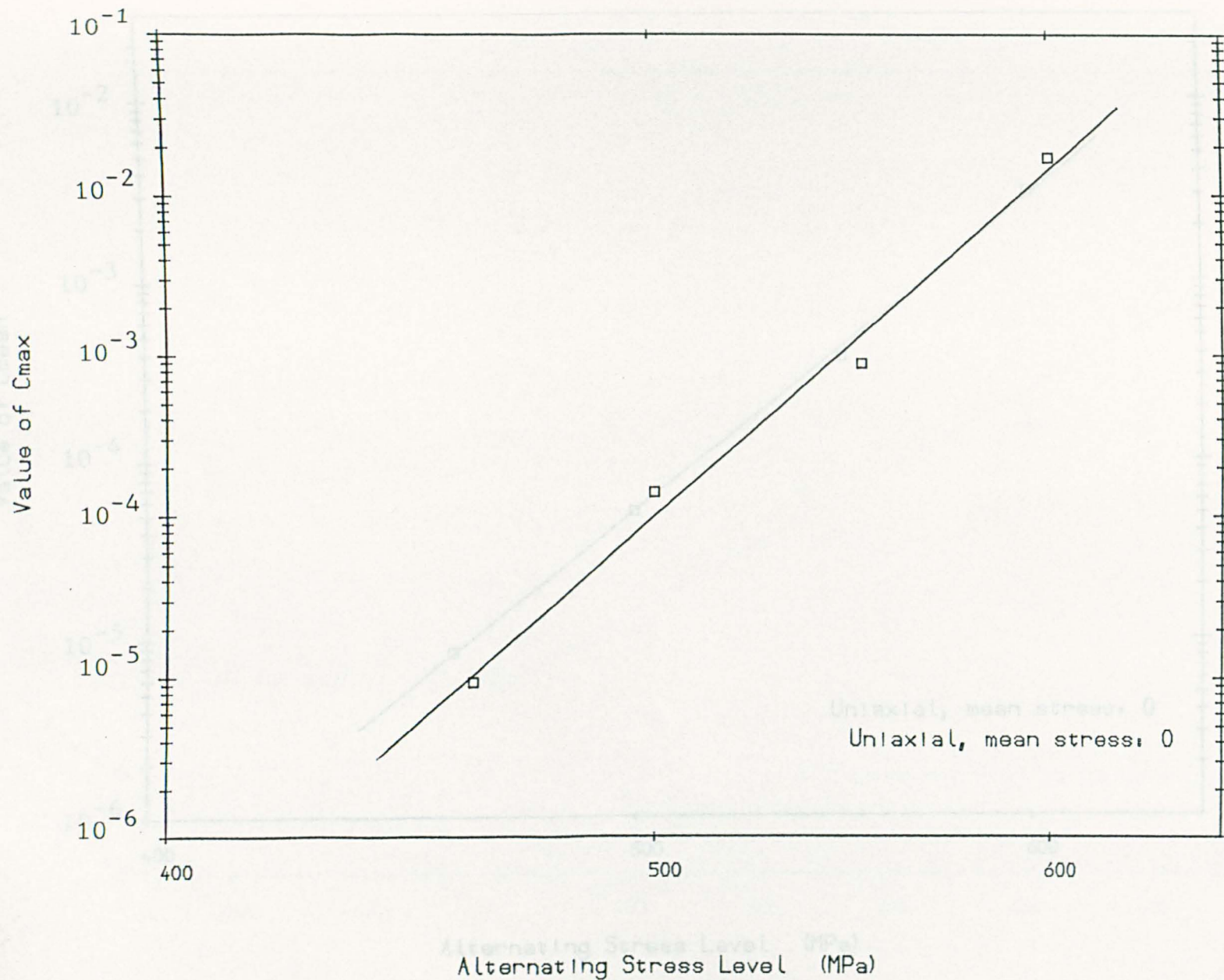
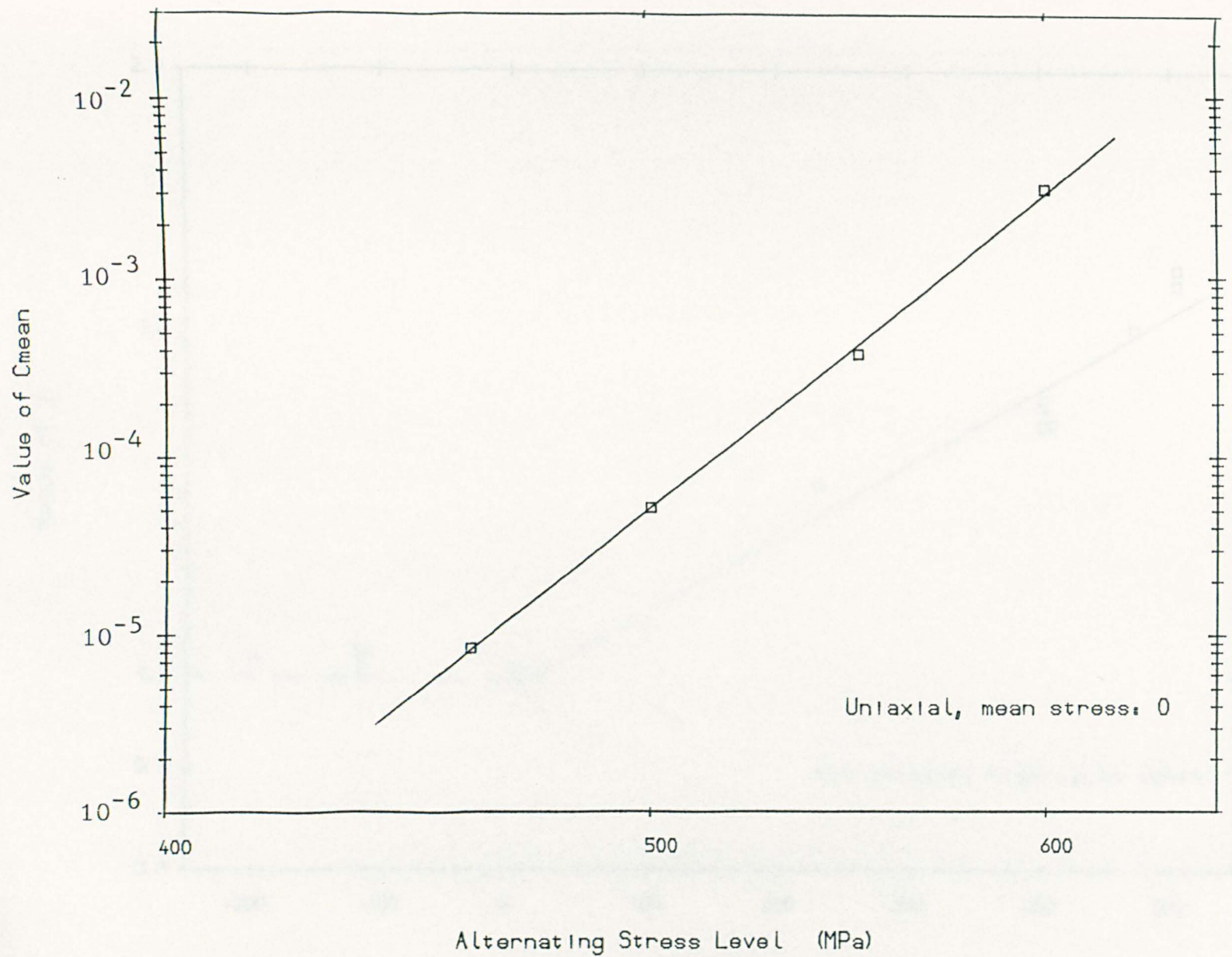


Fig. 6.13 Surface Crack Growth Rate versus d-a

Fig. 6.14a Values of C_{max} versus Alternating Stress Level

Fig. 6.14b Values of C_{mean} versus Alternating Stress Level

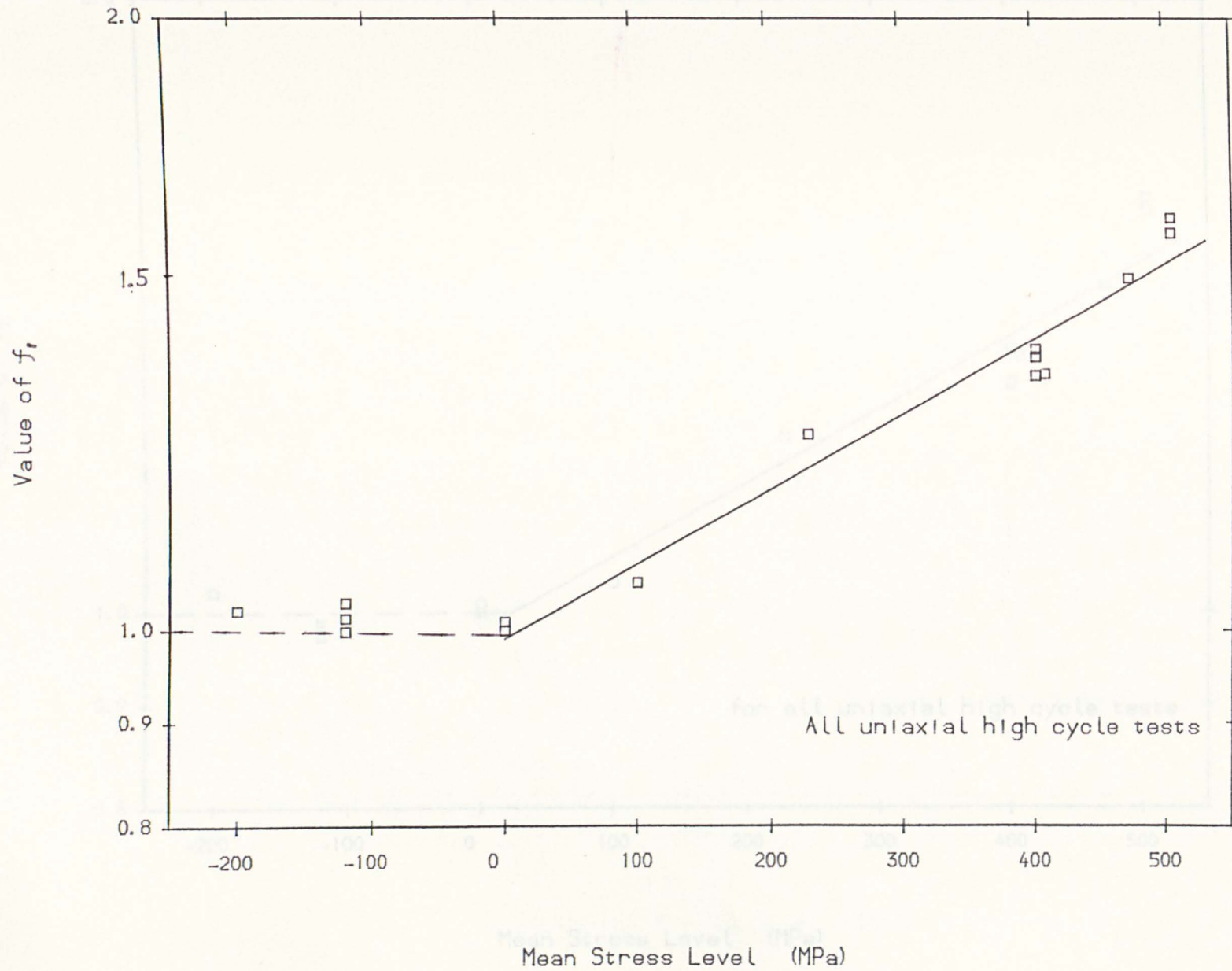
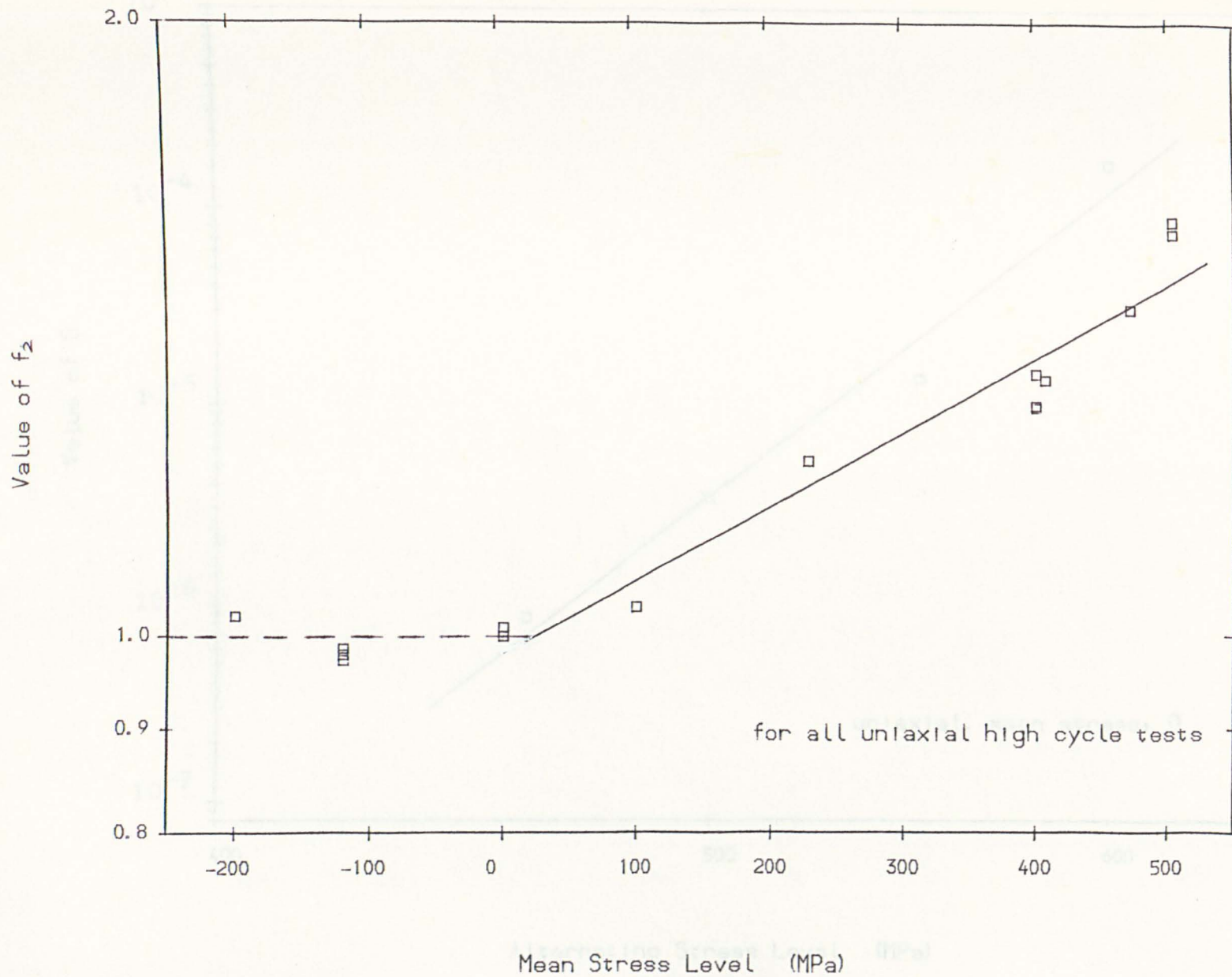


Fig. 6.15a Correlation between f_r and Mean Stress

Fig. 6.15b Correlation between f_2 and Mean Stress

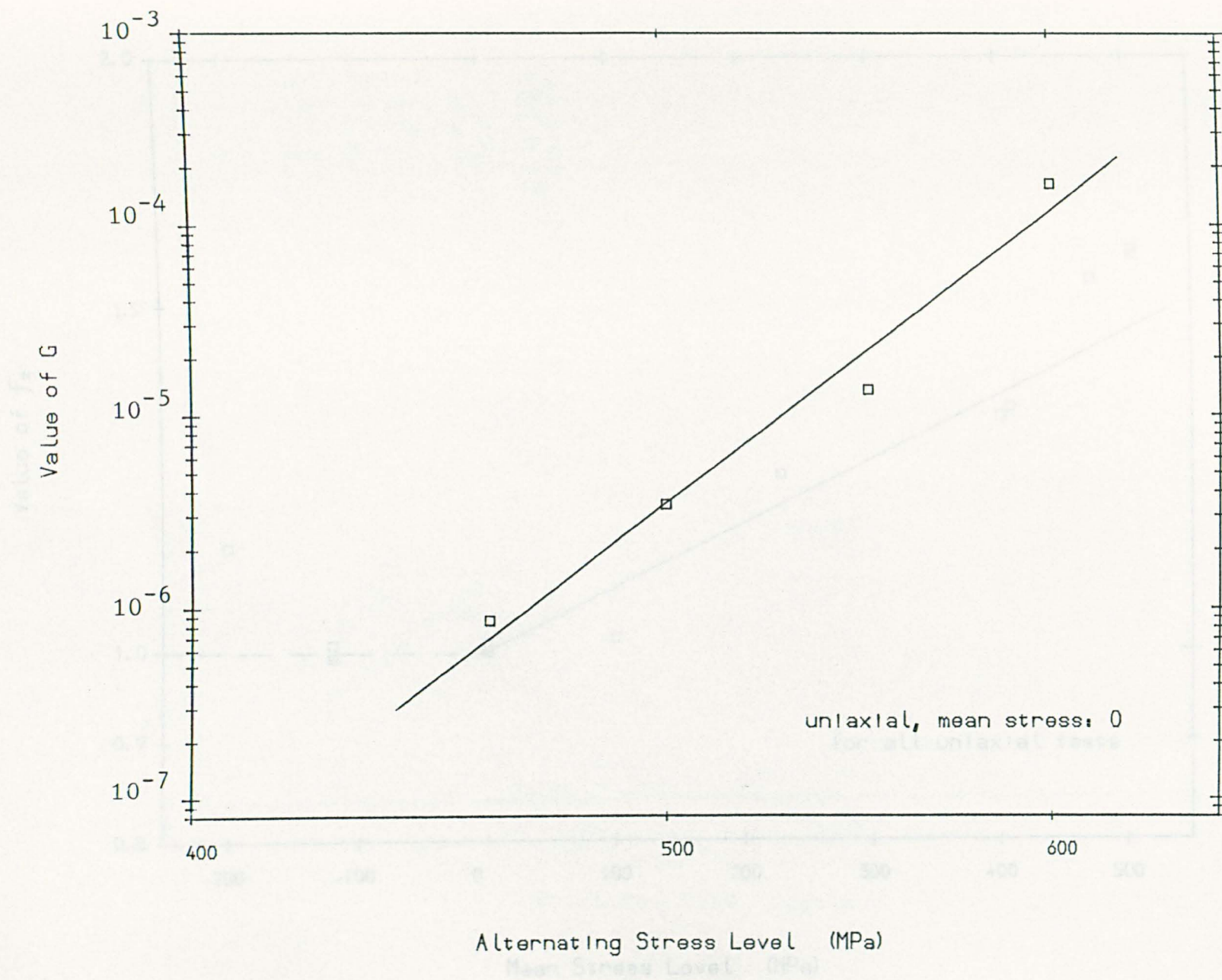
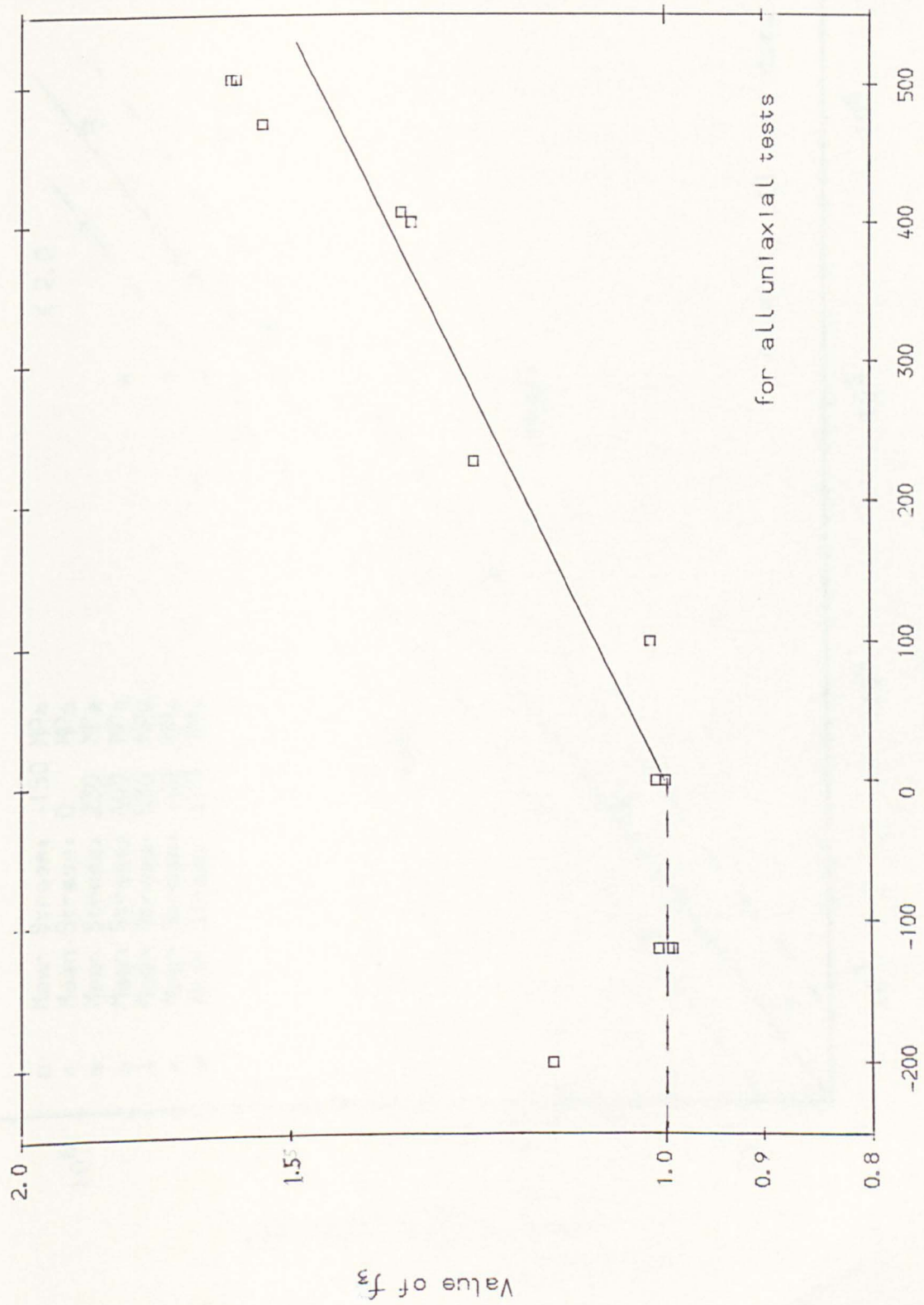


Fig. 6.16 Values of G versus Alternating Stress Level



Mean Stress Level (MPa)

Fig. 6.17 Correlation between f_3 and Mean Stress

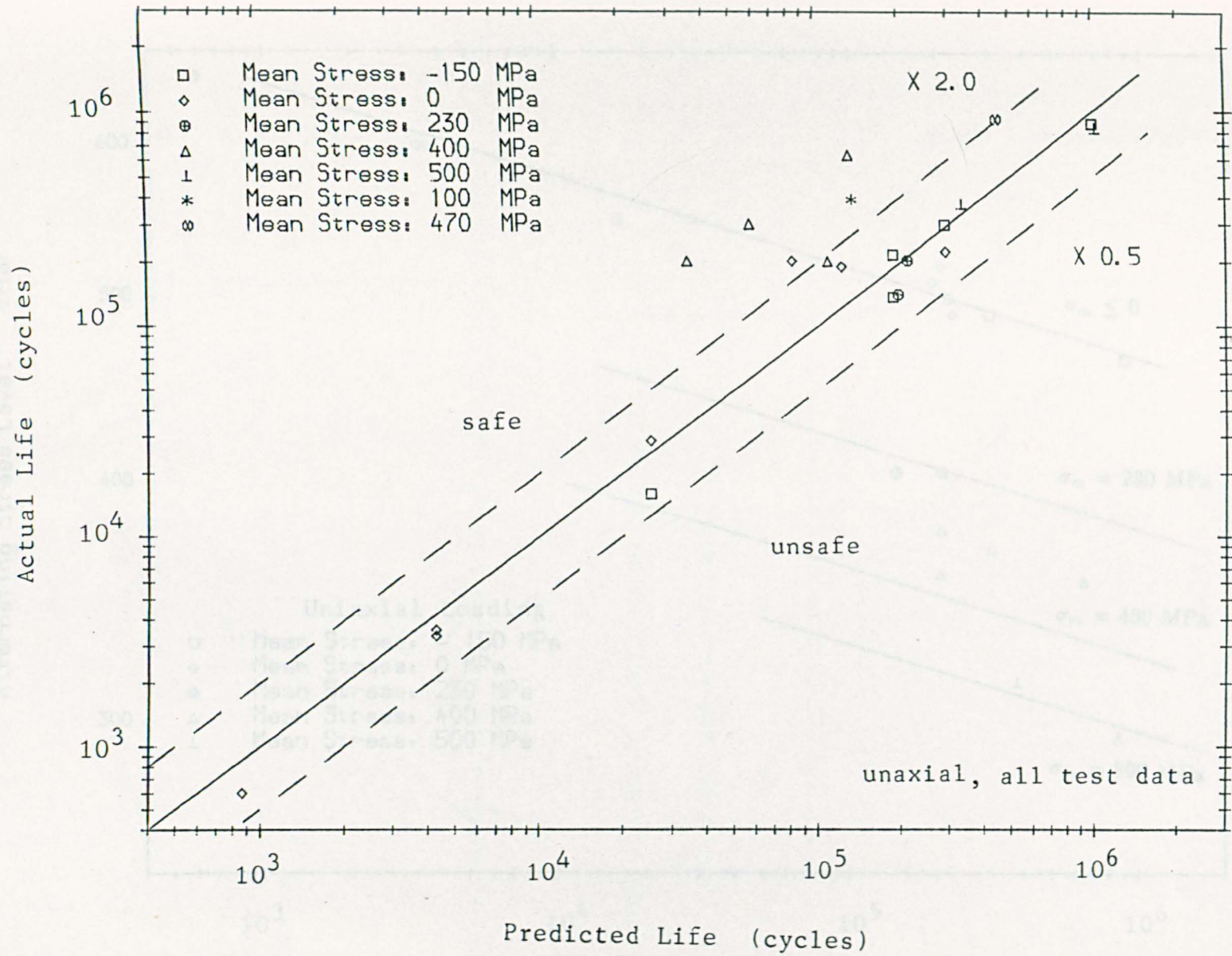


Fig. 6.18 Comparison between Actual Life and Predicted Life (uniaxial)

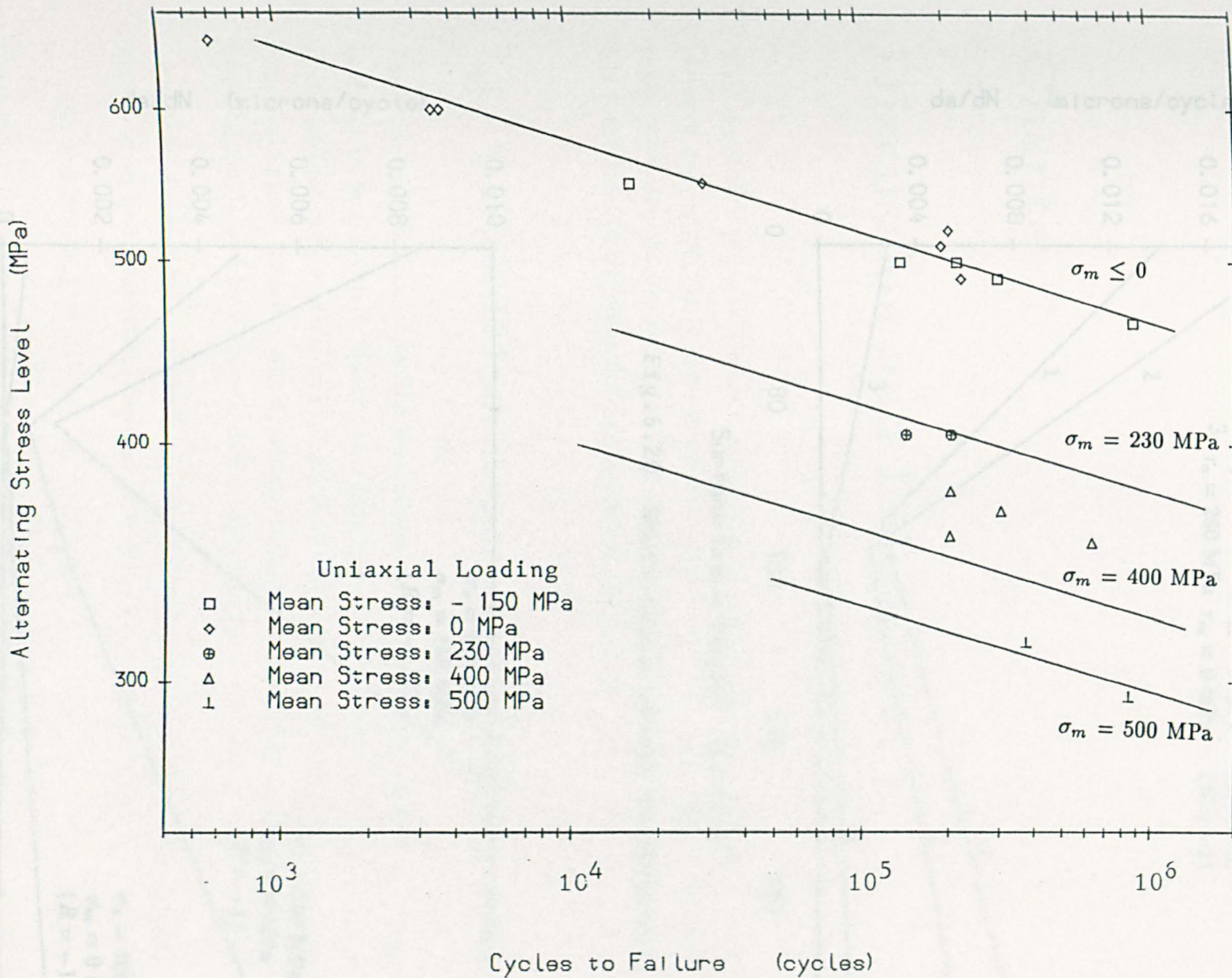


Fig. 6.19 Prediction of S--N Curves with Uniaxial Experimental Data

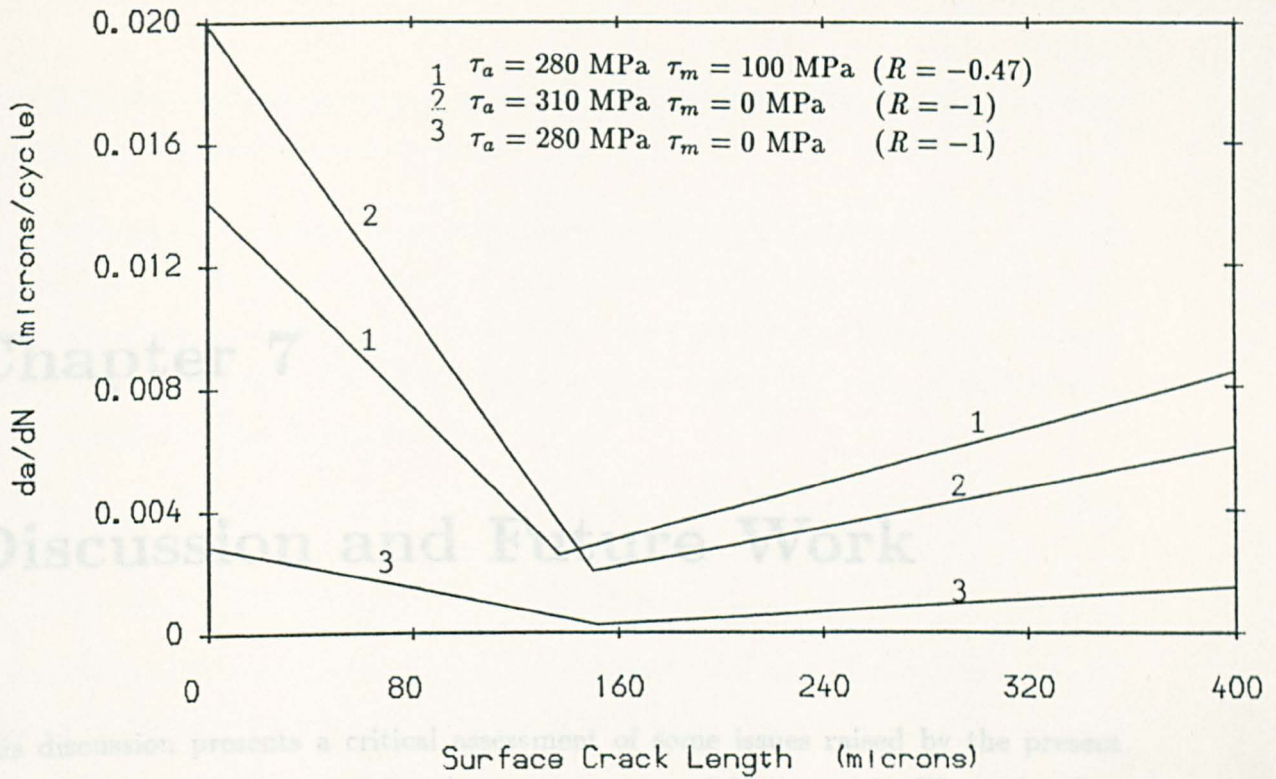


Fig. 6.20 Short Crack Growth in Torsion

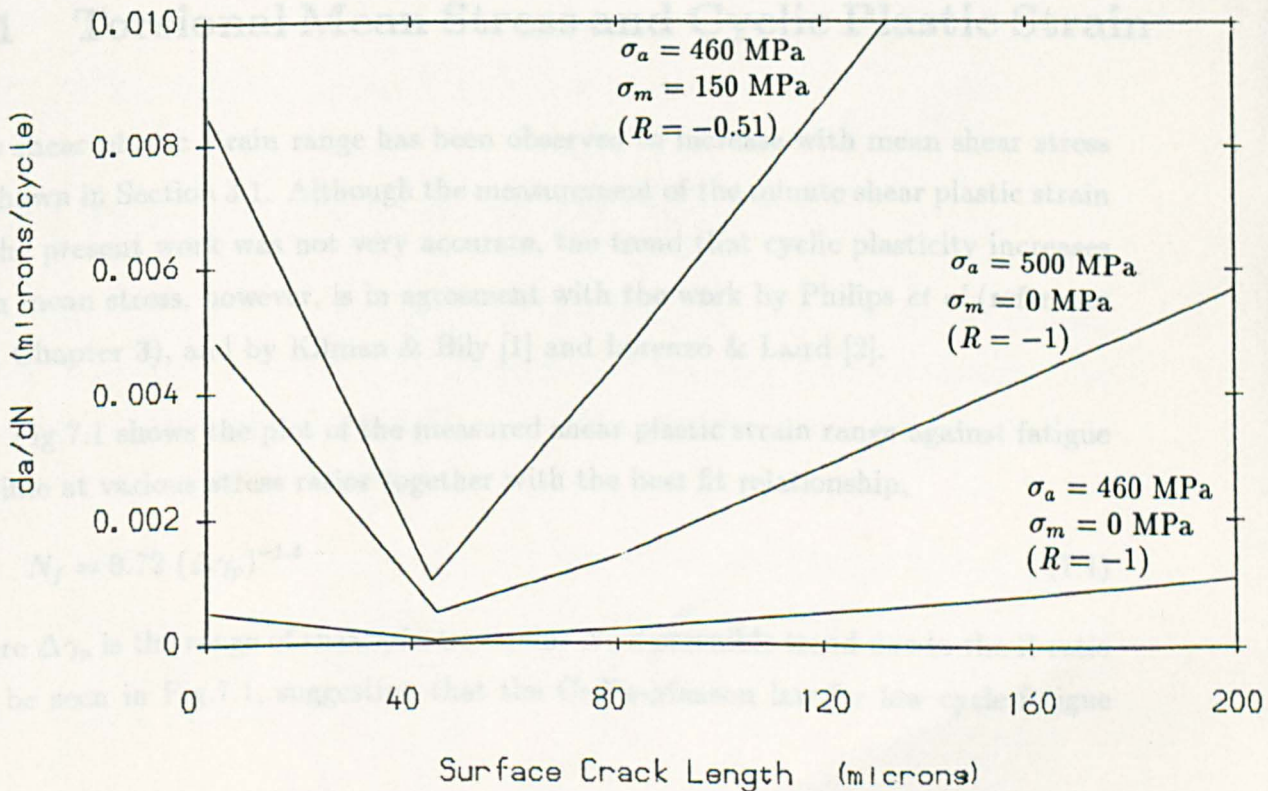


Fig. 6.21 Short Crack Growth in Tension

Chapter 7

Discussion and Future Work

This discussion presents a critical assessment of some issues raised by the present research and comments on their relevance to past and future work. The order that these issues are put forward in the following sections does not indicate any priority, but rather follows the chronological sequence in the present work.

7.1 Torsional Mean Stress and Cyclic Plastic Strain

The shear plastic strain range has been observed to increase with mean shear stress as shown in Section 3.1. Although the measurement of the minute shear plastic strain in the present work was not very accurate, the trend that cyclic plasticity increases with mean stress, however, is in agreement with the work by Philips *et al* (reference 2 in Chapter 3), and by Kilman & Bily [1] and Lorenzo & Laird [2].

Fig.7.1 shows the plot of the measured shear plastic strain range against fatigue lifetime at various stress ratios together with the best fit relationship,

$$N_f = 0.72 (\Delta\gamma_p)^{-1.5} \quad (7.1)$$

where $\Delta\gamma_p$ is the range of shear plastic strain. No discernible trend due to the R ratio can be seen in Fig.7.1, suggesting that the Coffin-Manson law for low cycle fatigue

under fully reversed loading may be extended to mean shear stress loading conditions provided cyclic plastic strain is present.

Following the same approach, MSC growth rate and PSC growth rate in torsion can also be correlated on the basis of $\Delta\gamma_p$ via the use of parameters C and B respectively which were used in the appropriate crack growth equations. For example, Fig.7.2 (a) and (b) show the plot of the maximum values of C and B against $\Delta\gamma_p$ together with the best fit relationships,

$$C = 7.65 \times (\Delta\gamma_p)^{1.372} \quad \text{MSC phase} \quad (7.2)$$

$$B = 5.48 \times 10^{-2} (\Delta\gamma_p)^{0.98} \quad \text{PSC phase} \quad (7.3)$$

The above results suggest that fatigue crack growth data and lifetime can be correlated using one single parameter — cyclic plastic strain range.

Some workers have shown that mean strain, under strain-controlled conditions, has no effect on fatigue behaviour if the mean stress is fully relaxed, e.g. see reference [1,3]. This is in agreement with the above analysis (see also Fig.7.1), since cyclic plastic strain is solely dependent on mean stress and is not affected by mean strain.

7.2 Plasticity Localization

7.2.1 Role of stress level and microstructure

While two different crack initiation sites were found in torsion tests, ie. in base material and at inclusions, only the former kind of initiating site (base material) was found in uniaxial tests. This is solely due to the size, shape, and orientation of the inclusions with respect to the stress field.

A plastic localization period (N_0) was observed for those cracks initiated in the base material both in torsional and uniaxial tests. However those cracks started from inclusions (ie. dominant cracks) corresponded to $N_0 = \text{zero}$. This could be ascribed to two reasons, namely:

(1) The cyclic softening characteristic of material. As crack initiation is primarily due to the yielding of surface grains and the formation of persistent slip bands, cyclic softening would enhance such process. In other words, under stress-controlled conditions, cyclic softening materials, like the present steel, could experience a transition from a very low-strain non-critical fatigue regime to a higher strain critical fatigue regime during the softening process. At low value of $\Delta\tau$ the initiated value of $\Delta\gamma_p$ may be zero but can increase to a certain value thereby being sufficient to permit the creation of cracks.

(2) The bainitic microstructure of the material. Prior austenite grains are divided into bundles which are composed of small packets of a size about $3 \mu m$ in diameter. The boundaries between packets and the boundaries between bundles are high angle ones which could pose a strong resistance to the movement of dislocations and the yielding of a whole grain in the initial phase of lifetime. Fig.7.3 shows the plot of the N_0 against the stress range in torsion and tension.

Inclusions elongated along the rotor axis are similarly aligned to the specimen axis since specimens were removed in the longitudinal direction of the forging. In torsion tests, these inclusions were aligned to the maximum shear strain direction and dominant (ie. failure) cracks were found to have been initiated promptly from inclusions and no plastic localization period was observed due to the stress concentration induced by the inclusions. However in uniaxial tests, inclusions were not found to start cracks as early as in torsion tests although some cracks did initiate from inclusions. In other words, inclusions had a significant effect on short crack growth under torsional loading but not in the case of uniaxial loading.

7.2.2 Effect of mean stresses

Torsional mean shear stress

The present investigation has revealed that crack initiation from the base material is strongly dependent on mean stress, especially the mean shear stress through its control of the cyclic strain range. Since fatigue crack initiation is primarily due to the yielding

of surface grains and the formation of PSBs in these grains, an increase in mean shear stress would cause the yielding of more surface grains and reduce the alternating stress level required to trigger the plasticity localization for the fracture process. This is supported by the experimental data. The minimum value of the plasticity localization period (N_0 , of those cracks started from base material) decreases with the increase of mean shear stress in torsion tests as shown in Fig.7.4, the regression relationship being,

$$N_0 = 98486 \times e^{-\tau_m/46.6} \quad (7.4)$$

Mean uniaxial stress

Since the initiation of MSCs is preceded by the formation of PSBs in the maximum shear plane under uniaxial loading condition, both the local mean shear stress and the local mean normal stress upon the maximum shear plane would affect the formation PSBs.

Mean uniaxial stress would introduce mean shear stress and mean normal stress on the plane 45° degrees to the loading direction. A mean tensile and compressive stress obviously can result in tensile and compressive local mean normal stress, respectively (see Section 4.3.1). The mean normal stress may modify the internal friction stress and the movement of dislocations as well. Thus the tensile normal stress facilitates and the compressive normal stress hinders the formation of PSBs. Therefore, it is not surprising that mean tensile stress can significantly shorten the plasticity localization period while compressive mean stress does not (see Table 6.3), i.e for the present material,

$$N_0 = 2.97 \times 10^{66} e^{-\sigma_m/51.5} \sigma_a^{-23} \quad (\sigma_m \geq 0) \quad (7.5)$$

See Section 6.7.2.

7.3 Microstructurally Short Crack Growth

7.3.1 Effect of torsional mean shear stress

MSCs are known to initiate and propagate in the relatively large surface grains having the most favourable inclined slip system, the growth rate being controlled by the shear stress or shear strain developed within the intensive shear bands. Based on various models proposed within the frame-work of EPFM, the sliding movement between crack faces is principally determined by the cyclic stress amplitude, since mean shear stress is almost fully relaxed within the shear bands at the crack tip. Consequently, the frequently used theory that crack advance is proportional to the crack tip sliding displacement would suggest that mean shear stress has no effect on the crack growth rate.

The present results however, indicate that mean shear stress (τ_m) can considerably increase the MSC growth rate as illustrated in Eq.6.14. Such an enhancing effect is possibly caused by the reduction of the re-welding effect and an increase of the proportion of the irreversible plastic deformation at the crack tip. Fatigue crack growth is considered to be generated by the cyclic sliding of crack faces under the action of cyclic loading. Since re-welding of the newly formed crack surface may occur during the unloading half cycle, the new crack surface is only a small part of the total plastic sliding displacement. The presence of mean shear stress, according to the present work, appears to reduce the possible effect of re-welding.

No rubbing or closure was observed in the MSC growth phase, indicating that the effect of mean shear stress upon short Mode II crack growth is not due to the change of crack closure or friction stress between crack faces. This suggests that mean shear stress plays a fundamental role in promoting short Mode II crack growth.

One important aspect of the effect of mean shear stress upon MSC growth is its insensitivity to polarity: mean shear stresses in two opposing directions have an identical effect on MSC growth. See the analysis in Section 3.6. This is not so in the case of mean uniaxial stresses.

7.3.2 Mean uniaxial stress

MSC growth under uniaxial loading is also sensitive to the level of mean stress: mean tensile stress ($\sigma_m \geq 0$) significantly increases the growth rate whilst mean compressive stress ($\sigma_m \leq 0$) has no influence (see Section 6.6.2). Two mechanisms are involved: (1) in the case of mean tensile stress, a tensile mean normal stress ($\sigma_{n,mean} \geq 0$) and a mean shear stress ($\tau_{n,mean}$) both act upon the MSC plane and both assist crack growth. Since a mean normal tensile stress may also reduce re-welding, the overall effect is therefore that crack growth rate increases significantly with the increase of mean tensile stress. (2) in the case of compressive mean stress, the counteracting effect of the compressive mean normal stress ($\sigma_{n,mean} \leq 0$) and that of the mean shear stress ($\tau_{n,mean}$) on the MSC plane result in the insensitivity of MSC growth to the compressive mean stress. This however is only true for low compressive mean stresses. For high levels of mean compressive stress, e.g. when the minimum stress level exceeds the yielding stress in compression, the maximum shear stress would control the growth of MSCs and the dominant crack may be in mode II (see Section 4.3.1).

7.4 A Model for the Effects of Mean Stress

In this section the Brown and Miller multiaxial fatigue theory (ref. [15] in Chapter 1) is modified to include mean stress effects. The modified model, involving two material dependent parameters (which can be obtained through fitting the results from mean shear stress torsional tests and fully reversed uniaxial tests) can predict the effects of mean tensile stress and mean compressive stress upon short crack growth. The high cycle fatigue lifetime can also be unified on the basis of this model.

The Dang Van criterion [5] was found to fail to correlate the fatigue life of both torsional and uniaxial tests under various stress ratios, although this criterion has claimed success in correlating finite fatigue life data under multiaxial stress states and mean stress loading.

7.4.1 Introduction

One simplified criterion put forward by Kandil, Brown and Miller (ref. [17] in Chapter 1) states that the effective shear strain amplitude which governs Mode II crack growth is

$$\gamma_a^* = \gamma_a + S \epsilon_{n,a} \quad (7.6)$$

Here γ_a and $\epsilon_{n,a}$ are the shear strain and normal strain amplitude on the crack plane. The coefficient S is a constant pertaining to a specific material.

In the present case, since the macroscopic plastic strain amplitude is negligible in the high cycle fatigue regime, the above equation can be rewritten in terms of stress, noting that

$$\epsilon_{n,a} = \frac{1-\nu}{2} \epsilon_a = \frac{1-\nu}{4(1+\nu)} \frac{2\sigma_{n,a}}{G} = 0.27 \frac{\sigma_{n,a}}{G} \quad (7.7)$$

here the Poisson's Ratio ν is taken to be 0.3 and G is the Shear Modulus of the material. Therefore the effective shear stress is,

$$\tau_a^* = \tau_a + 0.27 S \sigma_{n,a} \quad (7.8)$$

Assuming that the value of C_{max} is determined uniquely by the effective shear stress amplitude τ_a^* , the value of S can be obtained by correlating the fully reversed ($R = -1$) torsion and tension tests results.

In torsion tests, at a shear stress amplitude $\tau_a = 280$ MPa ($\tau_a^* = 280$ MPa), the value of C is 1.61×10^{-5} (see Section 6.3) whilst in push-pull tests, the value of C is 0.9×10^{-5} (see Table 6.3) at a stress level $\sigma_a = 460$ MPa ($\tau_a = 230$ MPa; $\tau_a^* = 230 + 0.27 \times S \times 230$). It is clear that the shear stress amplitude required to produce the same C is reduced due to the effect of normal stress. For the present material, S is found to be 0.805 to correlate the data from fully reversed torsion and tension tests.

The above model only applies to fully reversed loading and should be modified to incorporate the effects of mean stresses.

7.4.2 The modified model

As can be inferred from the discussion in Chapter 4, there are four parameters that may promote Stage I crack growth under a mean stress uniaxial loading:

1. Shear stress amplitude τ_a .
2. Mean shear stress τ_m .
3. Normal stress amplitude $\sigma_{n,a}$.
4. Mean normal stress $\sigma_{n,m}$.

A simple form of the 'effective shear stress amplitude' is proposed here as,

$$\tau_a^* = \tau_a e^{\tau_m/Q} + 0.27 S \sigma_{n,max} \quad (7.9)$$

Here the effect of the normal stress in the present model is considered to be due to the maximum stress in a cycle instead of the amplitude.

It is worth noting that only two parameters (Q and S) so far have been involved in equation (7.9). These two parameters are material dependent, and have to be derived from experimental data. The parameter S for the present material has been found to be 0.805 (as shown in the previous section) to unify the fully reversed uniaxial and torsional test data, and Q should equal to 1194 to unify the mean stress torsional test data; see Eq.6.13.

Since mean shear stress does not show any polarity condition in promoting shear mode crack growth, this means that in the above equation the absolute value ($|\tau_m|$) of τ_m should be used for the case of compressive mean axial stress loading (see also Chapter 4).

Therefore the 'effective shear stress amplitude' which uniquely characterises the MSC growth behaviour under mean stress torsional or uniaxial loading of the present material is given by

$$\begin{aligned} \tau_a^* &= \tau_a e^{|\tau_m|/1194} + 0.27 \times 0.805 \times \sigma_{n,max} \\ &= \tau_a e^{|\tau_m|/1194} + 0.218 \sigma_{n,max} \end{aligned} \quad (7.10)$$

By replacing τ_m and $\sigma_{n,max}$ with $\frac{1}{2}\sigma_m$ and $\frac{1}{2}(\sigma_a + \sigma_m)$ and after some simplification, Eq.7.10 can be simplified as follows for tensile mean stress levels less than 500 MPa which applies to the present case,

$$\tau_a^* = 0.61 \sigma_a \left[1 + \frac{|\sigma_m|}{2904} + \frac{\sigma_m}{5.63 \sigma_a} \right] \quad (\text{for uniaxial loading}) \quad (7.11)$$

Denote the second term in Eq.7.11 as $F(\sigma_m)$,

$$F(\sigma_m) = 1 + \frac{|\sigma_m|}{2904} + \frac{\sigma_m}{5.63 \sigma_a} \quad (7.12)$$

and if a typical value $\sigma_a = 450$ MPa is used, then

$$F(\sigma_m) = \begin{cases} 1.0 + \sigma_m/1164 & \text{when } \sigma_m > 0 \\ 1.0 - \sigma_m/19608 & \text{when } \sigma_m < 0 \end{cases} \quad (7.14)$$

Obviously $F(\sigma_m)$ approximately equals unity for compressive mean stress between -200 and 0 MPa. It will be demonstrated in the next section that the experimental crack growth rate data from the following five types of tests carried out in the present study can be unified on the basis of this model:

1. Fully reversed torsional loading.
2. Mean stress torsional test.
3. Fully reversed uniaxial test.
4. Uniaxial test under tensile mean stress.
5. Uniaxial test under compressive mean stress.

The parity between $F(\sigma_m)$, $f_1(\sigma_m)$ and $f_2(\sigma_m)$ (see Section 6.6.2), in fact, shows that Eq.7.11 is a general expression of the above mentioned three functions and indicates the potential of this model in correlating the fatigue lifetime.

As a conclusion, the 'effective shear stress amplitude' (τ_a^*) can be expressed as,

$$\tau_a^* = \tau_a e^{|\tau_m|/1194} + 0.218 \sigma_{n,max} \quad (7.14)$$

where $\sigma_{n,max}$ equals zero in torsional tests. The terms τ_a , τ_m and $\sigma_{n,max}$ are equal to $\sigma_a/2$, $\sigma_{mean}/2$ and $\sigma_{max}/2$ in uniaxial tests, respectively.

7.4.3 Application of the model to experimental results

Unification of short crack growth rate data

In what follows it will be demonstrated that the model can unify the short crack growth rate data obtained in the present work, e.g. the value of C_{max} in mean stress tensile tests as shown in Eq.6.42 can be predicted from the torsional test results and vice versa. This is not surprising because crack growth is a shear stress-shear strain dominated process.

The predicted C_{max} of the uniaxial tests from the torsion test results (Eq.6.14) is,

$$\begin{aligned} C_{max} &= 3.68 \times 10^{-52} (e^{\tau_m/1194} \tau_a)^{19.07} \\ &= 3.68 \times 10^{-52} (\tau_a^*)^{19.07} \end{aligned} \quad (7.15)$$

where τ_a^* , the effective shear stress amplitude is given by Eq.7.14. The predicted values together with the experimental data from uniaxial tests are shown in Table 7.1. An overall good prediction is observed irrespective of some under-estimation of the value of C_{max} in the high strain, low cycle regime, which is possibly due to the fact that the present model is mainly concerned with cases of low plasticity. Even so, in comparison with the large scatter encountered in the MSC growth phase, the prediction is still acceptable.

Therefore the MSC growth rate under both mean shear torsional and mean stress uniaxial tests can be expressed as

$$\frac{da}{dN} = 3.68 \times 10^{-52} (\tau_a^*)^{19.07} (d - a) \quad (7.16)$$

where $d = 166 \mu m$ for torsional loading and $d = 50 \mu m$ for uniaxial loading and the short crack growth rate under both tensile mean and compressive mean stress can be predicted from the torsional test results, and vice versa.

Correlation of fatigue lifetime

Although the present model is proposed on the basis of experimental MSC growth data, the parity between functions $F(\sigma_m)$ and $f_3(\sigma_m)$ (see Eq.6.57) suggests PSC growth rate under mean stress uniaxial loading can be unified by the model, although the PSC growth mode under uniaxial loading is mainly Mode I instead of Mode II. For instance, for uniaxial loading Eq.6.55 can be rewritten as,

$$\begin{aligned} G_{max} &= 2.346 \times 10^{-58} \left[\sigma_a \left(1.0 + \frac{\sigma_m}{1083} \right) \right]^{19.33} \\ &\approx 2.346 \times 10^{-58} \left[\sigma_a F(\sigma_m) \right]^{19.33} \\ &\approx 2.346 \times 10^{-58} \left[\frac{1}{0.61} \tau_a^* \right]^{19.33} \quad (\text{see also Eq.7.11}) \end{aligned} \quad (7.17)$$

The microstructural parameters d_1 (torsional loading) and d_2 (uniaxial loading), however, cannot be unified by the model, since these two parameters are dependent on the stress system and microstructure. Large shear type cracks can exist under torsional loading (see Section 3.3), but not in tension tests since the normal stress component would assist the transition of Mode II cracks to Mode I cracks.

Even so the model still exhibits a potential in unifying the fatigue life data from both torsion and tension tests at various stress ratios. Fig.7.5 shows the plot of the 'effective shear stress amplitude' against the fatigue lifetime of all torsion and tension tests under various stress ratios (type A specimens) carried out in the present research together with the power-law relationship,

$$\tau_a^* N_f^{0.0755} = 733 \quad (7.18)$$

It can be seen from Fig.7.5 that 96% of the experimental data points are within a $\pm 50\%$ error band, a surprisingly good prediction.

7.4.4 Comments

One recent established multiaxial fatigue theory—the Dang Van criterion [5]—has claimed success in finite life multiaxial fatigue correlation as well as in accounting for

the effect of mean stress on the fatigue limit. The application of this model will be discussed here in comparison with the present model.

The Dang Van criterion suggests that, in the high cycle fatigue regime, the constant endurance limit follows the following criterion,

$$\tau_a + \alpha p = b \quad (7.19)$$

where τ_a is the shear stress amplitude and p is the hydrostatic pressure. The two parameters (α and b) may vary with the lifetime. This model assumes that mean shear stress does not contribute to the growth of short cracks. In the case of uniaxial loading, the above equation is reduced to,

$$\frac{\sigma_a}{2} + \alpha \frac{\sigma_{max}}{3} = b \quad (7.20)$$

For an endurance life of 10^6 cycles, τ_a equals 280 MPa in torsion and σ_a equals 460 MPa in tension for the present material, thus the two parameters b and α can be obtained as 280 MPa and 0.326 respectively. It follows that the criterion for constant finite fatigue life under uniaxial loading for the present material is,

$$\sigma_a + 0.178\sigma_m = 460 \quad (\text{MPa}) \quad (\text{for any } \sigma_m) \quad (7.21)$$

Obviously, for the present material, the above equation is non-conservative for both tensile and compressive mean stress. For example, in the regime of tensile mean stress loading, the equation for the constant fatigue life of 10^6 cycles is (see also Eq.4.12 and Eq.4.13),

$$\sigma_a + 0.33\sigma_m = 460 \quad (\text{MPa}) \quad \sigma_m \geq 0 \quad (7.22)$$

and in the case of compressive mean stress loading, the experimental results showed that the mean compressive stress does not have a beneficial effect on the endurance limit, whereas the Dang Van criterion (Eq.7.19) predicts that the stress amplitude increases with an increase of mean compressive mean stress.

Comparing the present model with the Dang Van theory, the main difference is whether the effect of mean shear stress should be taken into account or not. Apparently when the parameter Q in Eq.7.9 is taken to be infinity, in other words, mean

shear stress is considered to have no effect on the fatigue crack growth, the present model reduces to a similar form to the Dang Van criterion.

The inclusion of the effect of the mean shear stress in correlating the fatigue initiation period was also reported by Jacquelin, Hourlier and Pineau [6], and in reference [7] McDiarmid reported that mean shear stress can affect the equivalent shear stress level. However, many researchers believe that mean shear stress does not have much effect on the torsional fatigue limit or uniaxial fatigue limit. More work is therefore required in which the level of mean shear stress can be accurately monitored and controlled, since it has been found that to maintain the mean shear stress constant throughout the torsion test is very difficult (see Section 3.2); mean shear stress may be relaxed to a lower level than the initial value. It may be more so for combined stress states in which cyclic creep would cause re-distribution of stresses.

7.5 Physically Short Crack Growth

7.5.1 Torsional loading

Two kinds of crack path were observed in the PSC growth phase as shown in Section 3.5: a zig-zag path and a bifurcated crack path. Examination of these two types of crack path revealed that PSCs mainly propagated in the tensile mode under an influence of the shear mode along the surface, especially the dominant cracks. Since a tensile or a compressive mean stress has been induced by the applied shear stress on two 45° planes inclined to the maximum shear plane, only the growth of one bifurcated branch crack is favoured whereas that of another is being hindered or terminated by the action of mean compressive stress.

In what follows an attempt will be made to offer an explanation of the effect of mean shear stress upon the dominant PSC (bifurcated at Stage I crack tip) growth behaviour.

It has been established in Chapter 3 that mean shear stress can increase the

maximum plastic zone size and reduce the effect of crack closure. For those PSCs that bifurcated into Mode I and propagated at 45° to the Stage I crack plane, the applied mean shear stress induces a normal tensile stress on one branch crack and a compressive mean stress on the other one. Fig.7.6 shows that the maximum values (B_{max}) and the mean values (B_{mean}) of B against the ratio of maximum plastic zone size to crack length ($r_{p,max}/a$) which can be obtained from Eq.3.15 as

$$\frac{r_{p,max}}{a} = \sec \left[\left(\frac{\pi}{2} \right) \left(\frac{\tau_a + \tau_m}{2\tau_u - \tau_a - \tau_m} \right) \right] - 1 \quad (7.23)$$

here τ_u is taken as half of the UTS of the material and equals 420 MPa.

Fig.7.6 suggests that the ratio of the maximum plastic zone size to the crack length ($r_{p,max}/a$) provides a good correlation to the upper bound of crack growth rate (B_{max} of the PSC phase) and mean value (B_{mean} of the PSC phase). The correlation equations are,

$$B_{max} = 9.16 \times 10^{-6} \left(\frac{r_{p,max}}{a} \right)^{0.767} \quad (7.24)$$

$$B_{mean} = 6.12 \times 10^{-6} \left(\frac{r_{p,max}}{a} \right)^{0.751} \quad (7.25)$$

Apparently the crack growth rate of PSCs not only depends on the reversed plastic zone size, but also depends on the maximum plastic zone size. In the present case, The PSC growth rate under constant shear stress amplitude can be correlated with $r_{p,max}$, this highlights the mechanism of how the mean shear stress affects the PSC growth behaviour in torsion. For those PSCs which followed a zig-zag path, the growth rate may also increase with an increase of mean shear stress because the applied mean shear stress would not only increase the maximum plastic zone size but also assist in overcoming the microstructural barriers.

7.5.2 Uniaxial loading

It is clear from the crack growth rate data presented in Fig.5.12 that mean tensile stress not only significantly changes the MSC (less than 50 microns) growth, but also drastically enhances the PSC growth. The PSC growth rate under uniaxial loading

with tensile mean stress can be rewritten in terms of stress ratio, see Eq.6.60,

$$\frac{d a_s}{dN} = \left[1 + \frac{\sigma_a}{1083} \frac{1+R}{1-R} \right]^{19.33} \sigma_a^{19.33} a_s^{1.405} - D \quad (7.26)$$

Here the stress ratio R should be higher than -1 .

It can be seen that the crack growth rate is strongly dependent on the stress ratio and the effect of stress ratio on short crack growth rate is much more pronounced than on LEFM type of cracks. For example, for $\sigma_a = 460$ MPa, if the stress ratio increases from -1 to -0.5 , the PSC growth rate is increased by more than 9 times. But in the LEFM regime, the crack growth rate (for a certain crack length) may be doubled if stress ratio increases from -1 to 0 for a constant stress range as stated in Section 5.2. Moreover, for short cracks, it can be expected that if the alternating stress is maintained constant, crack growth rate can be significantly affected by stress ratio, although in practice a high mean stress level with high alternating stress may cause ratcheting failure rather than fatigue failure.

The experimental crack growth rate data seem to suggest that the PSC growth under high strain level is dominated by bulk deformation rather than by the stress concentration induced by crack itself. In other words, the PSC can be considered as being embedded within a field having a high shear strain level with un-relaxed mean shear stress. Crack advance is known to be produced by shear decohesion (ie. in [4]) and this is illustrated by the high exponent number in the crack growth equation (Eq.6.14 and Eq.6.30). The applied mean shear stress enhances such a decohesion process in a similar way as in the case of the MSC growth. This is possibly the reason why mean tensile stress is still effective in enhancing fatigue crack growth processes when crack closure is not present. This also explains why mean compressive stress showed no preference on the PSC growth in the present experiments: the preference of crack closure under low stress ratio is nulled by the effect of mean shear stress; it should be noted that compressive mean stress also introduces mean shear stress on the maximum shear plane, and mean shear stress is always effective.

7.6 Effect of Mean Stress and Crack Closure of Short Cracks

Long crack (LEFM type crack) growth is controlled by the local plastic deformation which is governed by the stress concentration (e.g. the stress intensity factor K) induced by the crack itself. Extensive studies on the closure of long cracks have led to the conclusion that both crack growth rate and crack growth threshold can be unified by a single parameter—effective stress range, provided crack growth is in a striation mode. The underlining reason is that once crack faces come into contact, the disappearance of the stress concentration means that any subsequent unloading does not contribute to crack growth.

However in the short crack regime, crack growth is not only controlled by the local plastic deformation induced by the crack itself but also, possibly more dominantly, the applied stress (or strain) as indicated by the high exponent number in the crack growth equations (see Eq.6.14 and Eq.6.30). Short crack growth, therefore, cannot be considered to be governed only by the portion in which crack is open, more explanations being as follows,

1. In the present work, SEM observations showed that short cracks keep open under high mean stresses, for example when $R > 0$, although they do close at low stress ratios ($R \leq 0$). However, the experimental crack growth rate data showed that mean stress is still effective at high stress ratios, suggesting that the effect of mean stress upon short crack growth behaviour cannot be accounted for by crack closure. It follows that even if the closure stress level could be accurately measured, it would not provide faithful predictions and valid explanations of the effect of stress ratio.
2. In the LEFM regime, crack closure plays a key role in crack growth under unsymmetrical loading. Consequently a larger grain size will result in lower threshold value and lower crack growth rate for the same $\Delta\sigma$ (or ΔK), due to the more severe crack closure caused by the deflection of crack path in comparison with small grains. By contrast, the fatigue limit of smooth specimens has been

known to decrease with the increase of grain size. The recent experimental results reported by Slade [8] showed that the stress level required to generate the same growth rates in both the MSC and the PSC phases decrease with grain size, indicating that the more severe roughness of the crack path in the large grain size material does not reduce the crack growth rate. The opposing trend in the effect of grain size on crack growth threshold and crack growth in the LEFM regime and the short crack regime suggests that the use of the 'crack closure' concept can be misleading and non-conservative, although cracks may close during the fatigue process. For instance the recent experimental results reported by James and Sharpe [9] suggest that short crack growth rate cannot be unified on the basis of their measured crack opening stress level.

3. The MSC propagating in a shear mode (e.g. in torsion test) or in mixed Mode I and Mode II (e.g. in tensile test), is dominantly controlled by the shear strain or shear stress. Shear cracks or stage I cracks in torsion have been found in the present work to be smooth and no rubbing or closure has been observed between crack faces in torsion tests. It is postulated that if a low compressive mean stress is superimposed to close the crack, shear crack growth will not be significantly affected since only a very low friction stress may be produced between the smooth crack faces. Some recent work on the fatigue crack growth under rolling contact, e.g. in reference [10], shows that Mode II cracks can grow under compressive rolling contact stress although such a stress apparently contrives to close the crack rather than open it. Thus the effective stress range based on the experimentally measured crack closure stress level may lead to non-conservative predictions to crack growth rate, since in this case the contribution of Mode II growth is totally ignored.

From the above comments the crack closure stress level has been known to be dependent on many factors (see the discussion in Chapter 5), for instance, alternating stress level, mean stress level, environment, crack length, stress-strain state, grain size, crack growth mode, etc. The measurement is also strongly affected by the technique being used, the position where the crack tip opening displacement is monitored and so on. In particular, it is more difficult to measure the closure stress level of short

cracks (see Section 5.4).

In summary, crack closure is not the only mechanism that plays an important role in the effect of stress ratio, especially in the short crack regime, and it is almost impossible to quantify crack closure in simple terms. Therefore the readily available field parameters such as stress level and mean stress rather than the microscopic parameter (e.g. crack closure stress level), are more important to engineers and it is in this context that continuum models should be developed.

7.7 Fatigue Life Prediction

Fatigue failure is considered as the result of fatigue crack propagation, as verified by the torsional and uniaxial fatigue tests on smooth specimens. Although crack coalescences were also observed at later stages of fatigue life, they did not significantly affect the fatigue lifetime in the mid-range and high cycle fatigue regime.

Therefore the fatigue lifetime can be considered to be consist of three periods: plasticity localization period (N_0), the MSC growth period (N_{MSC}) and the PSC growth period (N_{PSC}).

$$N_f = N_0 + N_{MSC} + N_{PSC} \quad (7.27)$$

where N_{MSC} and N_{PSC} can be obtained by integrating the crack growth equations.

The first two periods (plasticity localization and MSC growth phases) are strongly affected by physical aspects such as microstructural details and the stress system, therefore the following two cases should be treated differently:

1. Under torsional loading, since the inclusions were aligned to the maximum shear direction, dominant cracks would initiate immediately hence the plasticity localization period can be neglected. Even more, to be conservative, the initial crack (MSC) length should be taken to be the largest size of the inclusions.
2. In the case of uniaxial loading, since the inclusions were aligned to the applied tensile loading, they do not introduce considerable stress concentration. The

effects of these inclusions on both the plasticity localization period and the MSC growth phase can be neglected.

However, if the loading axis is perpendicular to the orientation of inclusions, both the MSC growth phase and PSC growth phase may be effected, since the length of the largest inclusions is greater than the dominant microstructural barrier distance ($d_2 = 50 \mu m$). Thus the initial crack length should be taken to be the size of the largest inclusions, therefore the fatigue lifetime and the endurance limit will be significantly reduced. This is confirmed by the experimental results reported in [11].

Now the different fatigue $S - N$ curves at various mean stresses can be obtained by integrating crack growth equations as shown in Section 6.6 and Section 6.7, thus the $R - M$ diagrams can be better appreciated through quantifying the crack growth behaviour under various combinations of alternating and mean stresses.

7.8 Future Work

The present work concentrated on the behaviour of naturally initiated short cracks in smooth specimens under various mean stresses. More work is required to generalize the models put forward in the present work. Several interesting points are therefore raised:

Surface finish is known to influence the fatigue limit: a lower surface finish grade will result in a lower fatigue limit (see reference [11]). This is an very important aspect of the application of fatigue studies to engineering problems since many engineering components do not have a high standard of surface finish. However, the associated crack growth behaviour is still unknown, especially in terms of growth rate. If the present model is extrapolated to low stress levels, the predicted crack growth rate would be too low to be realistic. In other words, another set of equations is needed to bridge the gap between the short crack regime and the LEFM regime. This would be of value to understanding the growth behaviour of cracks started from

surface scratches under a stress level below the fatigue limit of smooth specimens but above the stress level for which the LEFM approach is valid.

Mean compressive stress is found not to be beneficial to short crack growth and the fatigue strength of smooth specimens for the present material. Since the reason for this phenomenon is that the mean shear stress, introduced by the uniaxial compressive mean stress, may cancel the beneficial effect of the normal compressive mean stress. However, if the compressive mean stresses are equal-biaxial or triaxial, then no mean shear stress will be introduced, the compressive mean stress would be beneficial. Therefore it is very important to distinguish between uniaxial compressive mean stress and equal-biaxial or triaxial compressive mean stresses. This is closely related to the conventional surface hardening technique. More work is required to ascertain this speculation.

A new model has been put forward based on current multi-axial fatigue theories and it has been shown that the new model can satisfactorily correlate the effect of mean shear stress, mean tensile stress and mean compressive stress on the MSC growth and high cycle fatigue lifetime. One interesting aspect of this model is that it also provides good predictions of the PSC growth behaviour (in terms of G_{max}) under mean stress uniaxial loading, this is illustrated by the similarity between $F(\sigma_m)$ and $f_3(\sigma_m)$ (see Section 6.7.2). However further study in which multi-axial fatigue tests under mean stress are involved is needed to ascertain this conclusion.

References

1. Kilman, V. and Bily, M. (1980) Influence of Mode Control, Mean Value and Frequency of Loading on the Cyclic Stress Strain Curve, *Material Science and Engineering, Vol.44*, pp.73-79.
2. Lorenzo, F. and Laird, C. (1984) A New Approach to Predicting Fatigue Life Behaviour under the Action of Mean Stress, *Material Science and Engineering, Vol.62*, pp.205-210.
3. Koh, S. K. and Stephens, R. I. (1989) Mean Stress Effects on Low Cycle Fatigue for a High Strength Steel, to be published in *Fatigue & Fracture of Engineering Materials and Structures*.
4. Tomkins, B. (1968) Fatigue Crack Propagation—An Analysis, *Philosophical Magazine, Vol.18*, pp.1041.
5. Dang Van, K., Cailletaud, G., Flavenot, J. F., Douaron, A. Le., and Lieurade, H. -P. (1989) Criterion for High Cycle Failure under Multiaxial Loading, *Biaxial and Multiaxial fatigue, EGF3* (Edited by M. W. Brown and K. J. Miller), Mechanical Engineering Publications, London, pp.459-478.
6. Jacquelin, B., Hourlier, F., and Pineau., A. (1985) Crack Initiation under Low-Cycle Multiaxial Fatigue, *Multiaxial Fatigue, ASTM STP 853*, K.J. Miller and M.W. Brown Eds., American Society for Testing and Materials, Philadelphia, pp.285-313.
7. McDiarmid, D. L. (1989) The Effect of Mean Stress on Biaxial Fatigue where the Stress Are Out-of-Phase and at different frequencies, *Biaxial and Multiaxial Fatigue, EGF3*(Edited by M. W. Brown and K. J. Miller), Mechanical Engineering Publications, London, pp.605-610.
8. Slade, J. E. (1990) The Effect of Grain Size on the Propagation of Short Fatigue Cracks, *Ph.D Thesis*, University of Sheffield.
9. James, M. N. and Sharpe, W. N. JR (1989) Closure Development and Crack Opening Displacement in the Short Crack Regime for Fine and Coarse Grained A533B Steel, *Fatigue and Fracture of Engineering Materials and Structures, Vol.12, No.4*, pp.347-361.
10. Bower, A. F. (1987) Some Aspects of Plastic Flow, Residual Stress and Fatigue Cracks due to Rolling and Sliding Contact, *Ph.D Thesis*, Cambridge University.

11. Suhr, R. W. (1986) The Effect of Surface Finish on High Cycle Fatigue of a Low Alloy Steel, *The Behaviour of Short Fatigue Cracks*, EGF Publication No.1 (edited by K. J. Miller and E. R. de los Rios) pp.69-86.

Table 7.1:
Comparison between the Predicted C_{max} and Actual C_{max}
(Uniaxial Tests)

Specimen No.	Stress Amplitude (MPa)	Mean Stress (MPa)	Predicted C_{max} ($\times 10^5$)	Actual C_{max} ($\times 10^5$)	Predicted/Actual Ratio
A55	464	-120	1.80	2.36	0.763
A56	490	-120	6.68	8.73	0.765
A59	500	-120	9.82	9.83	1.0
A50	500	-200	10.6	18.4	0.576
A52	460	0	1.78	0.82	2.17
A53	456	0	1.51	0.95	1.59
A31	500	0	8.74	8.66	1.01
A32	500	0	8.74	14.1	0.62
A33	500	0	8.74	5.01	1.75
A42	550	0	53.8	88.9	0.61
A41	600	0	283	447	0.633
A44	600	0	283	1710	0.166
A51	460	100	8.74	6.00	1.46
A40	405	228	4.76	14.5	0.33
A34	378	400	13.1	12.1	1.08
A35	369	407	8.10	7.53	1.08
A36	360	400	4.70	6.30	0.75
A37	355	400	3.65	5.45	0.67
A57	315	471	0.85	1.92	0.44
A58	310	504	3.48	4.96	0.70
A60	295	504	0.701	0.79	0.89

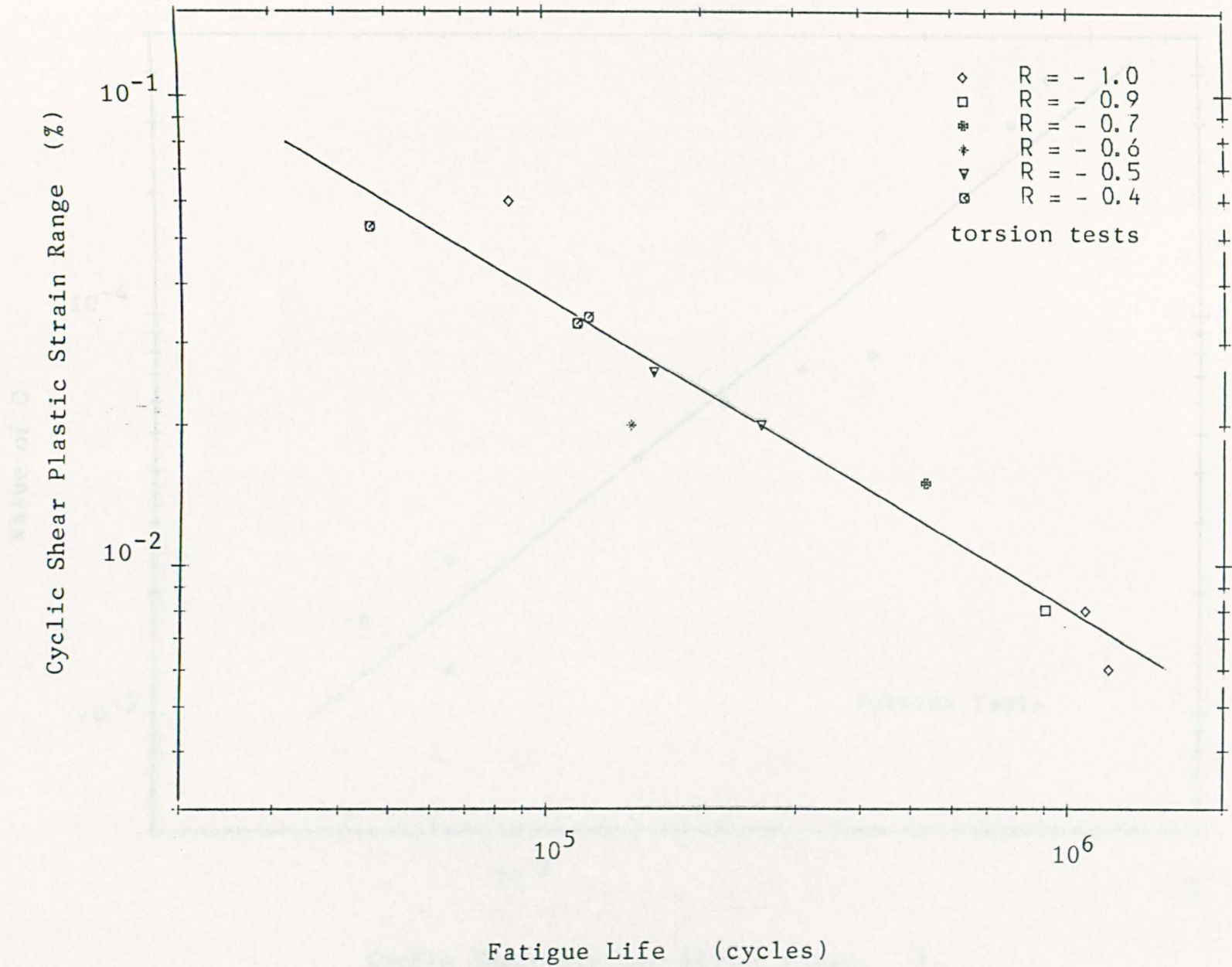


Fig.7.1 Torsional Fatigue Life versus Cyclic Plastic Strain

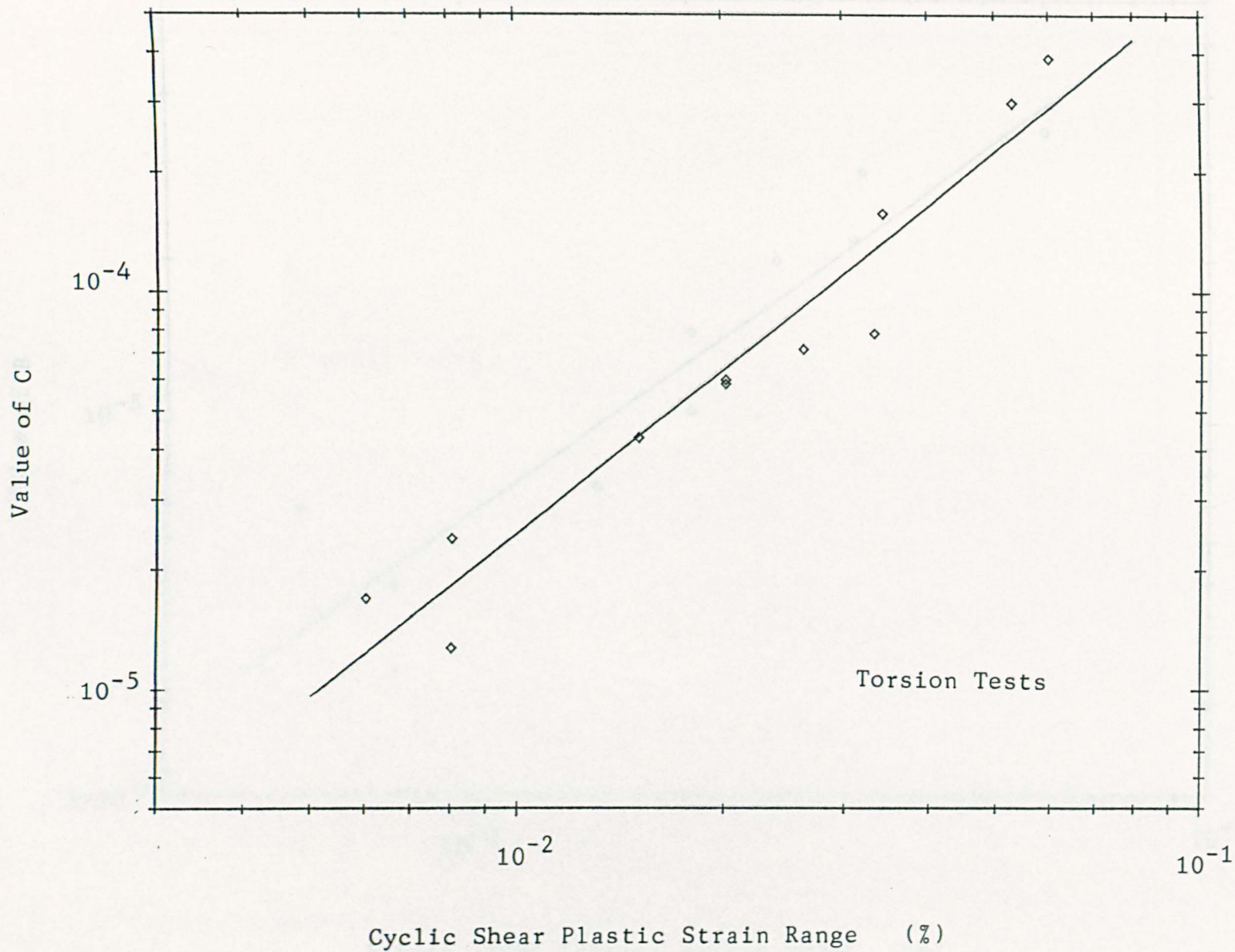


Fig.7.2a Values of C versus Cyclic Plastic Strain

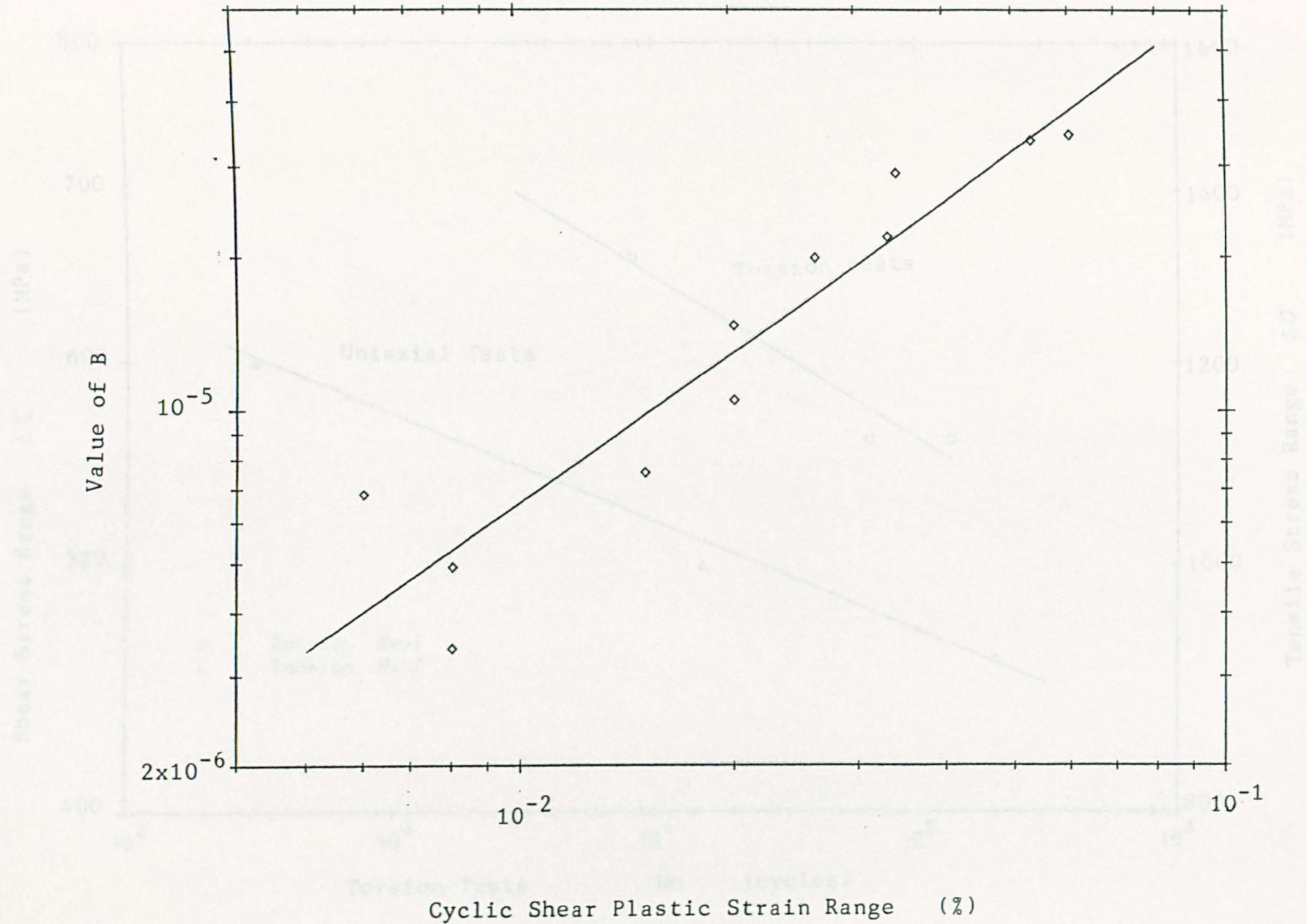


Fig.7.2b Values of B versus Cyclic Plastic Strain

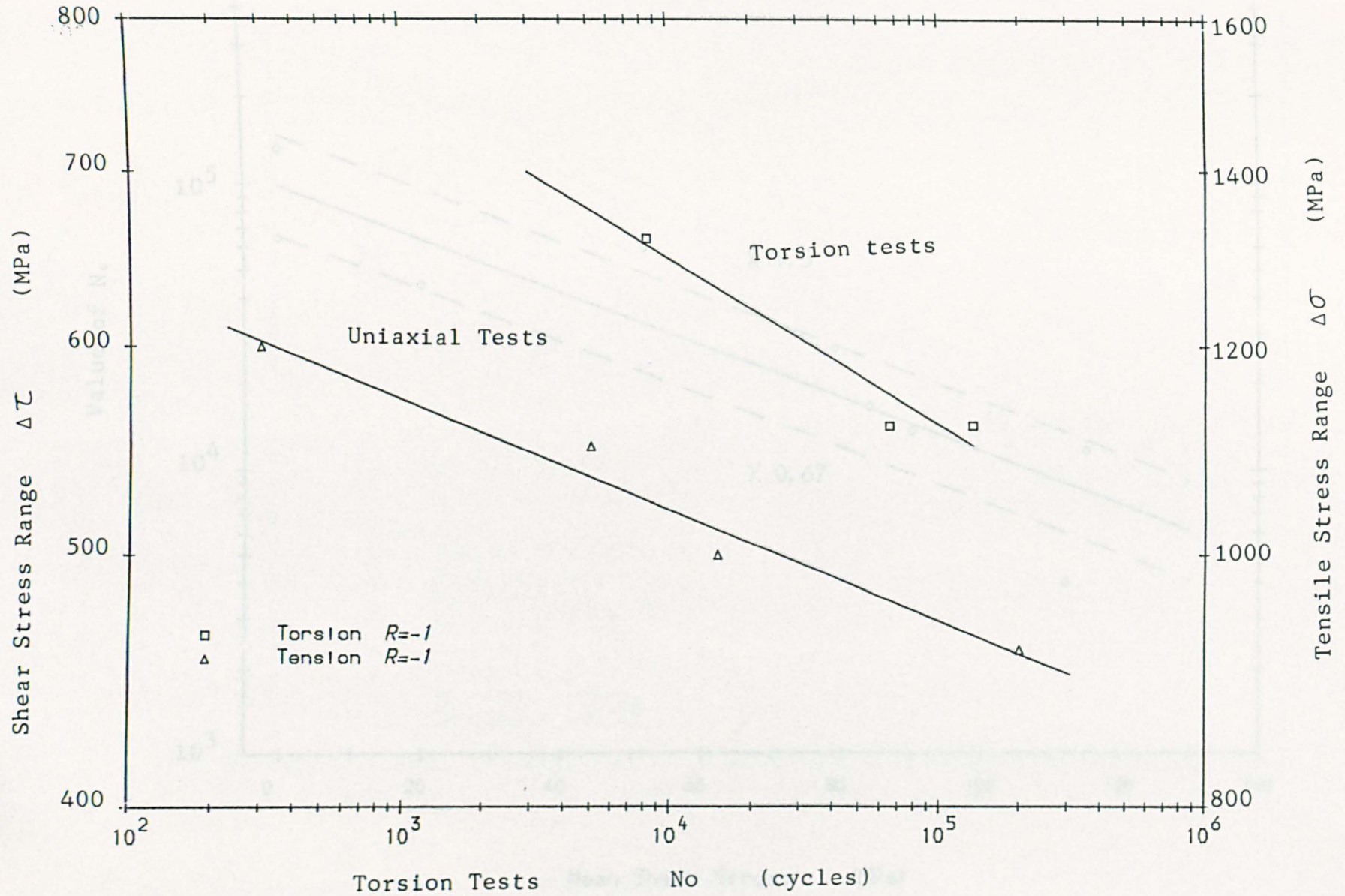


Fig.7.3 Stress Range versus N_o (number of cycles to crack initiation)

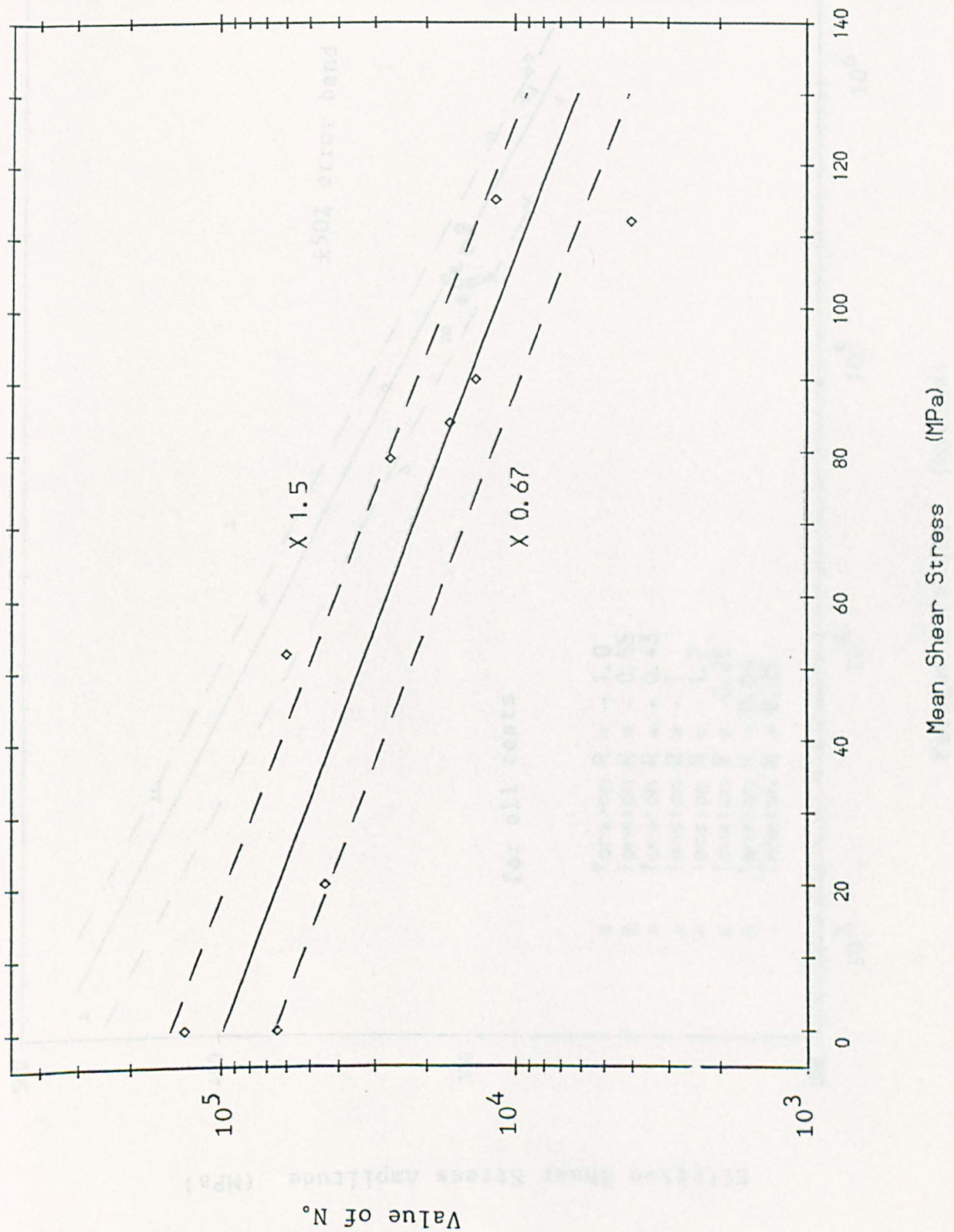


Fig.7.4 No versus Mean Shear Stress (constant alternating stress)

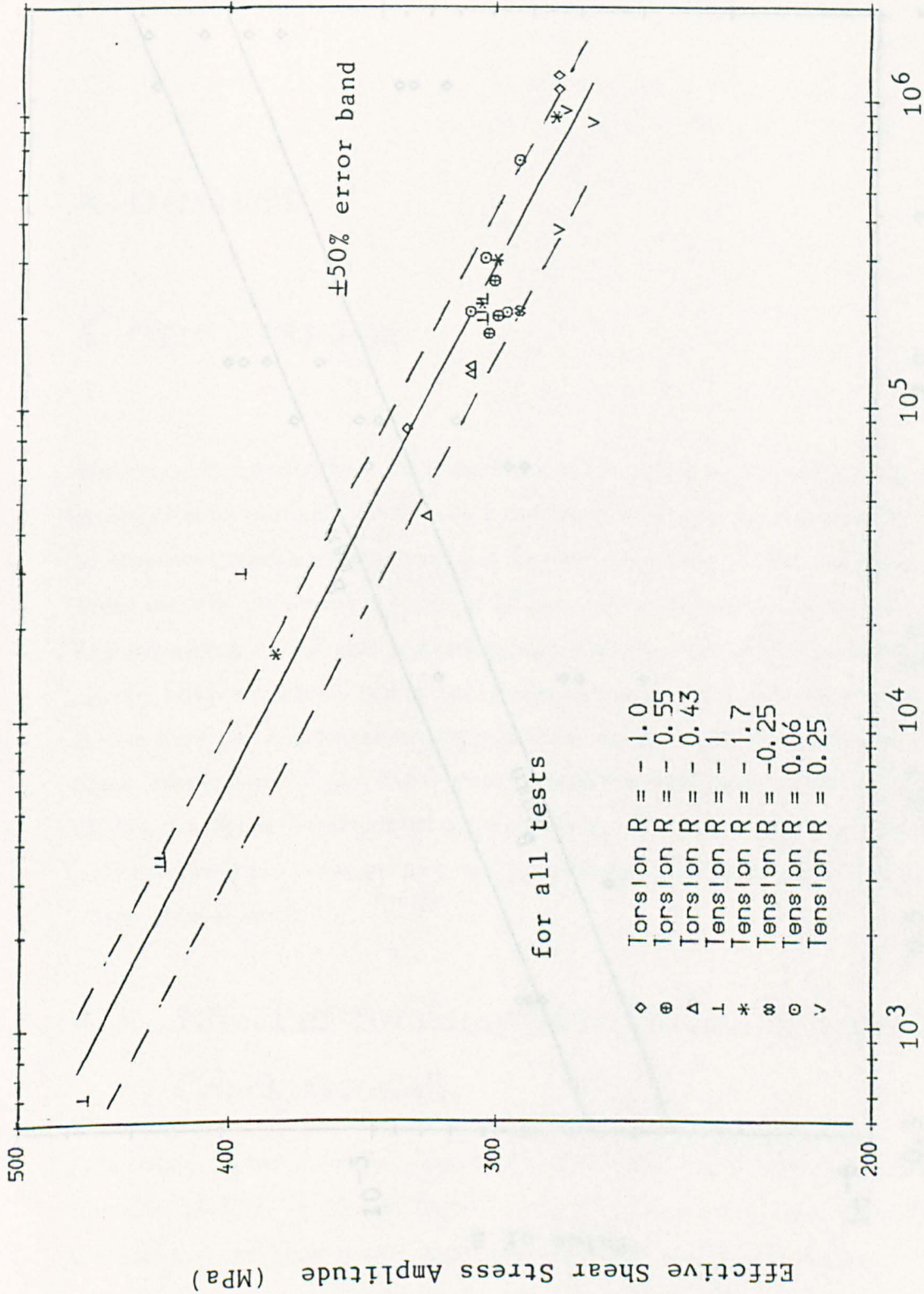


Fig.7.5 Correlation of Fatigue Life against Effective Shear Stress

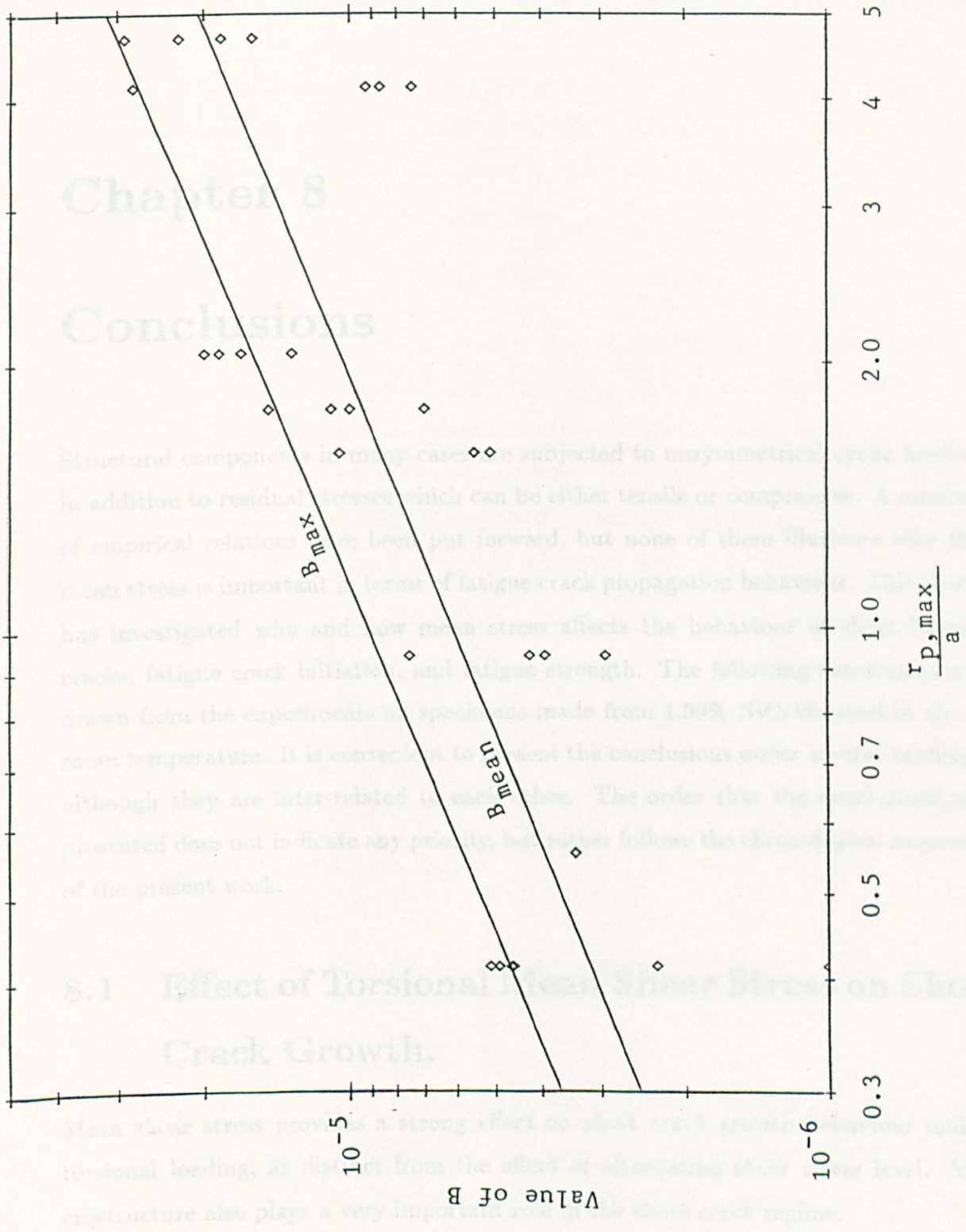


Fig.7.6 Value of B versus $r_{p,max}/a$

Chapter 8

Conclusions

Structural components in many cases are subjected to unsymmetrical cyclic loading in addition to residual stresses which can be either tensile or compressive. A number of empirical relations have been put forward, but none of them illustrate why the mean stress is important in terms of fatigue crack propagation behaviour. This thesis has investigated why and how mean stress affects the behaviour of short fatigue cracks, fatigue crack initiation, and fatigue strength. The following conclusions are drawn from the experiments on specimens made from 1.99% NiCrMo steel in air at room temperature. It is convenient to present the conclusions under several headings although they are inter-related to each other. The order that the conclusions are presented does not indicate any priority, but rather follows the chronological sequence of the present work.

8.1 Effect of Torsional Mean Shear Stress on Short Crack Growth.

Mean shear stress provides a strong effect on short crack growth behaviour under torsional loading, as distinct from the effect of alternating shear stress level. Microstructure also plays a very important role in the short crack regime.

1. Mean shear stress can considerably enhance the microstructurally short crack (MSC, Mode II) growth rate and this effect is independent of the polarity of the mean shear stress. Since no rubbing effect or crack closure was observed in the experiments, the mean shear stress plays a fundamental role in the short crack growth behaviour as witnessed by the equation:

$$\frac{da_s}{dN} = 3.68 \times 10^{-52} e^{\tau_m/62.6} \tau_a^{19.07} (d - a_s) \quad (\mu m/cycle) \quad (8.1)$$

where $d = 167 \mu m$.

2. MSC growth rate is a function of a characteristic dimension (d) of the microstructure as well as the crack length (a). This characteristic dimension is found to be dependent on stress state but not on the stress level: under torsional loading, the average value of d is $167 \mu m$ (about three times the average prior austenite grains size) which is independent of the mean shear stress level, whereas under uniaxial loading, the value of d is about $50 \mu m$.

3. Under torsional loading, mean shear stress is found to increase the Physically Small Crack (PSC) growth rate by inducing a mean tensile stress upon a re-oriented or branch crack and enhances its growth. Consequently the complementary branch crack growth is hindered. This is represented by the equation

$$\frac{da_s}{dN} = 1.09 \times 10^{-34} e^{\tau_m/66.5} \tau_a^{11.712} a_s - D \quad (\mu m/cycle) \quad (8.2)$$

where $D = 5.1 \times 10^{-4} \mu m/cycle$.

8.2 Effect of Mean Uniaxial Stress on Short Crack Growth.

1. Mean tensile stress increases the MSC growth rate under uniaxial loading. Mean compressive stress, however, does not have any bearing on MSC growth provided the minimum stress does not exceed the (cyclic) yield stress of the material in compression. The PSC growth rate under tensile mean stress is given by

$$\frac{da_s}{dN} = 3.894 \times 10^{-78} \left(e^{\sigma_m/1171} \sigma_a \right)^{27.2} (d - a_s); \quad \text{when } \sigma_m \geq 0 \quad (8.3)$$

where $d = 50 \mu m$. In the case compressive mean stress, the MSC growth rate is equal to that under zero mean stress loading.

2. Mean tensile stress can significantly increase the PSC growth rate in uniaxial fatigue, but a compressive mean stress has no effect. The PSC growth rate under tensile mean stress is represented by

$$\frac{da_s}{dN} = 2.346 \times 10^{-58} \left(e^{\sigma_m/1083} \sigma_a \right)^{19.33} a_s^{1.405} - D \quad (\mu m/cycle) \quad (8.4)$$

where $D = 2.76 \times 10^{-34} e^{\sigma_m/137} \sigma_a^{11.1} (\mu m/cycle)$. In the case compressive mean stress, the PSC growth rate is equal to that under fully reversed loading.

3. A new model has been put forward which can satisfactorily account for the effects of mean torsional shear stress, mean tensile stress and mean compressive stress on MSC growth behaviour through an effective shear stress amplitude as given by

$$\tau_a^* = \tau_a e^{|\tau_m|/1194} + 0.218 \times \sigma_{n,max} \quad (8.5)$$

where τ_a , τ_m and $\sigma_{n,max}$ are the macro shear stress amplitude, macro mean shear stress and the macro maximum normal stress across the MSC plane.

4. PSC growth rate under asymmetrical loading can also be accounted for by the model.
5. The experimentally achievable stress ratios under which fatigue crack growth data can be obtained from smooth specimens under uniaxial loading are within the range between -2 and 0.3 . Either no fatigue failure or ratcheting failure occurred for stress ratios outside of this range.
6. Mean tensile stress increases the crack growth rate and for high stress ratios ($R \geq 0$) short cracks do not close. Signs of crack closure at low stress ratios are found from SEM observations.

8.3 Effects of Mean Stress on Crack Initiation Processes.

1. The effect of mean shear stress on cyclic plastic deformation was investigated because it is the cyclic deformation and plasticity that provides the driving force for fatigue crack initiation and fatigue failure. The cyclic shear plastic strain range is found to increase with mean shear stress, e.g. for constant shear stress amplitude equal to 280 MPa, the cyclic shear plastic strain range is given by

$$\Delta\gamma_p = 6.72 \times 10^{-5} e^{\tau_m/71.1} \quad (8.6)$$

2. The crack growth rate under torsional loading can be predicted on the basis of the measured cyclic plastic strain amplitude under different mean shear stress, as can be the torsional fatigue lifetime, from the equations 7.2 and 7.3.
3. A plasticity localization period was found under stress-controlled conditions in which no crack initiation occurred. This was partially due to the cyclic softening characteristic of the material. Mean shear stress and mean tensile stress shorten the period of plasticity localization and the formation of PSBs. A mean compressive stress has no effect. For example, under tensile mean stress uniaxial loading, the number of cycles spent in the plastic localization phase is given by

$$N_0 = 2.97 \times 10^{66} e^{-\sigma_m/51.5} \sigma_a^{-23} \quad (8.7)$$

4. The major effect of microstructure is due to the misorientation between different grains or bundles rather than the absolute boundary strength, since cracks were found originating from grain boundaries, packet boundaries and base material.
5. Both mean shear stress and mean tensile stress increase the ability to overcome these microstructural barriers. Prior austenite grain boundaries represent barriers confining the short cracks to within one to three grains. Substructures, i.e. boundaries between packet bundles in the present alloyed steel, also provide obstacles to short crack growth at low stress levels.

6. Inclusions can cause anisotropy in crack growth behaviour under torsional loading, viz, cracks along one of the maximum shear planes tend to be initiated earlier than in the complimentary direction. Inclusions have no effect on the subsequent growth of MSCs and PSCs under torsional loading.
7. Under uniaxial loading, however, inclusions do not show any effect on crack initiation and growth with specimens removed from the longitudinal direction of the rotor.

8.4 Effects of Mean Stress on Fatigue Lifetime.

The effect of mean stresses on fatigue lifetime and the fatigue endurance limit can be better understood via quantification of short crack growth behaviour.

1. The fatigue lifetime can be accurately predicted by integrating the short crack growth equations derived in this thesis plus the plasticity localization period which equals zero in the case of torsion tests due to the favourable orientation of inclusions.
2. Fatigue strength under uniaxial loading decreases with the increase of mean tensile stress. The effect can not be adequately represented by a Goodman diagram or a Gerber relationship. A SWT parameter is found to provide a reasonably good prediction of the effect of mean tensile stress on fatigue endurance, but not for the case of compressive mean stress.
3. Mean tensile stress is additionally effective in reducing the fatigue endurance beyond the point where the maximum stress level exceeds the monotonic or cyclic yield stress.
4. Mean compressive stress has no beneficial effect on fatigue strength for the steel being studied. Both the SWT parameter and the Goodman relationship overestimate the beneficial effect of a compressive mean stress on the fatigue strength. The Gerber relationship illustrates such an effect but lacks physical significance.

5. The final failure of specimens under torsional loading is mainly due to cracks which bifurcate into Mode I propagating cracks.
6. High cycle fatigue failure under uniaxial loading occurred as a result of the propagation of a single crack to a very large size and the eventual merging with other cracks. Crack coalescence, if it exists, does not show a recognisable effect on the final fatigue life.
7. Low cycle fatigue failure under uniaxial loading occurs when two or more long cracks are linked. However due to the fact that this rapid event happened in later stages of fatigue life, the life can still be accurately predicted by integrating the single crack growth equations, assuming that failure is due to the propagation of a single crack. The error in the above mentioned fatigue life prediction is within the order of the scatter of the experimental results.
8. The combination of a high shear stress amplitude and a mean shear stress enables cracks to grow in the shear mode under uniaxial loading, since such a stress system can set up a predominant single slip system rather than a multi-slip system thereby facilitating Mode II crack growth.
9. A satisfactory correlation was achieved between the fatigue lifetime and the 'effective shear stress amplitude' (τ_a^*) proposed in the present work. The value of τ_a^* is given by Eq.8.5.

Appendix A

Torsion Test Data

No of Crack	Replica Stage (cycles)	Crack Length (μm)	δa_a (μm)	δN (cycles)	$\delta a/\delta N$ ($\times 10^3$) ($\frac{\mu\text{m}}{\text{cycle}}$)	$a_{s,mean}$ (μm)	C ($\times 10^5$) (cycle^{-1})	d (μm)
A1-1	0	50						
	3000	56	6	3000	2.0	53.0		
	16440	100	44	13440	3.27	78.0		
	42628	137	37	26188	1.41	118.5	1.76	207
	56066	140	3	13438	0.223	138.5		
	62618	140	0	6552	0.0	140.0		
	65410	140	0	2792	0.0	140.0		
A1-2	0	66						
	2000	76	10	2000	5.0	71.0		
	16440	110	34	14440	2.35	93.0	5.01	146
	26617	130	20	10177	1.97	120.0		
A1-3	0	2						
	36617	2						
	62618	77	75	26001	2.88	39.5		
	85296	99	22	22678	0.97	88	2.06	170
	92830	113	14	7534	1.85	106		
A1-4	0	2						
	26440	2						
	42628	77	75	16188	4.63	39.5	3.06	194
	62618	135	58	19990	2.90	106.0		
	85296	163	28	22678	1.23	149.0		
A2-1	0	2						
	4034	2						
	7070	202	200	3036	65.9	102.0	29.9	335
	9140	289	87	2070	42.0	245.5		
	11566	293	4	2426	1.65	291.0		
A2-2	0	60						
	4034	130	70	4034	17.4	95.0		
	7070	165	35	3036	11.5	147.5	21.8	180
	9140	165	0	2070	0.0	165.0		

No of Crack	Replica Stage (cycles)	Crack Length (μm)	δa_a (μm)	δN (cycles)	$\delta a/\delta N$ ($\times 10^3$) ($\mu\text{m}/\text{cycle}$)	$a_{s,mean}$ (μm)	C ($\times 10^5$) (cycle^{-1})	d (μm)		
A2-3	0	2								
	4634	2								
	9140	100	98	4506	21.7	51.0	18.4	160		
	11566	112	12	2426	4.95	106.0				
	14230	136	24	2664	9.01	124.0				
	21359	160	24	7129	3.37	148.0				
23460	160	0	2101	0.0	160.0					
A2-4	0	2								
	9140	2								
	11566	2								
	16985	103	101	5419	18.6	52.5	21.1	139		
	21359	120	17	4374	3.89	111.5				
	23460	131	11	2101	5.24	125.5				
29140	135	4	5680	0.70	133.0					
A2-5	0	2								
	9140	2								
	14230	2								
	16985	85	83	2755	30.1	43.5	15.77	222		
	21359	140	55	4374	12.6	112.5				
	23460	164	24	2101	11.4	152.0				
	25583	189	25	2123	11.8	176.5				
	29140	198	9	3557	2.53	193.5				
A3-1	0	2								
	60050	2								
	79008	101	99	18958	5.22	51.5			3.50	211
	91306	153	52	12298	4.23	127.0				
	101695	163	10	10389	0.963	158.0				
A3-2	0	2								
	60050	2								
	79008	2								
	91306	45	43	12298	3.55	23.5	4.27	105		
	101695	65	20	10389	1.93	55.0				
	123759	87	22	22064	0.997	76.0				
	150322	100	13	26563	0.489	93.5				
	179593	100	0	29271	0.0	100.0				
201021	105	5	21428	0.233	102.5					
A3-3	0	50								
	11801	88	38	11801	3.22	69.0			2.20	217
	44262	157	69	32461	2.13	122.5				
	91306	197	40	47044	0.850	177.0				
	101695	201	4	10389	0.385	199.0				
A3-4	0	2								
	60050	2								
	79008	68	66	18958	3.48	35.0	1.88	251		
	91306	103	35	12298	2.85	85.5				
	101695	145	42	10389	4.04	124.0				
	123759	188	43	22064	1.95	166.5				
	150322	188	0	26563	0.00	188.0				

No of Crack	Replica Stage (cycles)	Crack Length (μm)	δa_a (μm)	δN (cycles)	$\delta a/\delta N$ ($\times 10^3$) ($\mu m/cycle$)	$a_{s,mean}$ (μm)	C ($\times 10^5$) ($cycle^{-1}$)	d (μm)
A4-1	0	40						
	3841	40						
	10029	58	18	6188	2.91	49.0	5.29	111
	26516	101	43	16487	26.1	79.5		
	43238	101	0	16722	0.0	101.0		
A4-2	0	2						
	36155	2						
	43238	28	26	7083	3.67	15.0		
	61861	40	12	18623	0.644	34.0		
	90815	64	24	28954	0.829	52.0	3.61	85
	114838	64	0	24023	0.0	64.0		
	123466	74	10	8628	1.16	69.0		
148532	92	18	25066	0.718	83.0			
A4-3	0	2						
	16516	2						
	26155	39	37	9639	3.84	20.5		
	43238	46	7	17083	0.410	42.5		
	54848	63	17	11610	1.46	54.5	5.85	73
	70773	66	3	15925	0.188	64.5		
	79813	66	0	9040	0.0	66.0		
98875	82	16	19062	0.839	74.0			
A4-4	0	31						
	10029	83	52	10029	5.18	57.0	3.11	223
	36155	164	81	26126	3.10	123.5		
A5-1	0	50						
	8042	88	38	8042	4.73	69.0		
	23504	116	28	12546	1.81	102.0	7.17	131
	28156	122	6	4652	1.29	119.0		
	34457	126	4	6301	0.635	124.0		
A5-2	0	2						
	13504	2						
	30240	20	18	16736	1.08	11.0		
	37546	70	50	7306	6.84	45.0	2.15	290
	50412	88	18	12866	1.40	79.0		
59700	138	50	9288	5.48	113.0			
A5-3	0	2						
	30240	2						
	41094	38	36	10854	3.32	20.0		
	65025	38	0	23931	0.0	38.0		
	70117	51	13	5092	2.55	44.5	0.79	303
	86212	64	13	16095	0.808	57.5		
	97002	117	53	10790	4.91	90.5		
	107450	120	3	10448	0.287	118.5		
	117655	130	10	10205	0.980	125.0		

No of Crack	Replica Stage (cycles)	Crack Length (μm)	δa_a (μm)	δN (cycles)	$\delta a/\delta N$ ($\times 10^3$) ($\mu m/cycle$)	$a_{s,mean}$ (μm)	C ($\times 10^5$) ($cycle^{-1}$)	d (μm)
A5-4	0	2						
	13504	2						
	28156	2						
	37546	65	63	9390	6.71	33.5	5.22	151
	50412	95	30	12866	2.23	80.0		
	65025	132	37	14613	2.53	113.5		
	70117	137	5	5092	0.982	134.5		
A5-5	0	2						
	13504	2						
	28156	10	8	14652	0.546	6.0		
	30240	49	39	2084	18.7	29.5		
	37546	98	49	7306	6.71	73.5		
	41094	133	35	3548	9.86	115.5	2.84	346
	50412	180	47	9318	5.04	156.5		
	65025	207	27	14613	1.85	193.5		
	70117	217	10	5092	1.196	212.0		
	86212	220	3	16095	0.186	218.5		
A5-6	0	2						
	28504	2						
	31000	2						
	41094	10	8	10094	0.793	6.0		
	50412	62	52	9318	5.58	36.0		
	59700	84	22	9288	2.37	73.0	6.55	117
	65025	90	6	5325	1.13	87.0		
	70117	105	15	5092	2.295	97.5		
	86212	112	7	16095	0.435	108.5		
	91140	112	0	4928	0.0	112.0		
A6-1	0	2						
	11030	2						
	14123	10	8	3093	2.59	6.0	7.86	85
	21267	44	34	7144	4.76	27.0		
	30644	63	19	9377	2.03	53.5		
	43238	80	17	12594	1.35	71.5		
A6-2	0	2						
	21267	2						
	30644	10	8	9377	0.853	6.0		
	43238	80	70	12594	5.56	45.0	3.93	198
	57177	146	66	13939	4.73	113.0		
	62890	152	6	5713	1.05	149.0		
A6-3	0	2						
	3980	2						
	11030	2						
	14123	6	4	3093	1.29	4.0		
	21267	45	39	7144	5.46	25.5		
	30644	65	20	9377	2.13	55.0	—	—
	35607	82	17	4963	3.43	73.5		
	43238	109	27	7631	3.54	95.5		
	47568	128	19	4330	4.39	118.5		
57177	165	37	9609	3.85	146.5			

No of Crack	Replica Stage (cycles)	Crack Length (μm)	δa_a (μm)	δN (cycles)	$\delta a/\delta N$ ($\times 10^3$) ($\mu\text{m}/\text{cycle}$)	$a_{s,mean}$ (μm)	C ($\times 10^5$) (cycle^{-1})	d (μm)
A6-4	0	2						
	3980	2						
	11030	37	35	7050	4.96	19.5		
	14123	93	56	3093	1.81	65.0	7.34	154
	21267	99	6	7144	0.840	96.0		
30644	105	6	9377	0.640	102.0			
A6-5	0	2						
	14123	2						
	21267	44	42	7144	5.88	23.0	2.71	119
	30644	44	0	9377	0.0	44.0		
43238	68	24	12594	1.19	56.0			
A7-1	0	41	0					
	3000	41	0	3000				
	7591	100	59	4591	12.9	70.5	12.85	171
	10607	123	23	3016	7.63	111.5		
A7-2	0	2						
	26492	2	0	26492				
	30511	30	28	4019	6.93	16.0		
	34880	35	5	4369	1.14	32.5	7.98	88
	39404	61	26	4524	5.75	48.0		
49234	72	11	9830	1.12	66.5			
A7-3	0	2						
	30511	2	0	30511				
	34880	62	60	4369	13.7	32.0		
	39404	100	38	4524	8.40	81.0	14.82	129
	49234	124	24	9830	2.44	112.0		
56140	124	0	6906	0.0	124.0			
A7-4	0	2						
	11627	2	0	11627				
	15859	25	23	4232	5.43	13.5	15.73	48
26492	46	21	10633	1.97	35.5			
A8-1	0	2						
	4000	2	0	4000				
	20000	2	0	16000				
	146740	2	0	126740				
	227652	57	55	80912	0.680	29.5		
	274160	101	44	46508	0.946	79.0	0.474	218
	338384	145	44	64224	0.685	123.0		
408558	147	2	70174	0.0285	146.0			
A8-2	0	2						
	116760	106	104	116760	0.891	54.0		
	146740	106	0	29980	0.0	106.0	1.212	124
227652	128	22	80912	0.272	117.0			

No of Crack	Replica Stage (cycles)	Crack Length (μm)	δa_a (μm)	δN (cycles)	$\delta a/\delta N$ ($\times 10^3$) ($\mu m/cycle$)	$a_{s,mean}$ (μm)	C ($\times 10^5$) ($cycle^{-1}$)	d (μm)
A8-3	0	36						
	4000	36	0	4000				
	14725	63	27	10725	2.52	49.5		
	70334	97	34	55609	0.611	80.0	1.685	164
	116760	135	38	46426	0.819	116.0		
	174397	158	23	57637	0.399	146.5		
	227652	167	9	53255	0.169	162.5		
A9-1	0	2						
	44311	2	0	44311				
	89798	63	61	45487	1.34	32.5		
	129693	87	24	39895	0.602	75.0	1.72	110
	146760	93	6	17067	0.352	90.0		
A9-2	0	2						
	44311	2						
	89798	120	118	45487	2.59	61.0	2.39	167
	129693	145	25	39895	0.627	132.5		
	146760	155	10	17067	0.586	150.0		
A10-1	0	2						
	5000	2	0	5000				
	64571	2	0	59571				
	122283	65	63	57712	1.09	33.5	1.27	120
	189710	100	35	67427	0.519	82.5		
228466	107	7	38756	0.181	103.5			
A10-2	0	2						
	5000	2	0	5000				
	64571	2	0	59571				
	189710	36	34	125139	0.272	19.0		
	228466	59	23	38756	0.593	47.5	0.34	170
	281970	90	31	53504	0.579	74.5		
340463	106	16	58493	0.274	98.0			
A11-1	0	2		0				
	8132	2	0	8132				
	9785	70	68	1653	41.1	36.0		
	11371	106	36	1586	22.7	88.0	38.66	143
12776	121	15	1405	10.7	113.5			
A11-2	0	2		0				
	8132	2	0	8132				
	12776	96	94	4644	20.2	49.0		
	14195	112	16	1419	11.3	104.0		
	20137	136	24	5942	4.04	124.0	18.52	158
	30073	160	24	9936	2.42	148.0		
38845	160	0	8772	0.0	160.0			
A11-3	0	54						
	8132	110	56	8132	6.89	82.0		
	11371	136	26	3239	8.03	123.0	5.28	234
	14195	151	15	2824	5.31	143.5		
20137	165	14	5942	2.36	158.0			

Appendix B

Uniaxial Test Data

Specimen Number: A31

Test Conditions: $\sigma_a = 510$ MPa, $\sigma_m = 0$ MPa, $R = -1$
(uniaxial, high frequency)

loading cycles	surface crack lengths (μm)				
	Crack 1	Crack 2	Crack 3	Crack 4	Crack 5
0	2	2	2	2	2
5000	2	2	2	2	2
15000	2	2	6	2	2
25000	2	14	30	2	2
35000	30	14	30	2	2
45000	45	16	30	2	2
55000	45	16	30	2	2
65000	45	34	30	2	2
75000	45	34	30	2	31
85000	45	34	30	31	31
95000	74	66	30	31	31
105000	92	66	79	31	31
120000	124	91	79	63	33
135000	176	142	126	87	48
145000	220	176	158	114	64
156000	300	222	186	181	116
167000	444	290	274	307	149
178000	809	420	350	503	218
189000	1700	750	509	1500	232

Specimen Number: A32

Test Conditions: $\sigma_a = 520$ MPa, $\sigma_m = 0$ MPa, $R = -1$
 (uniaxial, high frequency)

loading cycles	surface crack lengths (μm)		
	Crack 1	Crack 2	Crack 3
0	2	2	2
10000	2	2	2
20000	2	2	2
30000	2	2	2
46000	44	2	2
51000	44	27	2
60000	44	27	2
68000	60	27	2
76000	60	27	2
84000	80	50	2
92000	80	50	2
106000	108	73	35
122000	180	73	78
130000	180	76	119
138000	220	85	162
146000	275	85	195
154000	322	119	245
162000	426	154	245
170000	558	213	315
178000	850	287	452
185000	1500	342	570
192000	1900	490	830
199000	3700	620	1340

Specimen Number: A33

Test Conditions: $\sigma_a = 490$ MPa, $\sigma_m = 0$ MPa, $R = -1$
 (uniaxial, high frequency)

loading cycles	surface crack lengths (μm)		
	Crack 1	Crack 2	Crack 3
0	2	2	2
12400	2	2	2
25000	2	2	2
50000	15	2	39
75000	60	15	46
100000	97	71	65
125000	186	71	136
150000	273	95	151
175000	522	138	182
200000	1200	152	185
212500	2100	175	190
225000	3500	250	193

Specimen Number: A34

Test Conditions: $\sigma_a = 378$ MPa, $\sigma_m = 400$ MPa, $R = 0.03$
 (uniaxial, high frequency)

loading cycles	surface crack lengths (μm)			
	Crack 1	Crack 2	Crack 3	Crack 4
0	2	2	2	2
15000	2	2	2	2
40000	2	2	2	2
48000	2	2	2	2
56000	2	2	35	19
64000	20	2	35	27
72000	20	15	42	75
80000	20	15	46	75
88000	26	15	77	75
104000	35	32	77	92
112000	61	36	90	92
120000	79	41	90	92
128000	115	57	108	92
136000	115	62	120	105
144000	145	95	162	137
152000	178	101	197	151
160000	234	125	197	185
168000	278	145	234	221
176000	428	156	253	246
184000	625	178	290	298
192000	1221	250	383	400
200000	2600	500	550	600

Specimen Number: A35

Test Conditions: $\sigma_a = 369$ MPa, $\sigma_m = 407$ MPa, $R = 0.05$
 (uniaxial, high frequency)

loading cycles	surface crack lengths (μm)		
	Crack 1	Crack 2	Crack 3
0	2	2	2
100000	2	2	2
140000	2	2	2
164000	2	2	2
170000	2	2	2
178000	24	2	2
198000	75	23	30
210000	75	36	30
220000	136	51	42
240000	232	75	42
260000	351	200	65
280000	750	276	160
300000	3800	1800	249

Specimen Number: A36

Test Conditions: $\sigma_a = 358$ MPa, $\sigma_m = 400$ MPa, $R = 0.05$
(uniaxial, high frequency)

loading cycles	surface crack lengths (μm)	
	Crack 1	Crack 2
0	2	2
10000	25	2
20000	31	22
30000	31	22
40000	42	22
50000	53	25
60000	56	36
70000	58	53
80000	70	58
90000	70	58
100000	86	58
110000	125	71
120000	125	98
130000	140	98
140000	171	106
150000	196	122
160000	331	151
170000	353	157
180000	518	166
195000	1400	240

Specimen Number: A42

Test Conditions: $\sigma_a = 550$ MPa, $\sigma_m = 0$ MPa, $R = -1$
(uniaxial, low frequency)

loading cycles	surface crack lengths μm					
	Crack 1	Crack 2	Crack 3	Crack 4	Crack 5	Crack 6
0	2	2	2	2	2	2
5000	2	2	2	2	2	2
12000	55	72	61	2	64	29
13500	88	73	78	24	105	32
15000	105	80	80	29	134	51
17000	126	108	130	52	191	70
19000	133	108	160	76	258	94
20000	207	271	199	87	349	131
23000	284	318	313	101	388	155
24500	383	364	347	186	469	195
25800	505	505	474	315	616	358
27000	727	649	529	341	715	572

Specimen Number: A37

Test Conditions: $\sigma_a = 355$ MPa, $\sigma_m = 401$ MPa, $R = 0.06$
(uniaxial, high frequency)

loading cycles	surface crack lengths (μm)	
	Crack 1	Crack 2
0	2	2
10000	8	2
80000	8	2
160000	8	2
240000	8	2
280000	8	2
290000	26	2
300000	26	16
313000	26	16
327000	26	16
340000	26	16
355000	32	16
382000	32	18
395000	32	34
408000	32	34
421000	38	45
434000	38	57
447000	44	57
460000	46	67
473000	67	71
486000	83	78
500000	83	81
513000	119	87
526000	119	87
539000	120	87
552000	157	87
565000	179	111
578000	250	112
591000	450	136
604000	730	168
617000	1300	218
630000	6800	400

Specimen Number: A41

Test Conditions: $\sigma_a = 600$ MPa, $\sigma_m = 0$ MPa, $R = -1$
(uniaxial, low frequency)

loading cycles	surface crack lengths (μm)			
	Crack 1	Crack 2	Crack 3	Crack 4
0	2	2	2	2
300	2	2	2	2
800	2	2	16	29
1400	57	104	33	54
2000	116	155	94	68
2500	218	324	192	109
3000	668	712	391	370
3200	1350	764	736	800

Specimen Number: A40

Test Conditions: $\sigma_a = 405$ MPa, $\sigma_m = 228$ MPa, $R = -0.28$
(uniaxial, high frequency)

loading cycles	surface crack lengths μm					
	Crack 1	Crack 2	Crack 3	Crack 4	Crack 5	Crack 6
0	2	2	2	2	2	2
20000	2	2	2	2	2	2
40000	2	2	2	2	2	2
60000	2	2	2	2	2	2
80000	2	2	2	2	2	2
100000	2	2	2	2	2	2
110000	20	10	2	2	2	2
130000	21	33	30	2	2	2
140000	49	33	30	39	2	2
150000	65	33	30	39	36	0
160000	88	40	30	41	36	0
170000	102	40	47	41	56	42
186000	140	40	54	41	56	42
200000	160	50	62	83	56	42
211000	258	80	74	118	85	74
226000	394	95	110	155	111	78
240000	710	160	135	208	124	81
250000	1300	183	168	251	194	159
260000	2300	198	190	350	266	181

Specimen Number: A38

Test Conditions: $\sigma_a = 405$ MPa, $\sigma_m = 232$ MPa, $R = -0.27$
(uniaxial, high frequency)

loading cycles	surface crack lengths (μm)		
	Crack 1	Crack 2	Crack 3
0	2	2	2
5000	2	2	2
10000	40	2	2
15000	57	30	5
20000	57	35	30
25000	94	41	39
30000	98	54	59
35000	100	68	59
40000	103	90	59
45000	117	90	65
50000	117	111	65
60000	145	111	71
70000	210	138	72
80000	257	180	79
90000	263	204	96
100000	418	287	104
110000	548	402	104
120000	868	588	140
130000	1800	1100	141
140000	2800	1600	141

Specimen Number: A43

Test Conditions: $\sigma_a = 500$ MPa, $\sigma_m = 0$ MPa, $R = -1$
(uniaxial, low frequency)

loading cycles	surface crack lengths μm		
	Crack 1	Crack 2	Crack 3
0	2	2	2
1000	2	2	2
6000	2	2	2
13000	31	35	2
20000	35	35	2
28000	45	40	30
35000	70	88	30
44000	109	100	50
56000	146	142	66
62500	164	149	152
70000	237	167	200
80000	322	212	220
94000	396	237	266
100000	482	286	350
106000	597	452	404
110000	660	491	447
118000	1119	604	581

Specimen Number: A44

Test Conditions: $\sigma_a = 600$ MPa, $\sigma_m = 0$ MPa, $R = -1$
(uniaxial, low frequency)

loading cycles	surface crack lengths μm		
	Crack 1	Crack 2	Crack 3
0	2	2	2
750	5	2	2
900	21	2	30
1050	21	35	36
1200	38	70	36
1350	56	70	36
1500	56	70	47
1700	65	70	66
1900	65	91	77
2100	89	105	147
2300	95	106	148
2600	190	135	190
2900	353	203	302
3200	706	405	707

Specimen Number: A51

Test Conditions: $\sigma_a = 464$ MPa, $\sigma_m = 100$ MPa, $R = -0.64$
 (uniaxial, high frequency)

loading cycles	surface crack lengths μm		
	Crack 1	Crack 2	Crack 3
0	2	2	2
20000	2	2	2
40000	2	2	2
60000	38	30	20
80000	38	30	20
130000	56	34	39
180000	80	36	69
230000	113	74	97
280000	198	139	164
350000	700	367	357
390000	4000	500	510

Specimen Number: A53

Test Conditions: $\sigma_a = 456$ MPa, $\sigma_m = 0$ MPa, $R = -1$
 (uniaxial, high frequency)

loading cycles	surface crack lengths μm		
	Crack 1	Crack 2	Crack 3
0	2	2	2
100000	2	2	2
300000	2	2	2
400000	30	33	29
450000	40	41	41
550000	42	64	51
610000	65	79	68
670000	106	94	77
730000	170	106	100
800000	384	126	113
870000	1650	167	117
890000	5600	192	159

Specimen Number: A55

Test Conditions: $\sigma_a = 464$ MPa, $\sigma_m = -120$ MPa, $R = -1.73$
(uniaxial, high frequency)

loading cycles	surface crack lengths μm			
	Crack 1	Crack 2	Crack 3	Crack 4
0	2	2	2	2
240000	2	2	2	2
320000	2	2	2	2
440000	40	25	19	0
480000	50	27	21	0
520000	64	44	21	0
560000	73	55	21	31
600000	102	66	43	40
640000	121	76	43	40
680000	168	76	43	77
720000	215	125	65	110
760000	351	156	84	135
800000	609	238	86	197
840000	1456	330	99	249
860000	2600	428	121	339
878000	9000	436	141	417

Specimen Number: A56

Test Conditions: $\sigma_a = 490$ MPa, $\sigma_m = -120$ MPa, $R = -1.65$
(uniaxial, high frequency)

loading cycles	surface crack lengths μm			
	Crack 1	Crack 2	Crack 3	Crack 4
0	2	2	2	2
20000	2	2	2	2
65000	2	2	2	17
80000	26	39	24	25
95000	26	44	26	26
110000	46	47	26	26
125000	73	51	36	26
140000	86	66	41	29
155000	103	83	42	52
170000	150	101	45	66
185000	158	107	59	69
210000	269	191	101	85
220000	298	223	114	111
230000	389	268	118	137
240000	468	324	141	138
250000	607	366	197	153
260000	838	514	198	201
270000	1000	670	228	245
280000	1704	789	334	357

Specimen Number: A57

Test Conditions: $\sigma_a = 315$ MPa, $\sigma_m = 471$ MPa, $R = 0.20$
 (uniaxial, high frequency)

loading cycles	surface crack lengths μm		
	Crack 1	Crack 2	Crack 3
0	2	2	2
480000	2	2	2
540000	23	28	49
570000	24	28	49
660000	48	37	49
690000	50	48	49
750000	58	86	49
800000	58	128	57
840000	58	208	57
870000	62	340	72
900000	83	800	112
923000	108	2900	174

Specimen Number: A58

Test Conditions: $\sigma_a = 310$ MPa, $\sigma_m = 504$ MPa, $R = 0.28$
 (uniaxial, high frequency)

loading cycles	surface crack lengths μm	
	Crack 1	Crack 2
0	2	2
100000	2	2
180000	37	2
204000	75	25
214000	90	46
224000	116	48
234000	119	53
244000	131	68
260000	151	83
278000	196	88
290000	240	115
302000	305	150
320000	467	213
330000	907	346
360000	2274	638
370000	6700	1056